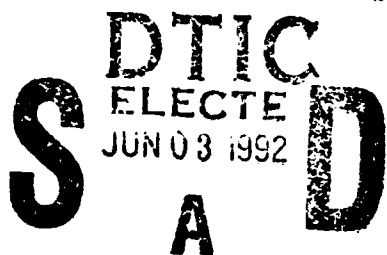AD-A251 466

Technical Document 2275
March 1992

A Method of Self Adaptive Rezoning for the Case of Large Deformation Finite Element Problems Utilizing Rezoning Indicators Derived From Eigenvalue Testing

B. L. Croft

DTIC
S ELECTE D
JUN 03 1992
A

92-14426

92 ⁕ 01 ⁚0⁚

NRaD

Technical Document 2275
March 1992

A Method of Self Adaptive Rezoning for the Case of Large Deformation Finite Element Problems Utilizing Rezoning Indicators Derived From Eigenvalue Testing

B. L. Croft

Accesion For	
NTIS CRA&I	☑
DTiC TAB	[]
Unannounced	☐
Justification	

By ....

Distribution /

Availability Codes

Dist	Avail and / or Special
A-1	

NAVAL COMMAND, CONTROL AND OCEAN SURVEILLANCE CENTER RDT&E DIVISION
San Diego, California 92152-5000

J. D. FONTANA, CAPT, USN
Commanding Officer

R. T. SHEARER
Executive Director

ADMINISTRATIVE INFORMATION

This work was performed as an independent research project for the Research, Development, Test and Evaluation Division of the Naval Command, Control and Ocean Surveillance Center, San Diego, CA 92152-5000.

Released by
T. H. Wickstrom, Head
Engineering Branch

Under authority of
J. D. Warner, Head
Weapons System Test and
Evaluation and Ranges
Division

ABSTRACT

Rezoning is required when elements within a
Lagrangian based finite element mesh become distorted due
to large deformations and strains. Rezoning halts the
solution process to correct distorted elements which
cause inaccuracies and ill conditioning. The solution is
restarted after the remeshing and the remapping of the
element variables in the rezoning regions. To date the
rezoning process has remained an interactive process with
very little theory.

A method for self adaptive rezoning is delineated
based upon finite element modeling assumptions of
structural problems involving large deformations and
strains. Linear isoparametric quadrilateral elements
using selective reduced integration are examined.

Geometrical measures of an element are defined in
terms of aspect ratio, taper ratio, and skew angle. The
amount of distortion of an element is related to these
terms when compared to the same terms for an ideal
element. An algorithm is developed to examine the finite
element mesh, element by element, to quantify the
geometrical relationships which are needed to quantify
the amount of distortion.

A key ingredient for self adaptive rezoning is the determination of rezoning indicators which provide information to determine when and how to rezone. Results of eigenvalue testing quadrilateral elements is used to derive the rezoning indicators. The process is theoretically and mathematically sound, but must be derived empirically due to the nonlinear nature of the stiffness matrix. A ratio of the strain energy density of an ideal to a distorted element is used in determining the rezoning indicators.

A remeshing technique is developed which requires user intervention and is based upon information determined by the rezoning indicators. An automatic remapping scheme is used to remap the element variables from the old mesh to the new rezoned mesh.

Two example problems are examined. An upsetting cylindrical billet simulates a quasi static metal forming process. An impacting cylindrical rod simulates a dynamic impact process. Both problems involve large deformations and strains. Results are compared to strain jump values, gradients of equivalent plastic strain, Mises stress, and strain energy density ratio, changes in the time step and increment sizes, and to similar cases from the literature.

TABLE OF CONTENTS

i

LIST OF TABLES

LIST OF FIGURES

CHAPTER 1

INTRODUCTION

1.1 An Overview

The overview is included as an aid to following the flow of the subject material presented in this thesis. There are three principal objectives of this thesis. The first objective was to develop rezoning indicators which allow for automatic detection of distorted elements and provide information required to create an optimized new mesh. The second objective was to develop a method for self adaptive rezoning which utilizes the determined rezoning indicators. The self adaptive rezoning method is used to overcome the limitations caused by distorted elements in a Lagrangian based mesh due to large strains and deformations. The third objective was to validate the first two objectives.

The information in Chapter 1 provides background information of the finite element method which applies to the rezoning method. This information is useful in determining why and how rezoning fits into the finite element method. The important considerations are the element formulations and the mesh reference frame used in

conjunction with large deformations and strains.

Chapter 2 describes the details of self adaptive rezoning in the finite element method. The theory behind the method is outlined along with some of the techniques used in development of self adaptive rezoning schemes. A general method of rezoning is explained which is similar to many of the methods cited in the literature.

An integral part of a self adaptive rezoner is the means to examine a finite element mesh at each time step or increment in order to determine if any distorted elements are present. A method was developed that describes an element's geometry in terms of aspect ratio, taper ratio, and skew angle, and this is compared to a distortion measure. This is described in Chapter 3. An ideal element shape was used as a reference.

A necessary and very important part of a self adaptive rezoner is the means to determine when an element is distorted to the point that the errors in the solution tend to grow more rapidly and cause havoc with the solution process. Chapter 4 outlines the method developed by the investigator to derive rezoning indicators. Rezoning indicators are the geometrical measures of an element that determine when an element is too distorted for use and rezoning must take place. The results of an eigenvalue problem solution of the element's stiffness matrix, incorporated into a strain

2

energy formulation, provides a valid method to derive the rezoning indicators.

Chapter 5 describes the remeshing procedure required for rezoning. In the rezoning process, the solution is halted and a new optimized mesh is created in the region of the distorted elements. This eliminates the distorted elements which create the inaccuracies and ill conditioning in the solution process.

Remapping of element variables from an old mesh to the new mesh that was created in the remeshing process (Chapter 5) is just as vital to the rezoning process as the remeshing itself. Interpolation of the element variables is required in order to restart the solution process.

Two test problems were chosen to test and validate the self adaptive rezoning process and the rezoning indicators derived from eigenvalue testing.

Finally, the results are examined and observations made regarding the rezoning indicators and the procedure of self adaptive rezoning developed by the investigator. A comparison between the nonrezoning and rezoning of the results of the test problems is used for verification of the usefulness of using the self adaptive rezoning method. Recommendations for improvement and further validation are given.

3

1.2 Basics of the Finite Element Method

An understanding of the finite element analysis process is required in order to conceptualize the purpose of rezoning found in some finite element analyses. A brief overview of the finite element analysis process will be examined.

In a finite element analysis a continuum is discretized into a series of elements which are interconnected at node points. This is done in such a fashion to properly describe the domain of the problem and to limit the infinite number of unknowns across the continuum by selecting a number of descriptive discreet points. A variety of element types exist to describe an enormous variety of problems. These problems can be found in such fields as solid mechanics, fluid dynamics, electromagnetics, acoustics, and many other fields which are beginning to use the analytical power of the finite element method.

Most finite elements are formulated to simulate the type of behavior representative of the problem and its geometry. The mathematical formulation of the element tries to simulate the behavior of real materials under given loading conditions. The nodes and integration points serve as convenient points within the elements to obtain the values of desired variables. Since only solid

4

mechanic problems are examined in this investigation these desired variables are such quantities as displacement, strain and stress.

The finite element method is advantageous in that a simple solution can be found for each individual element. A summation over all the elements is then used to derive the system of equations for the entire problem. In finite element analysis the element equations are formed using a variety of approaches. One of four general approaches can be used. The direct, variational, weighted residuals, or the energy balance approach. Once the system of equations are formed, by one of the mentioned approaches, the unknown nodal displacements are solved. The discrete displacement values at the nodes can then be interpolated to adequately describe the displacement field within each element. This process is usually achieved by using shape functions in the formulation of the element. The shape functions provide a mathematical means to interpolate between the solved displacements at the node points while representing an approximation to the true behavior of the continuum.

1.3 Strain Measures

An important feature in the finite element analysis of solid mechanics is the determination of strains. Strains can be derived from the finite element

displacement fields. This assumes that a proper measure of deformation was implemented into the equations of the analysis. One form of deformation that is commonly used is that of the stretch ratio. The stretch ratio is defined as the ratio of the current infinitesimal gage length of a particle to its initial gage length. This can serve as an adequate strain measure by itself. Many strain measures have been derived from the stretch ratio. Most assume that a measure of strain is a function of the stretch ratio. The function of stretch ratio that is assumed is dependent upon the application of the strain measure. Since strain is a link between the kinematic and constitutive theories one must base a derived strain measure on the ease with which the strain can be computed from the displacements and the appropriateness of the strain measure to a given constitutive law.

Nominal strain (Biot's strain) is a strain measure which is a function of the stretch ratio. This strain measure is most familiar to engineers who use results of uniaxially loaded test specimens. This is commonly used in small displacement, small strain problems. A second strain measure is that of logarithmic strain. This strain measure is commonly used in metal plasticity problems because it closely approximates the strain measured in 'sion, compression and torsion tests, where "true" stress (force per current area) is measured. This

6

is used with both small and large deformation and strain approximations. Finally, a third strain measure is that of Green's strain. This strain measure is used in cases of large motions but small strains. Proper choice of a strain measure must coincide with the problem to be solved whether it be for large deformations and finite strains, large deflections but small strains or simply small strains with small displacements.

1.4 Stress Measures

The stresses are a key ingredient to be derived from the finite element analysis. From the strains the stresses can be determined via the constitutive laws. For a given strain measure one can obtain a work conjugate stress measure (the product of stress and strain rate defines the work per current volume). The Cauchy (true) stress is one of the most practical stress measures in the finite element field because it measures the true stress at the current condition. This stress measure is practical for situations which model both large and small deformations and strains.

1.5 Constitutive Laws and Material Models

Constitutive laws are generally derived from tests which determine the material's behavior under various conditions. Many material models exist which try to

approximate material behaviors over a variety of conditions. Most commonly these model describe elastic and or plastic behavior. Included are such thing as yield criteria, hardening rules, flow rules, modulus of elasticity, bulk modulus, and any other pertinent parameters. Many of these models are provided in rate form so that history dependence of the response can be modeled.

The stresses can be determined from the strains by use of the constitutive laws which are formulated on a given material's properties and behavior. The finite element mesh variables provide the estimate to the kinematic solution which are in turn passed on to the constitutive laws to derive a corresponding material specific stress at a given point known as an integration point. Integration points are points that lie within the element and provide an optimum position for the computation of such state variables as the stresses.

1.6 Types of Applications

Finite element analysis problems are in general divided into either a static or dynamic type of problem which can be either linear or nonlinear. The majority of work done to date in the finite element field has extensively covered the linear static and dynamic applications. There still remains much to be done for

the improvement to solution techniques used in nonlinear static, quasi static and dynamic applications.

An application can become nonlinear in one of three ways. The material can exhibit nonlinear behavior as seen in plasticity models with large strains. The geometry can be nonlinear with large displacements and rotations. Finally, the loading conditions and kinematic constraints can be applied in a nonlinear fashion.

Dynamic applications deal with responses of the model over a period of time where the response changes sufficiently over that time period. The inertial properties tend to influence, to one degree or another, the outcome of the solution. The rate of the dynamics involved also plays an important part in the finite element modeling process. The nature of the application basically dictates how the finite element analysis is formulated.

1.7 Finite Element Mesh Reference Frame

An important factor in the finite element formulation is the reference frame of the finite element mesh to a given set of coordinates. In practice there has generally been two ways to reference a given finite element mesh to a coordinate system. If the nodes and elements remain coincident with a given spatial coordinate system, where each element and their nodes remain

9

fixed in space, and one lets the material points migrate from one element to the next, then this mesh is called a Euler mesh. Boundary conditions and definitions are almost impossible with this type of mesh. Generally these meshes handle large interior deformation problems such as might be found in fluid dynamic problems. They are also used for problems where there is a significantly high frequency content in the transient response. The solution techniques usually require many small time steps for dynamic problems but the equations are solved explicitly. This type of mesh is generally used in fluid dynamic problems.

In the second mesh type the nodes of the elements remain coincident with the same material point and the elements contain the same domain of material through out the deformation process. This is called a Lagrangian mesh. The boundary of the domain is well defined throughout the solution process in this mesh reference frame. Nodes and elements will always be able to describe the boundary, and therefore the motion of the boundary causes no problems. Lagrangian meshes, solved implicitly, allows one to use larger time steps in dynamic problems, and larger increments in static or quasi static problems. Implicit finite element codes are generally used for metal forming processes and structural analysis and design. Generally these involve static,

10

quasi static, and dynamic problems where there is a low frequency content to the response. Time step sizes can be up to three orders of magnitude greater than those used for Euler meshes.

Lagrangian meshes become disadvantageous when large distortions occur in the elements. The distorted elements cause inaccuracies and ill conditioning of the finite element solution. A solution to this problem has been to rezone the mesh. Rezoning, simply put, is the creation of a new acceptable mesh in the regions of poor element behavior due to distortion of the elements. A remapping of the old mesh variables to the new mesh is included in the rezoning process. The rezoning process depends upon many of the factors previously described concerning the finite element formulation process. The key factor for using a self adaptive rezoner is to allow one to use Lagrangian based finite element meshes and overcome the difficulties encountered with distorted elements due to large deformations and strains.

CHAPTER 2

ADAPTIVE REZONING - THEORY, ASSUMPTIONS, AND APPROACH

2.1 Theory and Method of Adaptive Rezoning

What is adaptive mesh rezoning? When and why is it used? What adaptive strategy does one use? How does one indicate when and how much rezoning should take place? What extent of the mesh should be rezoned? What will serve as proper indicators to initiate rezoning and to control how much and where it is done? Which meshing technique will best serve the purpose? How does one integrate rezoning into the solution process as well as manipulate the data structure containing the nodes and elements? How does one best transfer the nodal and element values from the old mesh to the new one? These questions are answered by examining the theory and assumptions upon which adaptive mesh rezoning is built. A method is outlined for a specific approach to developing a self adaptive rezoning algorithm.

The need for self adaptive rezoning stems from the use of Lagrangian based finite element methods and the desire for automation of the process. In finite element solutions which utilize Lagrangian meshes for large

12

deformation problems, the solution process tends to loose accuracy as the elements become distorted. This causes failure in convergence and inaccurate results in the implicit calculations and solution. Rezoning has been an answer to these problems. In many applications, especially those related to metal forming (implicit) and shock wave propagation in complex structures (explicit), the need to rezone the mesh becomes unavoidable. Due to the nature of some of these applications, the use of better elements or solution algorithms will not alleviate the need to rezone because of the amount of distortion in the elements. Rezoning should always be used for those applications where any part of the mesh becomes grossly distorted during the solution process.

2.1.1 Theoretical Background to Adaptive Rezoning

A brief overview of finite element error estimation and accuracy improvement is in order to better understand the theory behind adaptive mesh rezoning. In the literature there exists many suggestions and very little theory on how one can use error estimates to examine and improve the results and accuracy of a finite element solution [1-8]. Most of the work on improvement of mesh accuracies goes back to the field of self adaptive error analysis and improvement techniques known as a posteriori error estimation. This method has mainly been used with

static cases and the theory has only been proven for one dimensional cases. Practically no theory exists for higher order problems as well as any nonlinear problems. The main purpose of this technique has been to optimize the finite element mesh, generally for linear static problems, so that the inaccuracies caused by the mesh are minimized. An iterative technique is utilized to converge on an appropriately accurate solution via mesh refinement.

Typically a posteriori error estimators would be used in conjunction with either the h-type or p-type mesh refinement techniques to improve upon the finite element mesh. The h-type of mesh refinement involves the subdivision of the element domain into more and smaller elements. The p-type mesh refinement involves increasing the order of the element. Both techniques have proven effective in improving the finite element mesh to better the solution accuracy. Combinations of the two mesh refinement techniques have also been utilized.

The a posteriori error estimation procedure for static linear cases starts by running the solution process on an initial mesh. After the solution process ends, an error would be estimated, by a variety of means such as the method of residuals. This estimate would then provide a measure of the "goodness" of the mesh. The h and or p-type refinement process would then be

14

applied to refine the mesh by the amount indicated by the obtained error estimator. The solution would then be run again on the improved mesh. This process repeats itself until a limit on the convergence towards a more accurate solution via mesh refinement is achieved. This is an iterative optimization technique.

Adaptive mesh rezoning uses many of the principles of the a posteriori error estimation technique, however, there are a number of differences. First, rezoning is typically used in large deformation and quasi static or dynamic type problems. Second, it is assumed that the initial mesh is appropriate and that as one marches through time or the iteration process, it is the prevention and correction of grossly distorted elements that becomes the objective. During each correction of the mesh one attempts to obtain an optimum mesh for the newly rezoned region to reduce the amount of future rezoning. Most of the current rezoning techniques are not self adaptive and user intervention is required. There exists no indicators as to when and how to rezone. Generally the user of a finite element program which contains a rezoning algorithm, must stop the solution, decide if rezoning is required, and where and how the mesh should be rezoned. A good understanding of the elements used, the nature of the problem, and experience of when elements are distorted beyond use is required by

the user for these interactive rezoning processes. The need for a self adaptive (automatic) rezoner becomes obvious.

2.1.2 General Method of Rezoning

The first step in the adaptive rezoning process is to be able to determine the geometry of each of the finite elements in the mesh and provide some type of measures that define the current geometrical shape of each element. These measures would act as comparative criteria against some distortion indicators in order to determine if an element has undergone an excessive amount of distortion. Typically one would compare a relationship between an element's current geometrical configuration to that of an ideally shaped element. This process provides the means to examine the geometry of the mesh and define geometrical measures which can flag those elements which have been distorted beyond use.

The actual determination of when an element is distorted to the extent as to cause inaccuracies in the solution process can be achieved by the generation of distortion indicators. These indicators would be used in conjunction with a mesh geometry checking process. An elements current geometrical configuration or measure would be compared to distortion indicators. The distortion indicators would be given in the same terms as

16

the element's geometrical relationships. When an element's current geometrical shape relationship values exceed the distortion rezoning indicator values, then the element is flagged for rezoning. The amount of rezoning to be done to a finite element mesh would depend upon the number of elements flagged for being distorted as well as those elements that are near or approaching the distortion limit criteria. Proceeding several time steps or increments further into the solution after the first distortion limit criteria has been met would allow the determination of those elements that are near or approaching the distortion limit criteria. These elements would in most cases be rezoned (remeshed) along with the elements that reached the distortion limits. Examining the distortion pattern at latter time steps or increments would also allow the determination of how the rezoning (remeshing) should be accomplished.

Typically the indicators for when and where the rezoning process should take place have been quantities closely related to the solution variables in the finite element solution process. For example, one might measure the amplitude and gradient of such quantities as strain, stress, displacement and strain energy density. Noting areas in the mesh of extreme values or jumps in values, as well as areas of high gradient values near or at distorted elements, have served as an indicators for

17

rezoning these regions. The rate form of quantities, such as strain rate, would also be of interest as rezoning indicators. Strain rate versus a quantity such as the plasticity index might provide a means to determine when the solution has exceeded the strain rate capacity of the material. To date there has been no set rules or paths to take as to which type of rezoning indicator to use.

The a posteriori error estimators are used in a self adaptive manner where the estimators are used in the reformulation of the same mesh to arrive at an optimized mesh layout. This process proceeds automatically without user input. For rezoning to be adaptive like the approach taken with the a posteriori error estimators, the rezoning indicators and the process must be able to specify when and where the rezoning is to be done, and by how much and in what manner this is to be accomplished. This is a key ingredient. The few rezoners that exist today rely heavily on user input to perform this task.

The determination of the regions to be rezoned is in general not too much of a problem given some appropriate rezoning indicators and following the procedure previously described. Usually the rezoning is restricted to a local region of the mesh. The actual rezoning must extend out past the elements that were flagged for rezoning and those deemed near or approaching the

18

distortion limit criteria. According to Saint Venants principle the effect of a distorted element to the surrounding elements dies out the further away one is from that element [9]. Thus, if the distorted element is in a region of little interest one might not even bother to fix it since its effect is localized. For rezoning purposes, the amount of the mesh away from the distorted elements and those elements that are near or approaching distortion, that must be included in the region to be rezoned is a topic of debate. A minimum good rule of thumb in the remeshing process is to include at least those element which surround the distorted elements and those near or approaching distortion.

Once it has been determined that rezoning is required and the region for rezoning has been flagged, then that region must be remeshed. The nodes and elements of the new mesh must be of an acceptable nature. Rezoning is of no benefit if the newly created mesh is no better off than the previous mesh. Further more, one is interested in remeshing to an extent that the region will remain valid (no rezoning required) for at least a number of time steps or increments. This implies that the new mesh or remesh is to be optimized in some fashion in accordance with the pattern of the future distortions in the mesh as well as those elements flagged by the rezoning indicators. The boundaries of the mesh must

19

also remain the same. The remeshing can either reshape the existing elements to a more acceptable element shape, or refine the mesh in the given area with acceptable smaller elements. A combination of these two is most likely to occur.

Once the new mesh is created the element variables from the old mesh must be mapped over to the new mesh. The manner in which this procedure is performed is important. If the rezoning process and indicators are precise in determining when and how rezoning should take place, and the remeshing part of rezoning is optimal, yet the remapping of the element variables is shoddy or erroneous, the effort is wasted. Most remapping techniques use some type of interpolation or weighted parameters based on the positions of the old mesh to that of the new mesh. It should be noted that the old mesh means the mesh prior to the solution which was flagged for rezoning.

Once the rezoning process is complete one usually checks the element variables for discontinuities. If discontinuities in the variables are present and of sufficient size then this serves as a final rezoning check. Under such conditions rezoning either occurred too late in the process or the mesh during the rezoning was not sufficiently refined. There may also exist the chance that the remapping of the variables was incorrect.

If this is encountered then the rezoning process can be repeated or even stepped back. Another option is to decrease the time step or increment size. If the discontinuities are relatively small then the solution can proceed until the next rezoning process is flagged. Several examples from the literature cite similar rezoning processes which follow the general method of rezoning that was developed in this section [10-22].

2.2 Assumptions for Adaptive Rezoning Problems

The adaptive rezoning process could be implemented into finite element codes in various ways. The adaptive rezoning process can be focused to be applicable to certain types of applications under certain conditions and assumptions. An approach similar to the description in section 2.1.2 for the rezoning process will be formulated based upon a given set of conditions and assumptions. These conditions and assumptions help to narrow the applications of rezoning to those of interest.

2.2.1 Types of Applications to be Studied

Nonlinear quasi static and dynamic problems of large deformations, large strains, and for some problems high strain rates are the main applications which require the rezoning process. Specifically such problems would entail impact problems at high velocities, metal forming

21

processes, and large deformation problems in general. A
large variety of these type of problems can be modeled
using two dimensional elements. The focus of this
investigation will be on axisymmetric, plane strain, and
plane stress elements undergoing large deformations and
strains. This process, however, could easily be extended
to other types of elements and three dimensional cases.

2.2.2 Finite Element Solution Technique

The applications of interest are either dynamic or
quasi static. In general they will always be nonlinear.
For such problems a direct integration technique is used
in the solution process. A standard implicit time
integration operator which would be a slight modification
of the trapezoidal rule called the Hilber-Hughes-Taylor
operator is used. This implicit time operator solves the
nonlinear dynamic equilibrium equations at each time step
and does so iteratively by Newton's method. An automatic
time incrementation scheme is used which adjusts the time
increment after such events as a sudden impact. This of
course, assumes the use of a Lagrangian based mesh. This
solution technique is used in ABAQUS' solver algorithm.

2.2.3 Elastic-Plastic Material Modeling

Most metals are considered to behave in a ductile
fashion and exhibit relatively small amounts of elastic
deformation in comparison to the amount of plastic or

22

inelastic deformation which they can achieve before failure. This behavior can be approximated or modeled by the elastic-plastic models common to many finite element codes. Finite element models of elastic and inelastic behavior of metals are therefore considered to be valid assumptions for adaptive rezoning. The inelastic response is simulated with a plasticity model. In plasticity theory the elasticity part of the model is not effected by the inelastic deformation. The elasticity theory assumed is the one standard to most text books.

The logarithmic strain measure is used since it is the measure commonly used in metai plasticity problems. This is appropriate for cases where the elastic part of the strain in a elastic-plastic analyses can be assumed to be very small. Many structural metals typically have their elastic modulus two to three orders of magnitude larger than the yield stress, and thus elastic deflections are comparatively small. This can be used to advantage in that the inelastic and elastic responses can be separated into the deformation of recoverable (elastic) and non recoverable (inelastic) parts. An additive relationship between the strain rates is utilized. This is the classical strain rate decomposition of plasticity theory. The rate of deformation will be used as the strain rate measure. Total strain is defined as the integral of the rate of

deformation in large displacement analysis. This class of problems therefore is based on finite strain formulation.

The inelastic (plastic) response is assumed to be fully incompressible in metals undergoing large plastic flow. When the material is flowing plastically the inelastic part of the deformation is defined by a flow rule. A single flow potential is assumed. The plasticity model uses isotropic hardening. Increases in strain rates typically cause an increase in the yield stress of the material. This is modeled since high strain rates are typical for the class of problems being considered. Metal plasticity models use the Mises stress potential for isotropic metal behavior. They depend only on the deviatoric stress so that the plastic part of the response is incompressible. True or Cauchy stress and logarithmic strain will generally be the element variables sought besides the displacement.

2.2.4 Element Selection and Conditions

The emphasis is focused on two dimensional first order isoparametric quadrilateral elements using selective reduced integration. These elements will be either plane strain, plane stress, or axisymmetric elements. The elements are first order or linear in interpolation with only four nodes, one at each of the

24

corners. This type of element has been chosen for the applications of interest, that being large deformations and strains leading to an incompressible material response. Note that the choice of elements could be extended to higher order elements without too much difficulty. The sides of the elements will be assumed to remain straight. A lump mass versus consistent mass matrix is used in the finite element models. Using lumped mass is generally easier and more appropriate with dynamic problems. The elements are formulated for finite strains and large displacements. Finite element distortion is most likely element type sensitive, therefore restrictions on the choice of element type aids in focusing the study on rezoning.

In problems where plastic flow ends up dominating the response, and the material behavior is near or fully incompressible, as seen in such cases as metal forming problems. The element choice and the integration scheme of the element's stiffness matrix is important. The elements must accommodate the incompressible flow assumption in the plasticity theory. Usually for these cases reduced integration elements are utilized. Occasionally one might use hybrid type elements. Reduced integration, however, can lead to singular or hourglass modes. These modes can grow in an unbounded fashion if uncontrolled. Singular or hourglass modes cause

25

irregularities and ill conditioning in the solution
process. Fully integrated first order continuum
elements, however, can be used with selective reduced
integration, where just the volumetric strain is
calculated at the centroid (reduced integration point) of
the element instead at other integration points. In
selective reduced integration the order of integration is
reduced for selected terms in the fully integrated
element like the volumetric strain used in this case.
This helps in the prevention of mesh locking which would
normally occur in fully integrated elements when the
response is incompressible. The volumetric strain is
then extrapolated to the four integration points in the
two by two Gauss quadrature integration scheme. First
order elements with selected reduced integration are
therefore suitable for the applications of interest in
this investigation [17, 18, 23].

2.3 Adaptive Rezoning Approach

Given the basis or the need for adaptive rezoning of
finite element meshes, and provided with a specific class
of problems, one can focus in on determining an approach
to the rezoning method which will be most effective.
This provides a means to specifically delineate the
method used for adaptive rezoning of large deformation
finite element problems.

26

First, one must inspect the finite element mesh for distorted elements. The geometrical measures of quadrilateral element shapes can be classified as aspect ratio, taper ratio, skew angle, triangular quadrilaterals, and inverted elements. These geometrical values must be examined for each element at each step in the solution. See Section 3.5 for details.

A rezoning indicator is used to determine if an element is distorted or approaching the point of being distorted. The rezoning indicators are given in terms of the same measures used in defining the geometry of the elements. The rezoning indicators therefore become a comparative criteria with the geometrical measures. Eigenvalue testing serves as an excellent means to derive rezoning indicators. The examination of large magnitudes or jumps in magnitudes of displacement, strain, stress and strain energy density, as well as steep gradients of these values, in the regions of distorted elements, permits the confirmation of the rezoning indicators derived from eigenvalue tests.

The rezoning indicators derived from eigenvalue tests are formulated by comparing ratios of strain energy density of distorted element shapes to an ideally shaped element under controlled conditions. The formulation of the strain energy density values is based on the eigenvectors and eigenvalues derived from an eigenvalue

27

test of the element's stiffness matrix. Chapter 4 provides more specific details on how these rezoning indicators are formulated.

The important point to realize is that the rezoning indicators act as the focal point in a self adaptive rezoning process. The element distortion limits set by the rezoning indicators permit the flagging of distorted elements as well as allowing the examination of the mesh to determine which elements in the future increments or time steps will reach the distortion limits set by the rezoning indicator criteria. This information is utilized in the remeshing phase of rezoning.

A new finite element mesh is generated based on the information obtained when examining the old mesh and comparing its geometrical relationships to the rezoning indicators. The new mesh formulation is based on the previous, present, and future deformation patterns exhibited by the finite element mesh. The knowledge of which elements are being distorted throughout the solution process, as well as the pattern and type of distortion, allows one to reshape the mesh anticipating and correcting for the distortions.

With the insight provided by the rezoning indicators as to when the distortions occur throughout the process, a new mesh at a given increment or time step can be optimized to reduce the number of future rezonings.

28

Caution should be applied so as not to loose valuable

information obtained in the remeshing. For example, an

area of refined element size should remain refined during

the remeshing if the refined region was put there to

achieve more accuracy in the solution, such as stress

concentration points. Such a technique is difficult to

incorporate into an self adaptive rezoning algorithm.

Expert type systems would be required to effectively

achieve this task. In addition, initial user input would

be required to define the desired parameters of the

problem. In this investigation interactive user input

was utilized to achieve the desired remeshings of the

rezoning process. The remeshing, however, was based on

the use of the rezoning indicator procedure just

described with the aid of various existing mapping

techniques.

The final step is to remap the element variables of

the old mesh onto the newly created mesh. This is

usually done by an interpolation scheme. ABAQUS a finite

element code was used to perform the remapping process.

The code contains an automatic remapping algorithm. This

allowed for an efficient remapping of all the solution

variables. The remapping itself can also serve as a

rezoning indicator. Chapter 7 provides more details on

the remapping of solution variables.

This entire process is repeated at any time step or

increment during the solution process when the rezoning
indicators flag elements of the mesh for rezoning.
Optimizing each step of the process will help to reduce
the number of rezonings required. This is important
since each rezoning adds additional computational effort
to the solution process and hence added cost and time to
obtain the solution.

2.4 Implementation of a Finite Element Code for Rezoning

There are many finite element codes which are
adequate as a finite element solver that can not only
solve large deformation problems, but can also be used to
implement an adaptive rezoning algorithm. Two finite
element codes which fit this description were examined.
These codes are NIKE2D and ABAQUS.

NIKE2D is an implicit finite deformation, large
strain finite element code for static, quasi static, and
dynamic analysis of two dimensional structural
calculation problems. Plane stress, plane strain and
axisymmetric problems can be solved. NIKE2D has a built
in interactive rezoning algorithm. It is also supplied
with a variety of material or constitutive models which
cover the desired range of problems. NIKE2D uses four
node quadrilateral elements with lumped mass [24].
Research by this investigator found NIKE2D to be lacking
in documentation, user friendliness, and the capability

to interface it to an adaptive rezoning algorithm. For these reasons NIKE2D was dropped as a candidate as a finite element code to be interfaced to the adaptive rezoner.

ABAQUS is an implicit Lagrangian finite element code. It is suited for all of the conditions and assumptions such as proper material models, as well as finite strain and large deformation capabilities [17, 18]. It contains many if not more features than those of the NIKE2D code. ABAQUS is setup to allow the eigenvalue testing of elements with only a simple manipulation of the mass matrices. This allows one to use the code to obtain the required data to derive the rezoning indicators. ABAQUS also allows one to stop the solution process and restart it again at a desired time step or increment. This is a typical restart procedure. This allows one to integrate a rezoning algorithm at this point. ABAQUS does contain a rezoning algorithm but it is strictly a user specified procedure. Various output procedures allow access to the element and nodal data bases for changes to be made during rezoning. ABAQUS' rezoning algorithm has a built in interpolation algorithm designed specifically to remap the nodal and element variables from the old mesh to the new mesh. This can be incorporated to eliminate the need to provide for this procedure in the rezoning algorithm.

31

The use of the ABAQUS code allows for a semi-self adaptive rezoning procedure. It is semi-self adaptive due to the fact that user intervention is still required to perform the "self adaptive" rezoning process. This limitation is due to the fact that direct implementation of the rezoning algorithm and its components into the ABAQUS code was not permissible.

CHAPTER 3

FINITE ELEMENT MESH INSPECTION

3.1 Introduction

The first item required for a finite element rezoner
is an algorithm that examines the finite element mesh at
each time step or increment. This algorithm determines
all required geometrical relationships within each
element of the mesh. Typically for quadrilateral
elements these are aspect ratio, taper ratio, skew angle,
triangular quadrilaterals, and inverted quadrilaterals.
Triangular and inverted quadrilaterals can be classified
as subsets of the skew angle. The discussion here is
limited to quadrilateral elements, however, it could as
easily apply to other type of elements such as the three
dimensional brick elements. The geometrical measures are
compared to the same type of measures for an idealized
element. An idealized element is defined as an element
that provides an optimum value for each of the
geometrical measures of its shape. Refer to Section 3.3
for the definition of an ideal element.

The geometry inspection of the elements of the mesh
is an essential key in the rezoning process. The fact is

that all rezoning indicators will eventually relate back to the geometry of the elements and all changes to the mesh will be related to the physical geometry of the mesh. A robust method of element geometry inspection is therefore required.

3.2 Focus on Quadrilateral Elements

This investigation focuses on the use of quadrilateral elements in finite element models and in the rezoning process. The procedure to inspect the geometry of other types of elements would be similar in nature. Many applications of large deformation finite element codes which require rezoning are modeled with quadrilateral elements either being plane strain, plane stress, or axisymmetric elements. Restriction to these elements provides for a concise exercise in the development of a rezoner and yet is applicable to a wide range of problems which are of interest.

Each element is isoparametric and limited to four nodes. Each element uses first order or linear interpolation. Lumped mass is assumed. This classification of elements greatly simplifies the procedure in developing an adaptive rezoner. Procedures used to examine the geometry of two dimensional first order isoparametric four node quadrilateral elements can be extended to other types and orders of elements. The

34

restrictions placed on the element choice is in agreement with statements from the literature which imply that such elements should be used for applications that involve large deformation and strain [17, 18, 23, 25].

3.3 Ideal Geometry of a Quadrilateral Element

In developing geometrical measures for quadrilateral elements one must have a frame of reference or some type of idealized geometry for comparison. A reference to an ideally shaped element would provide the most logical approach. If such a reference is made, then all distortions of a quadrilateral element can be compared to this ideal element to gain a quantitative as well a qualitative feel for the amount of distortion.

It has been documented that elements perform best if their shape is compact and regular [26-28]. Elements tend to loose accuracy as the aspect ratio increases, the corner angles become markedly different from one another, sides become curved, and if side nodes exist, when their positions become unequally spaced.

Ideally one would want a quadrilateral element with the aspect ratio near unity, the corner angles near ninety degrees, the side nodes (if they are used) at the element mid sides, straight sides or edges, and no great size differences between adjacent elements. The definition of an ideally shaped element would therefore

35

be square in shape, of unit dimension along each edge, corner angles would be ninety degrees, and lumped mass at the nodes. There are some exceptions to the definition of the ideal element. A rectangular shaped element under constant strain conditions can perform just as well as a square element shape. Close attention must be given when such cases arise.

3.4 Quadrilateral Element Geometry Definition

The geometrical relationships of a given quadrilateral element must be defined in order to describe and define the possible geometrical distortions of a quadrilateral element. The geometrical definition of a quadrilateral element is shown in Figure 3.1.
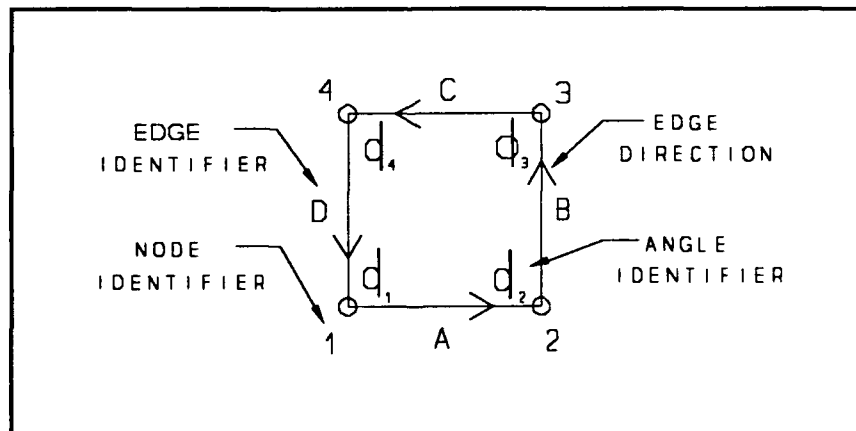
Figure 3.1.   Element geometry definition

The first important definition is the numeration of the nodes and their corresponding order. Each element

will have four nodes numbered such as 1, 2, 3, and 4.
Note that each node point will contain a unique node
number and an x and y coordinate value. The numbering
will be sequential from some starting node and marching
around the element in counter clockwise fashion as seen
from above the element. Any of the nodes can be defined
as the first node just as long as the sequential order is
given in a counter clockwise fashion.

The next step is to define or label each of the
edges of the element. From Figure 3.1 one can see that
the edges are defined as A, B, C, and D. Edge A lies
between the first and second nodes and the direction is
from node 1 to node 2. The other edges follow similar
suit, again in a sequential order going counter clockwise
around the element.

The final geometrical definition is that of the
angles of the element. All angles are defined to be
interior angles of the element. The first angle would be
made from edges D and A, the second angle would be made
from edges A and B, and so on. The angles are defined by
the interior angle between the intersecting edges at a
given node point. Ordered nodes with coordinate points,
directed element edges, and interior angles are all that
is required to define the geometry of two dimensional
first order four node quadrilateral elements.

3.5 Geometrical Distortions of Quadrilateral Elements

There are five main geometrical relationships that can be used to define the shape of a quadrilateral element. These relationships are (1) aspect ratio, (2) taper ratio, (3) skew angle, (4) triangular quadrilaterals, and (5) inverted quadrilaterals. These will be defined in a general sense and extreme cases of these values are depicted in Figure 3.2.
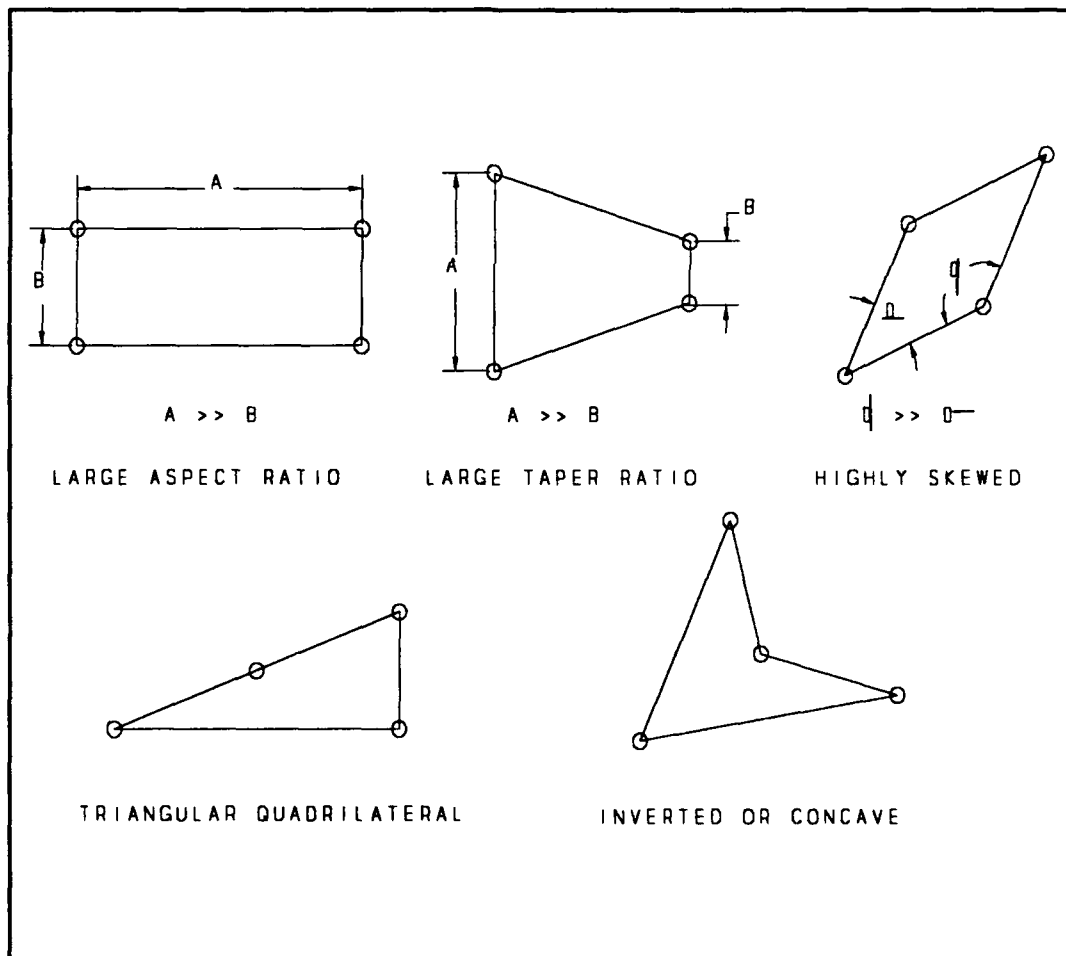
Figure 3.2. Geometrical distortions

Aspect ratio is defined as the ratio of the length of a given edge to the length of an adjacent edge. This makes possible four different aspect ratios. Note that their inverses would actually create four more possibilities but only four are required to uniquely define the possible aspect ratio combinations.

Taper ratio is defined as the ratio of the length of a given edge to the length of an opposite edge, not the adjacent edge. This makes possible two different taper ratios. Note that their inverses would actually create two more possibilities but only two are required to uniquely define the possible taper ratios.

Skew angle is defined as the value of the interior angle given by two adjacent edges at a given node. There are only four unique angles. Note that one could take ratios of the angles but the angles themselves are sufficient in defining the skew of an element.

Quadrilateral triangles are defined as having an element where three of the four nodes are collinear. Another definition is given by having one of the interior angles of the element equal to one hundred and eighty degrees. Generally such a situation should rarely be detected in rezoning owing to the fact that the angles given in the skew relationship should detect and initiate a fix on elements that have an interior angle which is approaching angles significantly lower than one hundred

39

and eighty degrees. Quadrilateral triangles are in essence a subset of the skew angle measure.

An inverted quadrilateral is defined as having a portion of the element turned inside out or concave. Put another way, one of the interior angle will have a value which exceeds one hundred and eighty degrees. In some cases the element will not be turned inside out but will be concave. This is an indication of extreme element distortion which causes great problems in the solution process. Inverted elements are also a subset of the skew angle measure.

3.6 Methodology to Determine Geometrical Relationships

The aspect ratio of a quadrilateral element is first determined by finding the length of each of the edges. Since first order quadrilateral elements have straight sides, one is only required to compute the distance between the beginning node and ending node of each edge. The x and y coordinates of each node point and hence the ends of each edge are known. Once the lengths are obtained then one finds the maximum ratio of adjacent edge lengths. This will indicate the largest aspect ratio for the element which in turn will be compared to an ideally shaped element and eventually to a rezoning indicator.

The taper ratio of a quadrilateral element is

determined in similar fashion to that of the aspect
ratio. The only difference between determining the tar ᵣ
ratio value and that of aspect ratio is that taper ratiᵤ
uses the ratio of opposite edge lengths instead of
adjacent edge lengths.

The skew angle of an element is determined by using
the dot product formula. One first determines which
interior angle is to be determined. Next, the two
intersecting edges that form the angle are selected as
the vectors to use in the dot product formula. The
direction of the first vector (edge) is reversed due to
the definition of the direction of the edges. The
magnitudes of the lengths of the vectors and each of
their x and y components is then determined and used in
the dot product formula. This equation can then be
manipulated in order to solve for the value of the angle.
The same element geometrical configuration of Figure 3.1
depicts the geometry used to obtain the skew angle given
in Equation (3.1b). The dot product is defined by

$$\vec{D} \cdot \vec{A} = |\vec{D}||\vec{A}|\cos\Phi_1 \qquad (3.1a)$$

and solving for the angle

$$\phi_1 = \cos^{-1}\frac{\vec{D}\cdot\vec{A}}{|\vec{D}||\vec{A}|} = \cos^{-1}\frac{|D_x||A_x| + |D_y||A_y|}{|\vec{D}||\vec{A}|} \qquad (3.1b)$$

41

where the angle is defined by element edges D and A of Figure 3.1.

The determination of a triangular quadrilateral is accomplished by either checking if any three consecutive nodes line along a straight line or if any two adjacent edges have the same slope. Another check is to simply use the skew angle equations and check for any interior angle which equals one hundred and eighty degrees.

Inverted or concaved quadrilateral elements can be determined by using the cross product formulation. This procedure is done in similar fashion to the determination of the skew angle. Two adjacent edges of the element are taken as vectors, with the vector direction of the first edge opposite to the way it is defined. The cross product formulation is then used. The sine of the angle term is not required. A negative value from just the z direction component of the equation defines a concave element. If the value is positive the element is neither concave nor turned inside out. This process is repeated for all four combinations until any one or none of the combinations indicate an inverted element. The geometry used to help develop Equation (3.2a) and Equation (3.2b) is identical to that depicted in Figure 3.1. The cross product in vector component form, which has its z direction component out of the plane of the element is given by

42

$$\vec{D} X \vec{A} = (D_y A_z - D_z A_y)\,\hat{i} + (D_z A_x - D_x A_z)\,\hat{j} + (D_x A_y - D_y A_x)\,\hat{k} \quad (3.2a)$$

and solving for just the sign of the z direction component

$$INVERT = SIGN(D_x A_y - D_y A_x)\,\hat{k} \quad\quad (3.2b)$$

where a negative sign indicates an inverted element.

Warping will not be considered. It is assumed that all quadrilateral elements will remain planar. By observation triangular and inverted quadrilaterals are definitely defined as distorted elements. The literature has provided some indication as to what quantitative degree an element becomes distorted so as to effect the accuracy of the solution. For an aspect ratio, limit values have ranged from fifteen to twenty. For skew angles, values below thirty, forty-five, or fifty degrees and above one hundred and thirty or one hundred and fifty degrees have been deemed as too distorted. Taper ratio values which exceed a two to one ratio have also been deemed as poor elements. Some have prescribed that values of any edge being less than one tenth of an average edge length will create inaccuracies. These quantitative values have been determined by experience and intuition. These values have also been used in mesh

43

checking routines of finite element codes and pre and
post processors [20, 27-31].

It is the objective of this investigation of self
adaptive rezoning to determine and quantify these values
in a more theoretical or experimental nature. It would
be logical that the geometrical distortion factors should
correlate to some degree with the values obtained by
experience and intuition that have been set as rules of
thumb for distortion values.

3.7 Computer Program for Geometry Inspection

A computer program , found in Appendix A, was
developed to inspect the geometry of each element in a
finite element mesh. Each element of the mesh is
systematically examined and the maximum values of aspect
ratio, minimum and maximum values of skew angles, minimum
values of taper ratios, the inversion of an element, and
coincident nodal points of each of the elements is
determined. These values are compared to rezoning
indicators and stored for use in the remeshing process.
If the comparison is less or exceeds the corresponding
rezoning indicator (depending on the criteria) the
element is flagged as distorted.

CHAPTER 4

REZONING INDICATORS DERIVED FROM EIGENVALUE TESTING

4.1 Introduction

A key ingredient in getting a self adaptive rezoner to work is to be able to automatically identify at what point and in what manner in the solution process one should rezone the finite element mesh. Eigenvalue testing of finite elements can be used to derive parameters which can be utilized as mesh rezoning indicators and measures of mesh correction.

Eigenvalue tests are tests of element quality. Eigenvalue testing is generally used to detect zero-energy deformation modes, lack of invariance, and absence of rigid-body motion capability. Eigenvalue tests have also served as a means to estimate the relative quality between different elements. In essence the eigenvalue test solves an eigenvalue problem which is formulated solely on the finite element stiffness matrix. The solution yields eigenvalues and eigenvectors which can be related to the strain energy associated with the element. The eigenvectors can also be associated with the possible deformation modes as well as rigid body

modes of the element. In short the eigenvalue test can
provide a good indication of how an element should
deform, and provide terms to generate a measure of the
energy associated with that deformation.

Rezoning indicators can be determined by using the
results of eigenvalue tests on elements of a given
distortion and comparing them against eigenvalue test
results on an ideal element. The eigenvalue test results
are incorporated into an equation to derive the strain
energy density. Doing this over a range of distortion
values for the various distortion parameters of aspect
ratio, taper ratio, and skew angle, provides a means to
determine at what point the element deformation pattern
and associated strain energy density begin to create
improper results in the solution.

4.2 Method of Deriving Distortion Indicators

The methodology that is used to derive the
distortion indicators from the results of an eigenvalue
test is founded on an equation presented in a paper by G.
L. Rigby and G. M. McNeice [32]. The main emphasis of
this paper is the development of a strain energy basis
for the study of element stiffness matrices. An equation
is developed which relates the eigenvectors and
eigenvalues from an eigenvalue test, along with an
assumed load vector, to the strain energy capacity of the

46

element. Rigby and McNeice believe that this principle
can be extended to investigate the effects and behavior
of geometrical distortions in the elements. This concept
serves as the foundation for the formulation of rezoning
indicators from eigenvalue tests used in this
investigation.

4.2.1 Mathematical Derivation of the Rezoning Indicators

Rezoning indicators which are derived from results
of eigenvalue tests can be shown mathematically to be
directly related to the parameters upon which the
deformation characteristics and strain energy content of
a quadrilateral element are based. This in turn leads to
the formulation of an equation which is based upon the
deformation characteristics and generates the strain
energy of a given element assuming a given load vector.

If one assumes that the displacement model of the
finite element is based on the minimum potential energy
principle then

$$[k]\{d\} = \{r\} \qquad (4.1)$$

This is the basic finite element equation which relates
the element stiffness matrix [k] and displacement vector
{d} to a load vector {r}. The assumption is made that
the load vector is proportional to the displacement
vector through a factor λ and Equation (4.1) becomes

47

$$[k]\{d\} = \{r\} = \lambda\{d\} \qquad\qquad (4.2a)$$

Rearranging the terms of Equation (4.2a) gives

$$([k] - \lambda[I])\{d\} = \{0\} \qquad\qquad (4.2b)$$

which is an eigenvalue problem where λ_i is an eigenvalue of the stiffness matrix [k]. Each λ_i has a corresponding eigenvector $\{\phi\}_i$ where

$$\{\phi\}_i^T\{\phi\}_j = \{ \frac{1 \; for \; i = j}{0 \; for \; i \neq j} \qquad\qquad (4.3)$$

defines how the eigenvectors are normalized. Multiplying each side of Equation (4.2b) by $\{\phi\}_i^T$ and examining the equation for each given mode gives

$$\{d\}_i^T[k]\{d\}_i = \lambda_i \qquad\qquad (4.4)$$

Recalling that strain energy is defined by

$$U = \frac{1}{2}\{D\}^T[K]\{D\} \qquad\qquad (4.5)$$

a parallel is drawn between Equation (4.5) and Equation (4.4). Equation (4.4) implies that the eigenvalue of a given mode λ_i is equivalent to twice the strain energy

48

for that mode with the normalized displacements or
eigenvectors being used, thus

$$2U_i = \lambda_i \qquad (4.6)$$

Equation (4.6) clearly states that the eigenvalues
derived from an eigenvalue test of an element's stiffness
matrix [k] are directly related to the strain energy of
the element associated with the deformation pattern of a
given mode. A summation of all the eigenvalues divided
by two would then determine the entire strain energy for
a given displacement. This same derivation is given by
Cook [27].

The derivation of strain energy can be taken one
step further to not only incorporate the eigenvalues but
the eigenvectors as well. This procedure is outlined in
Reference [32] and is summarized as follows. The
displacement vector of Equation (4.1) is equated to the
summation of each eigenvector times an assumed
coefficient such that

$$\{D\} = \sum_{i=1}^{n} c_i \{\phi\}_i \qquad (4.7)$$

where n in the summation is the number of degrees of
freedom in the element minus the number of rigid body

49

modes of the element. Equation (4.7) substituted into Equation (4.5) and using the relationship of Equation (4.4) yields

$$U = \frac{1}{2} \sum_{i=1}^{n} c_i \lambda_i c_i \qquad (4.8)$$

Utilizing Equation (4.1) , Equation (4.7), and Equation (4.4) the coefficient c_i can be determined along with premultiplying Equation (4.1) by each eigenvector. The coefficient is given by

$$c_i = \frac{\{\phi\}_i^T \{r\}}{\lambda_i} \qquad (4.9)$$

Substitution of Equation (4.9) into the strain energy relationship of Equation (4.8) causes the strain energy equation to become

$$U = \frac{1}{2} \sum_{i=1}^{n} \frac{(\{\phi\}_i^T \{r\})^2}{\lambda_i} \qquad (4.10)$$

It is clear from this derivation that Equation (4.10) formulates the strain energy content of an element

50

based on the eigenvectors and eigenvalues generated from
an eigenvalue test of the element's stiffness matrix.
The load vector utilized in the equation is the load
vector which creates the deformation pattern
characterized by the eigenvectors and therefore generates
strain energy within the element characterized by both
the eigenvectors and eigenvalues.

Equation (4.10) is used in a comparative ratio to
finally arrive at an equation which can be utilized to
quantify distortion or rezoning indicators. The ratio is
the strain energy of an ideal element to that of a
distorted element given by

$$\overline{U} = \frac{IDEAL\ STRAIN\ ENERGY}{DISTORTED\ STRAIN\ ENERGY} = \frac{\displaystyle\sum_{i=1}^{n} \frac{(\{\phi\}_i \{r\})^2}{\lambda_i}}{\displaystyle\sum_{k=1}^{n} \frac{(\{\psi\}_k \{r\})^2}{\eta_k}} \quad (4.11)$$

Calculating values generated from Equation (4.11) over a
range of the specified distortion parameters of aspect
ratio, taper ratio, and skew angle will create sets of
data which can be examined for discontinuities in the
change of the strain energy ratio values as compared to
the changes in given distortion parameter values.

It is also of interest to mathematically examine the
structure of a quadrilateral element stiffness matrix.
This permits one to see how the geometry of the element

51

is embedded in the equations that form the stiffness matrix. These geometrical terms can then be related to the specific distortion parameters of aspect ratio, taper ratio, and skew angle. This will illustrate how a change in the shape of the element can affect the performance of the element.

The standard finite element equation for the stiffness matrix is

$$[k] = \int_V [B]^T [E] [B] \, dV \qquad (4.12)$$

where [B] is the strain-displacement matrix and [E] is the material matrix. The equation is integrated over the volume of the element. A plane strain isoparametric element will be examined. The results for plane stress and axisymmetric isoparametric elements would only differ slightly, thus the plane strain case is representative of the other types of elements used in this investigation.

For a plane strain isoparametric element Equation (4.12) would be given as

$$[k] = \iint [B]^T [E] [B] \, t \, dx dy = \int_{-1}^{1} \int_{-1}^{1} [B]^T [E] [B] \, t J d\zeta d\eta \qquad (4.13)$$

where t is the thickness of the element, for this case t

is set equal to one, and J is the determinant of the Jacobian matrix. These quantities are required for the transformation of x and y coordinates to that of ξ and η of the isoparametric coordinates.

The geometry of the element is embedded in the strain-displacement matrix [B] and also the determinant of the Jacobian matrix J. The geometry of a four node quadrilateral element can be defined by just the x and y nodal locations. For isoparametric elements a coordinate transformation from the x and y coordinates to isoparametric coordinates ξ and η is given by

$$x = \sum_{i=1}^{4} N_i x_i \, , \quad y = \sum_{i=1}^{4} N_i y_i \qquad (4.14)$$

where N_i represents a shape function. The four shape functions used in the element formulation are

$$N_1 = \frac{1}{4}(1-\zeta)(1-\eta) \qquad (4.15a)$$

$$N_2 = \frac{1}{4}(1+\zeta)(1-\eta) \qquad (4.15b)$$

$$N_3 = \frac{1}{4}(1+\zeta)(1+\eta) \qquad (4.15c)$$

$$N_4 = \frac{1}{4}(1-\zeta)(1+\eta) \qquad (4.15d)$$

These relationships bind the two coordinate systems

53

together. If a relationship can be defined which correlates the x and y coordinate points of an element to the distortion measures of aspect ratio, taper ratio, and skew angle, it can then be transformed into the isoparametric coordinates utilizing Equation (4.15a) through Equation (4.15d). The shape functions, Equation (4.15a) through Equation (4.15d), and their derivatives are used extensively in the formulation of the strain-displacement matrix and the determinant of the Jacobian matrix. The relationship to the geometrical parameters which describe the shape of the element are therefore an integral part of the stiffness matrix.

Relationships between the x and y coordinates of the element and the distortion measures of aspect ratio, taper ratio, and skew angle can now be determined. The length of each of the edges as well as the lengths of the two diagonals formed from opposite nodes are easily determined from the nodal coordinate points. Two area equations can also be formulated. The first area equation is based on solving the area of the two triangles formed by the first diagonal. Simple geometrical relationships make this possible. The second area equation is identical, the only difference being the second diagonal, and the two resulting triangles that are used to determine the area.

The edge lengths, nodal coordinates, and edge

54

directions are all that is required to determine aspect ratio, taper ratio, and skew angle. Chapter 3 describes how these distortion measures are formulated. The four edge length equations, two diagonal length equations, and the two area equations, along with one of the distortion measure equations, can be used to simultaneously solve each of the eight coordinate values in terms of the given distortion measure. The solution of these equations is not included due to the length and amount of algebra involved. The important point is that the strain-displacement matrix and the determinant of the Jacobian matrix of the stiffness matrix can be formulated based on a given distortion measure in lieu of the x and y coordinates of the element. These equations would allow one to directly see the effects of a given distortion, such as aspect ratio, on the stiffness matrix of an element since the stiffness matrix becomes a function of the distortion measure. This in turn also allows one to study the effects on the deformation patterns and the strain energy content of the element in terms of the distortion measure.

The equations derived in this section could be solved to directly obtain the desired results. This is possible only if the equations are within the linear range. For large deformations and strains this is not the case. No closed form solution can be obtained.

Nonlinear solution techniques have to be employed. The best solution to this problem is to empirically derive the desired results. Using an existing finite element code which handles large deformation and strain problems would be the best choice.

4.2.2 Empirical Derivation of the Rezoning Indicators

Since large deformations and strains cause a finite element problem to be nonlinear, no nice closed form mathematical solution is possible. An empirical approach to deriving the rezoning indicators via eigenvalue testing is therefore required.

In this empirical method an eigenvalue test would first be run on an assumed ideal quadrilateral element. The normalized eigenvectors and their eigenvalues would be obtained for each mode. These are then summed over all the modes. The value that results is the amount of strain energy for an ideal element for a given load vector. Equation (4.10) is used for this purpose. The next step would be to repeat the same procedure but for an element with a known amount of distortion. Just one kind of distortion measure would be used in order to separate the effects caused by that type of distortion. This also simplifies the interpretation of the data. The strain energy for the distorted element is obtained using Equation (4.10).

In order to get a relationship between the two values of strain energy it is best to find the strain energy density of both the ideal and distorted elements instead of just the strain energy. Distorting elements of unit area under controlled conditions simplifies the procedure to obtain the strain energy density values. Applying specified displacements to the element in order to maintain a given type of distortion is a simple matter. Since plastic deformation is assumed to be incompressible, the area of the element can always be maintain at a value of one no matter how extreme the distortion. This provides for a "normalized" comparison and yields the strain energy density because the volume is also of unit dimension. For axisymmetrical cases, however, the revolved volume must be accounted for. The ratio of the strain energy density of the distorted element to that of the ideal element serves as an excellent comparison.

If the type of distortion is maintained but varied in degree then a range of comparative values can be obtained. For example one can vary just the aspect ratio from a one to one value up to say a forty to one value. In an empirical approach no function exists to generate a smooth continuous representation of the strain energy density ratios versus the range of a given distortion measure. Individual data points must be obtained and

57

then a curve fit between these values in order to obtain the intermediate values.

It is assumed that discontinuities seen in plots of the data will represent points at which an increase in the amount of distortion to the element will significantly increase the error in the solution process. This will identify the limit on the amount of distortion an element can handle before the amount of error gets out of hand. This limit value is the distortion or rezoning indicator for the given distortion measure being used. Section 4.4 provides the details on how this is accomplished.

4.3 Argument for Rezoning Indicators Derived from Eigenvalue Testing

The theoretical basis for the eigenvalue test is a direct extension of a normal modes analysis. In normal modes analysis one wishes to find the natural frequencies and mode shapes of an unconstrained object. These quantities provide important information concerning the deformation and vibrational characteristics of a given structure. If one reduces this down to a single element instead of a mesh of elements representing a structure, then theoretically, information that once identified the deformation modes and natural frequencies of a structure will now do so for a single element. This is important

58

because, from this, one can determine the possible modes of deformation and natural frequencies of a single element. A study can therefore be made on an element to element basis. This is essential to the rezoning process since each individual element must be examined instead of the entire mesh. Rezoning is associated with the remeshing of localized problems within the mesh cause by a single element or groups of elements.

In a normal modes analysis one solves the eigenvalue problem which involves the stiffness and mass matrices. The solution generally yields the square of the natural frequency for each mode. Using these values and a set of equations one, can then solve for the eigenvectors or mode shapes. The eigenvectors describe a normalized deformation pattern for a given mode. The summation of these deformation modes describes the overall deformation pattern. For eigenvalue testing the interest is in just the stiffness matrix. In eigenvalue testing the mass matrix as seen in the normal modes equation is set equal to an identity matrix. The procedure is then identical to that of the normal modes solution.

An assumption is made that if the normal modes analysis technique is changed ever so slightly to become an eigenvalue test, that the eigenvalue test might reveal the deformation characteristics and strain energy content of the element. The eigenvalues and eigenvectors end up

being related to the strain energy of the element, and the eigenvectors are also related to the possible deformation patterns.

The eigenvector and eigenvalue for each mode makes a contribution to the overall deformation and to the amount of strain energy. In essence it is the summation of these values that determines the given deformation pattern in the element as well as its strain energy content. The equations used in eigenvalue testing are described in Section 4.2. An eigenvalue test can therefore generate quantities that physically describe the deformation modes and strain energy associated with a given element. These in turn can be used to test the nature of the element under various distortions.

The number of eigenvalues and eigenvectors extracted should equal the number of degrees of freedom at each node times the number of nodes. There are three rigid body modes and iive displacement modes for plane strain and plane stress elements. One rigid body mode and six displacement modes for axisymmetric elements. In some cases deformation modes appear in mirror images with equal eigenvalues.

Generally an eigenvalue test is used to check that an element's stiffness matrix will provide as many rigid body modes as is expected. If too few are found this suggests that the element lacks the desired capability

60

for rigid body motion without strain. Too many suggests the presence of mechanisms. These results should be independent of where or how the element is located and oriented in global coordinates. Instabilities in the stiffness matrix can also be determine by the eigenvalue test. These characteristic quantities of an eigenvalue test tend to validate the assumption that eigenvalue testing an element can detect when an element is behaving poorly due to improper deformation modes caused by distortions of the element.

A closer examination of eigenvalue testing reveals that it tests the quality of the stiffness matrix. The stiffness matrix is derived in part from the shape functions of the element. These shape functions were implemented into the formation of the element in order to properly represent the deformation and strain energy characteristics of the given object being represented by the finite element. The shape functions are related to the geometry of the element and its expected deformation patterns. If the physical geometry of the element were to be distorted, this distortion is assumed to directly change the parameters used in the shape functions. This in turn affects the stiffness matrix which affects the possible deformation patterns and strain energy content of the element. This was pointed out in Section 4.2.1. Theoretically one should see differences in the strain

61

energy values of distorted elements when compared to the values for an ideal element.

The quantitative value of geometric distortion that can be applied to an element can be determined by examination of the range of values of strain energy density ratios of distorted elements to that of ideal elements. The idea is to determine a discontinuity in the pattern of change in the strain energy density ratios over a range of changing element distortion. For example, one would examine the change in the strain energy density ratios with respect to just the change in one element distortion measure such as aspect ratio. This would be examined from an ideal value of aspect ratio to that of an extreme aspect ratio value. A discontinuity such as a difference in the rate of change of strain energy density ratio values is assumed to indicate the point where the distortions in the element cause errors in the solution which are too large to ignore. This is the basic assumption to quantify distortion measures in order to derive rezoning indicators. The values of the distortion measures, such as aspect ratio, at the point of the discontinuity are then defined to be the rezoning indicators.

4.4 Implementation of Eigenvalue Testing

The methodology previously described to derive
rezoning indicators from eigenvalue tests was
implemented. Several techniques were attempted until a
workable solution was obtained. First, a simple case was
examined, that of a one dimensional bar element being
loaded axially. The simple problem was used to
demonstrate the relationships between eigenvalue testing,
deformation patterns, and strain energy content. Next,
MSC/PAL2 a finite element program was utilized to run
some normal modes case studies of single quadrilateral
elements. Attempts were made to distort the element's
shape from the ideal shape and note any differences in
the natural frequency values and especially any
differences in the shapes of the normal modes. This
technique proved interesting but inconclusive as to the
ability to distinguish any effect of the geometrical
distortion on the element. Changes were noticeable but
the results were inconsistent and thus no conclusion
could be drawn.

Another approach was made at making the results of
an eigenvalue test determine rezoning indicators. This
time Equation (4.10) and Equation (4.11) were used. The
equations contain the eigenvectors, eigenvalues, and a
load vector, which were all used in determining the

strain energy of an element under load conditions specified by the load vector. In the equations the normalized eigenvectors and the eigenvalues, not the square of the eigenvalues, are used. One uses a ratio of an ideal element's strain energy density to that of a distorted element for comparison in the amount of change in the strain energy density due to distortions in the element. Refer to Equation (4.11). It is the differences in the components of the eigenvectors and eigenvalues of an ideal to distorted element that makes a difference in the strain energy density content. The load vector is obtained by determining the resultant forces to an applied displacement of the element. The applied displacement corresponds to the amount of deformation required to achieve a given distortion measure.

The data required to calculate the strain energy density ratios, as given in Equation (4.11), is accomplished by running the normal modes program in the ABAQUS finite element code. First order elements in ABAQUS use lump mass at the node points. Care was taken to select density values so that the mass matrix became the identity matrix and the eigenvalue problem of Equation (4.2b) becomes the equation to solve. At this point the normal modes algorithm of ABAQUS becomes identical to an eigenvalue test algorithm. ABAQUS uses

64

the subspace iteration method so all possible modes are obtained. Only unconstrained cases were run.

In order to run the eigenvalue tests in ABAQUS a material had to be chosen to be able to input the required values to compute the stiffness matrix. A standard high strength steel was chosen. Assumptions as to the material values such as the elastic modulus had to be made. For metals these values are similar for a large variety of metals and thus was not a difficult choice. Material properties are specified in Figure 7.2.

Data is gathered by restricting each eigenvalue test run to a particular geometrical distortion. Examination of just aspect ratio, just skew angle, or just taper ratio is implemented to study the effects of just one distortion parameter at a time. An idealized element model is also solved for the comparison purposes essential to Equation (4.11). Unit area elements are used throughout the process.

ABAQUS was used to perform the eigenvalue tests. The input file was formulated to obtain the eigenvalues and eigenvectors for the range of distortion measures being considered. Initially an ideal element is formulated in the model. An eigenvalue test is then performed on the unconstrained ideal element. The next step is to use applied displacements on the element in order to plastically deform the element to the desired

distortion measure. An area of unit dimensions is maintained by controlling the values of applied displacement. At this point the reaction forces are obtained and used as the load vector in Equation (4.10) or Equation (4.11). The applied displacements are then released. The element will then relax by the amount of elastic recovery. This amount of relaxation is negligible in comparison to the permanent deformation cause by plastic straining. The error in the distortion measure caused by this relaxation is negligible. At this point an eigenvalue test is performed on the unconstrained, plastically deformed element of a given distortion measure. This yields the eigenvalues and eigenvectors for the given distortion. Applied displacements are again placed upon the element to achieve the next increment in distortion value. The process repeats itself and continues for all the desired values of the distortion measure. This process is performed for each of the distortion measures considered in this investigation.

Plane strain, plane stress, and axisymmetric elements are the elements of consideration. All distortions are assumed to take place upon an ideally shaped element which has edges that are aligned with the x and y coordinate axes. An aspect ratio is determined by elongating both of the element's edges

running in the x direction by equal amounts while the other two edges vary equally in the y direction to maintain an area of unit dimension yet arrive at the desired aspect ratio. Aspect ratios of 1, 2, 4, 6, 8, 10, 12, 14, 16, 18, 20, 22.5, 25, 30, 35, and 40 to 1 are used.

This method of achieving the aspect ratios maintains a rectangular shaped element throughout the entire range of aspect ratio values. This focuses the study of distortion effects to just the aspect ratio distortion measure. No taper ratio or skew angle effects are included.

To achieve the range of taper ratios, the upper element edge is consecutively reduced in length while the lower element edge is proportionally increased in length. This change is symmetric about a vertical axis. An area of unit dimension is held for each value of taper ratio. The element's vertical height to the length of its lower edge is maintained to be equal distances. Taper ratios of 1.0, 0.9, 0.8, 0.7, 0.6, 0.5, 0.4, 0.3, 0.2, and 0.1 are used.

The method of achieving the taper ratio is certainly not a totally inclusive way to achieve these values. Taper ratio maintains ties to skew angle and aspect ratio. The method used was chosen as one of the best ways to achieve a given taper ratio and yet reduce the

effects of skew angle and aspect ratio. Like aspect ratio the idea is to isolate the effect of taper ratio to be able to quantify its affect alone.

For skew angle the interior angle of two opposite element corners were equally reduced for each run while the other two opposing element corner angles were equally increased. Each edge length changed in equal proportion to achieve an area of unit dimension for any prescribed skew angle value. The element for each skew angle is held symmetric about a forty-five degree angle in the x-y coordinate plane. Skew angles of 90, 80, 70, 60, 50, 40, 30, 20, and 10 degrees are used.

Just like the taper ratio the manner in which the skew angle is achieve is not all encompassing. It does however, generate results which are typical of skew angles no matter how the skew angle is determined. Several different approaches were examined and the results tend to indicate that the manner in which the skew angle was achieved is representative of the majority of possible cases.

The manner in which the distortion measures of aspect ratio, taper ratio, and skew angle are achieved and examined, .s stated previously, are not totally encompassing. For example, combinations of two or more geometrical distortions is not considered. The effect of when the distortions do not occur in a symmetric pattern

68

about the element is also not considered. It is assumed that the manner used to determine values of the distortion measures in this investigation, is representative enough of the combined and nonsymmetric distortions cases to be able to account for such effects. The assumption is that the combined cases or nonsymmetric cases can be thought of as linear combinations of the type derived in this investigation. For example, if a distorted element exhibits combined distortions, each distortion is examined separately and its effect on the element is considered separately.

The data gathered from the eigenvalue test is manipulated and put in the form of Equation (4.10) and Equation (4.11). The values for the ratio of distorted elements strain energy density to that of an ideal element versus the distortion criteria were gathered over the ranges previously stated. Various curve fitting programs were examined. A least squares polynomial fit, a cubic spline fit, a linear fit, and a Lagrange polynomial fit were tried. Along with the fit, derivatives and the sensitivity of the curves were also determined. The derivatives and sensitivity of the values help indicate the discontinuities and therefore determine the rezoning indicators. The sensitivity plot is also used to examine how sensitive the strain energy density ratio, Equation (4.11), is to a change in a given

69

distortion measure.

A cubic spline curve fit was chosen since it most closely matches the data while maintaining continuous derivatives across each of the data points. This is important when one is trying to select the rezoning indicators based on a possible discontinuity in the curve or surface. If discontinuities arise due to the nature of the curve or surface fit used, then the determination of the rezoning indicators could be inconclusive.

4.5 Rezoning Indicator Results from Eigenvalue Tests

The rezoning indicators derived from the results of eigenvalue tests are summarized in tabular form in Table 4.1. These values were chosen based upon different types of plots that were developed to evaluate the strain energy density ratio versus a given range of the various distortion measures. A value was determined for each type of distortion measure for each type of element that was studied. It is interesting to note that the values for all three element types, axisymmetric, plane strain, and plane stress are very close in value. This implies that the general similarties exist since all the element are quadrilateral elements. Slight differences might be due to the difference in assumptions used in forming the element such as an axis of symmetry condition.

70

Table 4.1. Rezoning indicators

ASPECT RATIO REZONING INDICATORS

ELEMENT TYPE	VALUE
Plane Strain	18.59
Plane Stress	16.80
Axisymmetric	18.38

TAPER RATIO REZONING INDICATORS

ELEMENT TYPE	VALUE
Plane Strain	0.58
Plane Stress	0.63
Axisymmetric	0.55

SKEW ANGLE REZONING INDICATORS

ELEMENT TYPE	MIN VALUE	MAX VALUE
Plane Strain	43	137
Plane Stress	52	128
Axisymmetric	50	130

It is interesting to note that for most cases the element distortion values are within an acceptable range of the values stated in literature which were determined in essence by pure experience [20, 27-31]. The rezoning indicators were derived by examination of four plots of the results obtained through eigenvalue testing.

A three dimensional plot is generated which examines the relationship between the range of a given distortion measure, the derived strain energy density ratio values, and the load vectors obtained for each applied

71

displacement representative of a given distortion measure. In this plot the third dimension was added to gain insight into how a different load vector might effect the results of Equation (4.11). This surface plot illustrates the full impact of Equation (4.11). Figures for these three dimensional plots are found in Section 4.5.1 through Section 4.5.3.

The second type of plot is a two dimensional plot. This is a plot of strain energy density ratio versus a range of values of a given distortion measure. In essence this is a plot which is equivalent to the diagonal of the three dimensional surface plot. In this case only one load vector was used for a given distortion measure. The load vector used corresponds to the resultant loads obtained by the applied displacements which plastically deformed the element to the shape of the desired distortion measure. Figures for these two dimensional plots are found in Section 4.5.1 through Section 4.5.3.

The third type of plot is the derivative of the strain energy density ratio versus the given distortion measure. This is a plot of the derivative of the second plot. Since interest lies in finding discontinuities in the results of the eigenvalue tests, then a plot of the derivative of these result will more drastically illustrate the point at which this discontinuity occurs.

72

This helps to quantify the rezoning indicator value. Figures for the derivative plots are found in Section 4.5.1 through Section 4.5.3.

The fourth type of plot used is that of the sensitivity of the strain energy density ratio versus a given distortion measure. This plot is closely related to the derivative plot except that the sensitivity equation contains added terms to that of just the derivative. The equation for the sensitivity of the strain energy density ratio to a change in the aspect ratio is given by

$$S_{AR}^{\overline{U}} = \frac{AR}{\overline{U}} \frac{d\overline{U}}{dAR} \tag{4.16a}$$

where AR represents aspect ratio as a variable. The sensitivity for taper ratio is given by

$$S_{TR}^{\overline{U}} = \frac{TR}{\overline{U}} \frac{d\overline{U}}{dTR} \tag{4.16b}$$

where TR represents taper ratio as a variable. The sensitivity for the skew angle is given by

$$S_{SK}^{\overline{U}} = \frac{SK}{\overline{U}} \frac{d\overline{U}}{dSK} \tag{4.16c}$$

73

where SK represents skew angle as a variable.

The sensitivity plot is another technique used to quantify a given rezoning indicators value. This type of plot illustrates the relative sensitivity of a quantity to any degree of change. The more the amount of change the more dramatic this is illustrated in a sensitivity plot. The plots can therefore tune in on discontinuities. Any discontinuity in the plot of strain energy density ratio versus a given distortion measure will show up as a dramatic change in the nature of the sensitivity plot. Figures for the sensitivity plots are shown in Section 4.5.1 through Section 4.5.3.

Each of these four plots aid the others in attempting to determine where the discontinuities occur, and hence the value of the rezoning indicator. In some cases, but not all, at least two or more of these plots needed to be correlated in order to quantify the rezoning indicator values. When all four plot correlate to the same point of a given distortion measure as the rezoning indicator, one can assume with confidence that it is the appropriate rezoning indicator value.

4.5.1 Results for Aspect Ratio

Three dimensional plots shown in Figure 4.1 through Figure 4.3 were develop from resulting eigenvalue tests on axisymmetric, plane strain and plane stress elements.

74
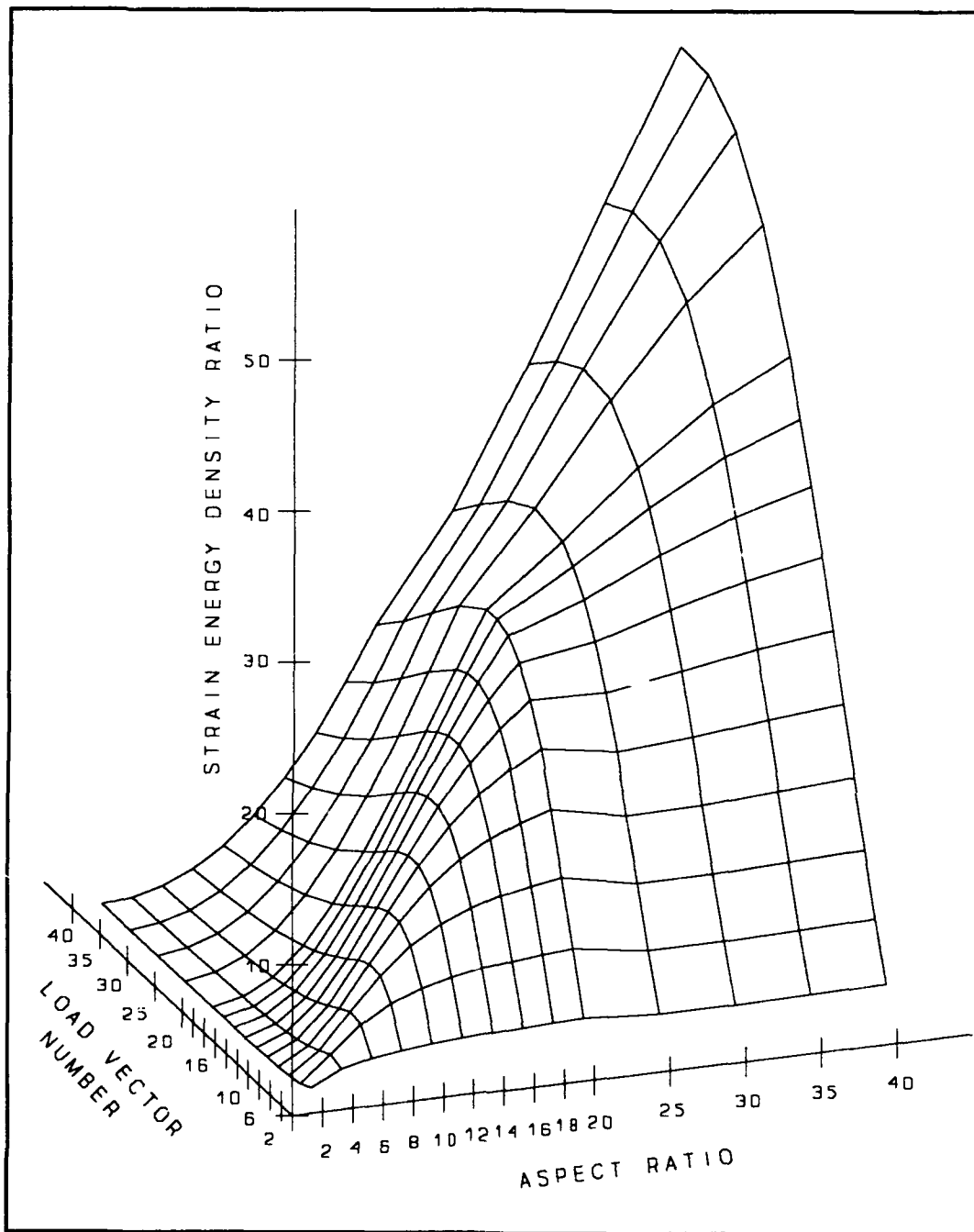
Figure 4.1. Three dimensional plot of strain energy density ratio varied over aspect ratio and load vector values for an axisymmetric element

75
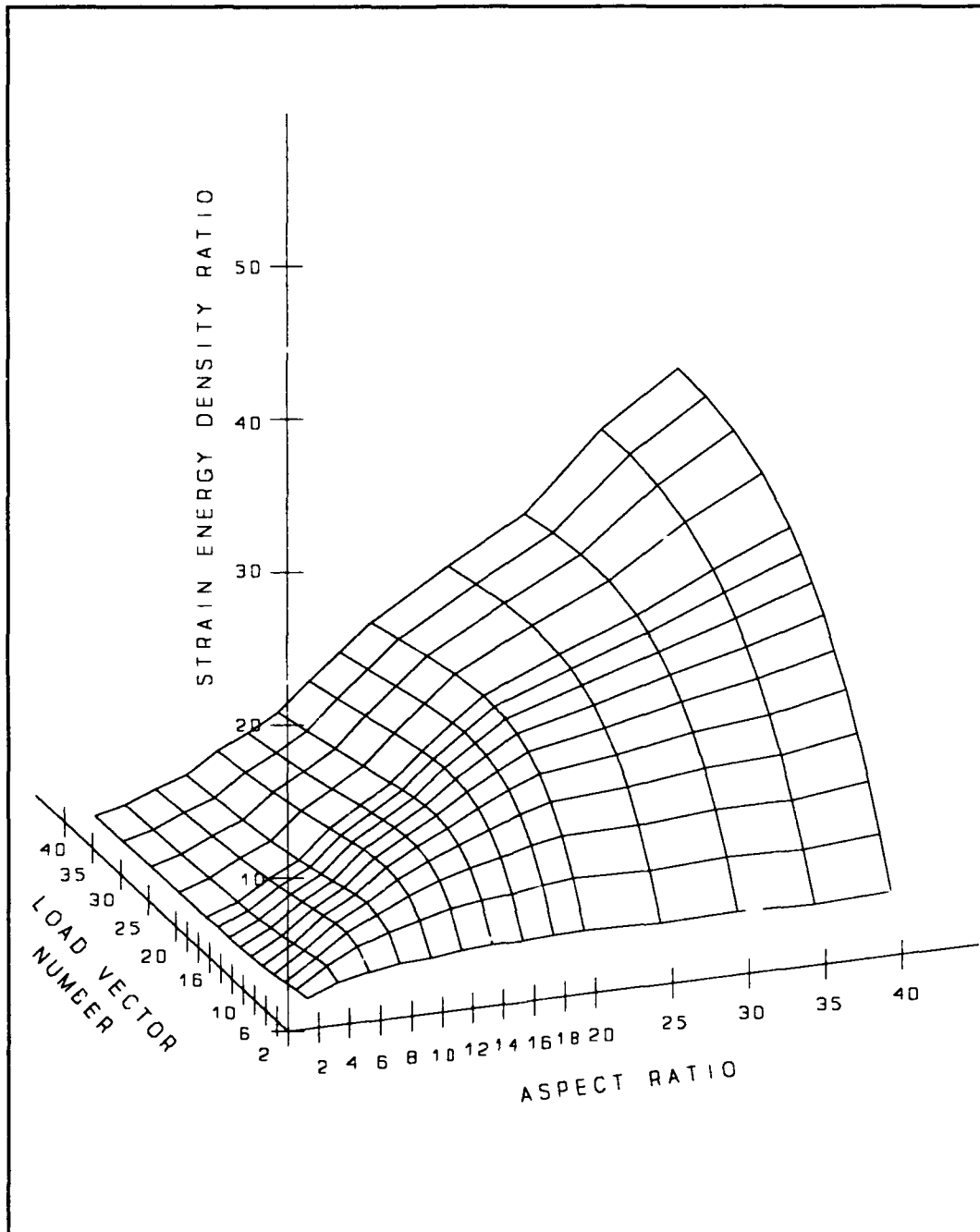
Figure 4.2. Three dimensional plot of strain energy
density ratio varied over aspect ratio and load vector
values for a plane strain element
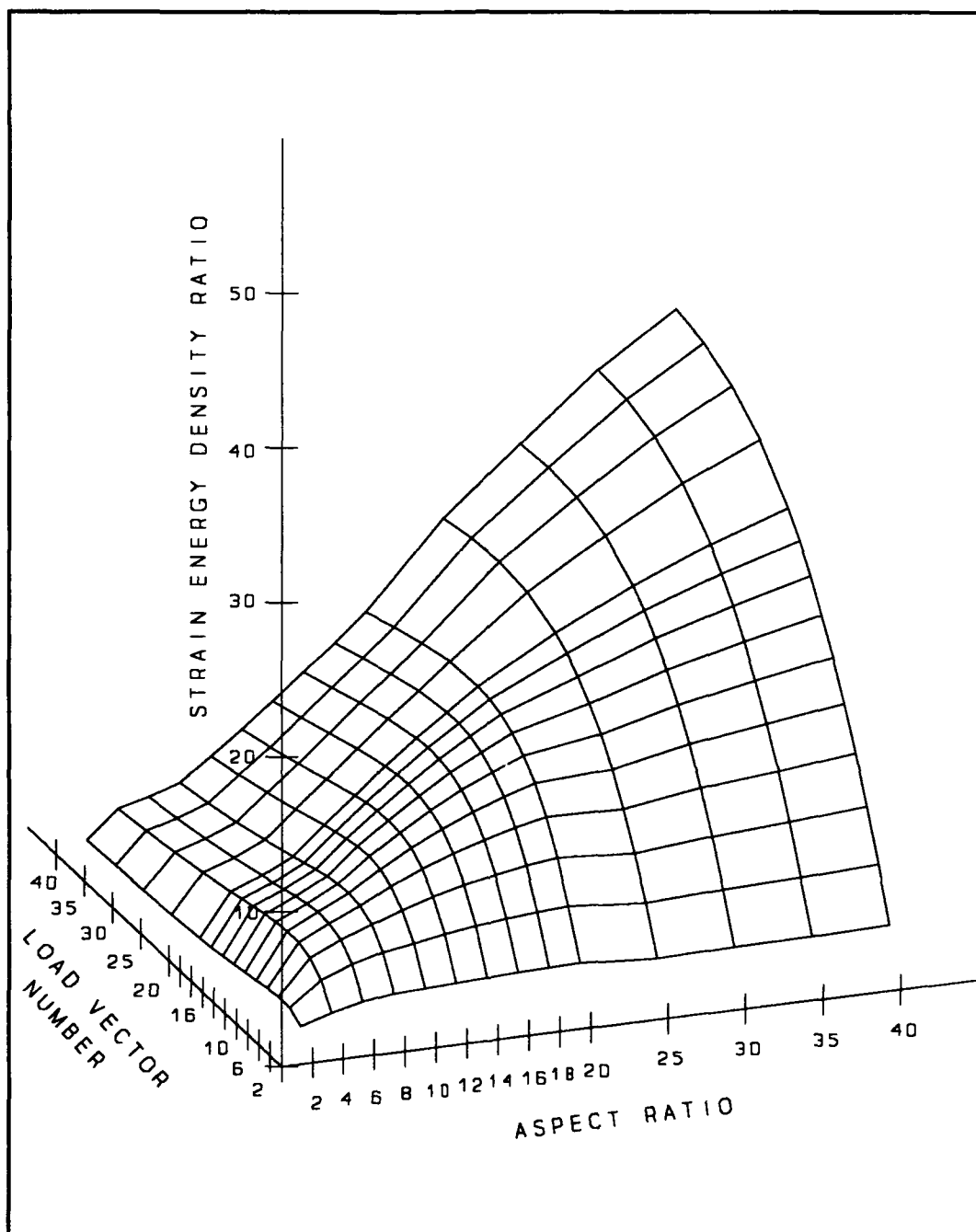
Figure 4.3. Three dimensional plot of strain energy
density ratio varied over aspect ratio and load vector
values for a plane stress element

In each of these three dimensional surface plots one can see the effects on strain energy density ratio due to changes not only in the aspect ratio but also in the load vector. The effects are most dramatic in Figure 4.1 for the axisymmetric case. In this case a discontinuity in the surface appears as a hump or bump around an aspect ratio of twenty. For this plot it is not certain exactly where it does occur but somewhere near a value of twenty. This discontinuity also tends to occur near the load vector value which corresponds to the load vector formed from the resultant load of an applied displacement to arrive at or near a aspect ratio of twenty. This discontinuity is less dramatic for the case of plane strain. Upon close inspection, however, it also appears to contain the same type of discontinuity in the same region. The plane stress case is the least dramatic of all three plots. The only discontinuities that appear seem to be away from those aspect ratios which would be the logical choices. No conclusion can be drawn on the plane stress plot.

The two dimensional plots of strain energy density ratio versus aspect ratio are equivalent to the three dimensional plots except only one load vector corresponds to a given aspect ratio. The two dimensional plots for each element type are shown in Figure 4.4 through Figure 4.6.
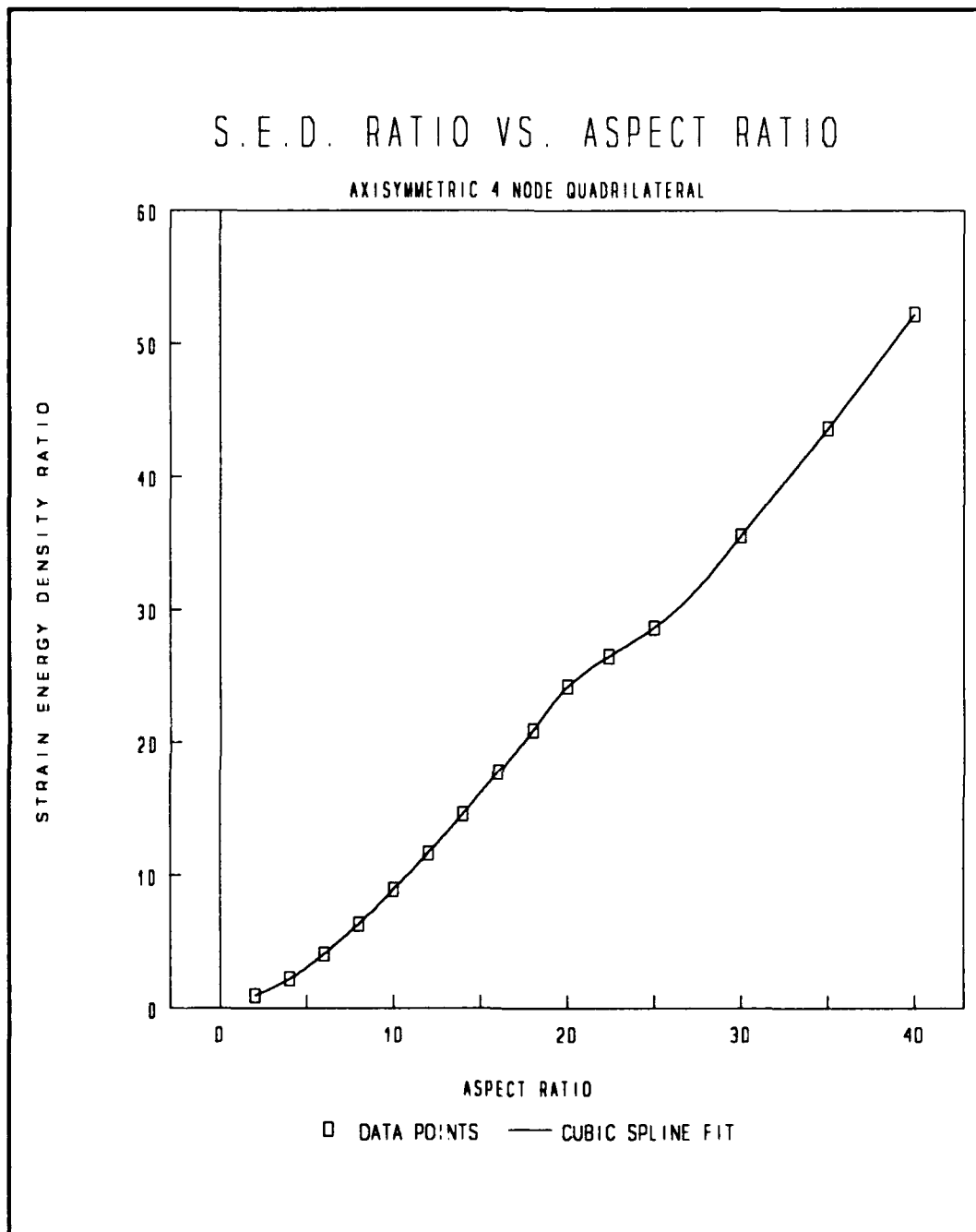
Figure 4.4. Strain energy density ratio versus aspect ratio for an axisymmetric element
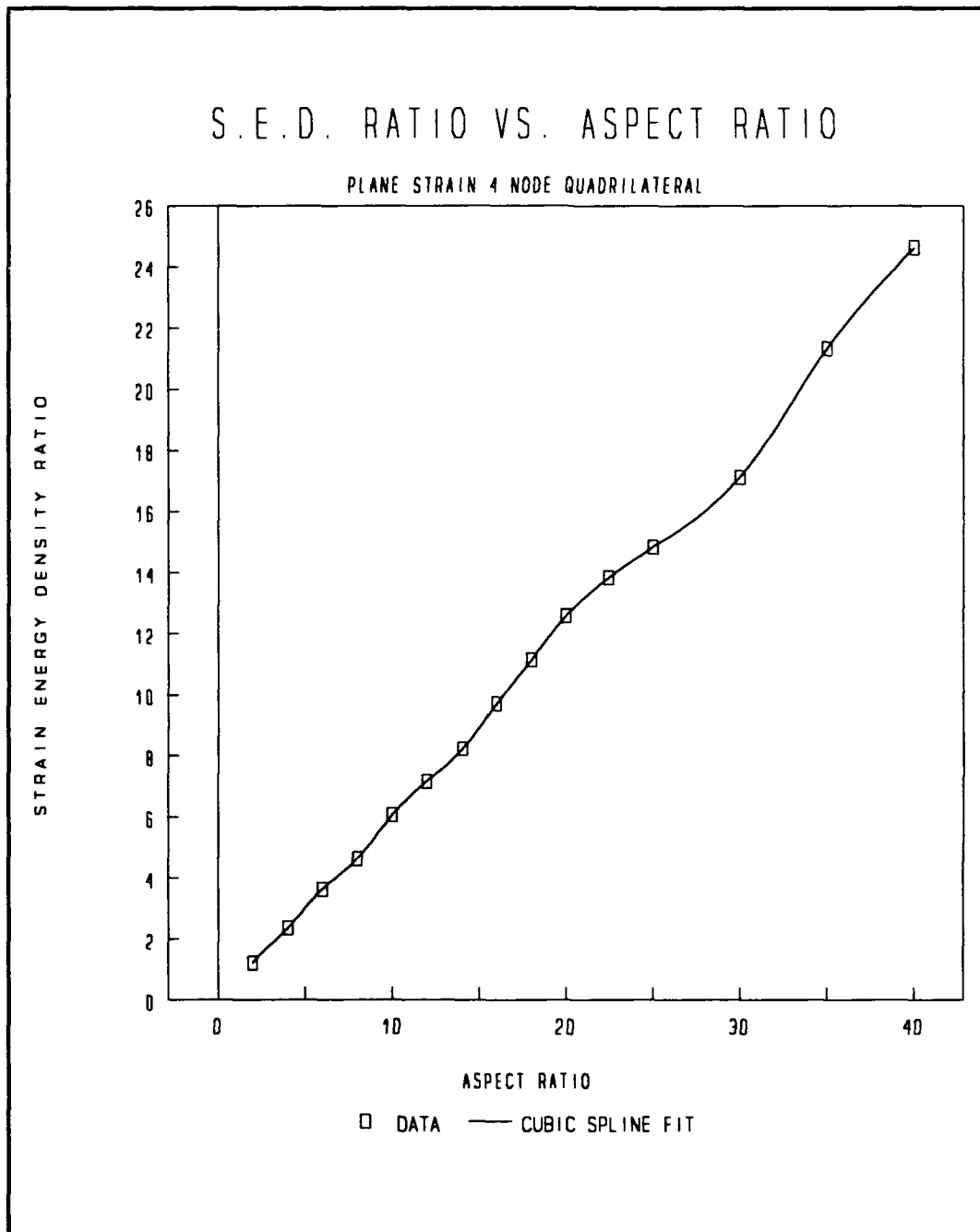
Figure 4.5.   Strain energy density ratio versus aspect ratio for a plane strain element

80
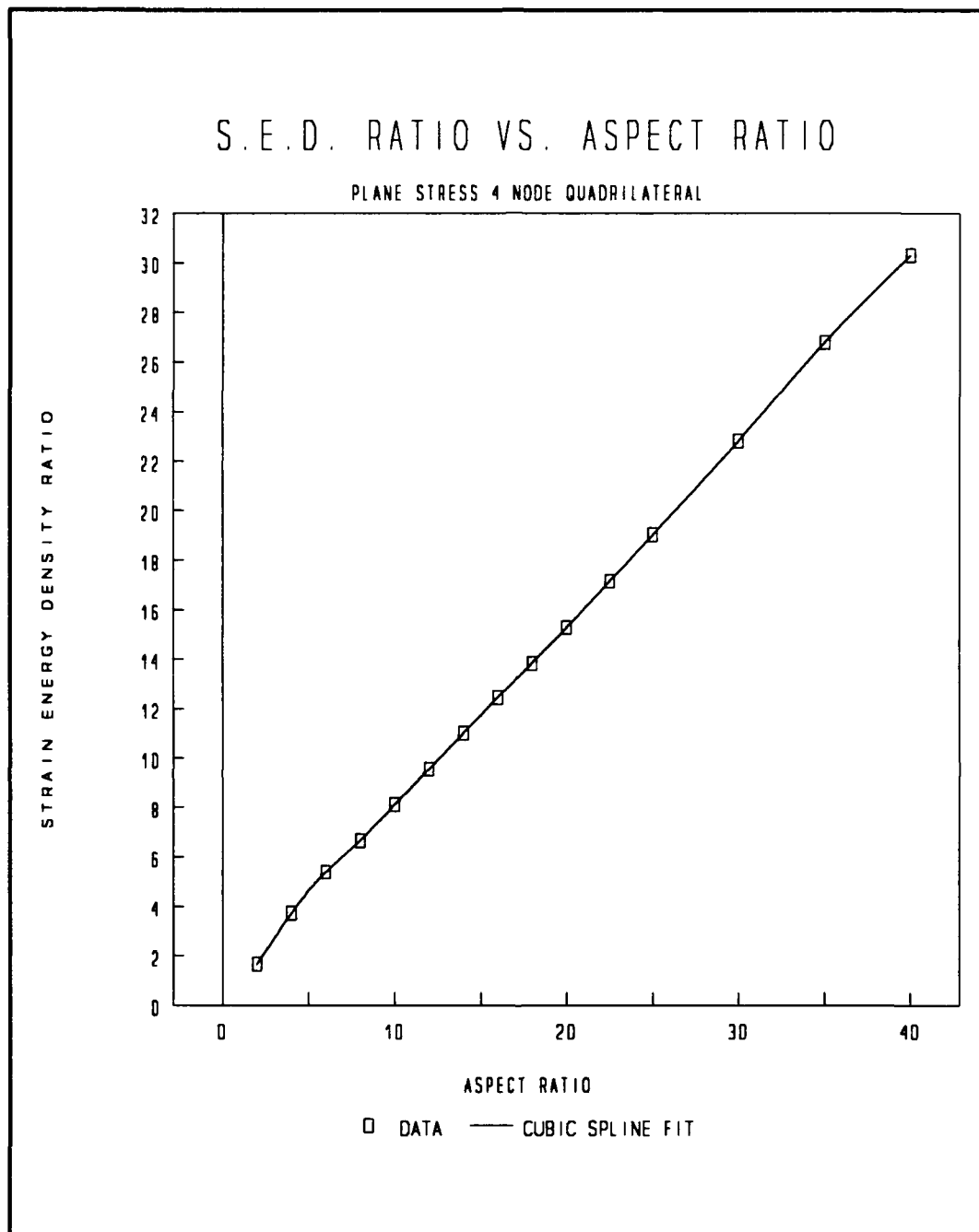
Figure 4.6.   Strain energy density ratio versus aspect ratio for a plane stress element

These two dimensional plots seem to correlate with the corresponding three dimensional plots in indicating the point at which a discontinuity appears in the plot. In Figure 4.4 for the axisymmetric case the slope seems to alter its direction or the radius of curvature changes its direction at about the point of an aspect ratio of twenty. This corresponds directly with the three dimensional surface plot of Figure 4.1. The same effect and correlation is noticed for Figure 4.5, the plane strain case. Here again the effect is less dramatic. In Figure 4.6 the plane stress case no discontinuities seem to be present. This is the same conclusion drawn from the Figure 4.3.

In the plots of the derivative of strain energy density ratio with respect to aspect ratio versus aspect ratio, the derivative of the curve was obtained through the cubic spline fit of the data points. For cubic spline fits, the derivative of the curve is continuous from one point to the next. More important is that it is also continuous at the point itself. This creates a smooth curve throughout and the derivatives obtained are reliable and do not induce discontinuities in the curve. These derivatives are used to help amplify and quantify possible discontinuities. The derivative plots for axisymmetric, plane strain, and plane stress elements are shown in Figure 4.7 through Figure 4.9 respectively.
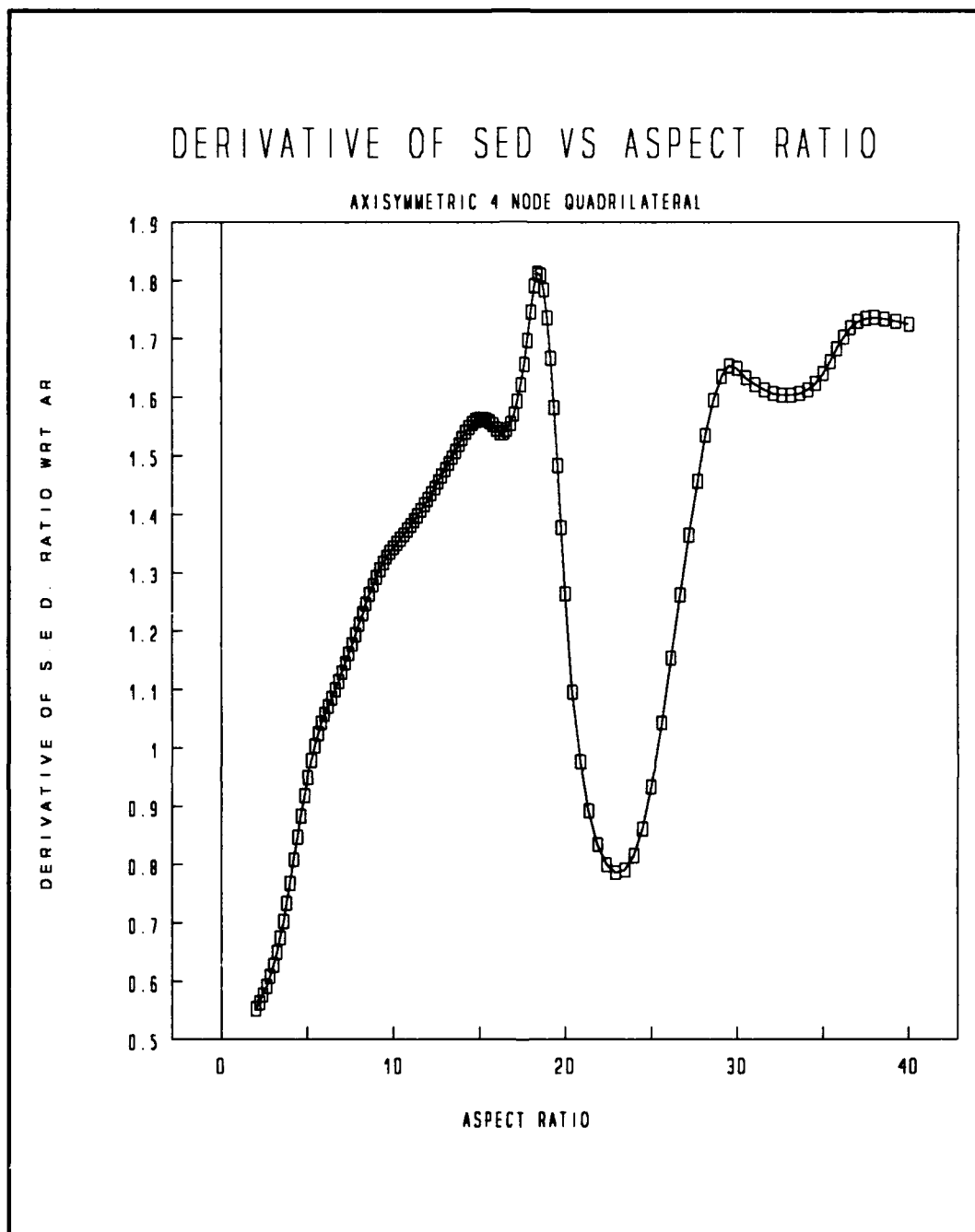
Figure 4.7. Derivative of strain energy density ratio with respect to aspect ratio versus aspect ratio for an axisymmetric element
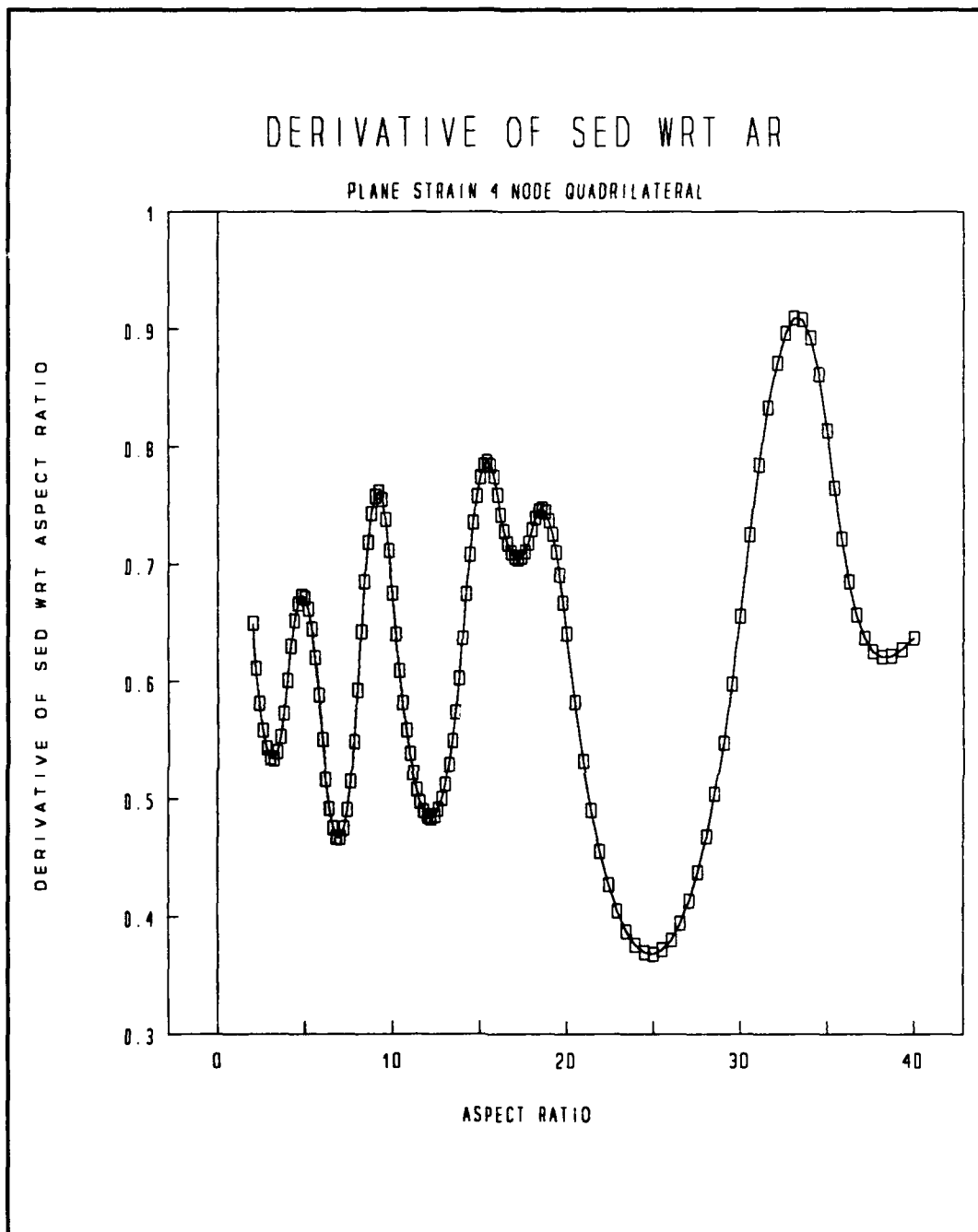
Figure 4.8. Derivative of strain energy density ratio with respect to aspect ratio versus aspect ratio for a plane strain element

DERIVATIVE OF SED WRT ASPECT RATIO

PLANE STRESS 4 NODE QUADRILATERAL
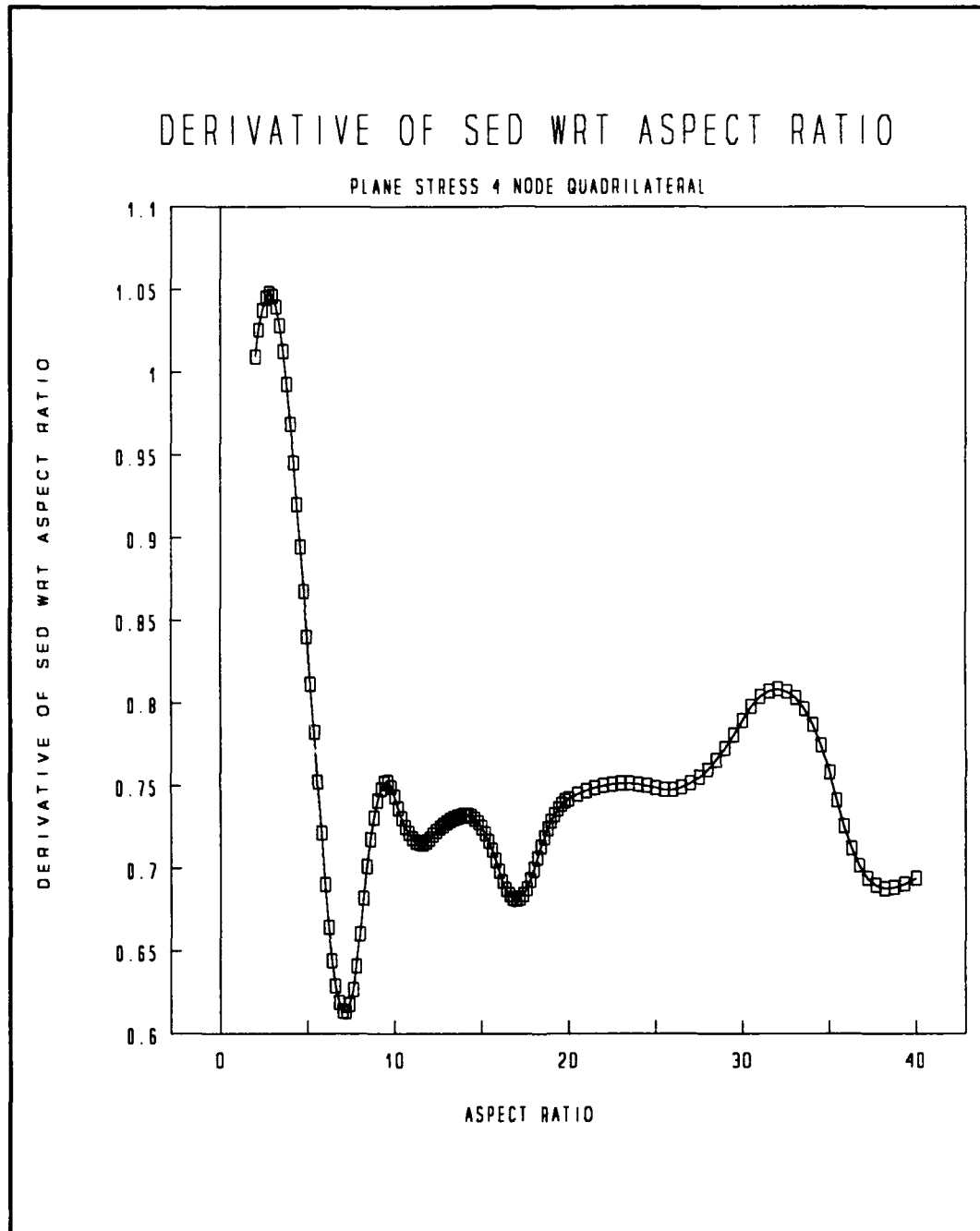
Figure 4.9. Derivative of strain energy density ratio with respect to aspect ratio versus aspect ratio for a plane stress element

85

These derivative plots clearly indicate the point of
the discontinuities seen in the three and two dimensional
plots. In Figure 4.7, the axisymmetric case, a dramatic
change in the derivative plot occurs at a peak value with
an aspect ratio value of 18.38. More interesting is the
fact that below this point the curve seems to oscillate
with small amplitudes and higher frequencies than the
portion of the plot above an aspect ratio of 18.38. This
point at which the change in amplitude and frequency
occurs corresponds to the point where the discontinuity
occurs in the two and three dimensional plots, Figure 4.1
and Figure 4.4 respectively. The exact same conclusions
can be drawn for Figure 4.8 the plane strain case. In
this case however, the peak value does not occur but the
same oscillation pattern does. The point of change in
the amplitude and frequency of the oscillations occurs at
an aspect ratio of 18.59. In Figure 4.9 the plane stress
case, there is finally some indication of where a
discontinuity or change in the effect due to aspect ratio
might occur. In this case the point at which the
oscillations change amplitude and frequency occurs at an
aspect ratio of 16.80. There may be some indication that
this value may extend up to an aspect ratio of 20.0,
however to be conservative a value of 16.80 is chosen.

Sensitivity plots are shown in Figure 4.10 through
Figure 4.12 for each element type.

SENSITIVITY OF SED VS ASPECT RATIO

AXISYMMETRIC 4 NODE QUADRILATERAL
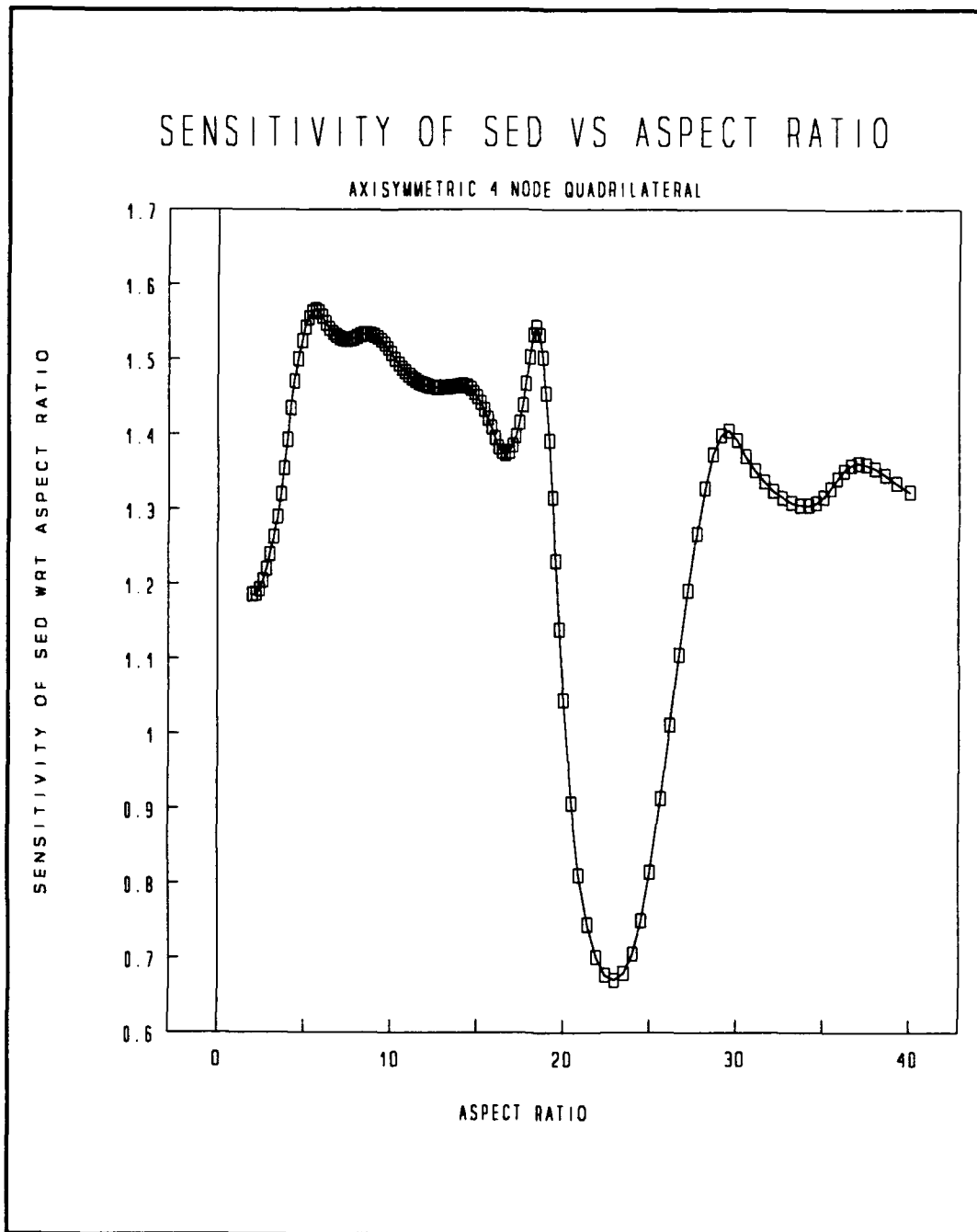
Figure 4.10.   Sensitivity of strain energy density ratio with respect to aspect ratio versus aspect ratio for an axisymmetric element

87

Figure 4.11. Sensitivity of strain energy density ratio with respect to aspect ratio versus aspect ratio for a plane strain element

88

Figure 4.12.   Sensitivity of strain energy density ratio with respect to aspect ratio versus aspect ratio for a plane stress element

These sensitivity plots tend to correlate exactly with the derivative plots, thus no further explanation is required. The fact that all four plots for each element type tend to point to the same rezoning indicator value adds further confidence to the choice of an aspect ratio rezoning indicator. A conclusion can be drawn that the aspect rezoning indicator values for the axisymmetric case is 18.83, for the plane strain case is 18.59, and for the plane stress case is 16.80.

4.5.2 Results for Taper Ratio

The results of eigenvalue testing an element's stiffness matrix that are implemented into Equation (4.11) for a range of taper ratios of can be illustrated in a three dimensional surface plot. This plot has the same form and was developed in a similar manner to the three dimensional plots of Section 4.5.1. It should be noted in this set of three dimensional plots that values of taper ratio along the taper ratio axis are worse nearer the origin of the plot than further away from the origin. The same idea applies to the load vector axis where the load vectors that correspond to worse taper ratios are closer to the origin of the three dimensional plot. Three dimensional plots shown in Figure 4.13 through Figure 4.15 were developed from resulting eigenvalue tests on the three element types.

90
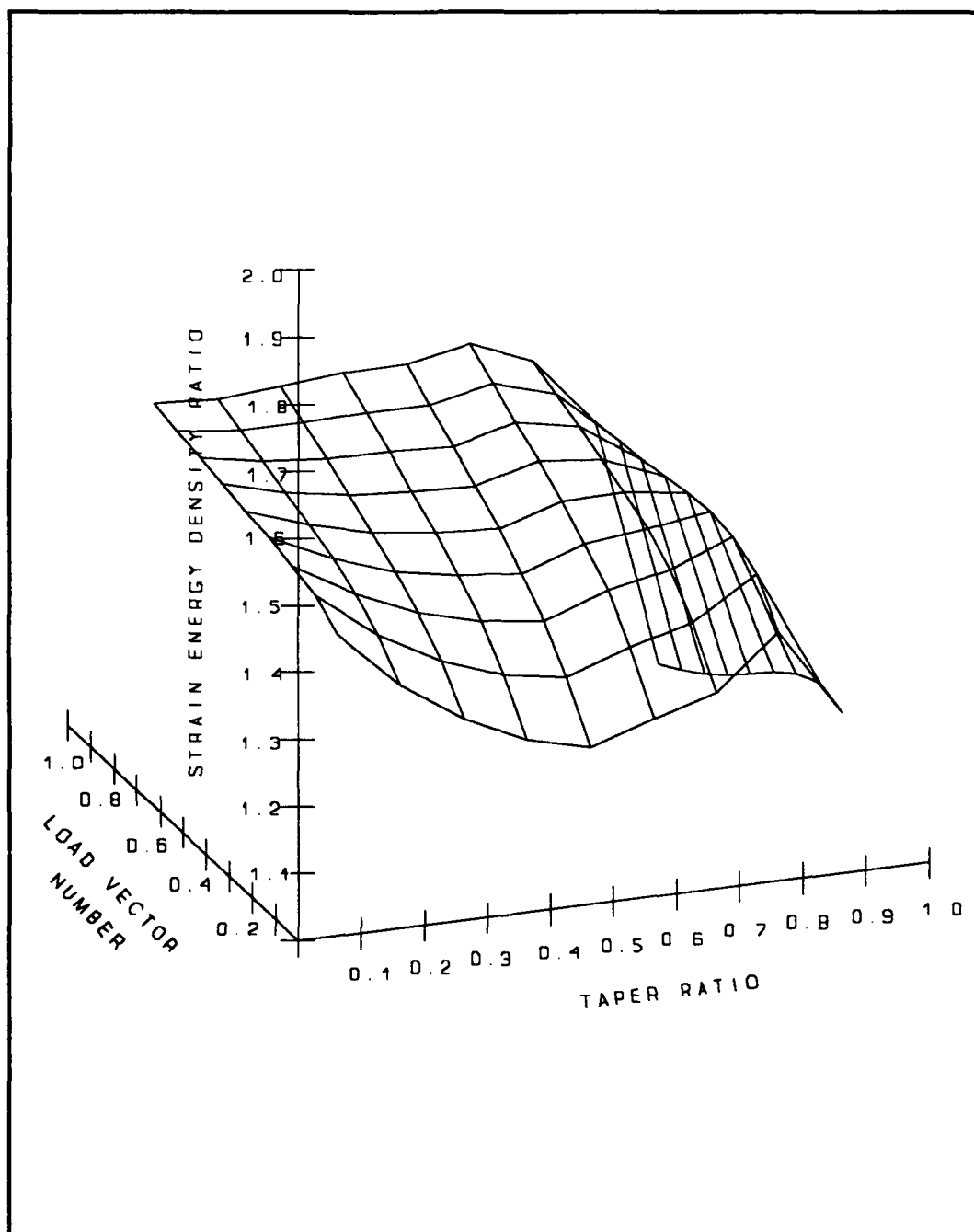
Figure 4.13. Three dimensional plot of strain energy
density ratio varied over taper ratio and load vector
values for an axisymmetric element
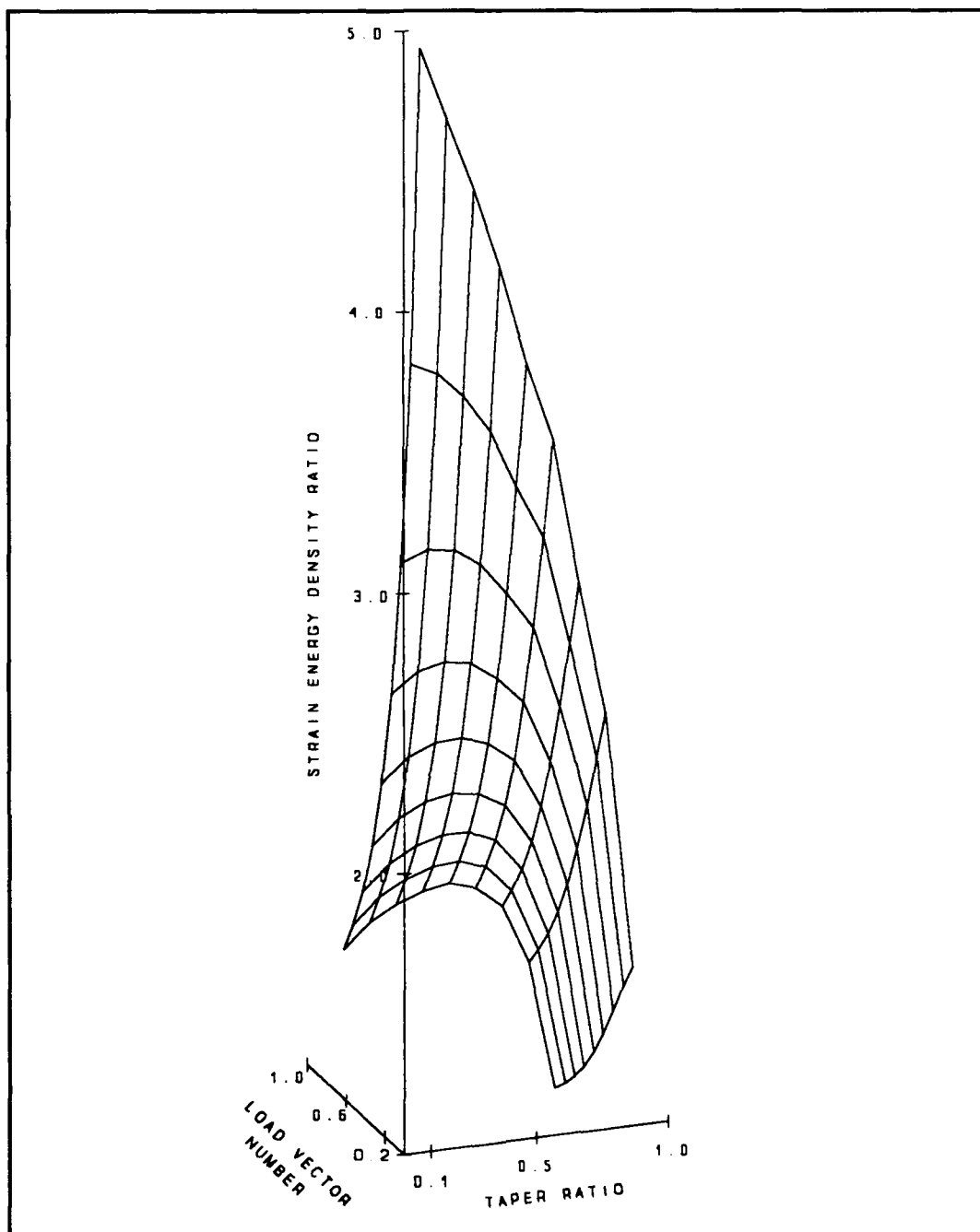
Figure 4.14. Three dimensional plot of strain energy density ratio varied over taper ratio and load vector values for a plane strain element
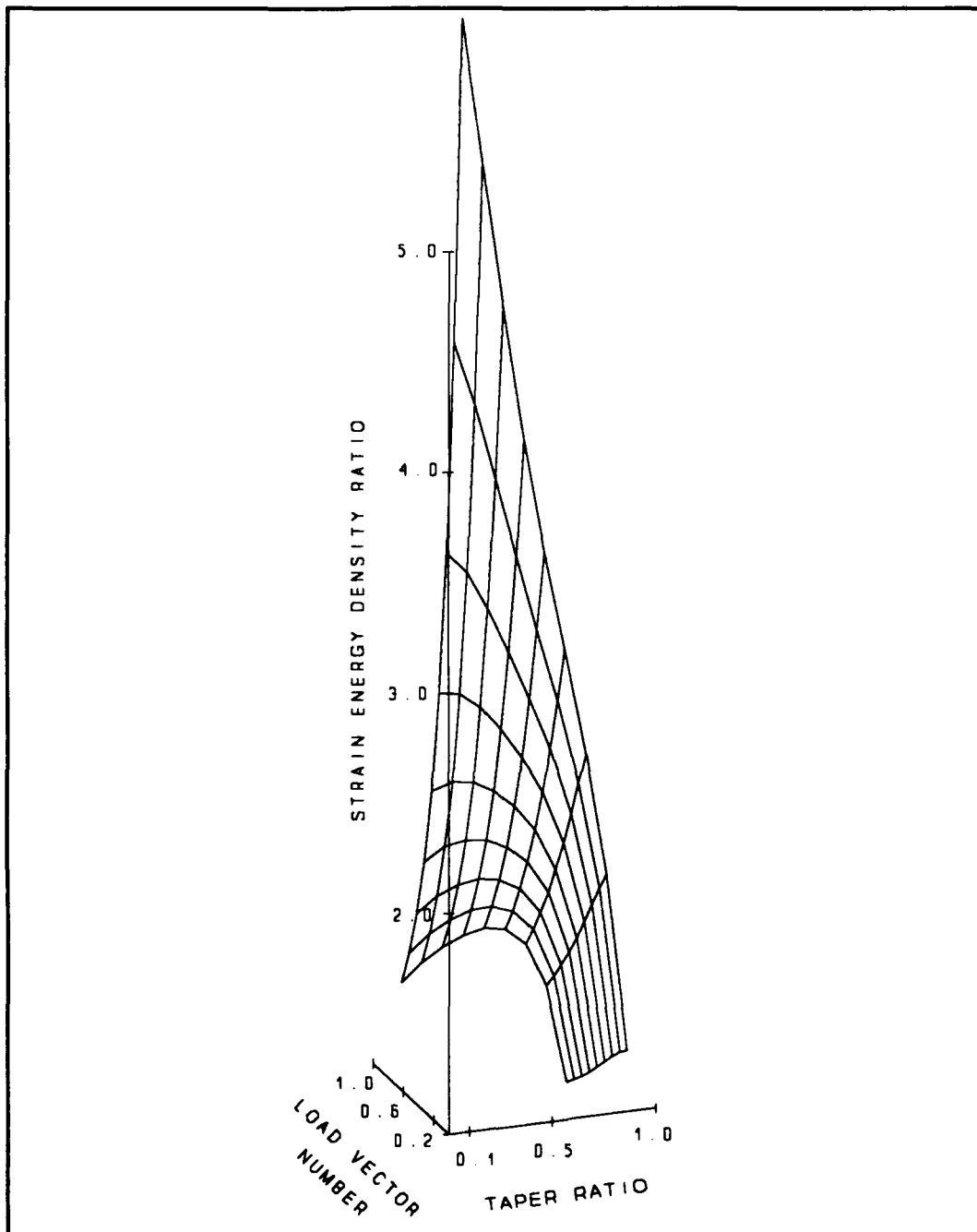
Figure 4.15.   Three dimensional plot of strain energy
density ratio varied over taper ratio and load vector
values for a plane stress element

In each of these three dimensional surface plots one can see the effects on strain energy density ratio due to changes not only in the taper ratio but also in the load vector. The plot in Figure 4.13 for the axisymmetric case, however, appears quite different from Figure 4.14 and Figure 4.15, the plane strain and plane stress cases respectively. The only logical explanation for this difference is that Equation (4.11) generates different results for taper ratio on axisymmetric elements. It is assumed that the axisymmetric case behaves differently due to the symmetric nature of the element and its implied restriction with respect to the axis of symmetry.

In the axisymmetric case, Figure 4.13, a discontinuity or change in the surface appears as a valley in the direction of the load vector axis around a taper ratio of 0.5. The plots for the plane strain and plane stress cases appear similar to each other, Figure 4.14 and Figure 4.15. A dramatic change in these plots is seen near a taper ratio value of 0.5 near the origin in the load vector direction. This value is slightly higher for the plane stress case, but both maximum points occur closer to the origin along the load vector axis.

Figure 4.16 through Figure 4.18 are two dimensional plots of strain energy density ratio versus taper ratio for axisymmetric, plane strain, and plane stress elements respectively.

94
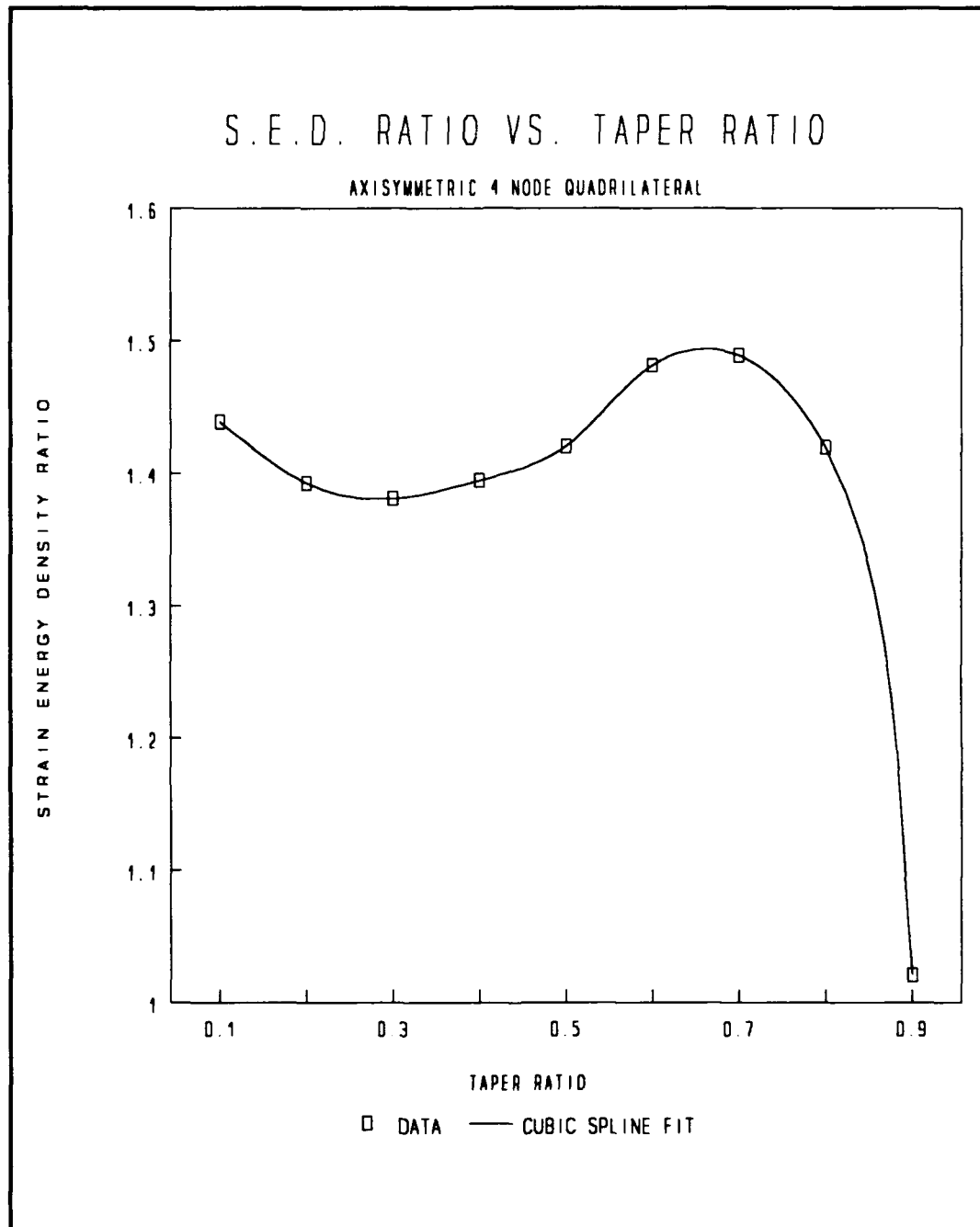
Figure 4.16.   Strain energy density ratio versus taper ratio for an axisymmetric element
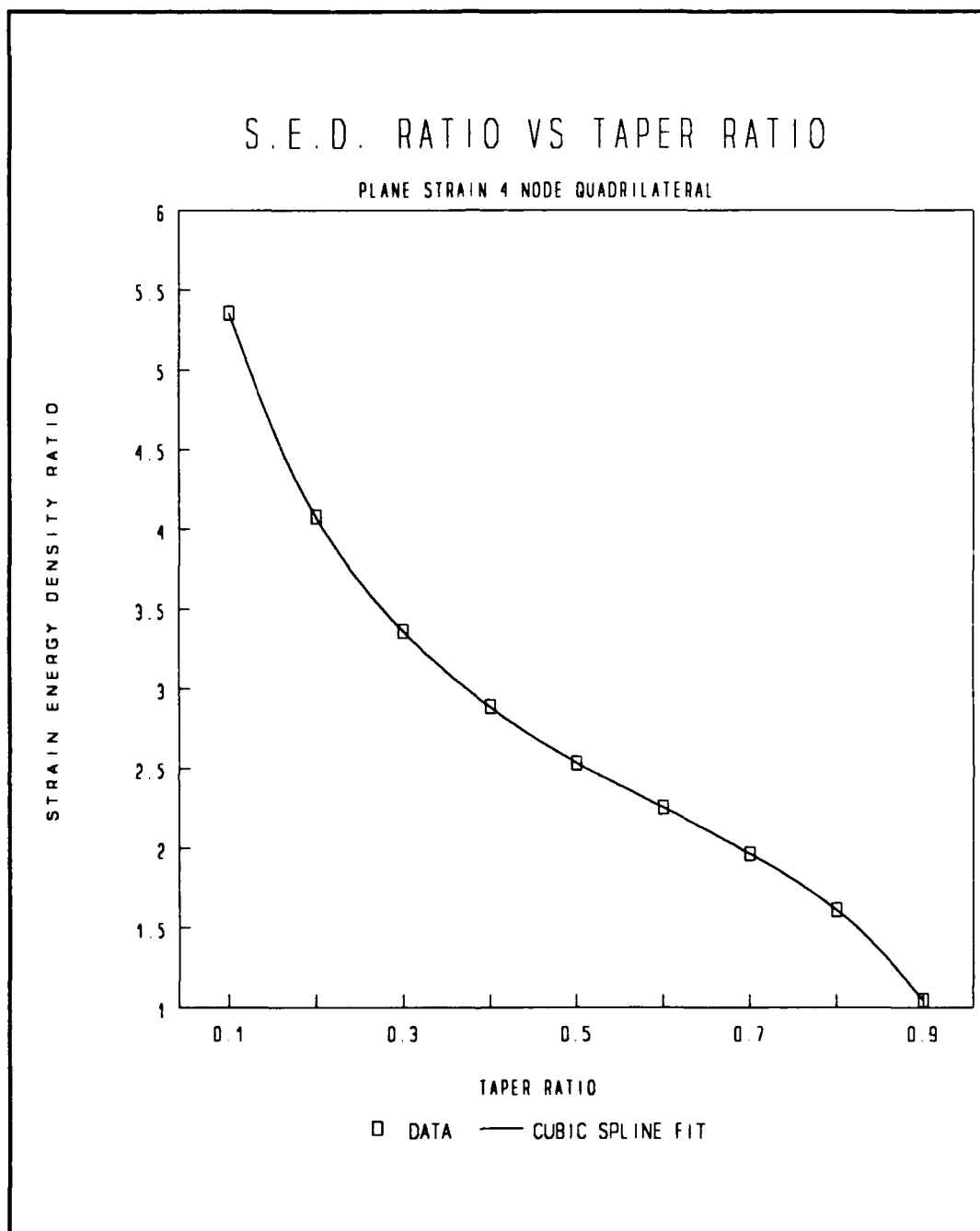
Figure 4.17. Strain energy density ratio versus taper ratio for a plane strain element

96
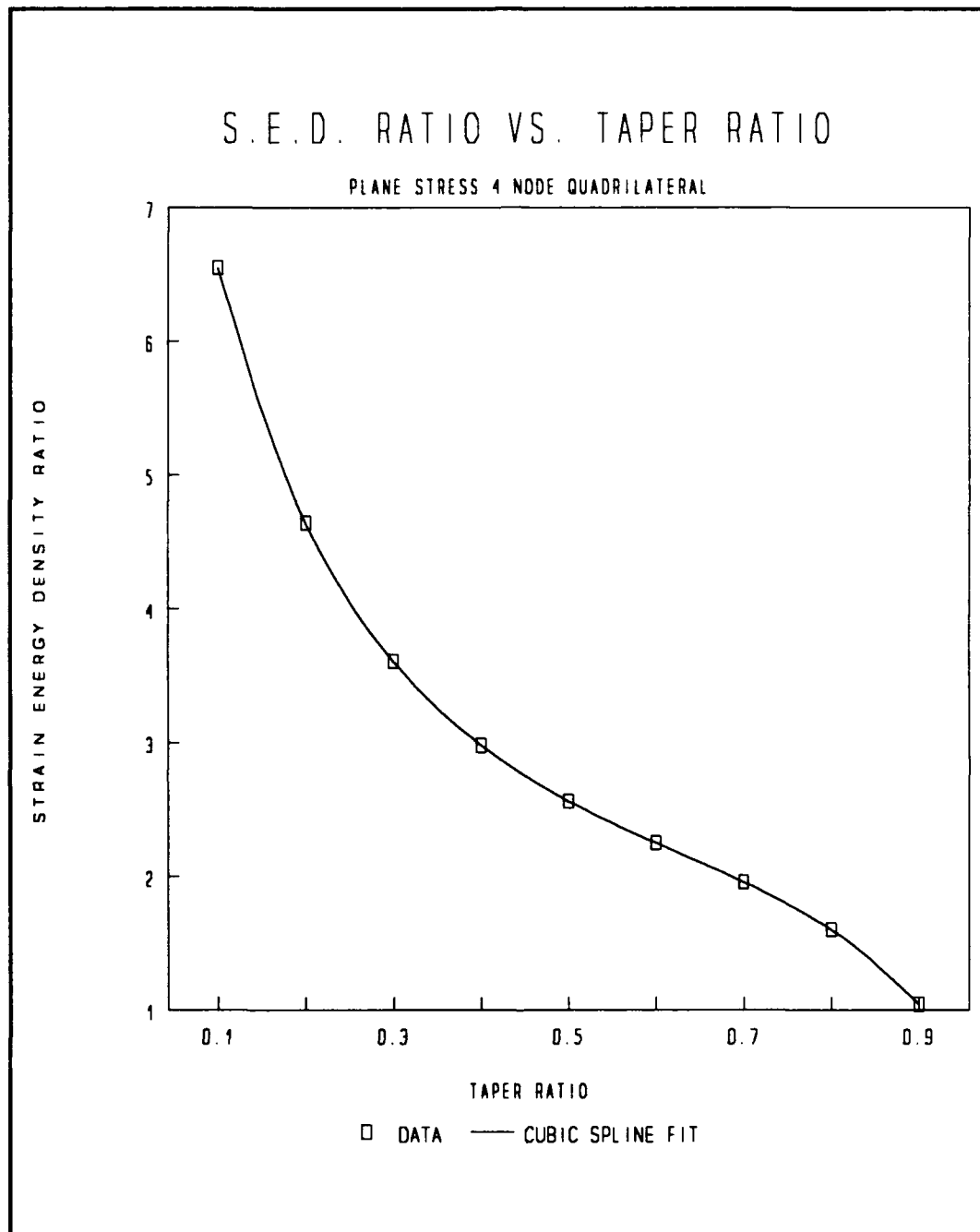
Figure 4.18.   Strain energy density ratio versus taper ratio for a plane stress element

These two dimensional plots seem to correlate with the corresponding three dimensional plots in indicating the point at which a discontinuity or dramatic change appears in the plot. In Figure 4.16 for the axisymmetric case, the curve seems to alter the direction of its radius of curvature at about the point of a taper ratio of 0.55. This corresponds directly with the location of the valley in the three dimensional surface plot, Figure 4.13. The same effect and correlation is noticed for Figure 4.17, the plane strain case. In this case the change in the radius of curvature or inflection point is noticed to occur at about a taper ratio of 0.55. This curve appears different than the axisymmetric case which is in agreement the differences in the axisymmetric case due to the axis of symmetry. In Figure 4.18 the plane stress case the same effect and correlation of the plane strain case is found. The change in direction of the radius of curvature or the inflection point of the curve seems to be at a taper ratio slightly higher than 0.6.

In the plots of the derivative of strain energy density ratio with respect to taper ratio versus taper ratio, the discontinuities are amplified in order to specify their value. The derivative plots are shown in Figure 4.19 through Figure 4.21. These plots are for axisymmetric, plane strain, and plane stress elements respectively.
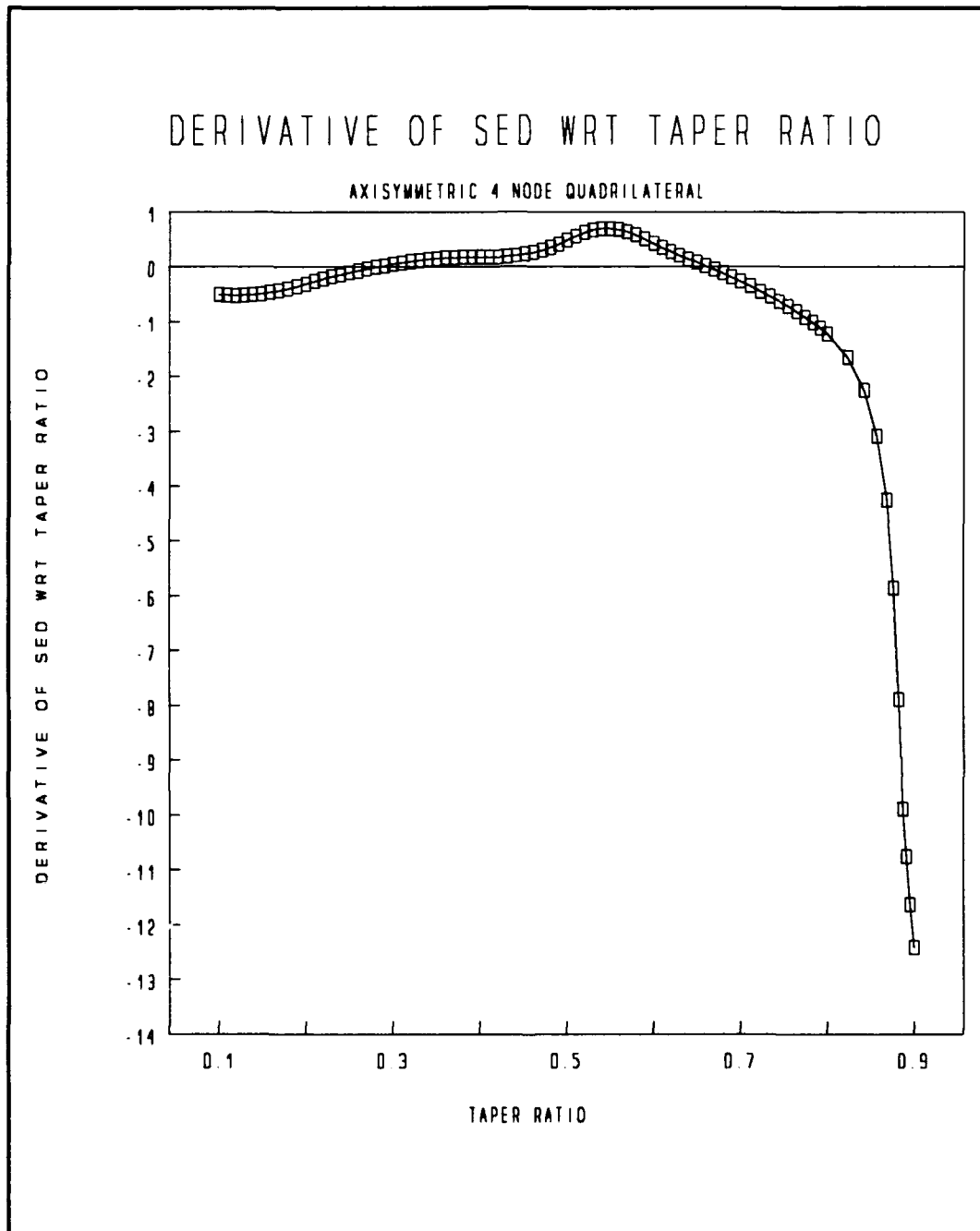
Figure 4.19. Derivative of strain energy density ratio with respect to taper ratio versus taper ratio for an axisymmetric element

99
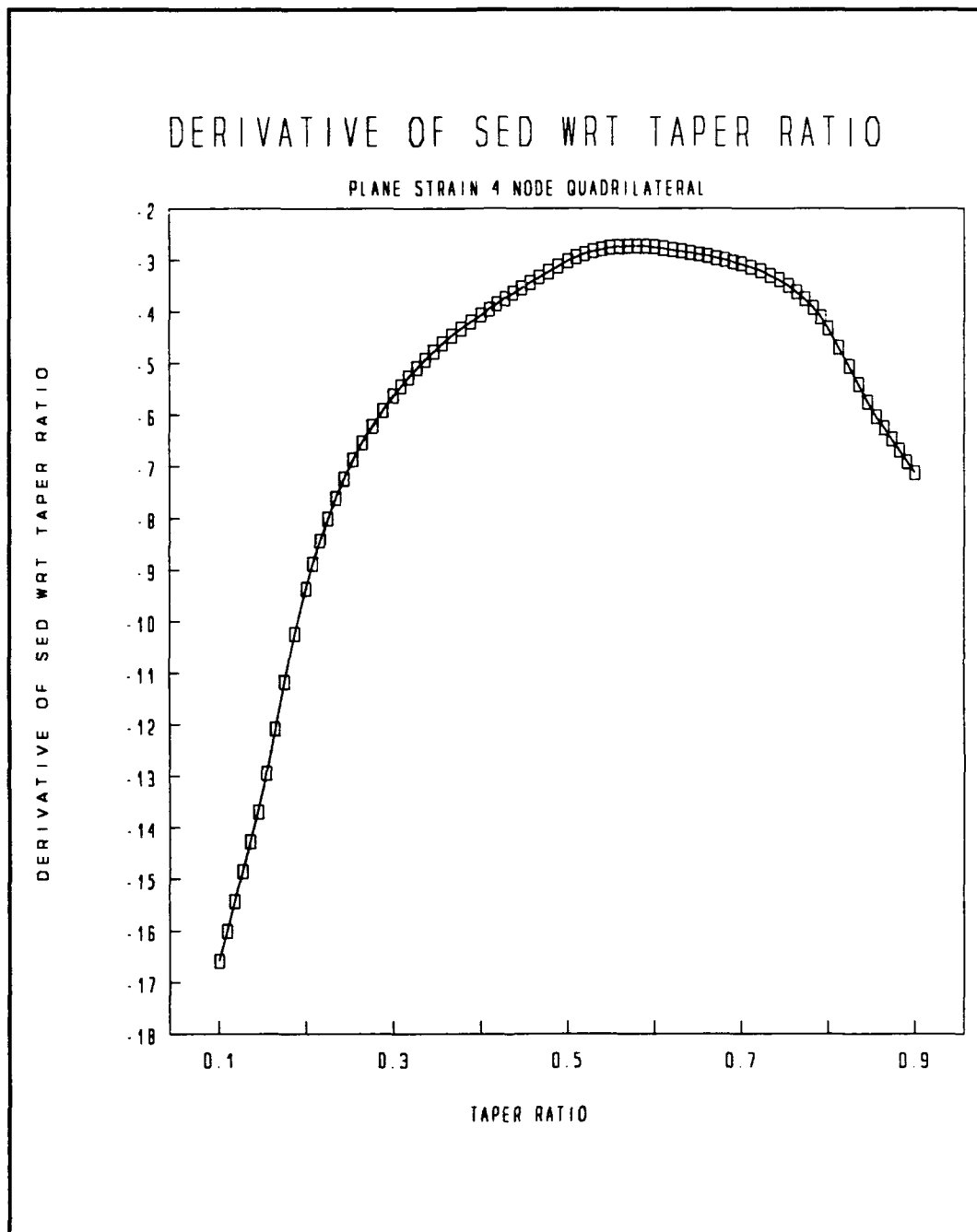
Figure 4.20. Derivative of strain energy density ratio with respect to taper ratio versus taper ratio for a plane strain element

100
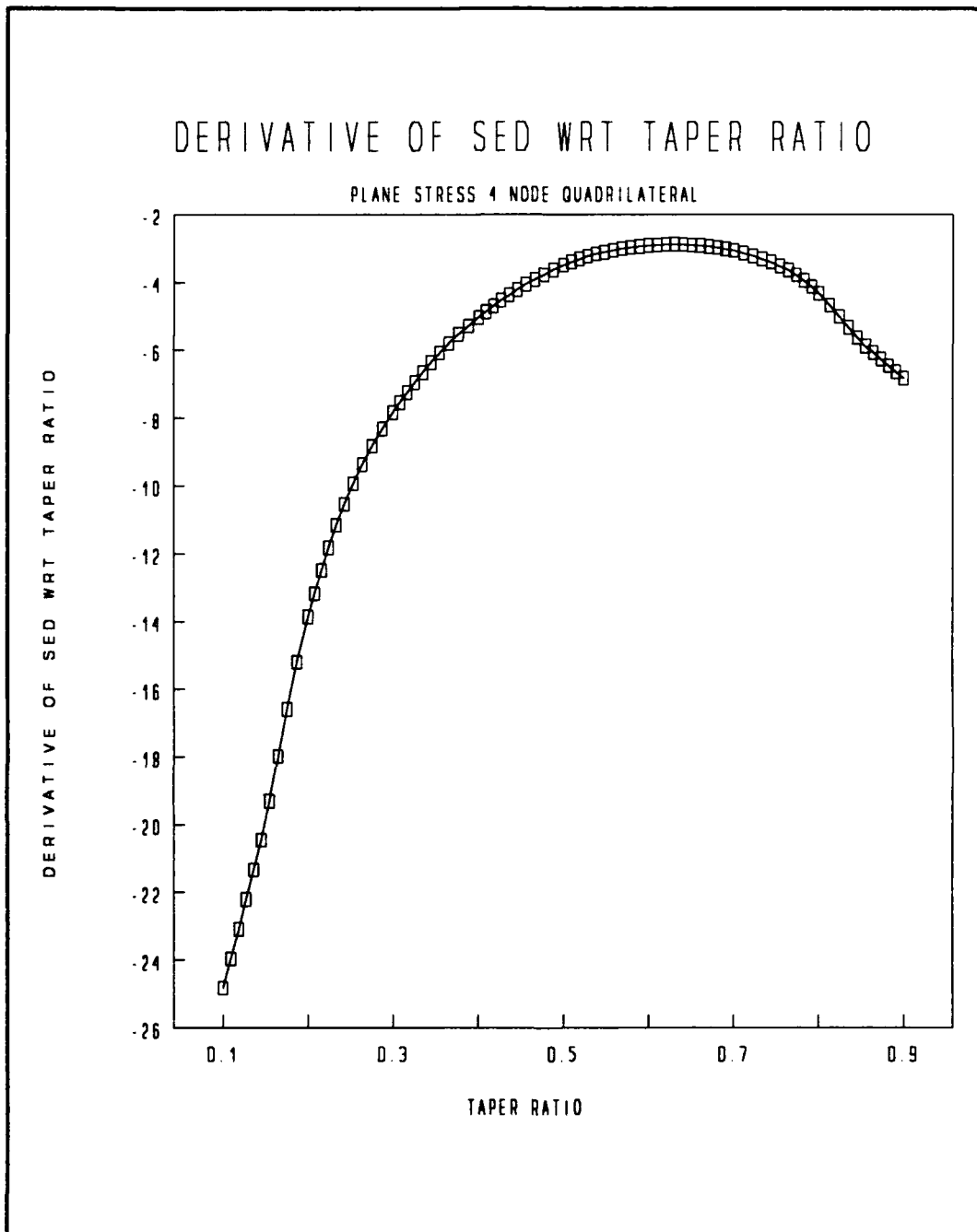
Figure 4.21. Derivative of strain energy density ratio
with respect to taper ratio versus taper ratio for a
plane stress element

101

These derivative plots clearly indicate the inflection point or point of change in the direction of the radius of curvature seen in the two dimensional plots. In Figure 4.19, the axisymmetric case, a dramatic change in the derivative plot occurs at a taper ratio value of 0.55. This appears as a peak value in the plot. The exact same conclusions can be drawn for Figure 4.20, the plane strain case, and for Figure 4.21 the plane stress case. In these latter cases however, the shape of the plots are similar to each other but different to the axisymmetric case. The effect of the axis of symmetry in the axisymmetric case causes the difference in appearance of the plots. The peak value in Figure 4.20, the plane strain case, is at a taper ratio value of 0.58. The peak value in Figure 4.21, the plane stress case, is at a taper ratio value of 0.63. All of these values are in agreement with the values determined from the two and three dimensional plots.

A similar trend is seen in the plots of the sensitivity of the strain energy density ratio with respect to taper ratio versus taper ratio. The sensitivity of the strain energy density ratio with respect to taper ratio versus taper ratio for the axisymmetric, plane strain, and plane stress cases are shown in Figure 4.22 through Figure 4.24.
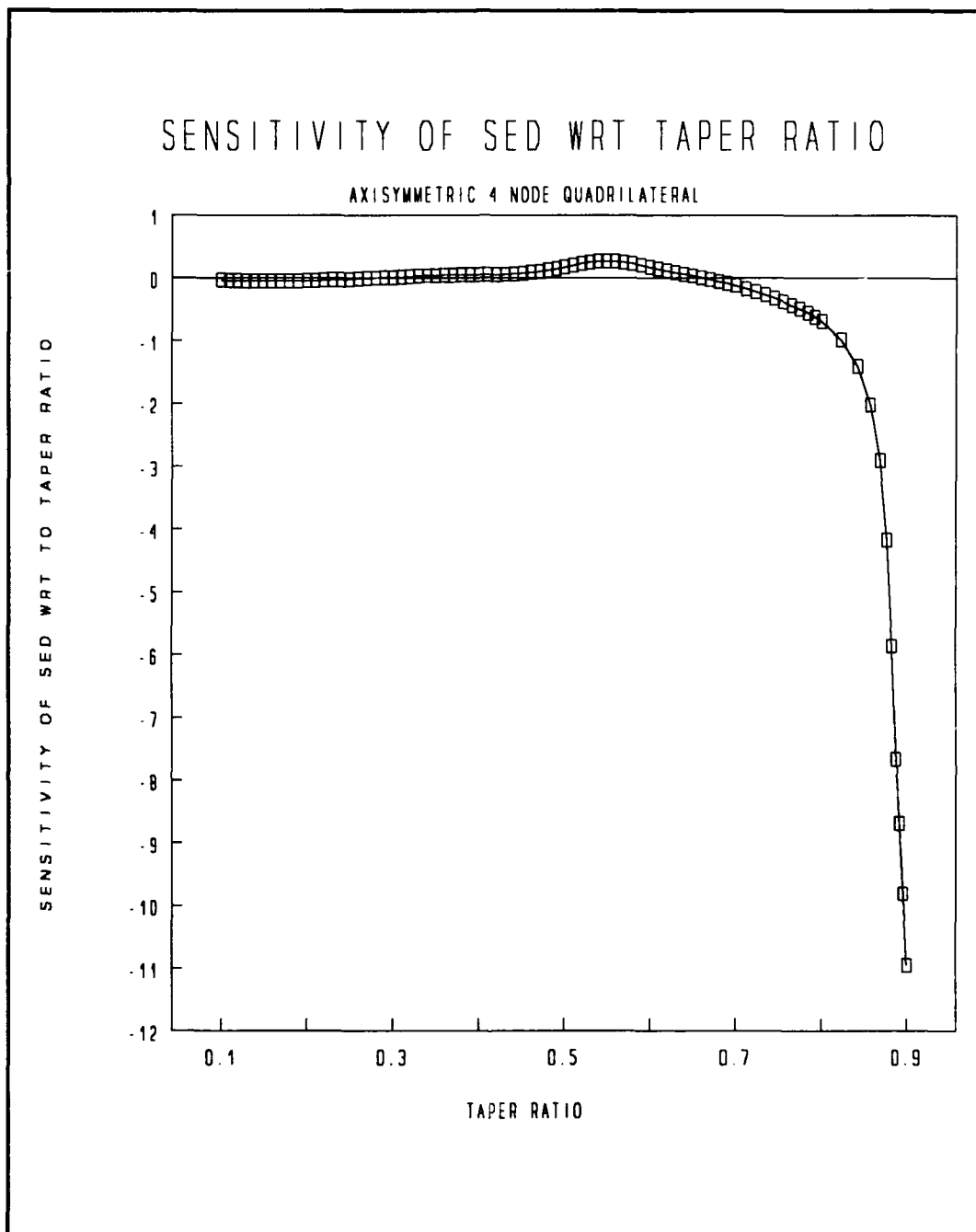
Figure 4.22. Sensitivity of strain energy density ratio with respect to taper ratio versus taper ratio for an axisymmetric element
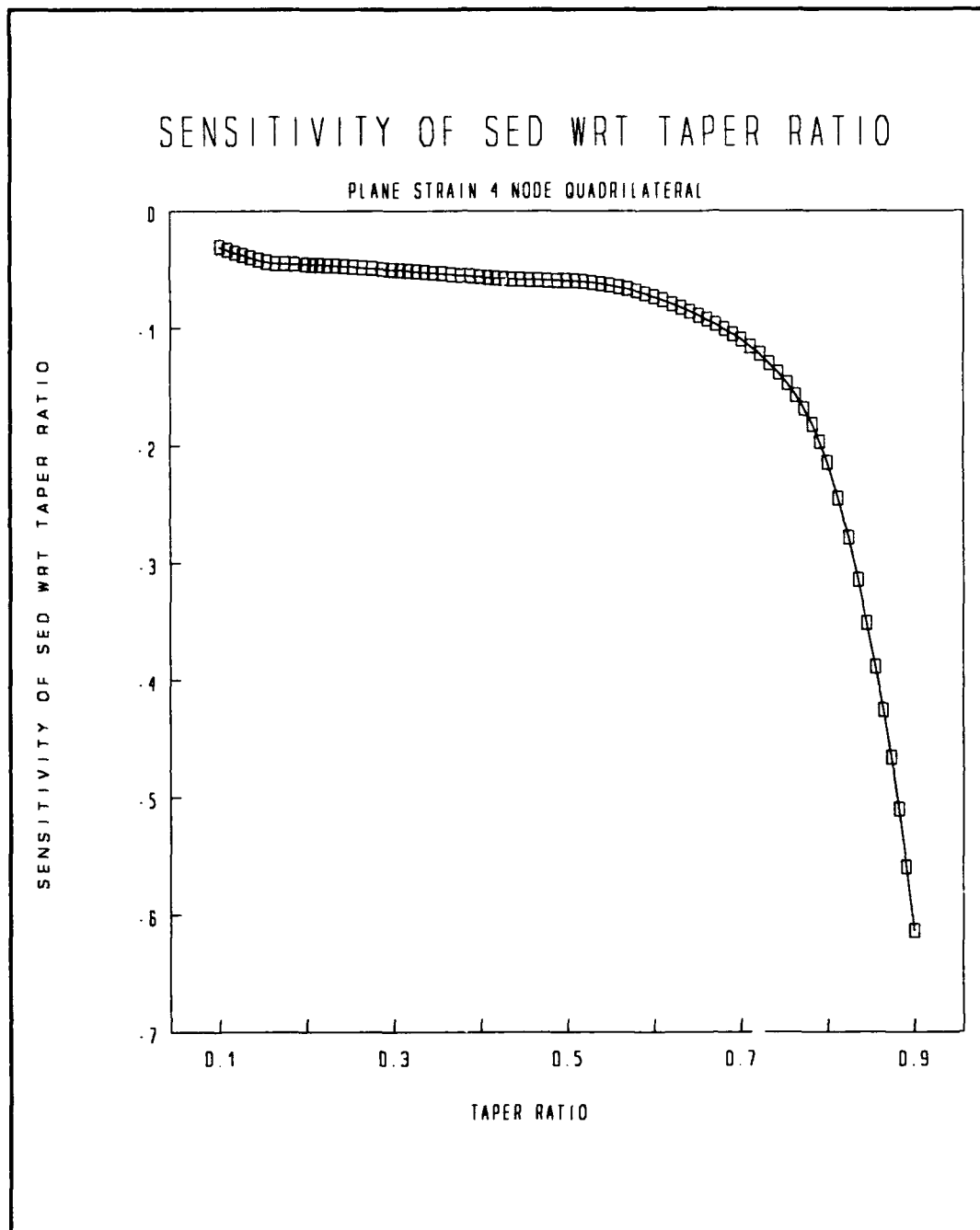
Figure 4.23. Sensitivity of strain energy density ratio with respect to taper ratio versus taper ratio for a plane strain element

SENSITIVITY OF SED WRT TAPER RATIO

PLANE STRESS 4 NODE QUADRILATERAL
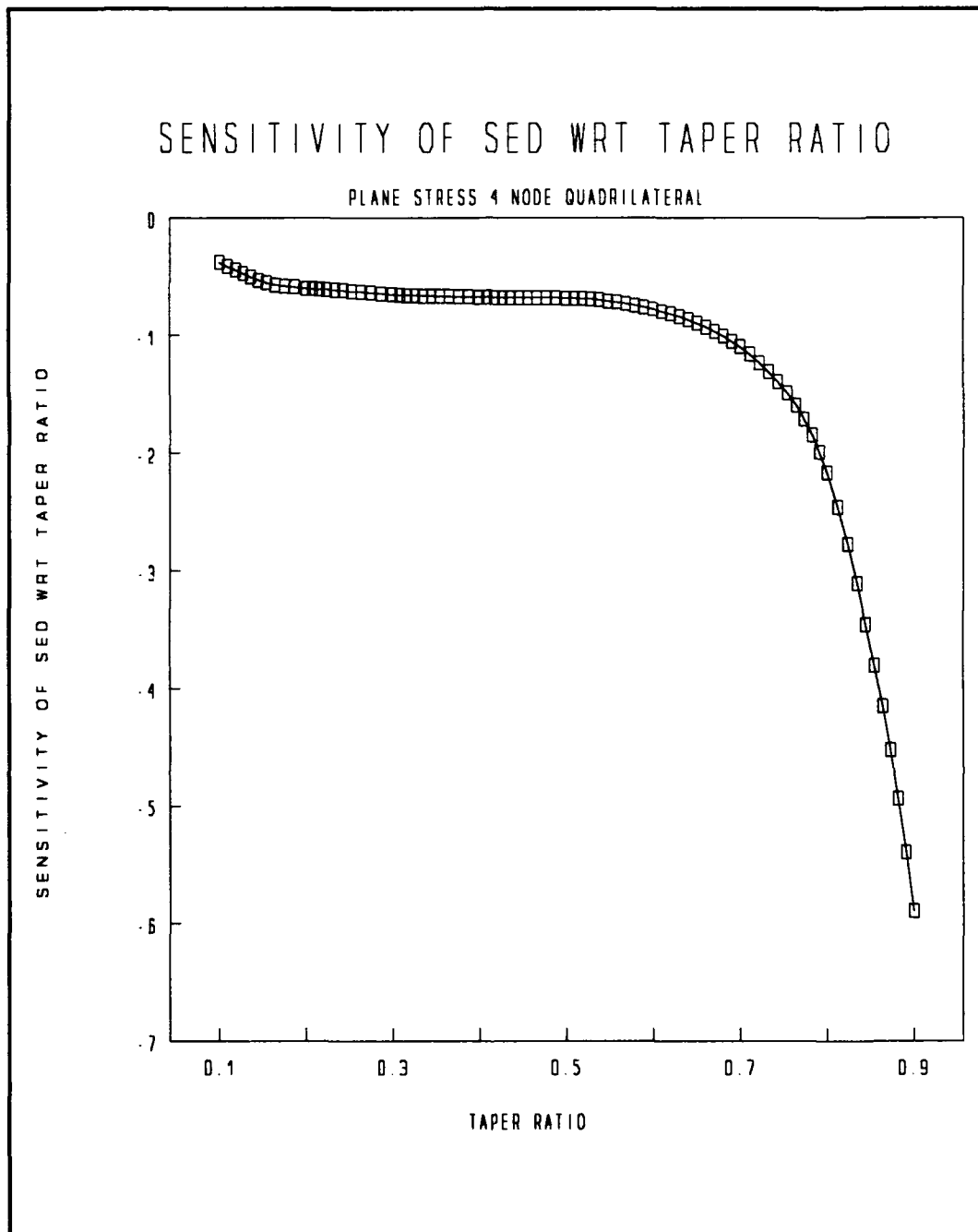
Figure 4.24. Sensitivity of strain energy density ratio with respect to taper ratio versus taper ratio for a plane stress element

These sensitivity plots tend to correlate overall with the derivative plots. In Figure 4.22, the axisymmetric case, a peak value occurs at a taper ratio of 0.55, the same location found in the derivative plot. For Figure 4.23 the plane strain case, and Figure 4.24 the plane stress case, no peak values appear. The only correlation that can be made is that the curves tend to level out at the peak points indicated in the derivative plots, thus some correlation exists. An interesting observation is that all three sensitivity plots are similar in shape. From this one can conclude that the sensitivity of the strain energy density ratio with respect to taper ratio is identical no matter the type of element used.

The fact that all four plots for each element type tend to point to the same rezoning indicator value adds further confidence to the choice of the taper ratio rezoning indicators. A conclusion is therefore drawn that the taper ratio rezoning indicator values for the axisymmetric case is 0.55, for the plane strain case is 0.58, and for the plane stress case is 0.63.

4.5.3 Results for Skew Angle

Three dimensional plots shown in Figure 4.25 through Figure 4.27 were developed from the results of eigenvalue tests on the three element types.
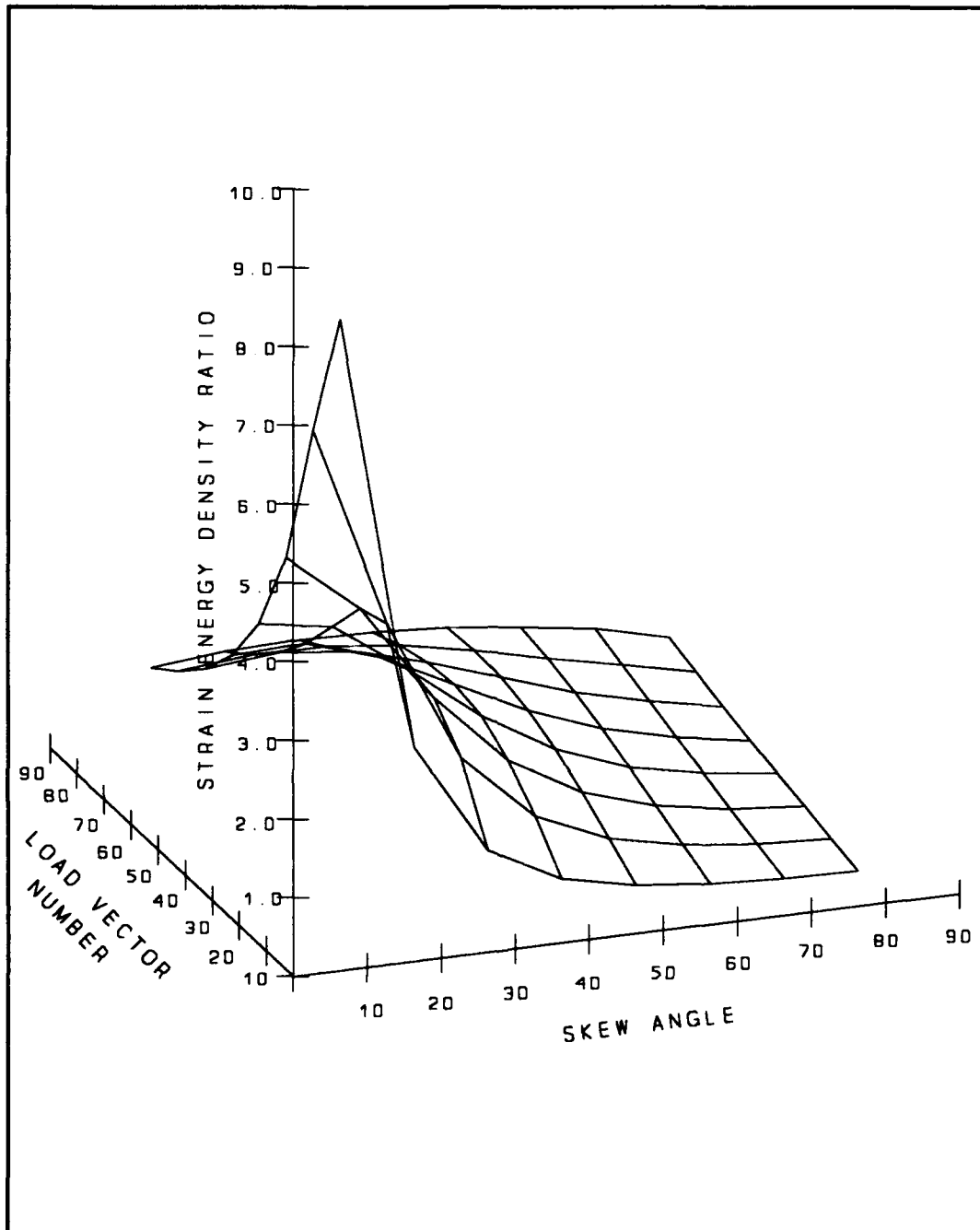
Figure 4.25. Three dimensional plot of strain energy
density ratio varied over skew angle and load vector
values for an axisymmetric element

107
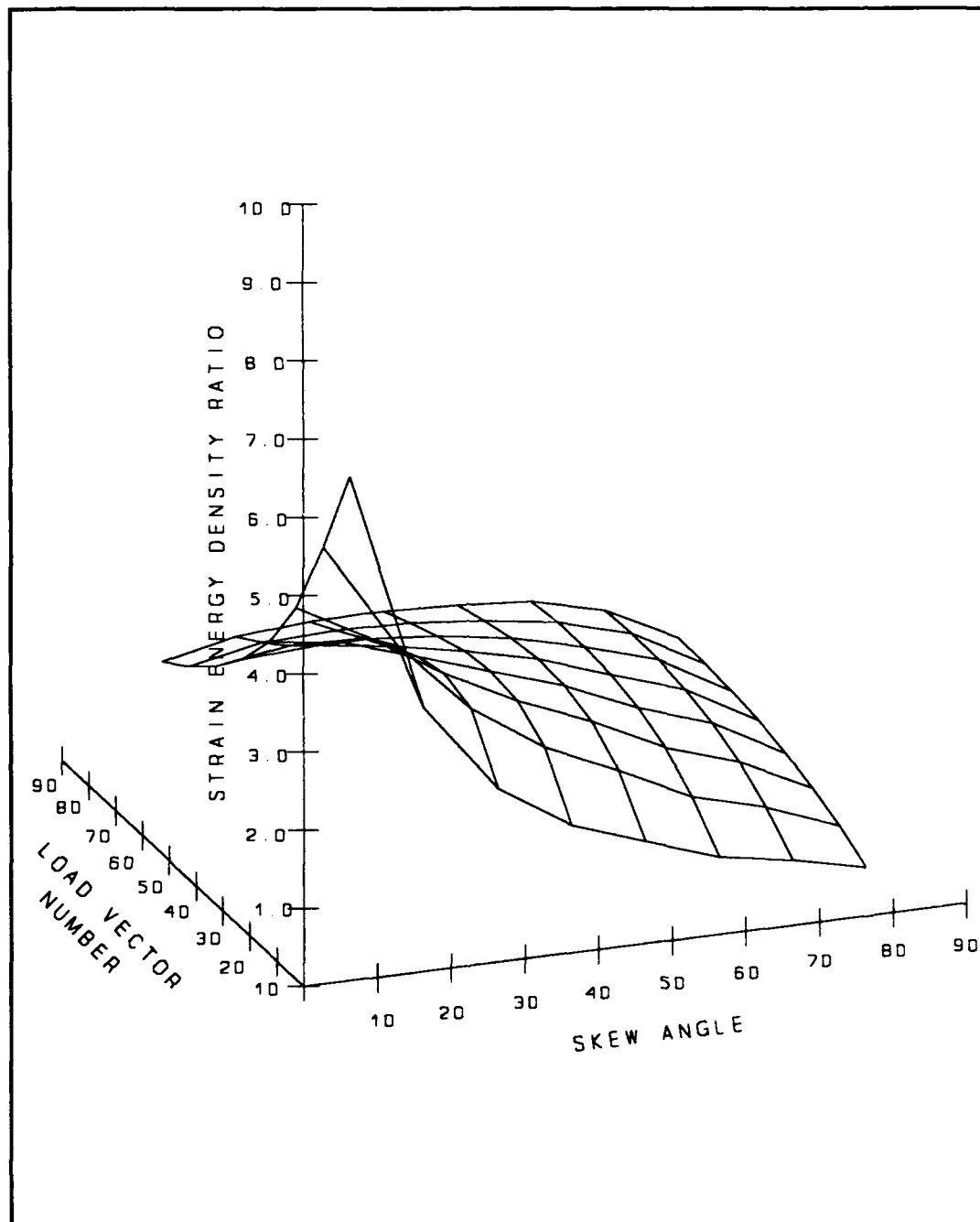
Figure 4.26. Three dimensional plot of strain energy
density ratio varied over skew angle and load vector
values for a plane strain element

108
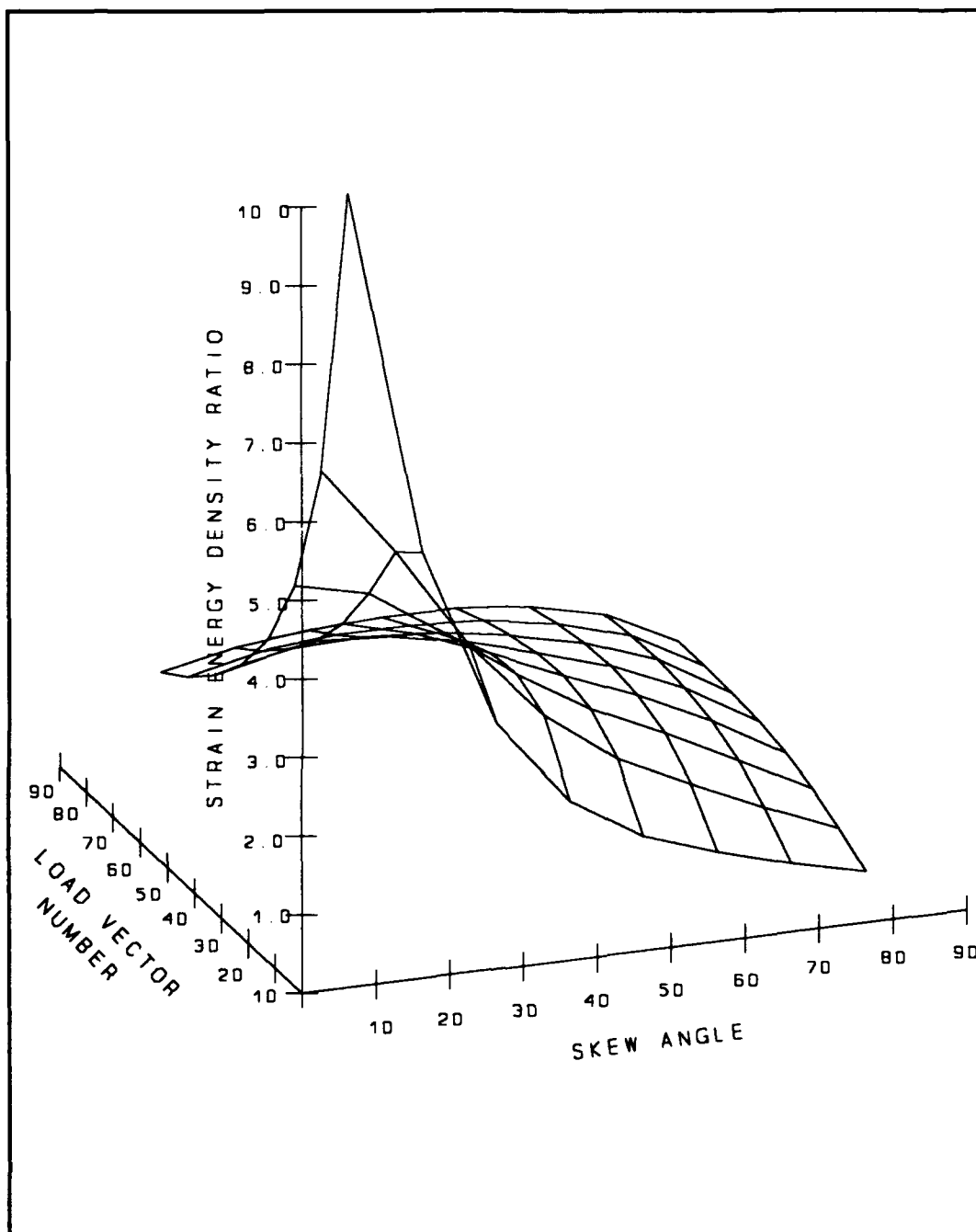
Figure 4.27. Three dimensional plot of strain energy density ratio varied over skew angle and load vector values for a plane stress element

In each of these three dimensional surface plots one can see the effects on strain energy density ratio due to changes not only in the skew angle but also in the load vector. The effects are similar for each element type. The general tend is that the surface peaks near the coordinate origin and quickly drops and then levels off the further one is away from both the skew angle and load vector axes. It is assumed that the point where the surface begins to change slope dramatically, in transitioning from the peak value to the flat part of the surface, is the point that would correspond to when the amount of skew angle drastically changes the results of the solution. In Figure 4.25 for the axisymmetric case, this change appears to occur at a skew angle near 50.0 degrees. In Figure 4.26 for the plane strain case, this change appears to be at a slightly lower value, some where near 40.0 degrees. In Figure 4.27 for the plane stress case, this change appears to be at about 55.0 degrees.

The two dimensional plots of strain energy density ratio versus skew angle follow. Note that a cubic spline curve fit was used to fit a curve to the data points. The two dimensional plots for the axisymmetric, plane strain, and plane stress case are shown in Figure 4.28 through Figure 4.30.
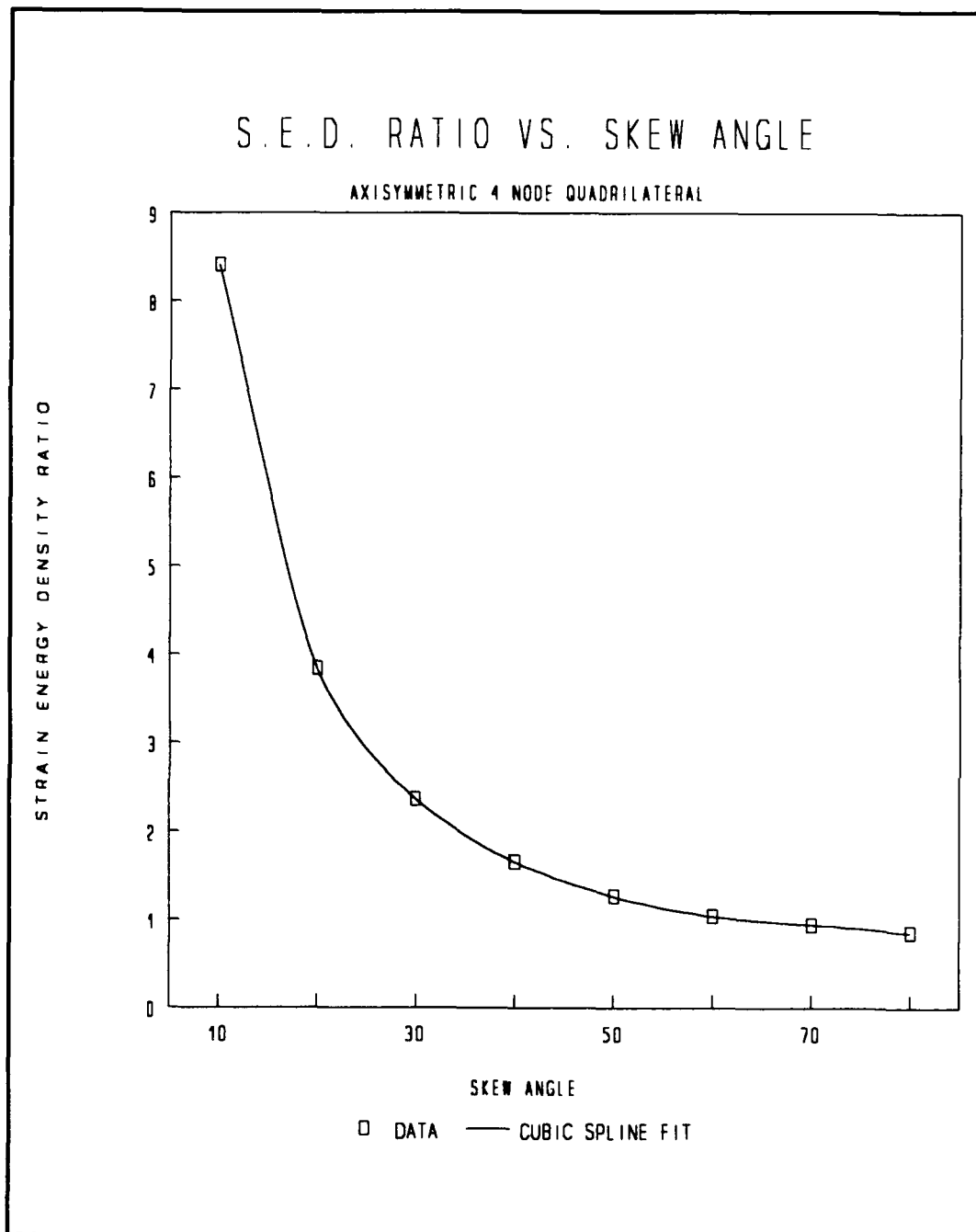
Figure 4.28. Strain energy density ratio versus skew angle for an axisymmetric element

111
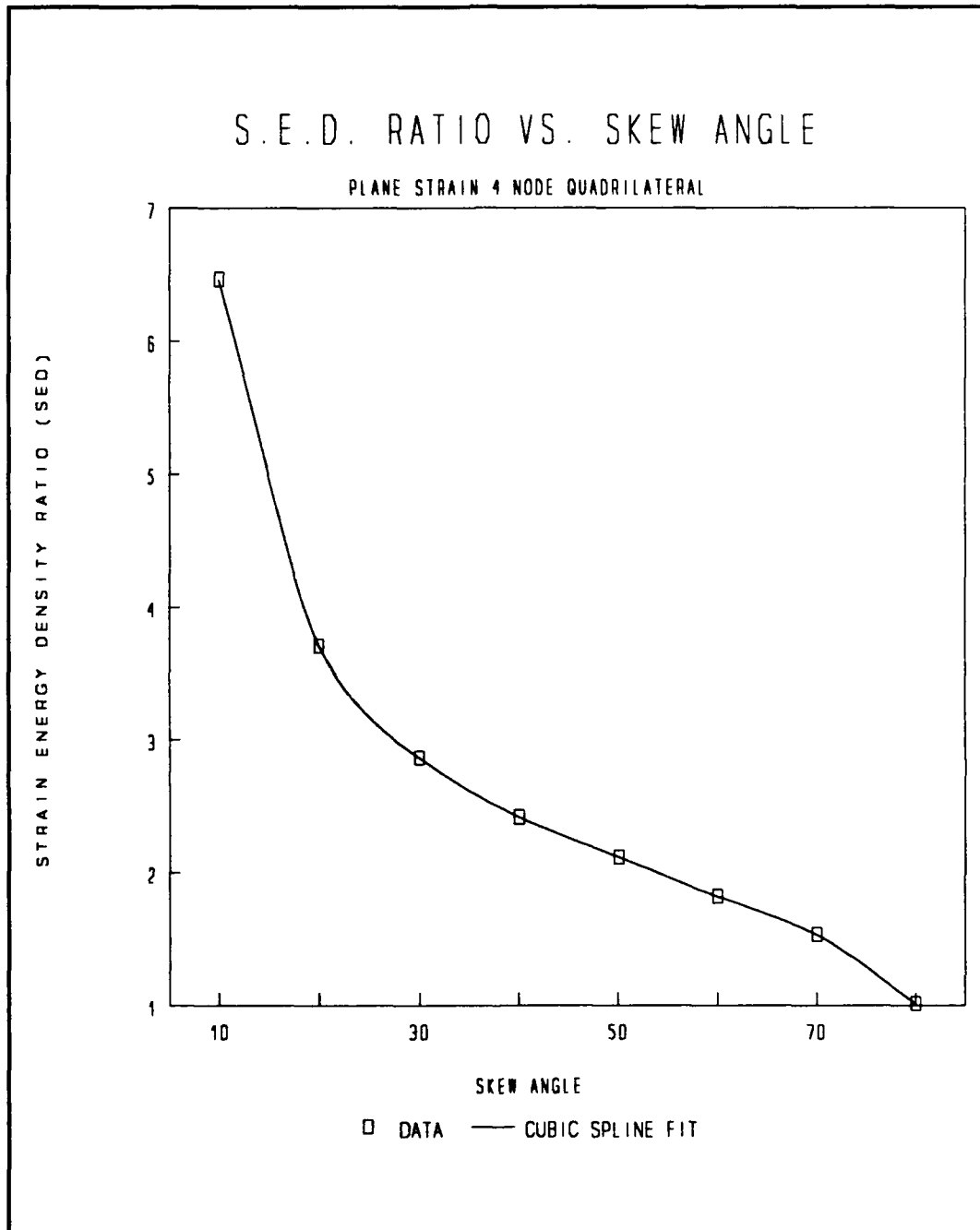
Figure 4.29. Strain energy density ratio versus skew angle for a plane strain element
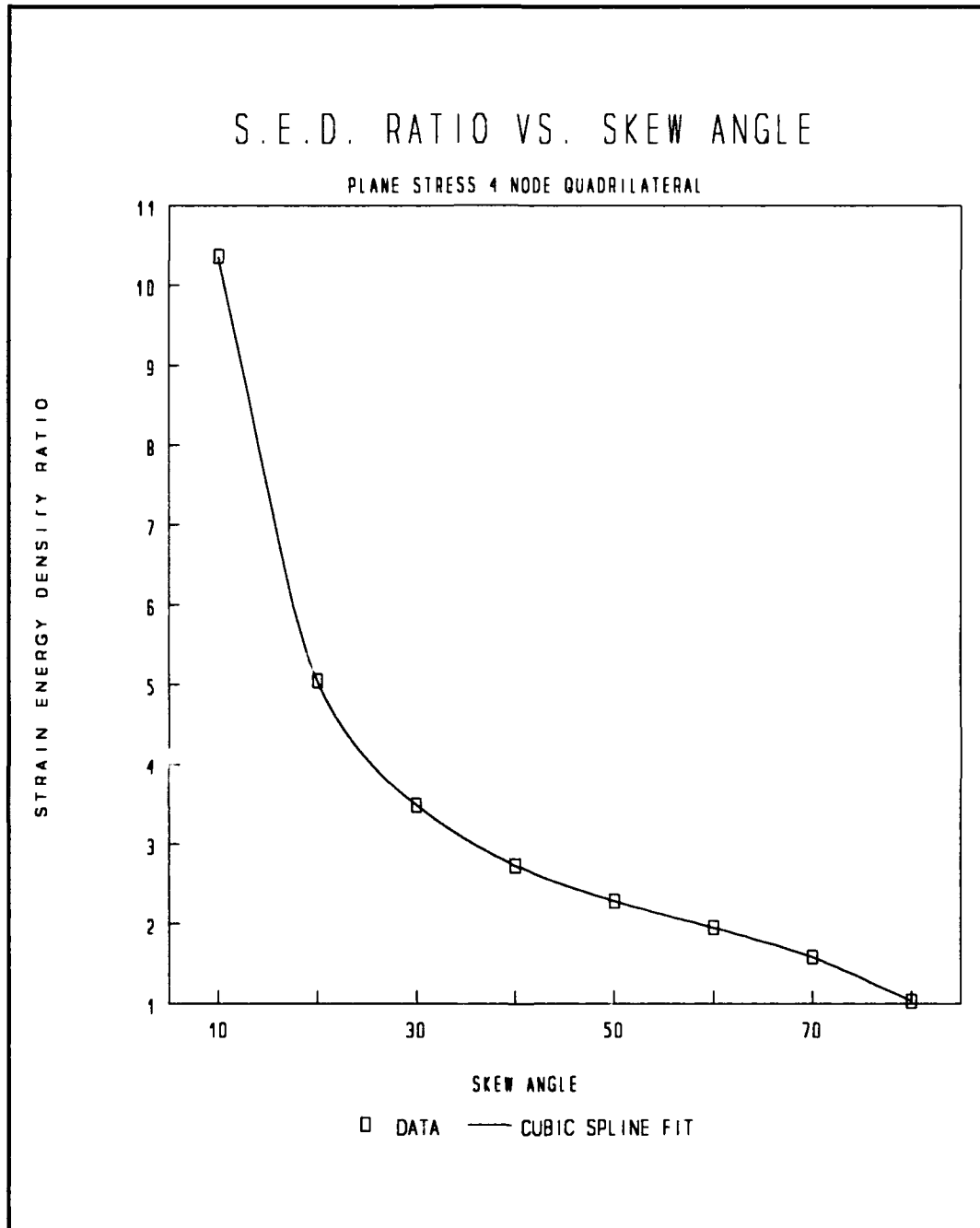
Figure 4.30. Strain energy density ratio versus skew angle for a plane stress element

113

The two dimensional plots seem to indicate in a general sense when the skew angle tends to dramatically change the effect of the solution. These values tend to correlate with the three dimensional plots. In Figure 4.28 for the axisymmetric case, no inflection point or change in the radius of curvature exits. One can, however, use the same assumption applied to the three dimensional plots that the point where the slope of the curve begins to change more quickly is the point of interest. This seems to occur at about 50.0 degrees. In Figure 4.29 the plane strain case, and in Figure 4.30 the plane stress case, there is a change in the radius of curvature direction or an inflection point in both plots. This seems to occur at about 47.0 degrees for the plane strain case, and at about 53.0 degrees for the plane stress case. These values correspond to those determined for the three dimensional plots.

In the plots of the derivative of strain energy density ratio with respect to skew angle versus skew angle, the values are determined by obtaining the derivative from the cubic spline curve fit. This is the same procedure used for the derivative plots on all of the distortion measures. The derivative plots are shown in Figure 4.31 through Figure 4.33 for the axisymmetric, plane strain, and plane stress cases.
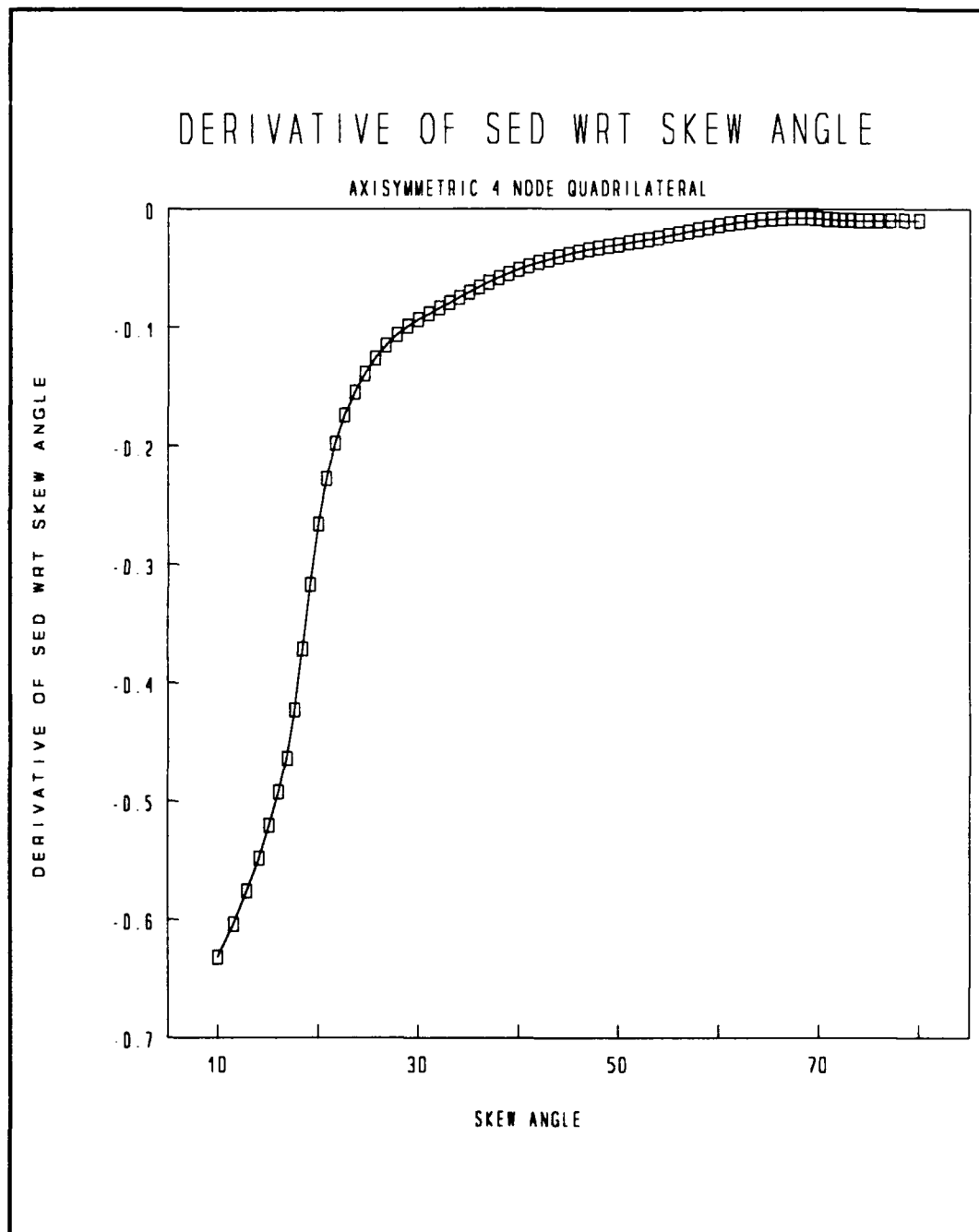
Figure 4.31. Derivative of strain energy density ratio with respect to skew angle versus skew angle for an axisymmetric element

DERIVATIVE OF SED WRT SKEW ANGLE

PLANE STRAIN 4 NODE QUADRILATERAL
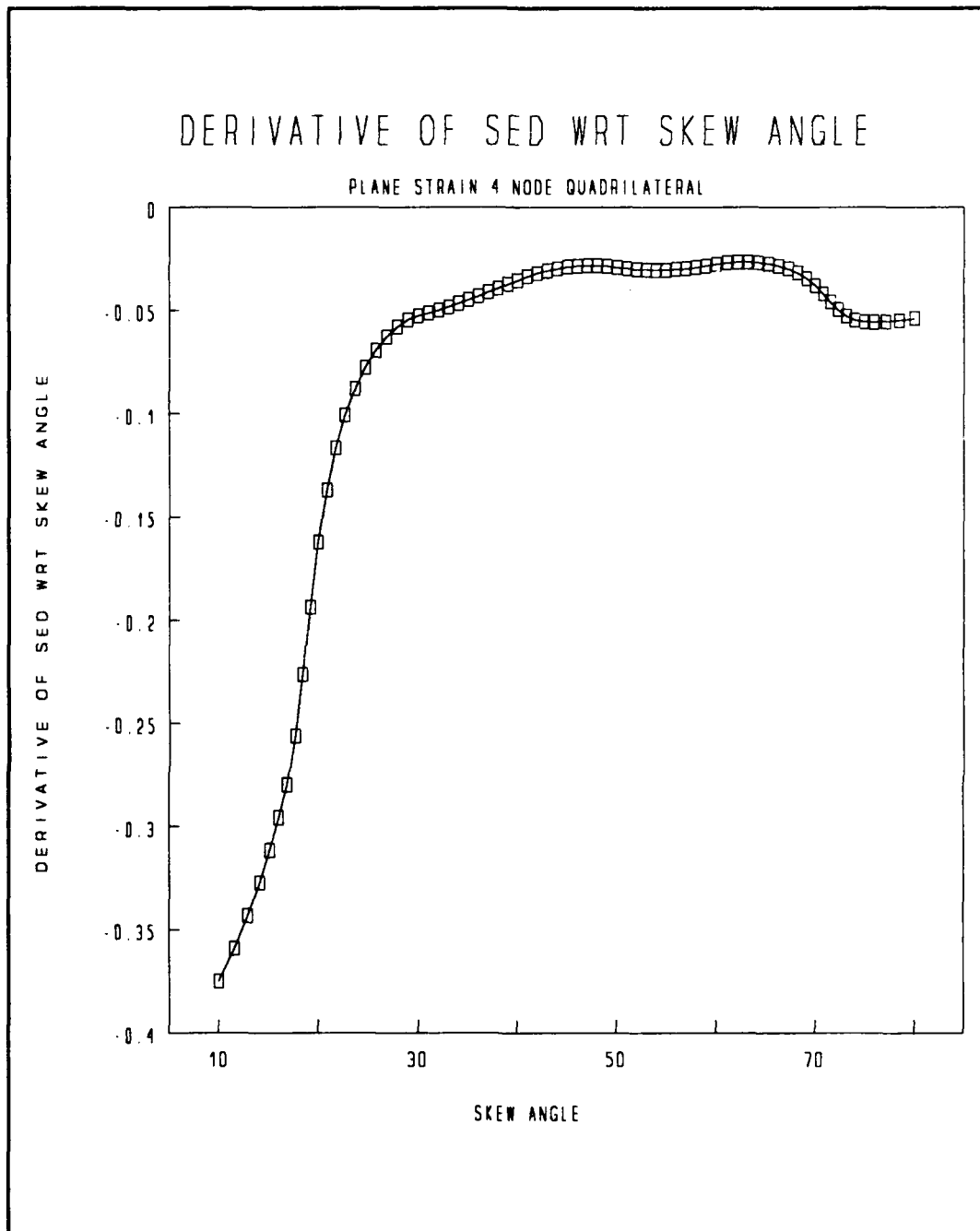
Figure 4.32. Derivative of strain energy density ratio with respect to skew angle versus skew angle for a plane strain element

116
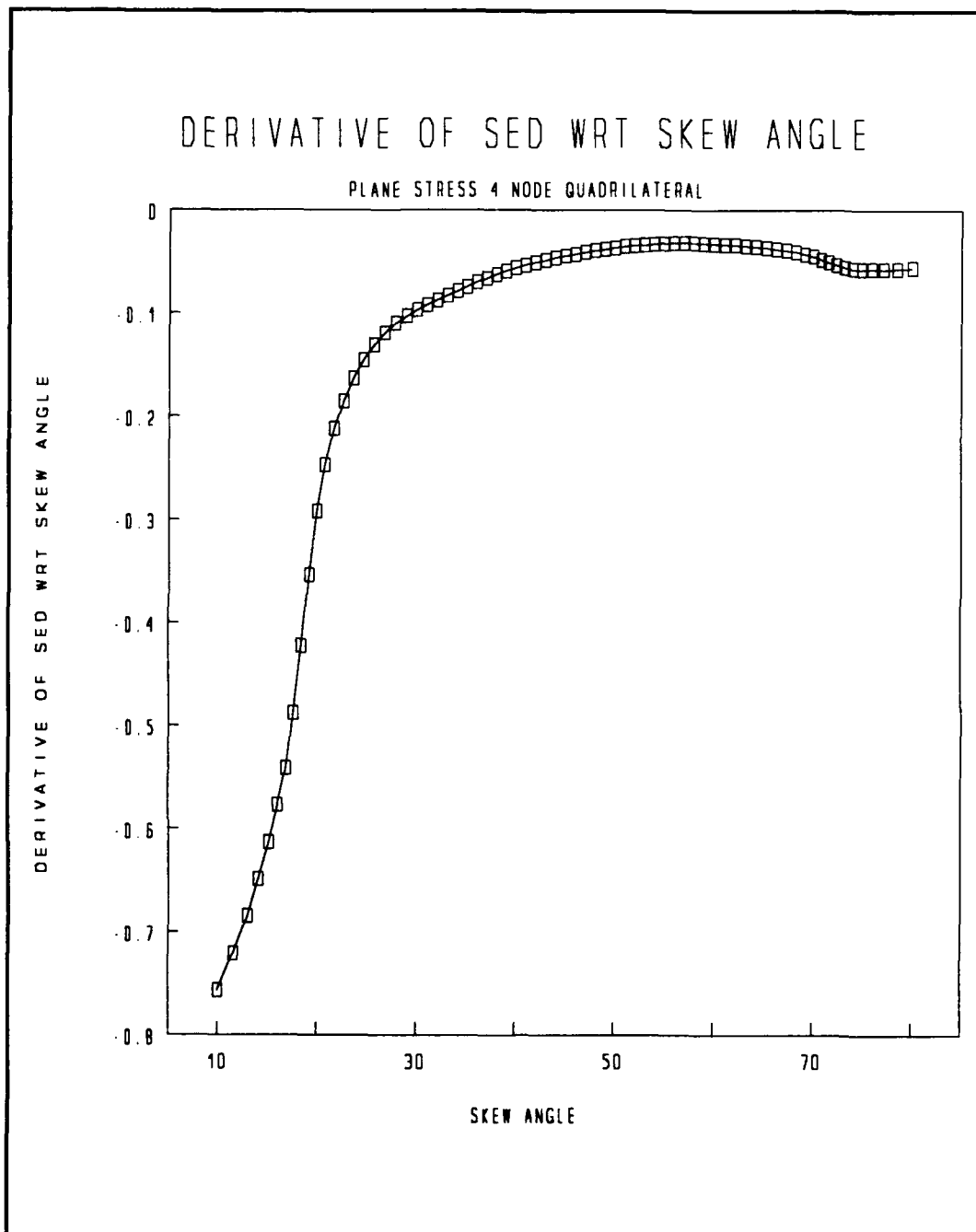
Figure 4.33. Derivative of strain energy density ratio with respect to skew angle versus skew angle for a plane stress element

The derivative plots indicate to some degree where the point of the change in direction of the radius of curvature or inflection points of the two dimensional plots occur. In Figure 4.31, the axisymmetric case, there is no real indicating point. The curve appears to have no change in the direction of the radius of curvature nor any discontinuities. All that one can assume is that an indicator point might occur somewhere in the range of 40.0 to 65.0 degrees. This assumption is based on the fact that the slope of the curve in this region is beginning to change rapidly. This might indicate the solution is increasing its error quicker within this region. In Figure 4.32, the plane strain case, at about a point of 45.0 degrees the plot seems to peak and level off. In Figure 4.33, the plane stress case, the plot here also peaks and levels off but at a point of about 55.0 degrees. These values correlate to the values determined from the two dimensional plots, Figure 4.28 through Figure 4.30. This correlation adds confidence to the values being selected for the rezoning indicators of skew angle.

In the plots of the sensitivity of the strain energy density ratio with respect to skew angle versus skew angle similar conclusions can be drawn. The sensitivity plots are shown in Figure 4.34 through Figure 4.36 for the axisymmetric, plane strain, and plane stress cases.

118

**SENSITIVITY OF SED WRT SKEW ANGLE**

AXISYMMETRIC 4 NODE QUADRILATERAL
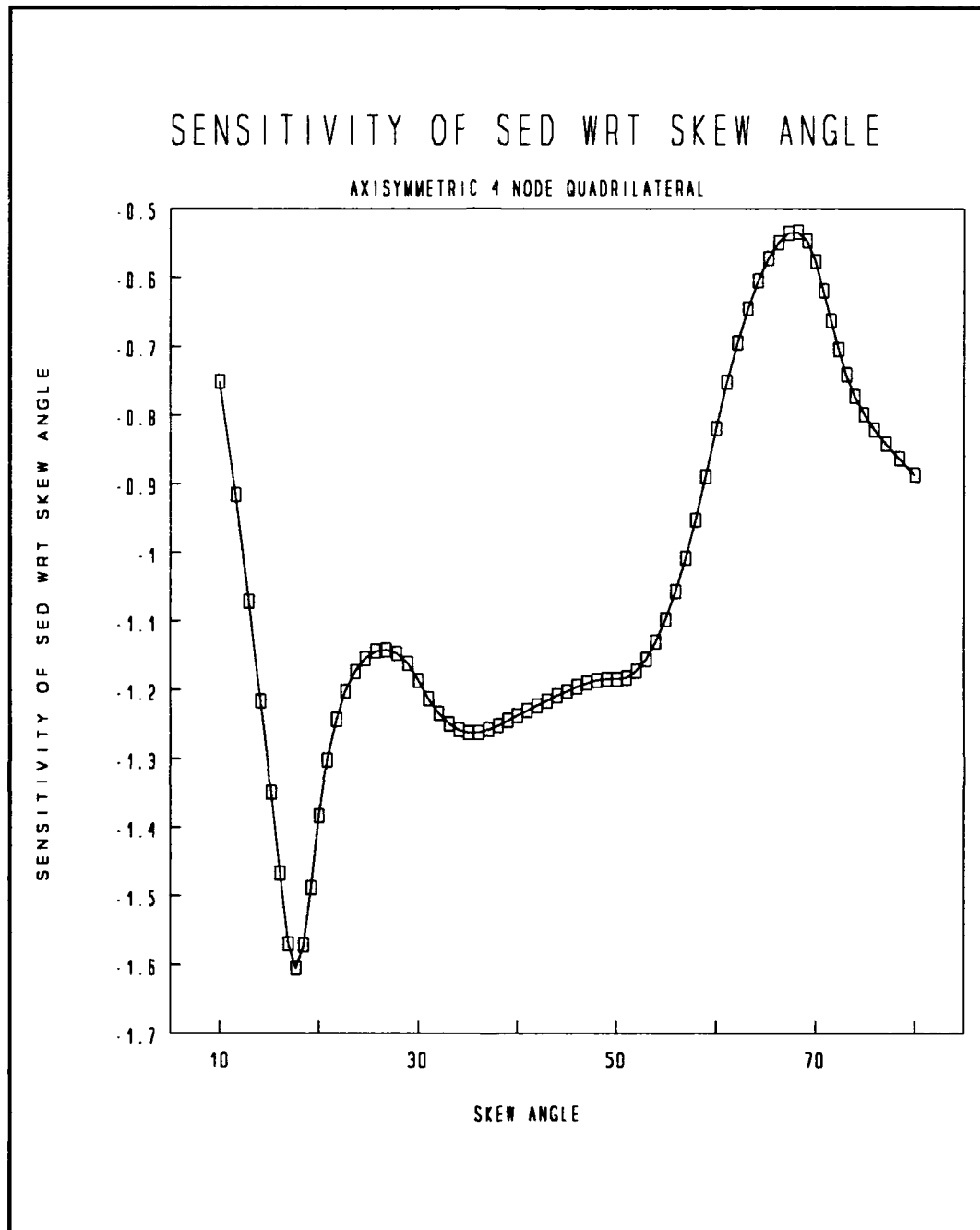
Figure 4.34. Sensitivity of strain energy density ratio with respect to skew angle versus skew angle for an axisymmetric element
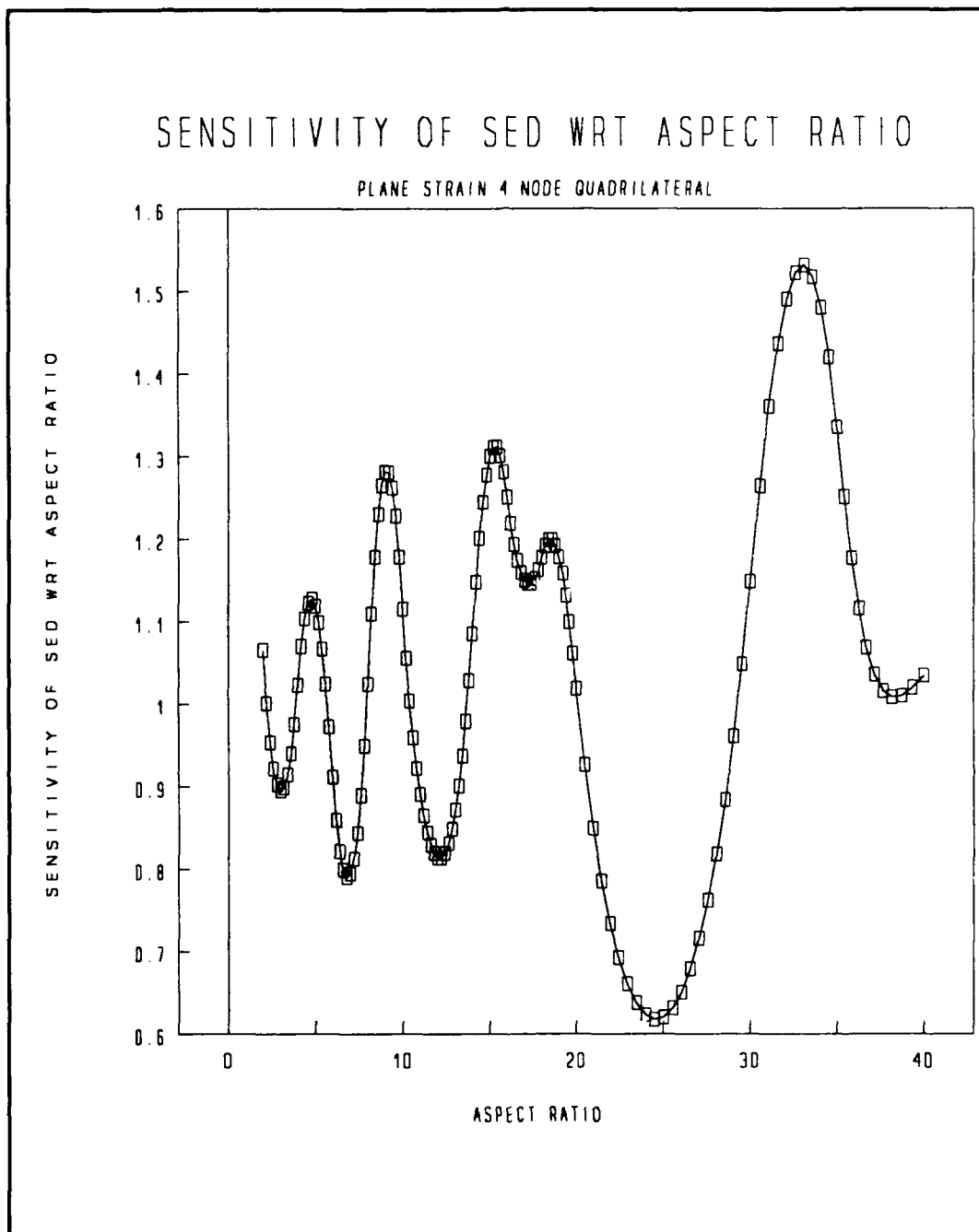
119
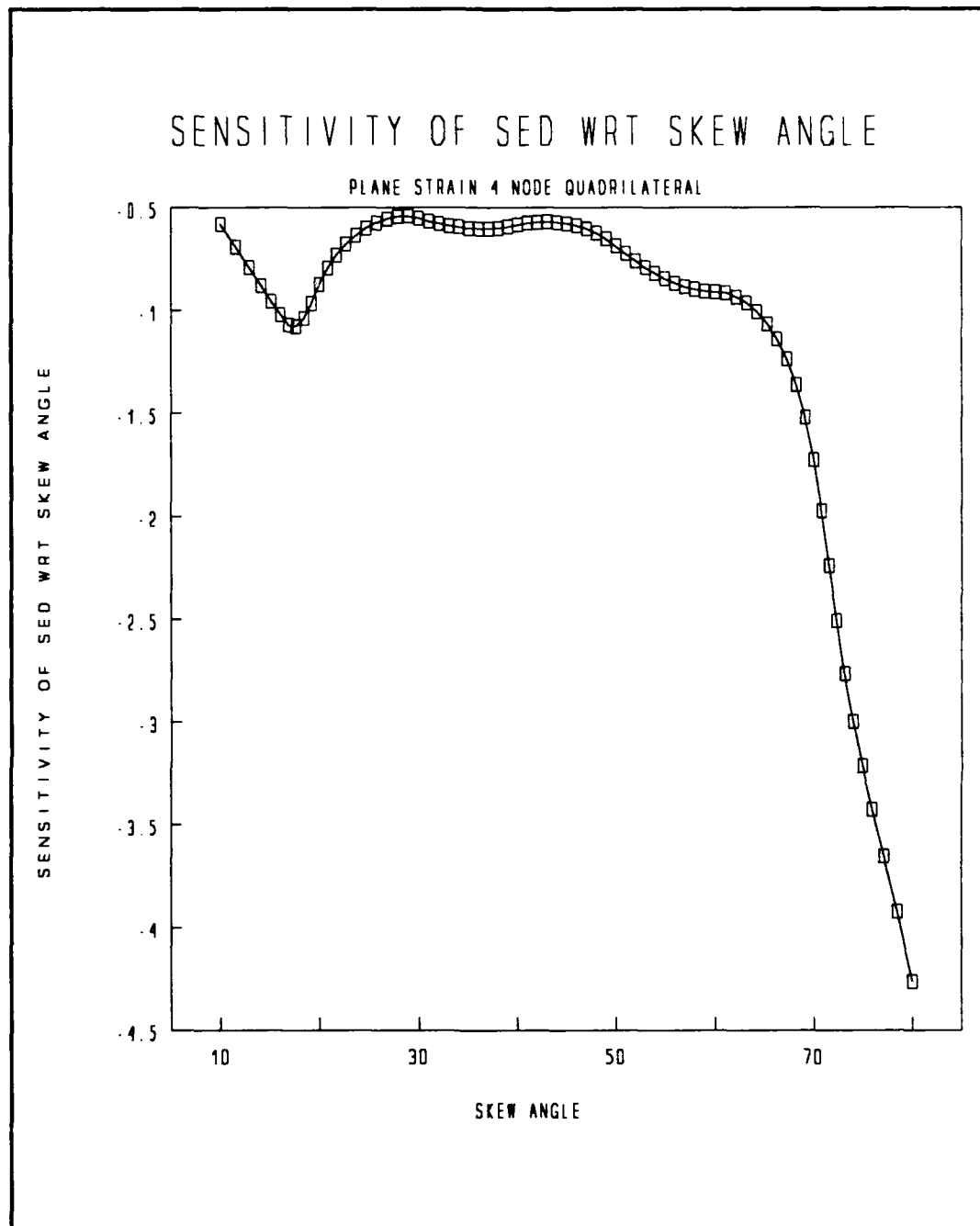
Figure 4.35. Sensitivity of strain energy density ratio with respect to skew angle versus skew angle for a plane strain element
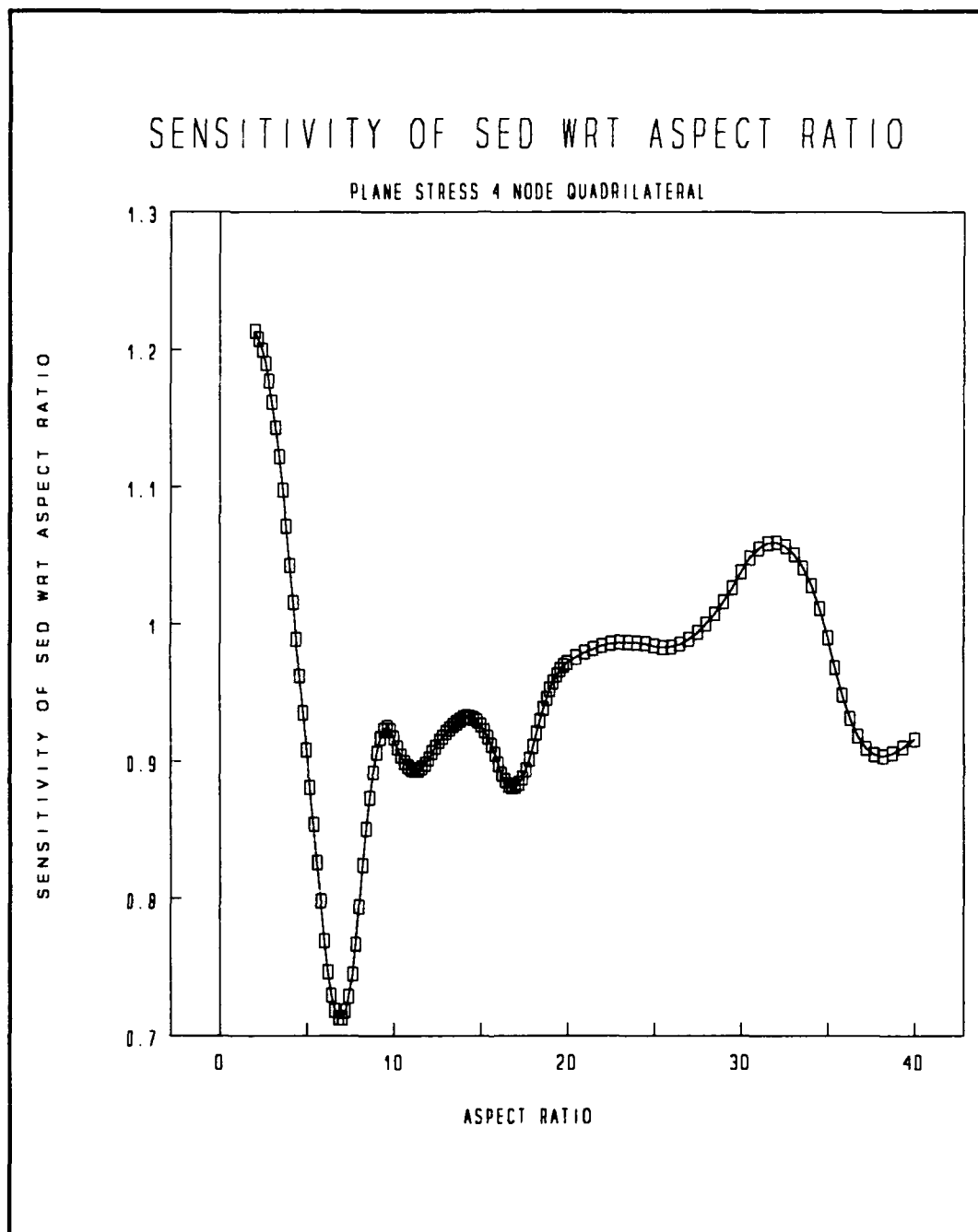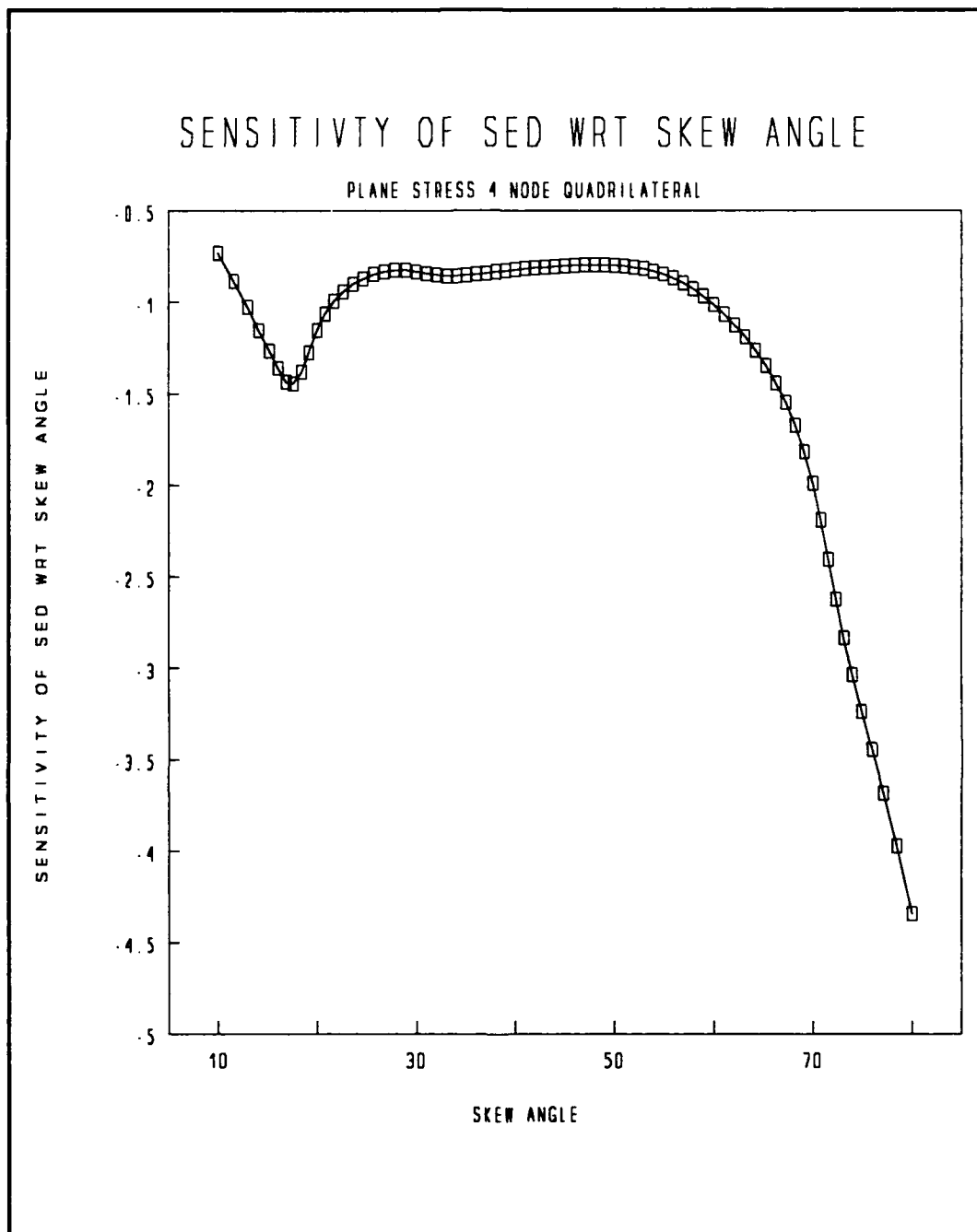
Figure 4.36. Sensitivity of strain energy density ratio with respect to skew angle versus skew angle for a plane stress element

121

The sensitivity plots tend to indicate more precisely the point of interest. In Figure 4.34, the axisymmetric case, one can observe the an oscillation pattern in the curve. At angles smaller than 50.0 degrees the amplitude is smaller and the frequency higher. Above 50.0 degrees the amplitude increases and the frequency is reduced. This sensitivity plot is different from the plane strain and plane stress cases. As seen in Figure 4.35, the plane strain case, at 43 degrees the plot tends to peak and level off. This same effect is seen in Figure 4.36, the plane stress case. In this case the peak point corresponds to when the curve levels off, which is at 52 degrees.

The fact that all four plots for each element type tend to point to the same rezoning indicator value adds further confidence to the choice of skew angle rezoning indicator. The skew angle rezoning indicator value for the axisymmetric case is 50 degrees, for the plane strain case is 43 degrees, and for the plane stress case is 52 degrees. An assumption is made that the decrease in the number of degrees in the skew angle from 90.0 degrees, to arrive at the skew angle rezoning indicator values, can be applied to angles that are also greater than 90.0 degrees. This provides a minimum and maximum range of values for the skew angle. Maximum skew angle values are 130 degrees for the axisymmetric case, 137 degrees for

122

the plane strain case, and 128 degrees for the plane stress case.

4.6 Verification Methods of Rezoning Indicators

State variables such as deformation, strain, stress, along with strain energy density are presently used as means to determine when and how rezoning should occur. These state variables provide a functional way of determining when, how, and to what degree to rezone. Since state variables are directly involved in the solution process they provide a direct link to how the solution is progressing. A link can also be made to the constitutive or material model to verify that values that are obtain are still within the bounds of the material behavior. In large deformation and strain problems many of the models are provided in rate form so as to be able to provide history response to the analysis. It would therefore be logical to look at the state variables in rate form. This would be especially true of strain rate. The sections that follow discuss how state variables and other solution processes can be used to indicate when and where rezoning should occur. This leads to the conclusion that such measures can be used to validate rezoning indicators derived from eigenvalue tests. If these rezoning measures are examined in conjunction with the eigenvalue test derived rezoning indicators, and if

123

they are in agreement, then one has validated the effectiveness of rezoning indicators derived from the eigenvalue tests by an independent means.

4.6.1 Jumps and Steep Gradients of State Variable Values

Deformations, strains, stresses, and strain energy densities can be very large in given areas of a mesh. If the gradients of these values are steep in areas of element distortion, then one has an indication that the solution process may have gone awry and rezoning will be required. Jumps in state variable values tend to indicate localized problems in the finite element mesh which could be due to distortions in the elements. Most of the work to date has been done in this regards by looking at deformations, strains, stresses, and strain energy density jumps or steep gradients of these values across a finite element mesh. Much of this work, however, has been for static linear finite element problems used in optimization of the mesh. There is, however, a fair amount of work done that has used jumps and steep gradients of displacement, strain, stress, and strain energy density as rezoning measures for quasi static and dynamic problems of large strains and deformations [19, 33-39].

The state variable gradient differentials or contours provide information as to when, where, and how

124

much rezoning should be done. The gradient differentials can not only indicate the elements that need to be reshaped but the regions of the mesh which need refinement as well. Generally this is accomplished via an h-type refinement. The refinement in the mesh helps to smooth out the discontinuities and provides more elements in areas of steep gradients thus assisting in the avoidance of numerical difficulties and solution inaccuracies.

The benefit of using these rezoning measures is that the information is directly available from the results of the solution. Contour plots make a visual inspection of these quantities and location of steep gradients possible. Examination of the data can determine the magnitude of the jumps in the values. Often this corresponds with the areas of steep gradients.

Correlation of the results obtained from jumps and steep gradients of displacement, strain, stress, and strain energy density to the rezoning indicators derived from eigenvalue tests would provide an excellent means for validation of the rezoning indicators. This correlation is made to some degree in this investigation by examination of contour plots of effective plastic strain, Mises stresses, and strain energy density. The examination of strain jumps is also included in this investigation. This process of examining the contour

plots of equivalent plastic strain, Mises stress, and strain energy density is used on two example problems. Chapter 7 and Chapter 8 describe the results of the comparison of these contour plots to the result obtained from the two example problems.

4.6.2 Changes in the Time Step or Increment Size

The time step plays a critical part in the solution process for dynamic problems. An implicit code is generally used so that the time step can be increased. If in the process a given element's distortion greatly exceeds the values determined by the rezoning indicators, this might indicate the need to reduce the time step size. As the solution progresses and things improve the time step can then be increased. This would be especially true in impact problems at the point of impact. Even if the rezoning process is performed properly the necessity to alter the time step may still be present. Generally the change in time step should be small. A dramatic or constant change in the size reduction of the time step would indicate the solution process is having difficulty in reaching equilibrium. This can be the result due to the difficult nature in solving the problem or could be an indication that distorted elements are playing havoc with the solution process.

126

Changes in increment size may also be required for quasi static problems. Often times the increment size on the applied forces causes solution difficulties when the size of the force is large. When this occurs the number of iterations required to reach equilibrium increases dramatically. Generally one can determine an appropriate load increment size prior to execution of the problem. Distortions in elements may in fact mislead the solution by creating pseudo load unbalancing. This causes the solution process to continually reduce the load increment size in an unwarranted fashion.

The repeated reduction of the time step or the increment size, that would cause a halt to the solution process or drastically slow it down, has several implications. The implication of interest would be that the repeated reduction is due to difficulties encounter by distorted elements in the mesh. The study of this effect was implemented in this investigation to help determine at what time step or increment one should stop the solution and examine the mesh for distorted elements. The use of this technique provides a qualitative measure for validation of rezoning indicators derived from eigenvalue tests.

4.6.3 Plasticity Index Versus Strain Rate

A useful indicator in adaptive rezoning is that of a strain rate measure. Many times in the finite element analysis false readings of strain and especially strain rate can be obtained. The results have the appearance that the solution is proceeding in a correct fashion, when in reality the strain rate may be exceeding the capabilities of the material, and is beyond its failure point. If one, however, looks at the time response of the variables, a different picture may develop. Such a case might indicate the need for rezoning based on the fact that an insufficient number of elements are present or the distortions in the elements cause the strain rate measure to exceed its proper bounds.

The plasticity index plotted against the strain rate for the true material behavior can be used as a means to curb the regions of proper and improper material behavior. Comparisons between this plot and the models behavior can be examined. This measure of strain rate behavior compared to the plasticity index can serve as an effective rezoning indicator.

Given a region which exceeds the strain rate capability one could determine first if the material has failed or if the elements are so distorted that they provide erroneous results. If there are distorted elements in this region marked by excessive strain rate

128

then one could use the plot of the plasticity index versus the strain rate to determine how much error there is in the model. This can be corrected and the mesh refined or corrected in this region.

The idea behind this is to refine the mesh in regions where the strain rate is high. In these regions differentials in strains will be high thus the region can more accurately be modeled and the discontinuities ironed out if the mesh is refined. The element distortions would be corrected along with the refinement process.

If the results of this rezoning measure are correlated with those of eigenvalue test rezoning indicators, then one can assume that eigenvalue test rezoning indicators can also make corrections to the finite element model to avoid the use of incorrect strain rates. Unfortunately no reference material was available for this type of rezoning process. This rezoning measure was not used in this investigation for the verification of eigenvalue test rezoning indicators.

CHAPTER 5

MESH MANIPULATION IN SELF ADAPTIVE REZONING

5.1 Introduction

The mesh manipulation procedure or remeshing process
of the rezoner provides the means to generate a new mesh
filled with valid and well shaped elements. The rezoning
indicators serve as identifiers of regions to be rezoned
as well as how the rezoning should take place within that
region. The region can be rezoned by reshaping the
existing elements, refining the mesh in the region, or by
a combination of both. Generally the region is selected
so that the boundary to this region is surrounded by
existing valid elements which will not be distorted
themselves within a number of time steps or increments
further into the solution process.   This helps to reduce
the number of rezonings that would be required. This
process permits elements near distortion to be reshaped
and thus be usable in an increased number of time steps
or increments than if left unrezoned. This is a
necessary requirement.

Once the mesh region to be rezoned has been
identified than a meshing technique is implemented to

generate the new mesh. The form, shape, and number of
elements of the new mesh is generated by the values of
the rezoning indicators when compared to the past,
present, and future states of deformation in the
elements.

5.2 Meshing Techniques

Many schemes or techniques exist to perform finite
element mesh manipulation or remeshing. Various mapping
techniques such as transfinite, laplacian, isoparametric
and conformal mapping are examples of such schemes.
Others that have been successful are subdivision by
quadtree encoding, a least squares method, and various
adhoc meshing methods [40-50].

One technique that has received much attention and
is vary powerful is that of non-uniform rational
b-splines or NURBS. NURBS can be used not only to
generate sculptured surfaces, but the technique has the
ability to fit a given set of data. A combination of
these qualities is required in a remeshing scheme. One
must fit the new mesh into a region of existing nodes and
elements. A match up to the nodes and elements which are
present and not part of the rezoning process is an
essential requirement. A fit to existing node points is
therefore required. A mesh must formed within the
boundary defined by these nodes of the old mesh which

were not included in the rezoning process. In this case the sculptured surface creation techniques of NURBS comes in handy.

NURBS have the properties of allowing local changes within a surface without effecting the rest of the surface. This allows one to use NURBS to locally move nodes about in order to optimize the shape of the remeshed region. NURBS generally follows the shape of the defining polygon, that is they exhibit strong convex hull properties. They can therefore be effective in matching up to the existing nodes and elements. The order of the fit is only limited by the number of points given in the definition of the NURBS surface. This allows for meshing of complex regions [51].

It is believed that NURBS used in some adhoc fashion or in combination with other schemes would provide an ideal mesh manipulation tool for rezoning. Many CAD and finite element pre and post processors utilize NURBS to be able to create a variety of surfaces. The control in using and fitting a NURBS surface to a given regions is excellent. This characteristic makes it an ideal choice for remeshing in the rezoning process. A combination of element reshaping as well as mesh refinement is generally required, and would be of no problem implementing an adhoc version of NURBS in possible combination with another mapping technique. To implement this in an

132

automatic fashion where the rezoning indicators are dictating how the NURBs formed mesh is generated, is at a minimum to say, a very difficult task.

5.3 Location and Manner of Remeshing

The determination of the where and how to remesh a given region of a finite element mesh, can in most cases be controlled by the rezoning indicators. This will not always be the case but a few simple rules can be implemented where the rezoning indicators can be used in the majority of the cases of remeshing elements that are flagged for rezoning.

First, it is desired that the new mesh be better than the previous mesh. Furthermore, it is desired that the region of the new mesh not require rezoning only after a couple of increments or time steps. This may not be possible in regions which involve a great amount of change on a constant basis. The rezoning process should still provide the best mesh for the given situation.

The region of rezoning must at a minimum cover all the distorted elements. Numerous localized regions or entire sections of the mesh can be considered. As a rule of thumb those elements which surround the distorted elements and surround those elements which are close to or approaching the limits set by the rezoning indicators, but do not fall into this category, should form the

133

boundary of the mesh rezoning region. According to Saint Venants principle the effect of a poor element is localized. As long as the local region of its effect is remeshed correctly then proper rezoning has taken place. The idea is to obtain a rezoning region of the mesh where the boundary nodes and elements to the region behave properly. When this region extends to the physical boundary of the mesh then this physical boundary must be maintained during the rezoning. Nodes and elements can shift along the boundary but must adhere to this physical dimension.

The amount of reshaping of the elements and refinement of the mesh is determined from the rezoning indicators. In some instances the physical geometry of the problem or the remeshing technique used may prohibit the amount of rezoning specified by the rezoning indicators. In this regards it is important to build in rules which apply to such cases. Generally the indicators will provide an indication of the amount of rezoning to be done and the remeshing technique employed should stay with in those bounds. When difficulties arise in this type of situation, the region of rezoning can be enlarged to include more of the valid elements if possible. This increases the total rezoning region in an effort to overcome any remeshing difficulties. Another solution is stay with in the specified regions but refine

the mesh. Increasing the number of elements in a given region may also aid in overcoming remeshing difficulties.

5.4 Updating the Finite Element Database

A key feature to the rezoning process is the ability to access and change the model database. First, access is required in order to examine the finite element mesh. Second, as the rezoning process occurs one must be able to update the newly rezoned regions into the finite element model. This means the deletion, creation, and movement of nodes and elements while still maintaining the linking relationships between the nodes and elements of the mesh. Generally a renumbering and relabeling of the nodes and elements will be required. The old mesh and its nodal and element values must also be stored as part of the rezoning process so that a comparison and remapping of the element variables can occur. This process is a simple bookkeeping technique.

5.5 Implementation of a Remeshing Technique

The remeshing technique described in this chapter can be effectively used in a self adaptive rezoning algorithm. As mentioned in Chapter 4 the implementation of such an algorithm would be at the level of creating an expert system. There are a lot of judgements to be considered in order to optimize the remeshing phase of

135

self adaptive rezoning. Each remeshing sequence of the rezoning process calls for a unique new mesh to be created. This, in combination with the infinite number and types of problems which involve rezoning, calls for a remeshing algorithm which has artificial intelligence.

Utilizing the rezoning indicators to determine the regions of the mesh to be remeshed is fairly straight forward. The difficult part is determining how to generate the new mesh in the rezoning region and do so in an optimized fashion. One must also consider if the variables from the old mesh can properly be transferred to the new mesh based on the layout of the new mesh, not on the remapping procedure. A user of a rezoner would not have much difficultly in performing this task if supplied with the proper data. This data is the results of examining the old mesh with the rezoning indicators. The important part is that this information is not only gathered for the present state but also for future states, and even past states of deformation. This allows the user to make judgement calls on how to create the new mesh. The data supplies information on the patterns of deformation within the mesh throughout a given portion of the solution. This data can therefore be used for information on how and when elements become distorted. This lets the user make judgement calls on how to best optimize the new mesh region. To create an algorithm to

136

take the users place and automate the process, is at best a tremendous undertaking and one not suited for this investigation.

In this investigation the focus has been placed first on the determination of rezoning indicators derived from eigenvalue tests of quadrilateral elements. The next level of emphasis was to define a specific technique required to obtain a self adaptive rezoning process. The remeshing phase for this investigation was built on an approach which required user intervention. The user takes the place of the so called expert system or artificial intelligence that would be required by a self adaptive remeshing algorithm. All judgements regarding how to remesh were based on results of the rezoning indicators. The user generates the mesh utilizing either a CAD program or a finite element pre and post processor. With a little work the user can arrive at an optimized mesh. This procedure was used in this investigation.

AutoCAD, a computer aided design program was used to help create the new meshes. Several drafting techniques and surface mesh routine within AutoCAD aided in the generation of new meshes. The old mesh was used as a template for the creation of the new mesh.

CHAPTER 6

REMAPPING OF VARIABLES TO THE REZONED MESH

6.1 Remapping Techniques

The final step to complete the rezoning process is to remap the nodal and element variables from the old mesh onto the new mesh. The solution process can then restart at the time step or increment which was flagged for rezoning.

Most remapping techniques use some type of interpolation, least squares fit or weighted parameters based on the position of the old mesh to that of the new mesh. The remapping process restores the values of the element variables at the new locations. Generally if the interpolation scheme utilized is based on the same interpolation function of the elements then the procedure works well. Remapping need only occur in the mesh regions which received changes from the rezoning process and not over the entire mesh [12, 20, 21, 52, 53].

Some finite element codes, which include interactive rezoners, have algorithms which allow the remapping or interpolation of the old mesh to the new mesh. It is clearly advantageous to use a built in remapper if it is

138

available and deemed to be appropriate. In most cases
these remapping schemes are created to provide the best
remapping possible for the given mesh with consideration
to computational effort. In this investigation the
remapping scheme in ABAQUS' finite element code was used.

The interpolation or remapping technique used in
ABAQUS is as follows [18]. One must obtain all the
element variables at the nodal locations. This is done
by extrapolating all the values from the integration
points to the nodes and then averaging the values of all
the elements that interface at that given node. One then
determines the integration points of the new mesh with
respect to the nodes of the old mesh. The element in
which a old mesh nodal point lies is found, and its
location in new element is determined. The variables are
then interpolated from the node of the old mesh to the
integration point or points of the new element. All the
variables are automatically interpolated within the
ABAQUS code. This is true for quasi static problems.
The remapping technique, however, was not implemented in
ABAQUS for dynamic problems. Dynamic problems, therefore
require the user to remap dynamic related variables such
as the velocities. For dynamic problems the strains, and
stresses are still remapped automatically.

A point of caution must be made. Like many visual
post processing results which average variables at the

nodes, remapping techniques which do likewise may in fact be smoothing over discontinuities in the solution. This very technique may introduce inaccuracies into the solution. For the most part the inaccuracies would only occur if the jumps or discontinuities at the nodal points are extreme in relative value. The rezoning process itself should continually correct the mesh such that these extremes in values would never be generated. The values averaged at the nodal points would therefore be relatively small in comparison. Proper and timely rezoning should avoid the "smoothing over" of discontinuities that might occur in the remapping phase.

6.2 Remapping as a Quality Control on Rezoning

As previously mentioned, when jumps or discontinuities in element values appear in the newly remapped region, this is an indication of either improper interpolation of the variables during remapping or that improper, insufficient, or belated rezoning has occurred. Either the element shapes were improper or more than likely the mesh was insufficiently refined. Lack of refinement is usually associated with discontinuities in the solution. On the other hand the rezoning process can be applied too late, letting too much distortion take place within the elements. A combination of these effects is also possible.

140

A quality control on the rezoning process can be achieved by examination of the element variables on the newly remapped region. This process in its own right can be included as a rezoning indicator. If this quality control indicator, the check for discontinuities in variables at the nodal locations, determines that there are discontinuities then one must rezone again, or even step back a few time steps or increments and then rezone. This assumes that the discontinuities were not caused by the remapping or interpolation of variables, but were due to lack of rezoning or element distortions. This same quality control may also indicate a need to change the time step or increment size.

CHAPTER 7

TEST PROBLEMS

7.1 Class of Large Deformation Problems

The class of problems that can be used as test examples of the rezoning process are those which involve large deformation, and finite strains. Impact and metal forming processes are typical of this class of problems. They would be representative of typical dynamic and quasi static problems involving large deformations and strains. Selecting a standard high strength steel as the material to be used in these problems allows one to use many of the elastic-plastic models that presently exist. ABAQUS contains all the key ingredients to solve this type of problem and is set up to be able to implement the adaptive rezoning algorithm. Two test problems have been selected as candidates to test the method of rezoning developed in this investigation. Rezoning indicators derived from eigenvalue tests were used in the rezoning process of these test problems to verify and validate their quantitative values as wells as their qualitative value to the self adaptive rezoning process.

7.2 Upsetting Billet - A Metal Forming Problem

The first problem involves the upsetting of a cylindrical billet. This is a classical metal forming problem in which a small cylindrical billet of metal is squeezed between two flat rigid dies. The rigid dies are modeled by flat rigid surfaces which are perfectly rough. Empirical data for similar problems exist in the literature [14, 15, 54]. This problem serves as an excellent study of the rezoning process in a quasi static metal forming problem.

Figure 7.1 illustrates the geometry and finite element model of the upsetting cylindrical billet. The cylindrical billet is 30 mm (1.18 inches) long, with a radius of 10 mm (0.394 inches).
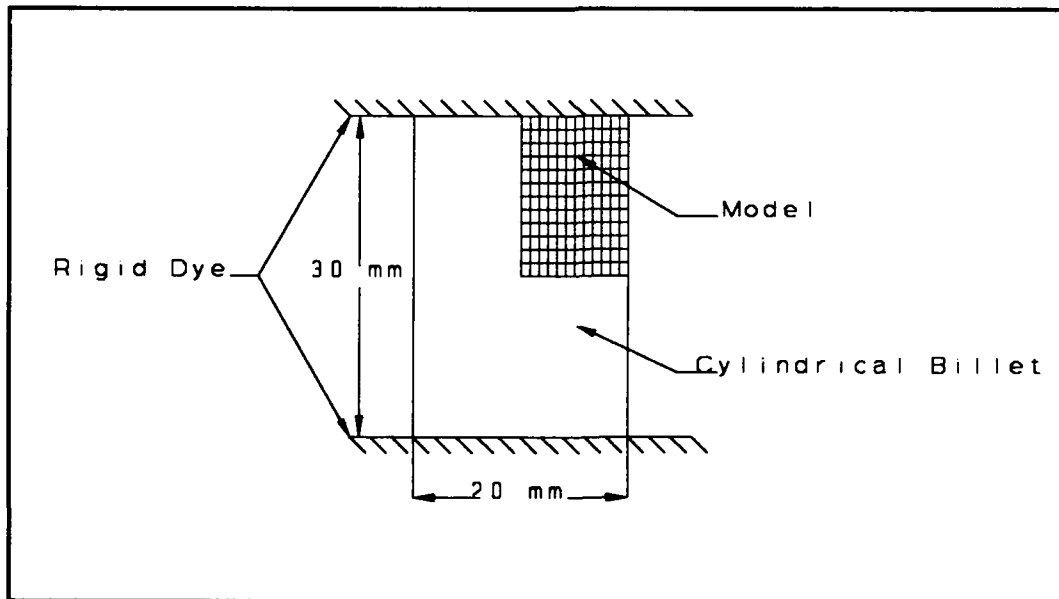
Figure 7.1. Model of the cylindrical billet

The material definition is the same that appears in
Lippmann [54] and in ABAQUS' example problems manual
[55]. The values correspond to typical steel and are
given in Figure 7.2.
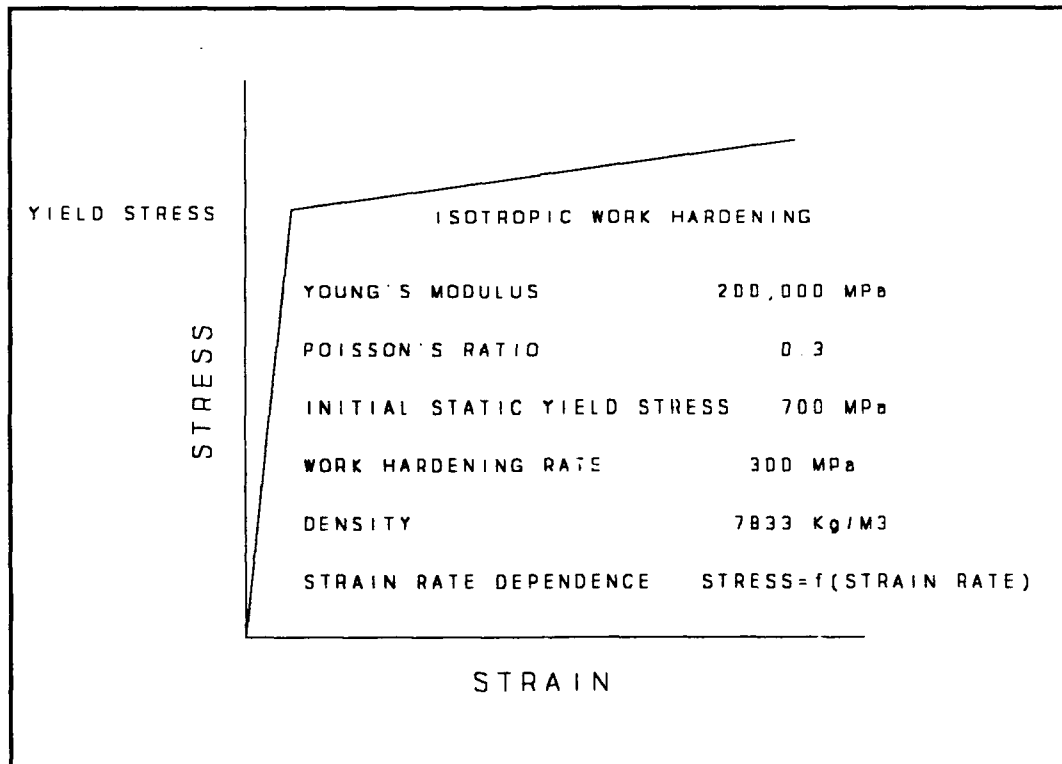
Figure 7.2. Material definition

The model uses four node, first order quadrilateral
elements. The elements used are axisymmetric elements.
As a point of interest the same problem could be run
using plane strain elements and hence plane strain
assumptions. In this case the model would represent a
long rectangular billet. The billet would be of such
length that plane strain assumptions can be applied.

144

This allows one to use nearly the exact same model used for this problem, with only slight modifications. This permits one to study a different element type with approximately the same model. The plane strain case of the problem was not computed since its results in relationship to rezoning parameters would not provide a great deal of new insights in comparison with the results using axisymmetric elements.

Due to the symmetry of the problem only one fourth of the cylindrical billet is modeled. The nodes along the central axis are constrained radially. The nodes along the midsection radius are constrained axially. There are a total of 169 nodes and 144 elements. The rigid surface is modeled to displace 9 millimeters axially downwards at a constant velocity. The total displacement of the rigid die or surface achieves a sixty percent reduction in the size of the cylindrical billet. Interface elements are used along the top surface for modeling the contact between the model and the rigid surface. The friction values between these two surfaces is modeled with very high values to achieve the perfectly rough surface contact. The definition of the finite element model in terms of the node and element numbers, and consequently the relationship between the nodes and elements is illustrated in Figure 7.3. Note that some node and element numbers are omitted for clarity. The

145

pattern for numbering, however, is quite clear. All
nodes and elements increase sequential across the mesh
and increase by a value of 100 in the vertical direction.
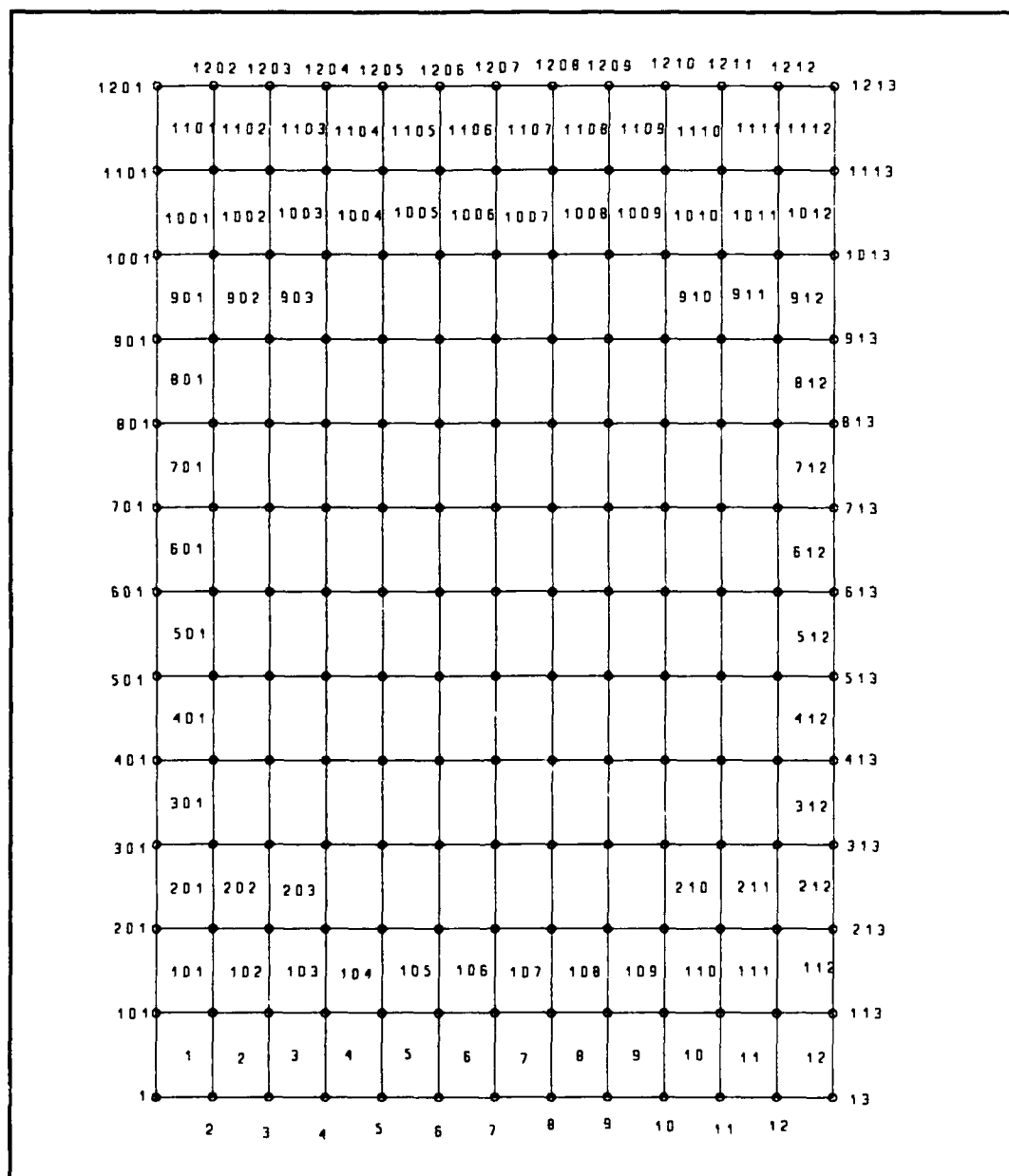
Figure 7.3.   Finite element model for the upsetting
billet problem

7.3 Results of the Upsetting Billet Problem

The upsetting billet metal forming problem was initially run without any rezoning used. The problem ran for forty increments. The problem ran to 93.9 percent completion as far as total percent traveled by the rigid die or surface which caused the billet to deform. The reason for failure to complete the analysis was due to excessive element distortions. This created numerical difficulties and excessive repeated attempts to reach equilibrium in the solution algorithm. This caused the solution process to terminate.

Figure 7.4 contains the deformed mesh at the point at which the solution was terminated. All elements that exceeded the distortion limits set by the rezoning indicators are shown with a dense double cross hatched pattern. Thirty-six elements were flagged as being too distorted. This is approximately twenty-five percent of the total number of elements in the mesh. One taper ratio violation, thirty-six skew angle violations, and two inverted elements were detected by the rezoning indicators. Sixteen elements were within twenty percent of the distortion limit values. These sixteen elements were not included in the thirty-six flagged for rezoning by the rezoning indicators. These elements appear as the lightly cross hatched elements in Figure 7.4.
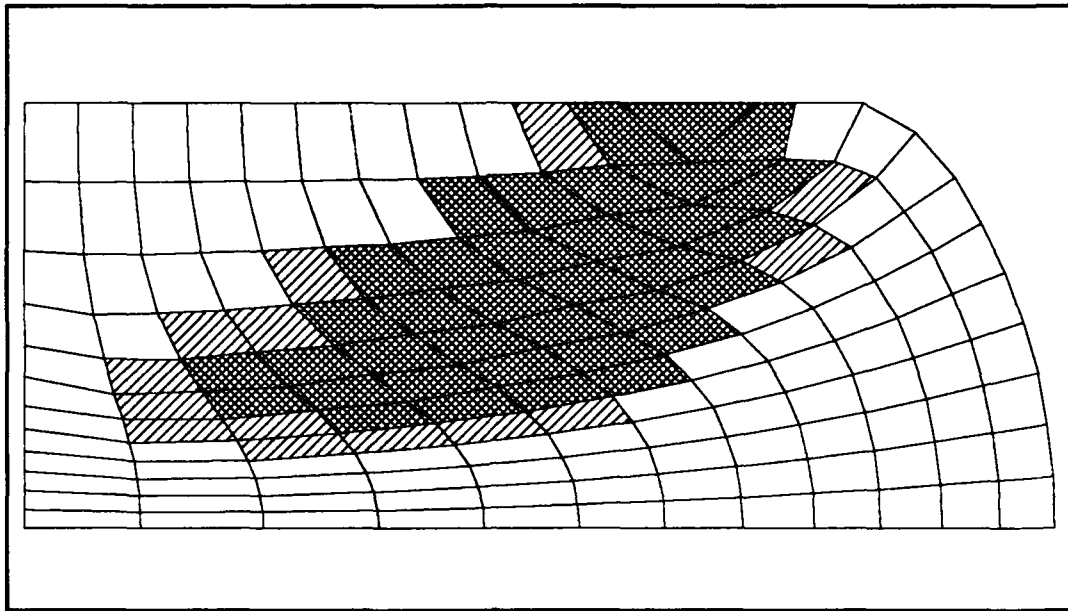
Figure 7.4. The mesh of the upsetting billet at the point of termination for the nonrezoning case

Figure B.1, Figure B.2, and Figure B.3, found in Appendix B, are contour plots of equivalent plastic strain, Mises stresses, and strain energy density respectively, for the final increment of the nonrezoning case before termination of the solution. Table B.1 of Appendix B contains a listing of strain jump values at the nodes of the element which were flagged for rezoning and those within twenty percent of this mark.

The problem was run again, this time using the rezoning technique with eigenvalue test derived rezoning indicators. A total of seven rezones were required during the solution process. Once the mesh was flagged for rezoning the solution process was still allowed to run to completion or as far as possible. An interesting

148

note is that after the first rezone the solution ran to completion.

The first rezone occurred at increment number ten with a total of 37.7 percent of travel of the rigid die completed. One element exceeded the rezoning indicator limits. This was a skew angle violation. This element is shown as the dense double cross hatched element in Figure 7.5. No elements were within twenty percent of reaching the distortion limits.
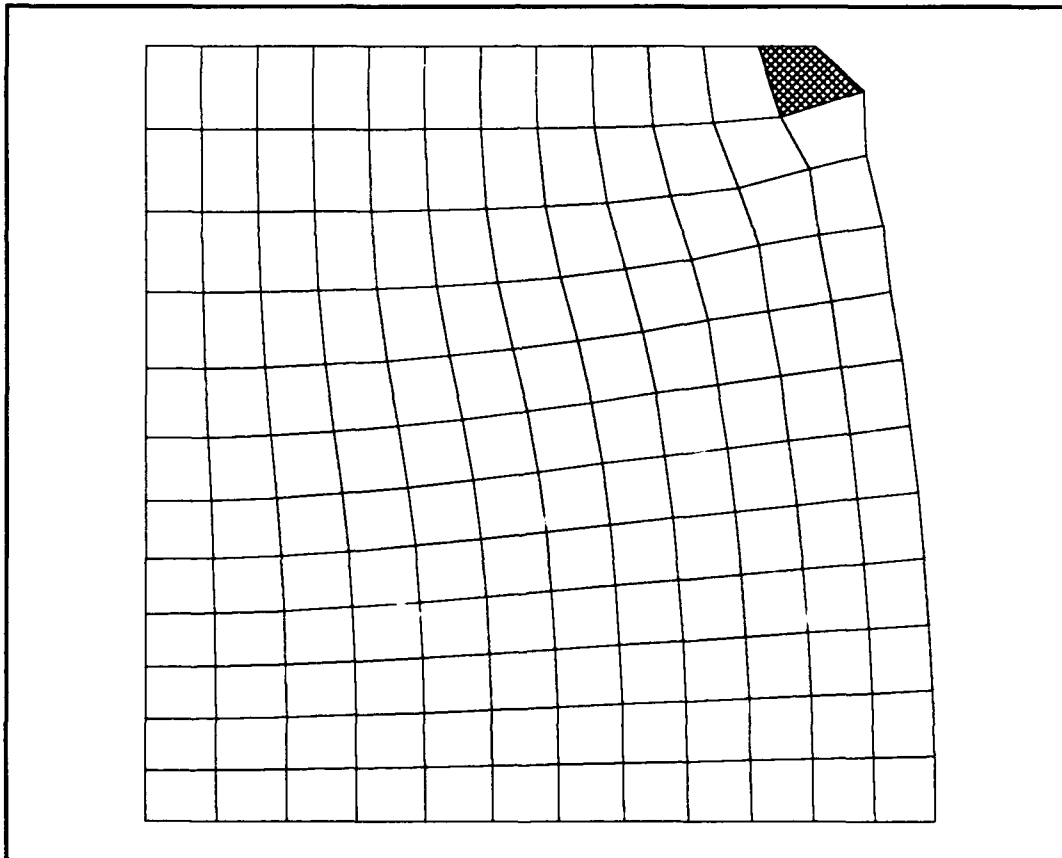
Figure 7.5. The mesh of the upsetting billet at the point of the first rezoning

149

Figure B.4, Figure B.5, and Figure B.6, found in Appendix B, are contour plots of effective plastic strain, Mises stress, and strain energy density respectively at the point flagged for the first rezoning. Table B.2 of Appendix B contains a listing of strain jump values at the nodes of the elements which were flagged for rezoning and those within twenty percent of the rezoning indicator values.

Figure 7.6 illustrates the new mesh that was created using the remeshing technique described in Chapter 5. The mesh changed from one hundred and forty-four to one hundred and sixty-five elements and from one hundred and sixty-nine to one hundred and ninety-three nodes. Fifty new nodes and sixty-five new elements were created. The old mesh variables were automatically remapped via ABAQUS' remapping algorithm.
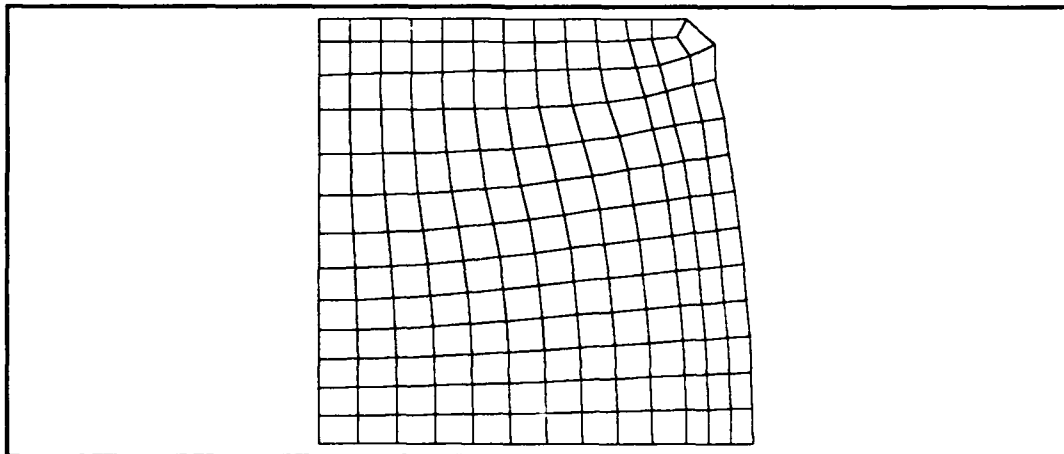
Figure 7.6.   The mesh of the upsetting billet after remeshing for the first rezoning

The second rezone occurred at increment number four after the first rezone with a total of 44.8 percent of travel of the rigid die completed. One element exceeded the rezoning indicator limits. This was a skew angle violation. This element is shown as the dense double cross hatched element in Figure 7.7. One element was within twenty percent of reaching the distortion limits. This is indicated as the less dense cross hatched element in Figure 7.7. One taper ratio of an element was within the twenty percent margin.
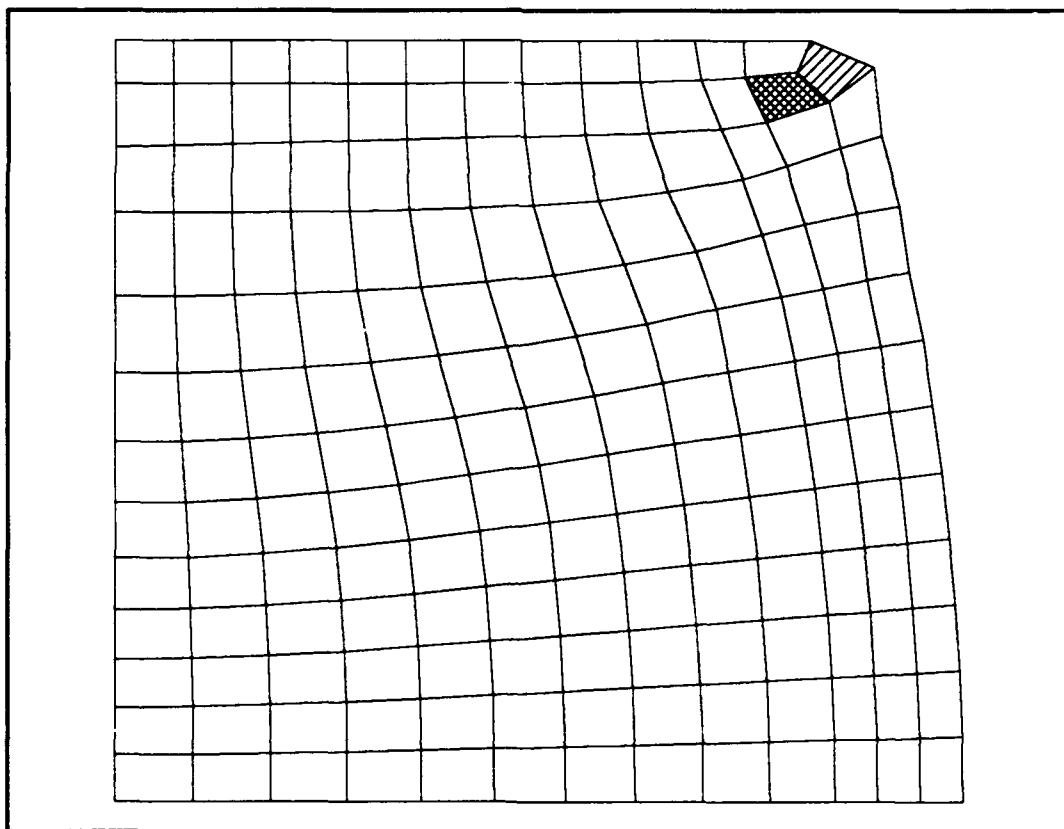
Figure 7.7. The mesh of the upsetting billet at the point of the second rezoning

151

Figure B.7, Figure B.8, and Figure B.9, found in Appendix B, are contour plots of effective plastic strain, Mises stress, and strain energy density respectively at the point flagged for the second rezoning. Table B.3 of Appendix B contains a listing of strain jump values at the nodes of the elements which were flagged for rezoning and for those that were within twenty percent of the rezoning indicator values.

Figure 7.8 illustrates the new mesh that was created using the remeshing technique described in Chapter 5. A total of six new nodal positions and thirteen new element positions were created in the remesh. No new elements were added to the mesh. The old mesh variables were automatically remapped via ABAQUS' remapping algorithm.
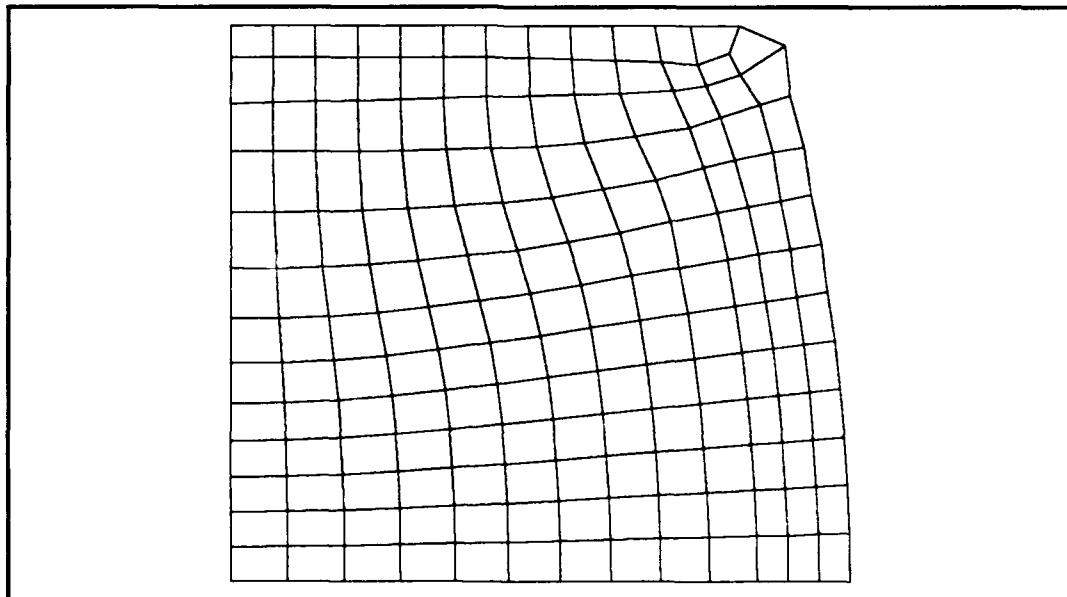
Figure 7.8. The mesh of the upsetting billet after remeshing for the second rezoning

The third rezone occurred at increment number five after the second rezone with a total of 61.2 percent of travel of the rigid die completed. Five elements exceeded the rezoning indicator limits. One taper ratio violation, and four skew angle violations were detected. These elements are shown as the most dense double cross hatched elements in Figure 7.9. A total of three elements were within twenty percent of reaching the distortion limits. These are indicated as the less dense cross hatched elements in Figure 7.9. Three skew angles of these elements were within the twenty percent margin.
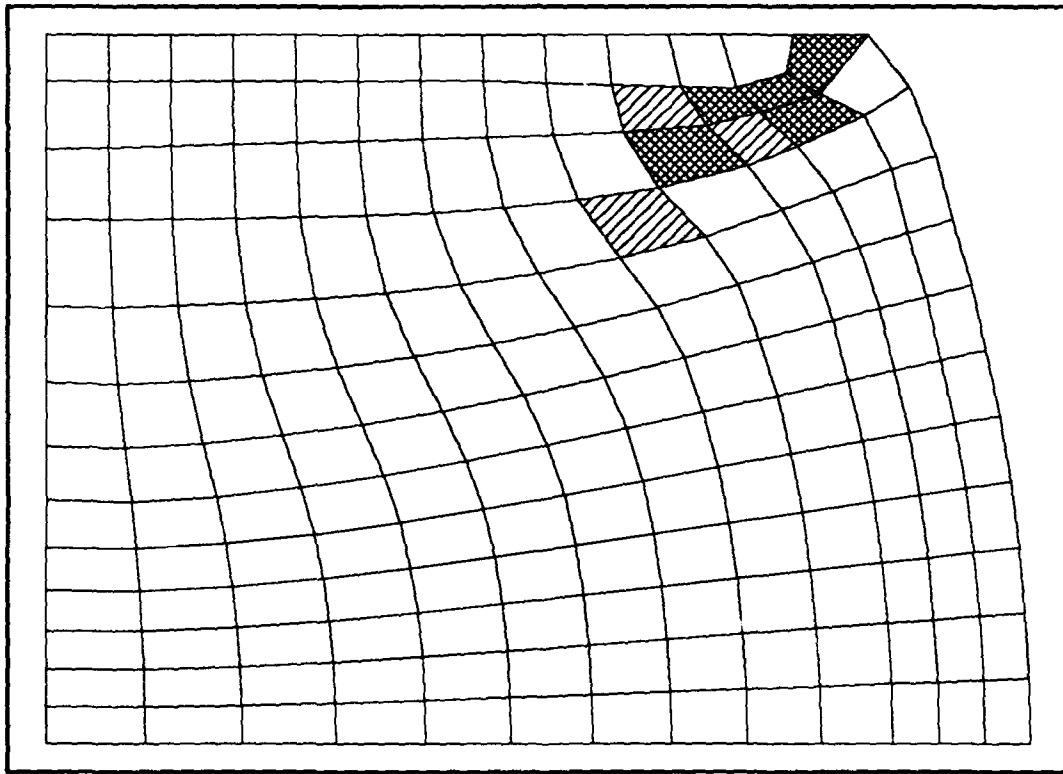
Figure 7.9. The mesh of the upsetting billet at the point of the third rezoning

Figure B.10, Figure B.11, and Figure B.12, found in Appendix B, are contour plots of effective plastic strain, Mises stress, and strain energy density respectively at the point flagged for the third rezoning. Table B.4 of Appendix B contains a listing of the strain jump values at the nodes of the elements which were flagged for rezoning and those which were within twenty percent of the rezoning indicator values.

Figure 7.10 illustrates the new mesh that was created using the remeshing technique describe in Chapter 5. The entire mesh was rezoned to help reduce future distortions. One hundred and fifty-five elements and one hundred and eighty nodes make up the new mesh. The old mesh variables were automatically remapped via ABAQUS' remapping algorithm.
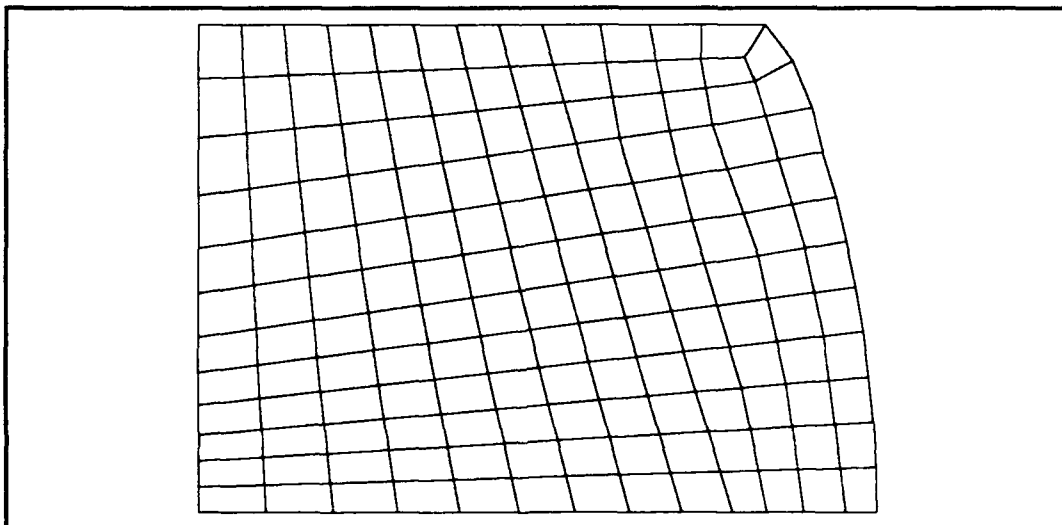
Figure 7.10. The mesh of the upsetting billet after remeshing for the third rezoning

The fourth rezone occurred at increment number four
after the third rezoning with a total of 69.7 percent of
travel of the rigid die completed. One element exceeded
the rezoning indicator limits. This was a skew angle
violation. This element is shown as the dense double
cross hatched element in Figure 7.11. A total of two
elements were within twenty percent of reaching the
distortion limits. These are indicated as the less dense
cross hatched elements in Figure 7.11. Two taper ratios
of these elements were within the twenty percent margin.
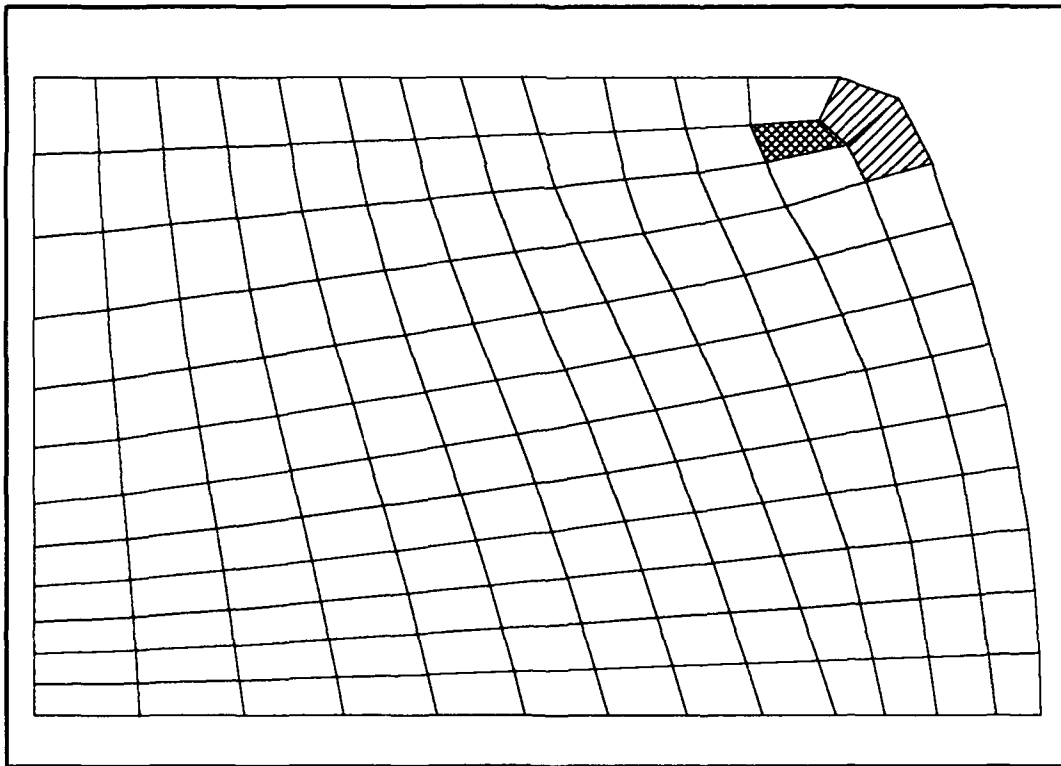
Figure 7.11. The mesh of the upsetting billet at the
point of the fourth rezoning

Figure B.13, Figure B.14, and Figure B.15, of Appendix B, are contour plots of effective plastic strain, Mises stress, and strain energy density respectively at the point flagged for the fourth rezoning. Table B.5 of Appendix B contains a listing of the strain jump values at the nodes of the elements flagged for rezoning and those within twenty percent of the rezoning indicator values.

Figure 7.12 illustrates the new mesh that was created using the remeshing technique described in Chapter 5. Twenty-eight elements were rezoned. No elements or nodes were added and twenty-one nodes were repositioned. The old mesh variables were automatically remapped via ABAQUS' remapping algorithm.
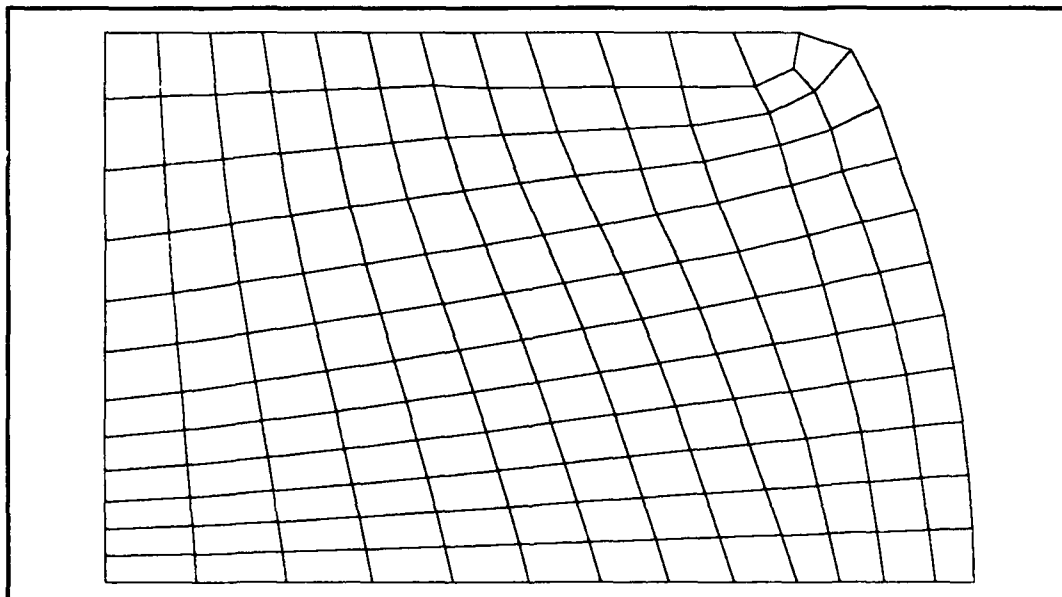
Figure 7.12. The mesh of the upsetting billet after remeshing for the fourth rezoning

The fifth rezone occurred at increment number five after the fourth rezone with a total of 78.5 percent of travel of the rigid die completed. One element exceeded the rezoning indicator limits. This was a skew angle violation. This element is shown as the dense double cross hatched element in Figure 7.13. A total of four elements were within twenty percent of reaching the distortion limits. These are indicated as the less dense cross hatched element in Figure 7.13. Three taper ratios, and three skew angles of these elements were within the twenty percent margin.
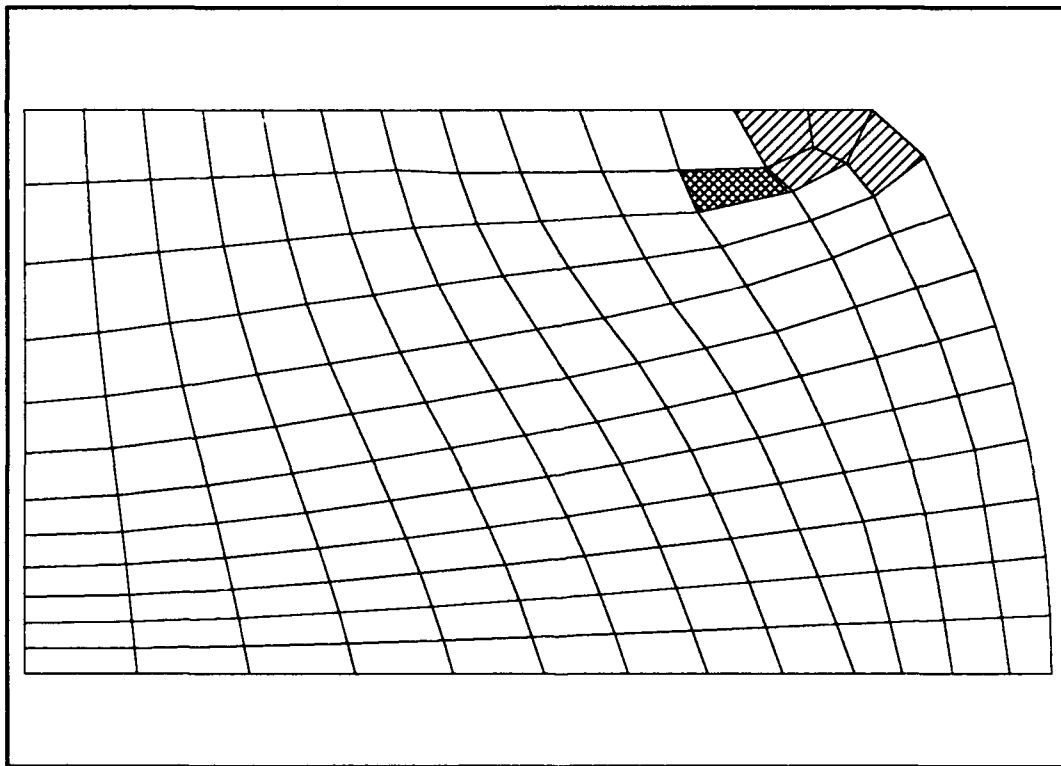
Figure 7.13. The mesh of the upsetting billet at the point of the fifth rezoning

Figure B.16, Figure B.17, and Figure B.18, found in Appendix B, are contour plots of effective plastic strain, Mises stress, and strain energy density respectively at the point flagged for the fifth rezoning. Table B.6 of Appendix B contains a listing of the strain jump values at the nodes of the elements flagged for rezoning and those within twenty percent of the rezoning indicator values.

Figure 7.14 illustrates the new mesh that was created using the remeshing technique described in Chapter 5. The entire mesh was totally rezoned to help reduce future distortions. A total of one hundred and seventy-nine elements and two hundred and six nodes are in the new mesh. The old mesh variables were automatically remapped via ABAQUS' remapping algorithm.
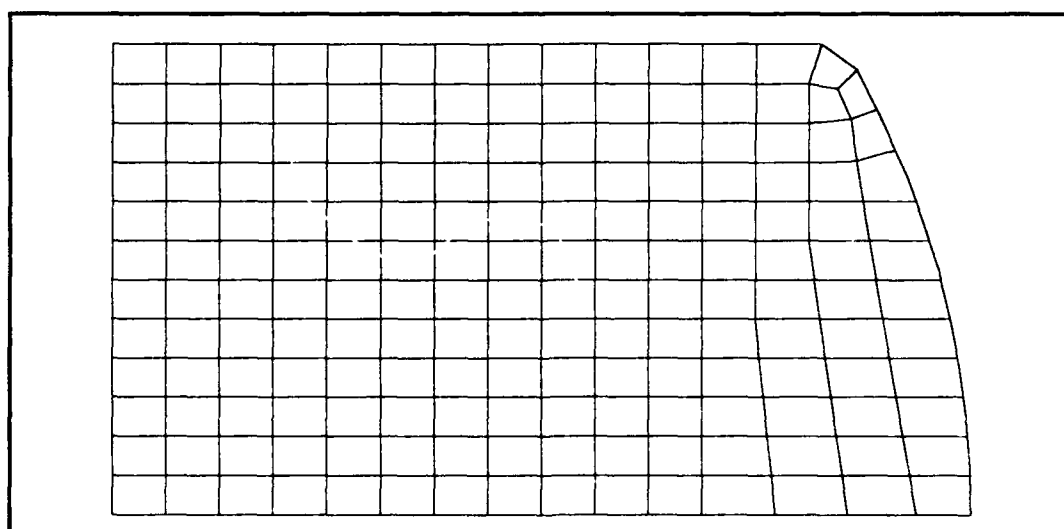
Figure 7.14. The mesh of the upsetting billet after remeshing for the fifth rezoning

The sixth rezone occurred at increment number six after the fifth rezone with a total of 89.4 percent of travel of the rigid die completed. No elements exceeded the rezoning indicator limits. A total of two elements were within twenty percent of reaching the distortion limits. These are indicated as the less dense cross hatched elements in Figure 7.15. One taper ratio, and one skew angle of these elements were within the twenty percent margin.
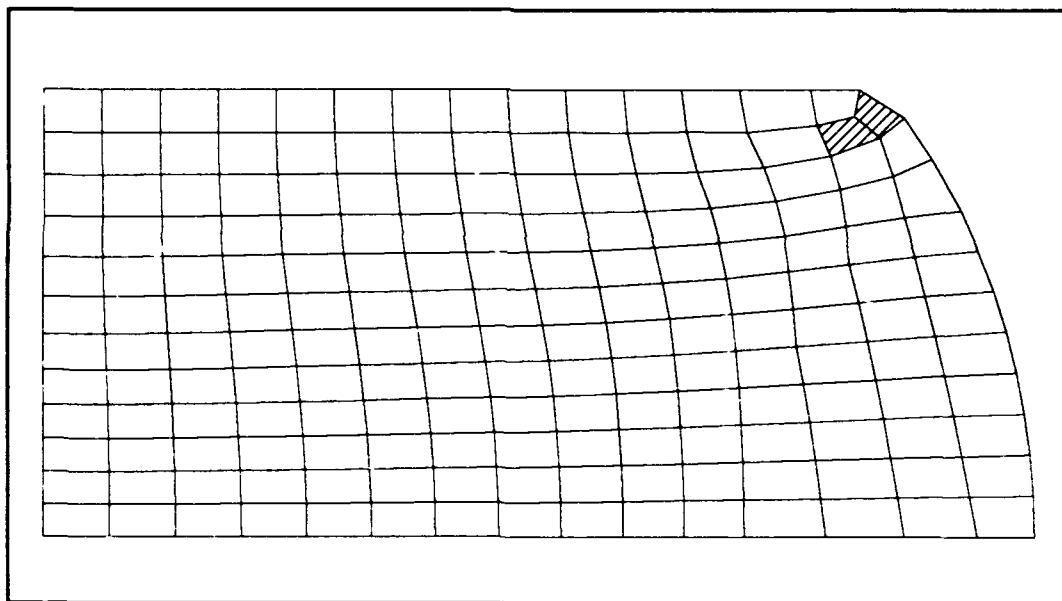
Figure 7.15. The mesh of the upsetting billet at the point of the sixth rezoning

Figure B.19, Figure B.20, and Figure B.21, found in Appendix B, are contour plots of effective plastic strain, Mises stress, and strain energy density respectively at the point flagged for the sixth rezoning.

159

Table B.7 of Appendix B contains a listing of the strain jump values at the nodes of the elements flagged for rezoning and those within twenty percent of the rezoning indicator values.

Figure 7.16 illustrates the new mesh that was created using the remeshing technique described in Chapter 5. A total of sixteen elements were rezoned. No new elements were added to the mesh and twelve nodal positions were changed. The old mesh variables were automatically remapped via ABAQUS' remapping algorithm.
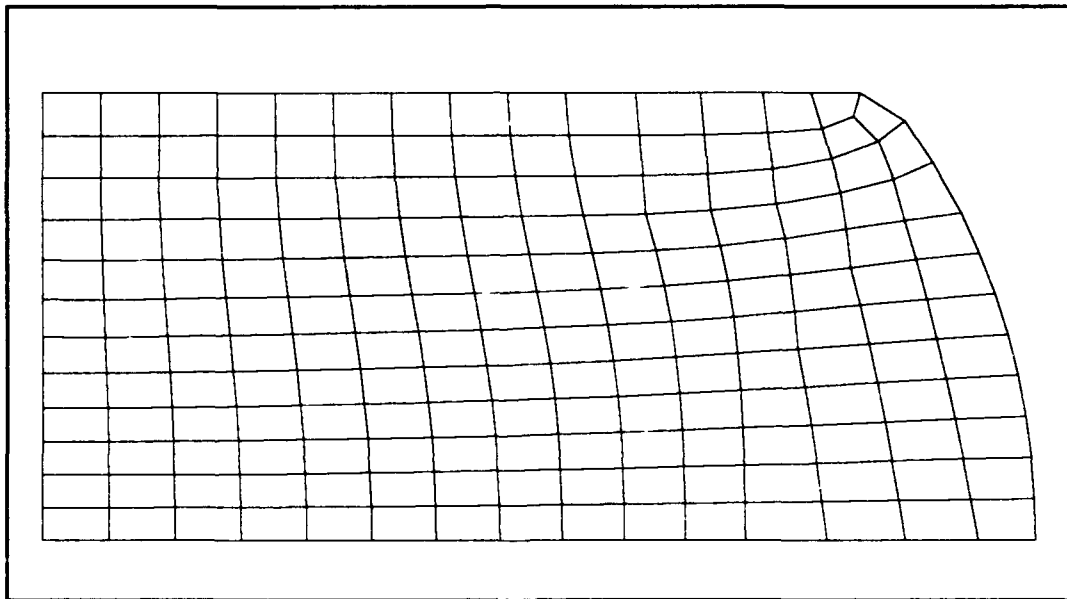
Figure 7.16. The mesh of the upsetting billet after remeshing for the sixth rezoning

The seventh rezone occurred at increment number three after the sixth rezone with a total of 94.5 percent of travel of the rigid die completed. Three elements

exceeded the rezoning indicator limits. One taper ratio violation, and two skew angle violations were detected. These elements are shown as the dense double cross hatched elements in Figure 7.17. No elements were within twenty percent of reaching the distortion limits.
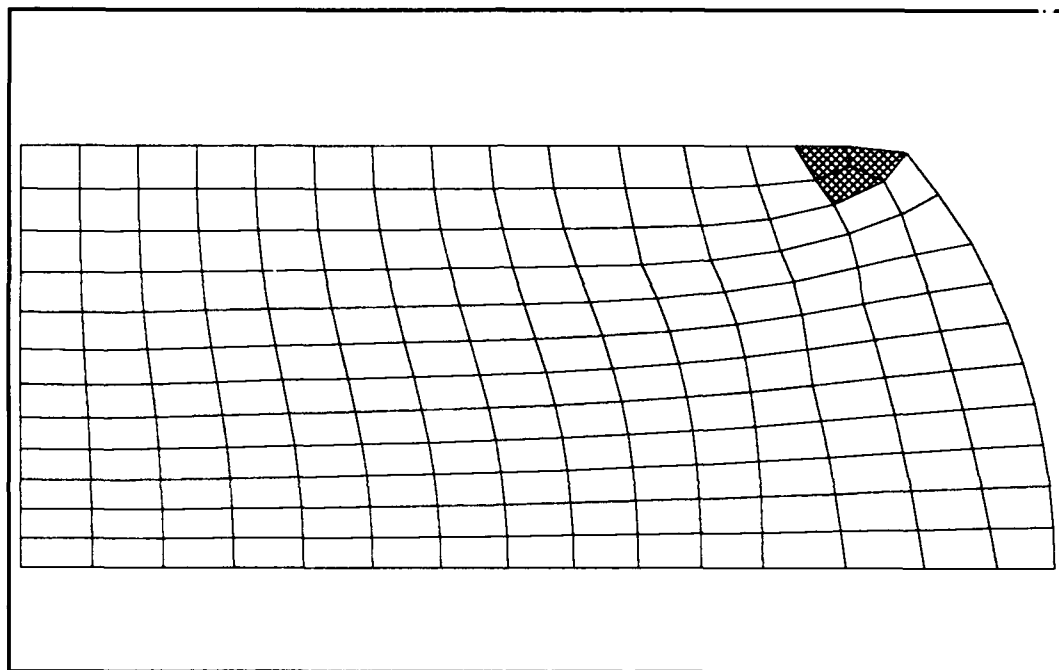
Figure 7.17. The mesh of the uosetting billet at the point of the seventh rezoning

Figure B.22, Figure B.23, and Figure B.24, found in Appendix B, are contour plots of effective plastic strain, Mises stress, and strain energy density respectively at the point flagged for the seventh rezoning. Table B.8 of Appendix B contains a listing of the strain jump values at the nodes of the elements that were flagged for rezoning and those that were within

twenty percent of the rezoning indicator values.

Figure 7.18 illustrates the new mesh that was created using the remeshing technique described in Chapter 5. A total of thirty-three elements were rezoned with one new element added to the mesh. Twenty-nine new nodal positions were created. The old mesh variables were automatically remapped via ABAQUS' remapping algorithm.
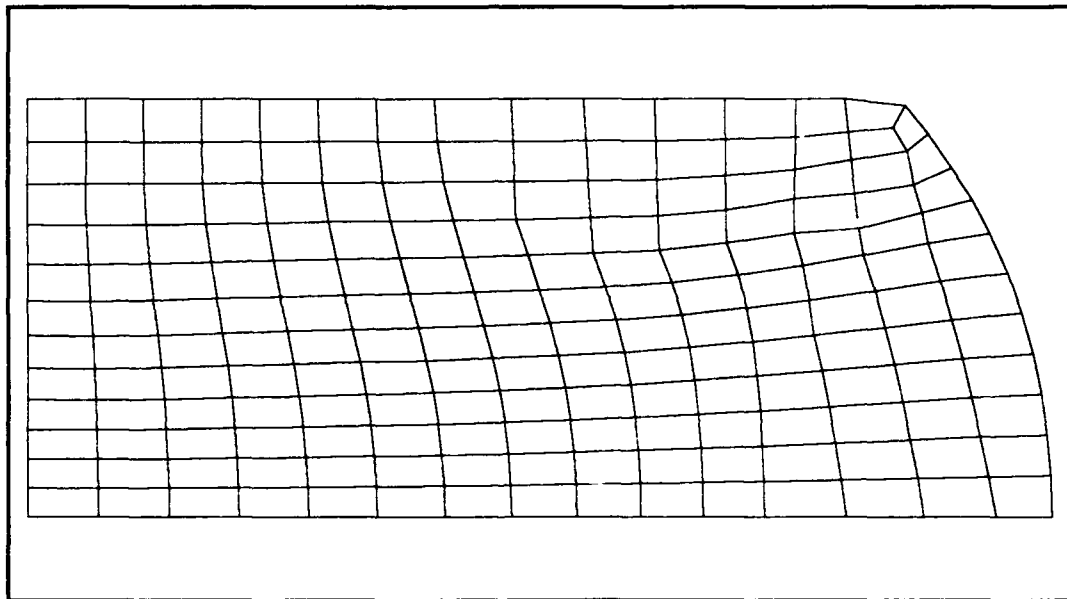
Figure 7.18. The mesh of the upsetting billet after remeshing for the seventh rezoning

The solution after the seventh rezone ran to completion in four more increments. The final mesh is depicted in Figure 7.19. Two elements just exceeded the rezoning indicator values. Both of these violations were skew angles. These are shown in Figure 7.19 as the dense

162

double cross hatched elements. A total of two elements were within twenty percent of reaching the distortion limits. These are indicated as the less dense cross hatched element in Figure 7.19. One taper ratio, and one skew angle of these elements were within the twenty percent margin.
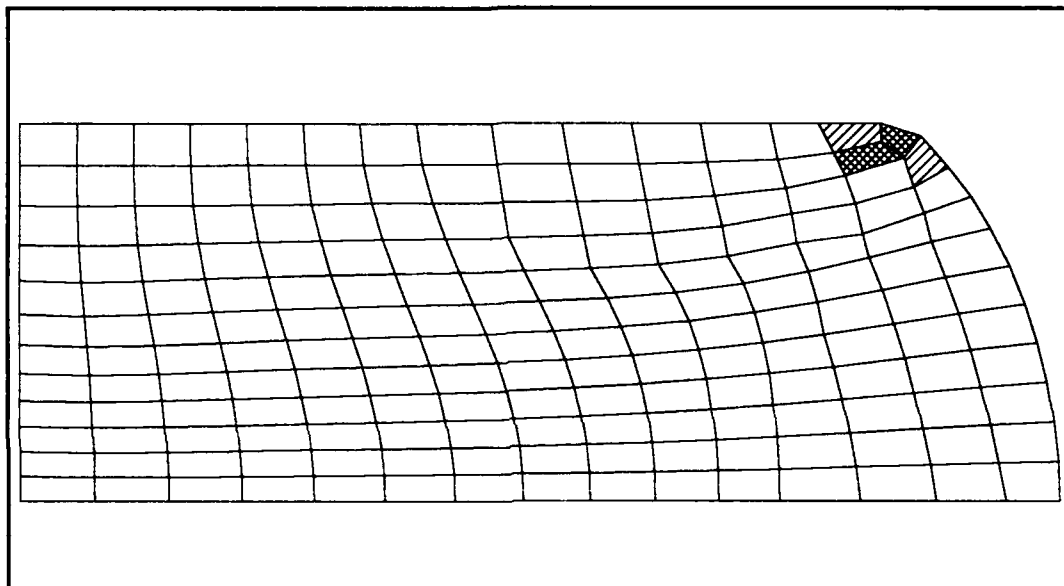
Figure 7.19. The mesh of the upsetting billet at the completion of the solution with seven rezonings

Figure B.25, Figure B.26, and Figure B.27, of Appendix B, are contour plots of effective plastic strain, Mises stress, and strain energy density respectively at the completion of the solution. Table B.9 of Appendix B contains a listing of the strain jump values at the nodes of the elements exceeding and within twenty percent of the rezoning indicator values.

163

7.4 Cylindrical Rod - An Impact Problem

The second problem involves a cylindrical rod impacting against a stationary smooth rigid surface. This is a dynamic problem. The geometry of the model is identical to the first problem illustrated in Figure 7.1 except for the rigid dies. Problems similar to this have been studied in the literature [11, 24, 56-60]. It can be thought of as a simulation of a bullet striking a rigid surface. This problem serves as an excellent study for the rezoning of dynamic related problems which involve large deformations and strains.

The material definition is identical to the first example problem illustrated in Figure 7.2. The strain rate dependence is more dramatic for this problem.

The finite element model is similar to the first example problem except for the fact that one half instead of one quarter of the model was used due to different symmetry conditions. This model initially contained one hundred and thirty-three nodes and one hundred and eight elements. The nodes along the vertical central axis are constrained radially. The rigid surface is modeled as a flat smooth surface which is stationary. The cylindrical rod has an initial velocity of 2,000 miles per hour or 894 meters per second. Impact speeds are large enough to create large deformations and strains. Interface

elements are used along the bottom edge of the rod
modeling the contact between the model and the rigid
surface. No frictional effects were included. The
finite element model is illustrated in Figure 7.20.
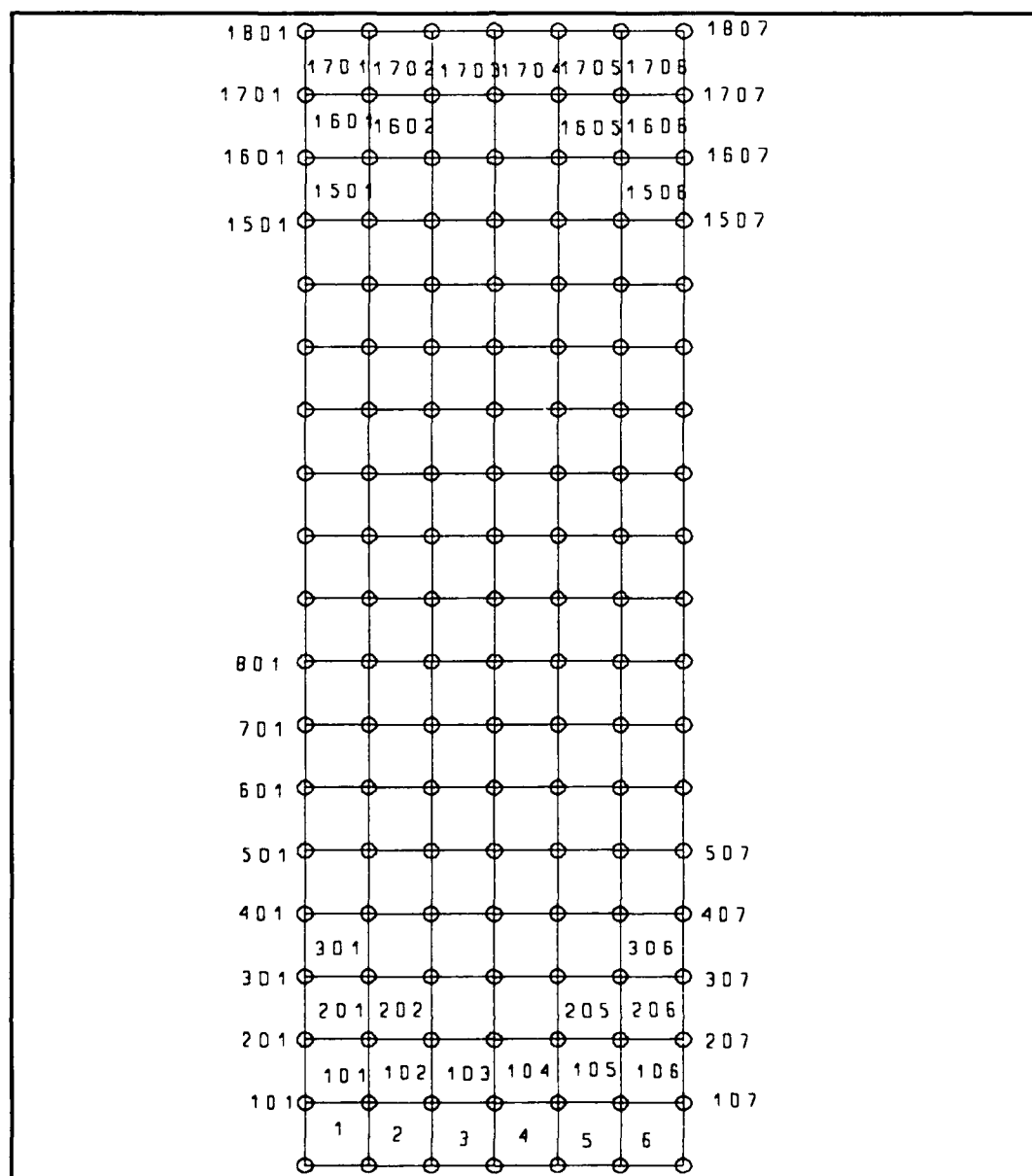
Figure 7.20.   Finite element model for the impacting
cylindrical rod problem

7.5 Results of the Cylindrical Rod Problem

The cylindrical rod impact problem was initially run without any rezoning used. The problem ran to completion in one hundred and thirty increments. The total time for the problem was one hundred microseconds. It should be noted that a good number of increments and time elapsed after the cylindrical rod had rebounded off the rigid surface. Several millimeters of distance of rebound was traveled prior to a total elapsed time of one hundred microseconds.

Figure 7.21 contains the deformed mesh at solution completion. Note that this would be in its rebounded state. Deformations and hence the element distortions may be slightly higher during impact. The difference should be negligible in terms of distortion. All elements that exceeded the distortion limits set by the rezoning indicators are shown with a dense double cross hatched pattern. Thirty-five elements were flagged as being too distorted. This is approximately 32.4 percent of the total number of elements in the mesh. Two aspect ratio violations, and thirty-three skew angle violations were detected by the rezoning indicators. Nine elements fell to within twenty percent of the distortion limit values. Of these values eight were skew angle values and one was a taper ratio value that exceed the twenty

percent margin.   These elements are lightly cross hatched
in Figure 7.21.
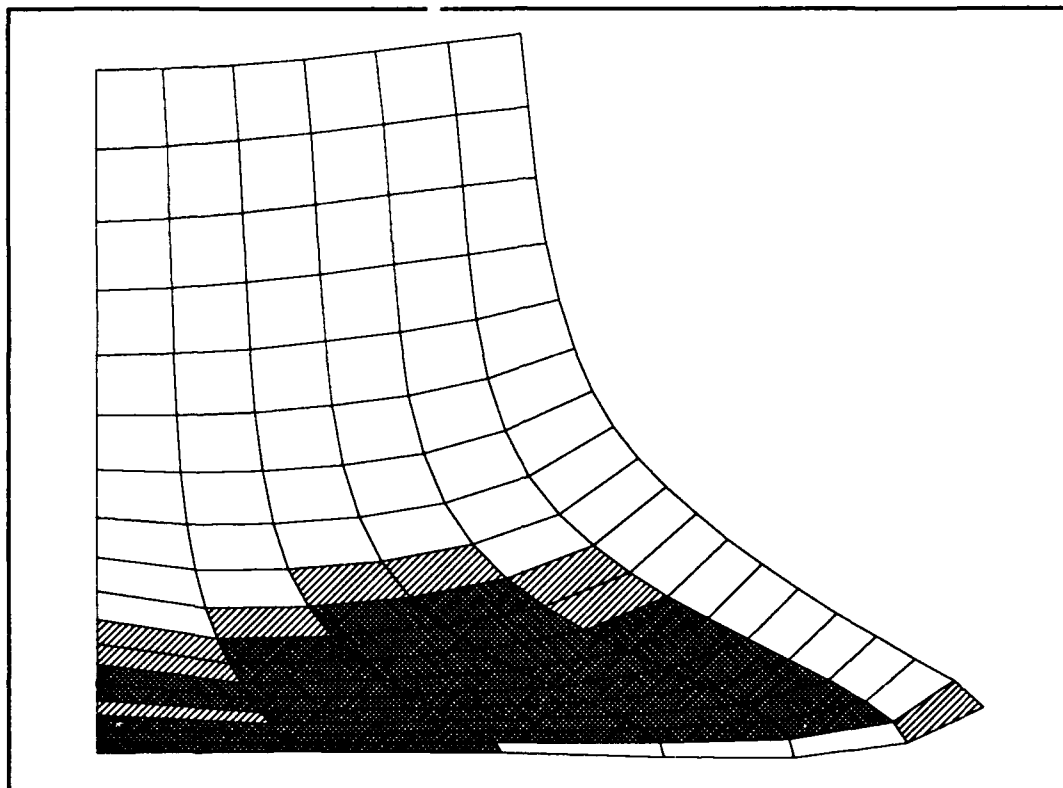
Figure 7.21.   The mesh of the cylindrical rod at the
completion of impact for the nonrezoning case

Figure B.28, Figure B.29, and Figure B.30, found in
Appendix B, are contour plots of equivalent plastic
strain, Mises stresses, and strain energy density
respectively, for the completed solution of the
nonrezoning case.   Table B.10 of Appendix B contains a
listing of the strain jump values at the nodes of the
elements that exceeded and were within twenty percent of
the rezoning indicator values.

167

The problem was run again, this time using the rezoning technique with eigenvalue test derived rezoning indicators. A total of two rezones were required during the solution process.

The first rezone occurred at increment number eighteen with a total of 6.048 microseconds of time elapsed. Two elements exceeded the rezoning indicator limits. Two skew angle violations were detected. These elements are shown as the dense double cross hatched elements in Figure 7.22. A total of four elements were within twenty percent of reaching the distortion limits. These are indicated as the less dense cross hatched elements in Figure 7.22. One taper ratio, and three skew angles of these elements were within the twenty percent margin.
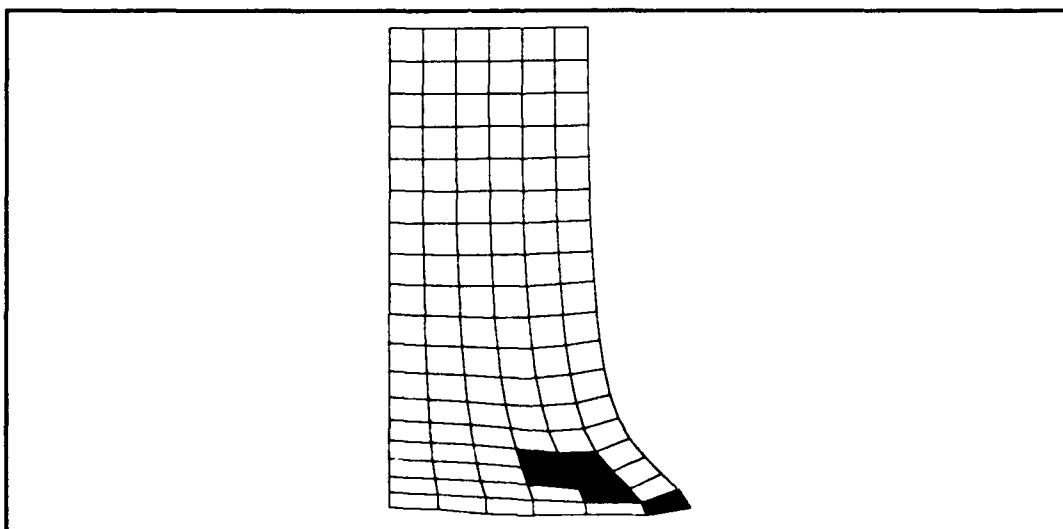
Figure 7.22. The mesh of the cylindrical rod at the point of the first rezoning

Figure B.31, Figure B.32, and Figure B.33, found in Appendix B, are contour plots of effective plastic strain, Mises stress, and strain energy density respectively at the point flagged for the first rezoning. Table B.11 of Appendix B is a listing of the strain jump values at the nodes of the elements that exceeded and that were within twenty percent of the rezoning indicator values.

Figure 7.23 illustrates the new mesh that was created using the remeshing technique described in Chapter 5. A total of fifty-two elements were remeshed. No new elements or nodes were added to the mesh. Fifty-five nodal positions were changed. The old mesh variables were automatically remapped via ABAQUS' remapping algorithm.
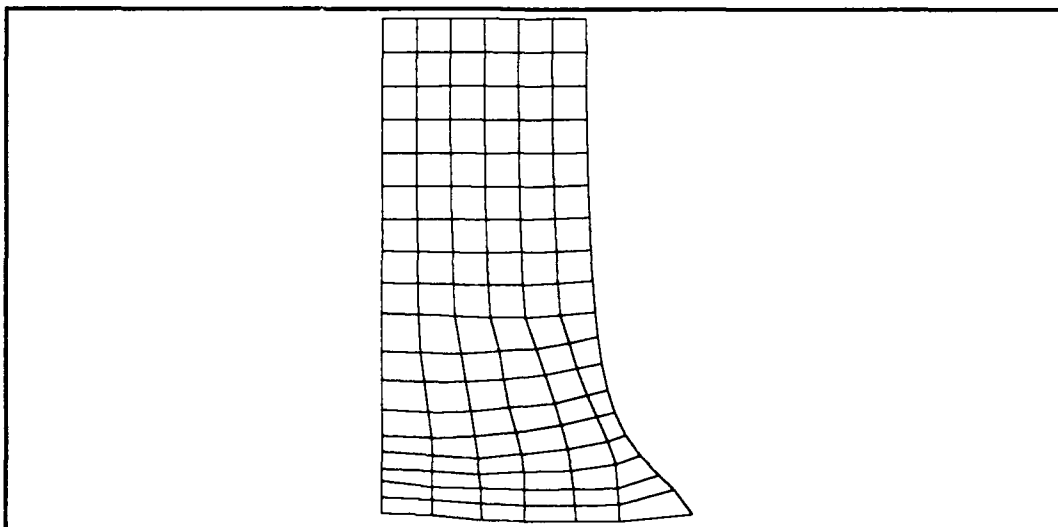
Figure 7.23. The mesh of the cylindrical rod after remeshing for the first rezoning

The second rezone occurred at increment number
twenty-three after the first rezone with a total of
16.758 microseconds elapsed. Twenty-two elements
exceeded the rezoning indicator limits. One taper ratio
violation, and twenty-two skew angle violations were
detected. These elements are shown as the dense double
cross hatched elements in Figure 7.24. A total of
thirteen elements were within twenty percent of reaching
the distortion limits. These are indicated as the less
dense cross hatched elements in Figure 7.24. Two aspect
ratios, three taper ratios, and nine skew angles of these
elements were within the twenty percent margin.
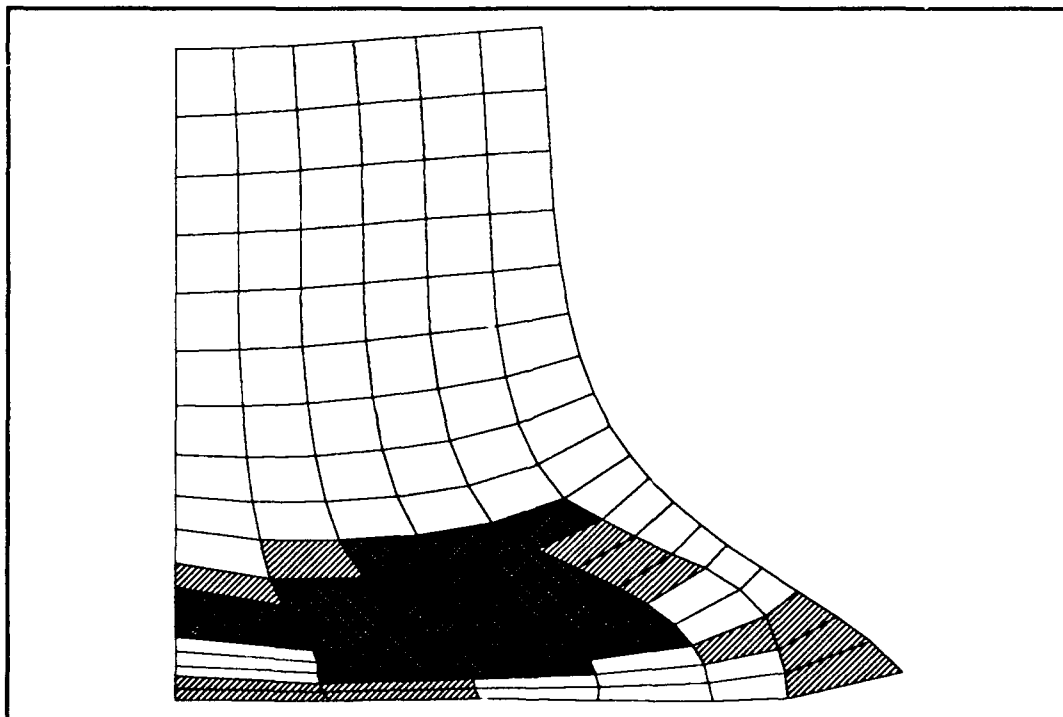
Figure 7.24.   The mesh of the cylindrical rod at the
point of the second rezoning

Figure B.34, Figure B.35, and Figure B.36, found in Appendix B, are contour plots of effective plastic strain, Mises stress, and strain energy density respectively at the point flagged for the second rezoning. Table B.12 of Appendix B contains a listing of the strain jump values at the nodes of the elements that exceeded and were within twenty percent of the rezoning indicator values.

Figure 7.25 illustrates the new mesh that was created using the remeshing technique described in Chapter 5. A total of sixty-nine elements were remeshed. No new nodes or elements were created in the new mesh. Fifty-nine nodal positions were changed. The old mesh variables were automatically remapped via ABAQUS' remapping algorithm.
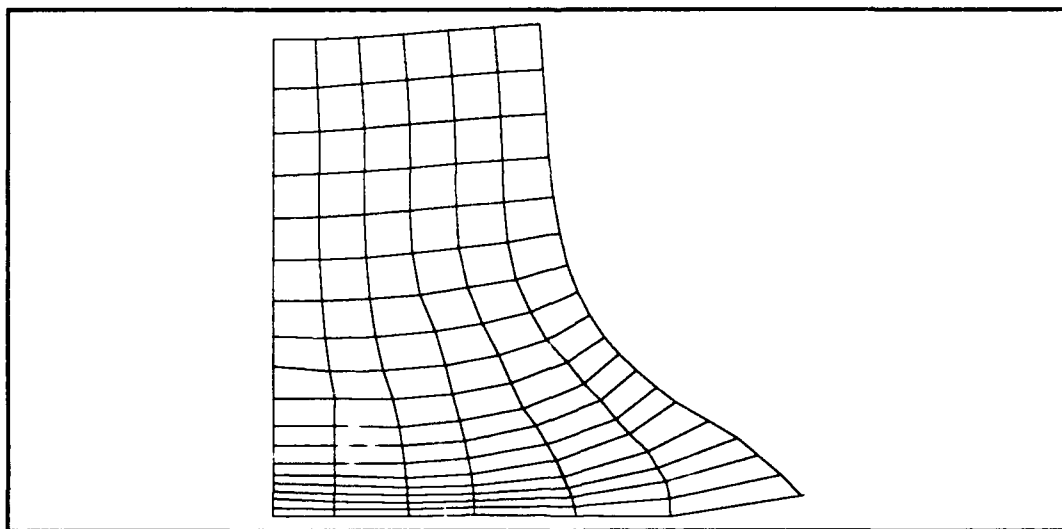
Figure 7.25. The mesh of the cylindrical rod after remeshing for the second rezoning

The solution after the second rezone ran to completion in sixty-four more increments for a final elapsed time of one hundred microseconds. Three elements were flagged by the rezoning indicators. Two exceeded the aspect ratio limits and one exceeded the taper ratio limits. In all three cases the values just exceeded the rezoning indicator values. These elements are depicted in Figure 7.26 as the dense double cross hatched elements. A total of thirteen elements were within twenty percent of reaching the distortion limits. These are indicated as the less dense cross hatched elements in Figure 7.26. Two aspect ratios, eight taper ratios, and seven skew angles of these elements were within the twenty percent margin.
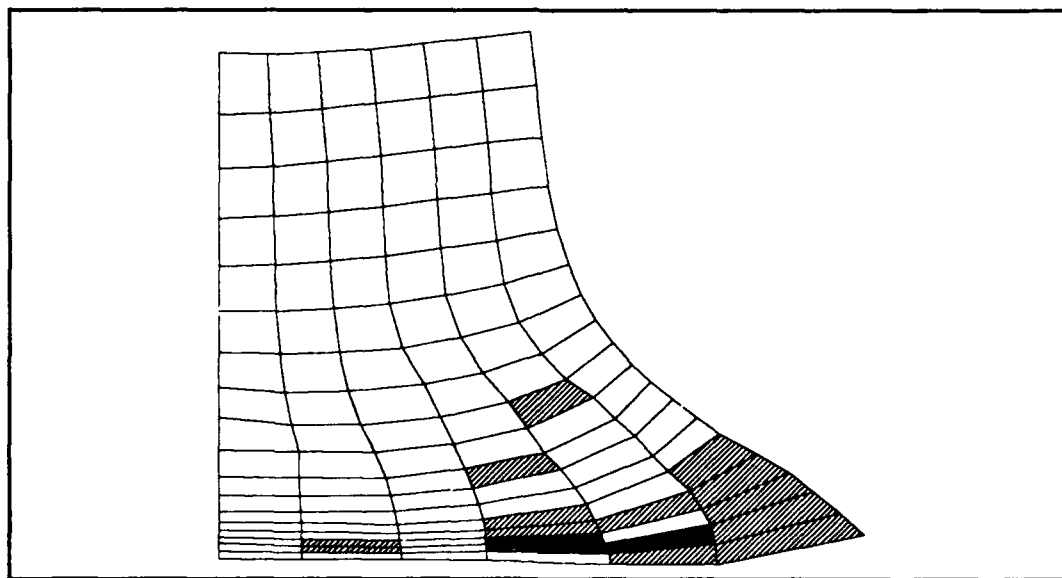
Figure 7.26. The mesh of the cylindrical rod at the completion of the solution with two rezonings

Figure B.37, Figure B.38, and Figure B.39, found in Appendix B, are contour plots of effective plastic strain, Mises stress, and strain energy density respectively at the completion of the solution. Table B.13 of Appendix B contains a listing of the strain jump values at the nodes of the elements that exceeded and were within twenty percent of the rezoning indicator values.

CHAPTER 8

ANALYSIS OF RESULTS AND OBSERVATIONS

8.1 Self Adaptive Rezoning Indicators

The derivation of rezoning indicators by eigenvalue
testing quadrilateral elements and implementing the
results into Equation (4.10) and Equation (4.11)
generates an effective means to examine the behavior of
geometrical distortions on the elements. The resulting
strain energy density ratio depicts the strain energy
content of an element over a given range of a distortion
measure. The ideal case provides a strain energy density
ratio of unit value. Departure from the ideal shape
tends to deviate the value from one.

Deviation from a consistent pattern in the strain
energy density ratios indicates a "departure from the
expected". This is exemplified in each distortion
measure that was studied. The "departure from the
expected" is illustrated as a discontinuity, a change in
the direction of the radius of curvature, a change in
amplitude and frequency of the plotted values, or a quick
change in the slope of the plot. All plots, Figure 4.1
through Figure 4.36, exhibited at least one of these behaviors.

174

As an element is distorted a departure from a unit value of the strain energy density ratio is expected since the results of a less ideal element will provide a slightly less accurate solution. In this case, a solution to the strain energy content of the element. A departure from the expected pattern of deviation from the unit value of strain energy density, as the distortion measure is increased, indicates that the solution has lost its reliability in providing accurate results. This value is the limit to the distortion measure that can be applied to an element before the errors tend to dramatically increase and the solution for the distorted element is no longer reliable. This limit of the distortion measure is the rezoning indicator for that measure.

In each case, the rezoning indicator values determined in this investigation were within the expected range of values that have been used to date for rezoning and for mesh formulations in general [20, 27-31].

8.1.1 Eigenvalue Testing - Mathematical Derivation

Section 4.2.1 of Chapter 4 outlined the mathematical derivation of rezoning indicators from a quadrilateral element's stiffness matrix. The underlying mathematics of rezoning indicators derived from eigenvalue tests is built solidly upon existing mathematical formulations

found within the finite element method. The only change is the incorporation of eigenvalues, eigenvectors, and a load vector into one equation to formulate the strain energy content of an element. This change, however, is a valid means of deriving a measure of strain energy both theoretically and mathematically. Since normalized displacements are used instead of real displacements, the true value of strain energy in the element is not obtained. An identical deformation pattern, however, is established. This creates a strain energy value proportional to the true strain energy content of the element. This proportionality to the exact strain energy value is sufficient to determine the effects of distortion on an element.

The stiffness matrix of the element is what defines the capability of the element. Eigenvalue test derived rezoning indicators are directly computed from the stiffness matrix. The theoretical and mathematic nature of these rezoning indicators is therefore sound.

8.1.2 Eigenvalue Testing - Empirical Derivation

Large deformations and strains call for a finite strain element formulation. Under such conditions the nature of the method is nonlinear. Rezoning indicators derived from eigenvalue tests fall into this category. No closed form mathematical solution exists. Nonlinear

176

techniques must be employed.

In this investigation the solution to obtaining the rezoning indicators was derived empirically using the finite element code ABAQUS. Sufficient data points were examined to define the nature of the strain energy density ratio over a wide range of distortion measure values. The spread in the data seemed not to inhibit the determination of the rezoning indicators.

The empirical technique used is tedious in nature. The manner in which the technique is applied allows one to study just one type of element with specific material properties. A generalization of the method to incorporate all element types and material properties is not possible, other than to gather data for each of the possible cases. Data can, however, be gathered for the more common type of elements and material models and still have use in numerous types of applications. The empirical technique does allow one to determine the rezoning indicators for elements and materials that are specific to a finite element code.

8.1.3 Aspect Ratio Rezoning Indicators

The aspect ratio rezoning indicator values as seen in Table 4.1 come within the expected range given by the general rule of thumb that has been to limit aspect ratios to less than twenty to one. The values determined

177

in this investigation are slightly lower. The lower values can be explained due to the fact that the rezoning indicators are the points at which the error in the solution begins to deviate drastically. Increasing the value of the aspect ratio slightly above the value of the rezoning indicator would still provide a reasonably accurate result. Experience indicates that values slightly higher than the rezoning indicator values for aspect ratio might still be useable. Derived rezoning indicators and values determined by experience are therefore in agreement. More accuracy and less problems in the solution will occur with the use of the derived rezoning indicators.

An interesting fact in deriving the rezoning indicator values for aspect ratio is that the location that specifies the value of the rezoning indicator in all four plots, Figure 4.1 through Figure 4.12, tend to correlate. This provides added assurance in the selection of these values.

8.1.4 Taper Ratio Rezoning Indicators

The taper ratio rezoning indicator values as seen in Table 4.1 come within the expected range give by the general rule of thumb that has been to limit taper ratios to less than two to one. The values determined in this investigation are slightly lower. The explanation for

the lower values is identical to the argument given for the aspect ratio. Derived rezoning indicators and values determined by experience for taper ratio are therefore in agreement. More accuracy and less problems in the solution will occur with the use of the derived taper ratio rezoning indicators.

The same interesting fact in deriving the rezoning indicator values for aspect ratio exists for taper ratio. The location that specifies the value of the rezoning indicator in all four plots, Figure 4.13 through 4.24, tend to correlate. This provides added assurance in the selection of these values.

8.1.5 Skew Angle Rezoning Indicators

The skew angle rezoning indicator values *as seen in* Table 4.1 come within the expected range given by the general rule of thumb that has been limit skew angles to less than one hundred and thirty degrees and greater than fifty degrees. The values determined in this investigation are within this range. An explanation similar to that given for aspect ratio can also be applied to the skew angle values. Derived rezoning indicators and values determined by experience for skew angles are therefore in agreement. More accuracy and less problems in the solution will occur with the use of the derived skew angle rezoning indicators.

179

The location that specifies the value of the rezoning indicator in all four plot types, Figure 4.25 through Figure 4.36, tend to correlate. This adds assurance in selecting these values.

8.2 Upsetting Billet Metal Forming Problem

The upsetting billet metal forming problem provided an excellent study of the rezoning method. When the model of this problem was run without rezoning, the solution technique used was unable to complete the entire solution process. Difficulties due to extreme distortions and continued reduction in increment size caused the termination of the solution process.

The problem was rerun using the rezoning technique developed in this investigation. After the first rezoning the solution ran to completion. This indicates the power behind the rezoning method. Correction of distorted elements helped to eliminate solution process difficulties. Additionally, increased accuracy to the solution was obtained through proper rezoning. The results of the solution indicate this. Comparison to references cited in the literature which are similar in nature to this problem is given in the next subsection.

This problem exhibited a behavior of distorting the elements in the upper right hand corner of the mesh (Figure 7.3) to an extreme after only a couple of

increments. This distortion was transferred through the mesh along a diagonal to the opposite corner of the mesh. This deformation behavior is what made this problem ideal for rezoning. Continuous rezoning of the upper right hand corner was required to obtain accurate results in this region. The displacements, strains, and stresses in this same region are of great importance to the analyst. Seven rezonings achieved the improvement in accuracy in the upper right hand corner as well as maintaining valid elements throughout the other regions of the mesh.

Observation and examination of the shape and element values of the finite element mesh, at each rezoning point, indicates that the determination of the values for rezoning indicators was appropriate. Higher or lower values of rezoning indicators would allow for too much distortion or not enough deformation capability. The effect of too much distortion has already been explained. Not enough deformation capability means that one must rezone the mesh more than is required. This causes an increase in time and cost for the solution. The seven rezonings required for this problem may seem like too many, except that the problems associated with extreme deformations occurring at the top right hand corner of the mesh are overcome by the repeated rezonings. A few of the elements in this region were continually undergoing an extreme amount of distortion to the point

of being inverted. The assumption of a perfectly rough

die surface in contact with the model, created was the

factor which caused the extreme deformations at the upper

right hand corner of the mesh.

8.2.1 Comparison to Similar Problems in the Literature

Several examples in the literature are similar in

nature to the example problem of the upsetting billet

[14, 15, 54, 55].

References [14, 15] contain examples of upsetting

billet problems. In these problems the physical geometry

and material properties differ from the ones used in this

investigation. The rigid die was not extended past the

billet material, thus in the deformation of the billet

its material extruded upwards once it was past the edge

of the die. The distortions in the elements, however,

tend to correlate with those seen in this investigation.

The elements at or near the edge of the die tend to

distort the most, even to the point of becoming inverted.

Rezoning was utilized for References [14, 15],

however, the problem was rezoned on regular intervals of

percentage reduction in the height. What can be

extrapolated from these examples is the fact the

distortion patterns seen in the model and individual

elements is in overall agreement with the results of this

investigation.

Reference [54] contained several examples of the upsetting billet problem which had the same geometrical shape, material properties, and loading characteristics used in this investigation. No rezoning, however, was utilized. Different types, and numbers of elements were used in the various investigations. In general the overall deformation patterns observed in this investigation correlate to those of Reference [54]. The same pattern of element distortion for the nonrezoning case in this investigation compares overall equivalent to that of Lippmann [54].

The final force required to achieve a sixty percent reduction in height is 1430 kN for a viscous-plastic case and 970 kN for a rigid-plastic case of Reference [54]. For this investigation a final force for the sixty percent reduction in height was 1038 kN for the nonrezoning case and 1029 kN for the rezoning case. Comparison of the force values for the rezoning case, the nonrezoning case, and from Reference [54] indicates that there is agreement in results and illustrates the improving effect rezoning has on the solution.

Reference [55] contained nearly the exact same problem used in this investigation. Three cases were examined. The first case included temperature effects and used eight node quadratic ordered elements. Fewer

elements in the mesh were used. No rezoning was applied. The die or rigid surface traveled to a full sixty percent height reduction of the billet, however, the speed of travel of the die was very slow. The final force for this case was approximately 960 kN. Distortions in the elements of the mesh for the final solution are quite noticeable, but in line with the results of the nonrezoning case of this investigation.

The second case of Reference [55] is identical to the first case except the rate of the application of the die was much faster. The final force was 1430 kN. It is interesting to note that in this case the top surface of the billet actually began to fold in on itself. This occurred at the corner of an element that was extremely distorted. The element was practically inverted. This folding may have been induced by the distorted elements in that region of the mesh. The distorted elements created false strains and stresses in that region of the model.

The third case of Reference [55] was practically identical to the problem used in this investigation except reduced integration elements were used. Only one rezoning was performed. No attempt to optimize the new mesh in terms of future deformations was taken into account. Elements within the mesh were far too distorted before the rezoning occurred. The elements of the final

mesh were also far too distorted. The final force to achieve the sixty percent reduction in height was 800 kN. This case, of all the references cited which contain upsetting billet problems, came closest, overall, to the model used in this investigation.

In the third case of Reference [55] the contours and values of effective plastic strain were, in general, equivalent to the contours and values obtained in the example problem of this investigation. Differences in the values and in the appearance of the contours was manifested in the mesh regions which contained the most distorted elements. This region is the top right hand portion of the mesh. For the third case of Reference [55], the extreme values and contours of effective plastic strain were shifted downwards and to the left as compared to the results of this investigation. The third case contours seemed to be affected by the distorted elements in the region of the upper right hand corner of the mesh. A one hundred and twenty percent strain was the peak strain value in this region for the third case as compared to a one hundred and forty percent peak strain value for the problem of this investigation. The furthest right hand point in contact with the die surface had an eighty percent strain for the third case and a forty percent strain for the case of this investigation. The strain gradients, of the two cases, across the top

185

surface of the billet only differed as one approached the upper right hand corner of the mesh, the mesh area corresponding to the region of greatest element distortion. The outside right hand edge of the mesh had a sixty percent strain value for the third case as compared to a twenty percent strain value for the problem of this investigation.

The results of the problem used in this investigation seems to be in overall agreement with the references cited. The differences illustrate an improvement in accuracy of the solution to the upper right hand corner of the mesh due to the rezoning method developed in this investigation. This rezoning method effectively dealt with the deformation difficulties generated in the right hand corner of the mesh in order to generate an accurate solution throughout the mesh.

The observations made concerning the performance of the upsetting billet results for the references cited are equivalent to some of the observations that can be made between the nonrezoning and rezoning cases studied in this investigation. These similarities tend to validate the effectiveness of the rezoning method and the eigenvalue test rezoning indicators used within the method. Since the nonrezoning case was similar to cases in the literature, and an improvement was seen between the nonrezoning and rezoning cases, the assumption of the

validity of the method of self adaptive rezoning using the rezoning indicators, appears to be in order. The improvement between the nonrezoning case and the rezoning case of this investigation is examined in the following subsections.

8.2.2 Comparison to a Nonrezoning Case

Figure 7.4 illustrates the deformations induced upon the elements in the mesh for the nonrezoning case. Two elements are inverted or near inversion. A good portion of the mesh is flagged as being distorted or near the distortion limits. Such results would not provide an accurate solution.

Figure 7.19 illustrates the mesh of the same problem near the same point in the solution as shown in Figure 7.4. In fact, this case is for the completed rezoned solution. A few distortions in the upper right hand corner are present. Upon examination of the values, the distortions just exceeded the limits set by the rezoning indicators. A solution for this case can definitely be considered more accurate. Seven rezonings is not a high price to pay for the increased accuracy and the completion of the solution.

8.2.3 Comparison to Strain Jump Values

Strain jump values for the upsetting billet problem are listed in Table B.1 through Table B.9 in Appendix B.

Extreme jumps or discontinuities between the strain values that occur at a given node shared by several elements is indicative of inaccuracies in the solution. Elements which connect to this node are providing quite different results in strain for the same nodal position. In some cases this can be expected where there exists a steep gradient in the strain field. This can be a natural tendency given the nature of the problem. In cases of constant strain this would not be expected.

In the upsetting billet problem strain jumps were relatively high in the regions of large deformations. This is expected since the model undergoes a sixty percent reduction in height. Upon comparison of the strain jump values for the non rezoning case (Table B.1) to those for the rezoning case (Table B.2 through Table B.9) one finds that the values for the nonrezoning case can be an order of magnitude higher. This is drastic for the strain values under consideration. Comparison of the final solution for the nonrezoning and rezoning cases indicate a factor of about five in difference between maximum strain jump values. Values of large strain jumps correspond nicely with regions of the mesh which are flagged for rezoning. Slightly less values are noticed in regions of the mesh which are within twenty percent of reaching the rezoning indicator limits.

8.2.4 Comparison to Equivalent Plastic Strain Values

Figures B.1, B.4, B.7, B.10, B.13, B.16, B.19, B.22, and B.25 in Appendix B are contour plots of the equivalent plastic strain for the upsetting billet problem. These contour plots provide a visual comparison of the mesh for regions of steep gradients of equivalent plastic strain. Regions of steep gradients would be indicative of large deformations confined to a small region. They could also be considered regions of discontinuities in the solution values and hence inaccurate results.

Visual examination of the rezoning contour plots seem to indicate smooth transitions of strain throughout the mesh rising to peak values in the critical regions. Elements flagged for rezoning occurred only within the regions of steep gradients. The smoothness of the contours is indicative of an accurate solution.

Comparison of the final meshes of the nonrezoning to rezoning cases illustrates the difference in strain values obtained. Some of the contour shapes and most of the peak strain values differ. This is indicative of an improvement in the solution caused by rezoning. Selection of rezoning indicators would also appear appropriate.

8.2.5 Comparison to Mises Stress Values

Figures B.2, B.5, B.8, B.11, B.14, B.17, B.20, B.23, and B.26 in Appendix B are contour plots of Mises stress values for the upsetting billet problem. These contour plots provide a visual inspection of the mesh for regions of steep gradients of Mises stress. Regions of steep gradients could be indicative of discontinuities in solution values and hence inaccurate results.

Visual examination of the rezoning contour plots seems to indicate smooth transitions of stress throughout the mesh rising to peak values in the critical regions. Rezoning the distorted elements ironed out the regions of steep gradients. The smoothness of the contours is indicative of an accurate solution which in part is due to the rezoning process.

Comparison of the final meshes of the nonrezoning to rezoning cases illustrates the difference in strain values obtained. Some of the contour shapes and most of the peak stress values differ. The contours of the nonrezoning case appear to be erratic in nature. This is indicative of errors in the solution. The rezoning case is much smoother. This is indicative of an improvement in the solution caused by the rezoning. Selection of rezoning indicators would also appear appropriate.

190

8.2.6 Comparison to Strain Energy Density Values

Figures B.3, B.6, B.9, B.12, B.15, B.18, B.21, B.24, and B.27 in Appendix B are contour plots of strain energy density for the upsetting billet problem. These contour plots provide a visual inspection of the mesh for regions of steep gradients of strain energy density. These regions of steep gradients could be indicative of large deformations and strains as well as the expenditure of energy confined to a small region. They could also be considered regions of discontinuities in solution values and hence inaccurate results.

Visual examination of the rezoning contour plots seems to indicate smooth transitions of strain throughout the mesh rising to peak values in the critical regions. Elements flagged for rezoning occurred only within the regions of steep gradients. The smoothness of the contours is indicative of an accurate solution.

Comparison of the final mesh of the nonrezoning to rezoning case illustrates the difference in strain energy density values obtained. Some of the contour shapes and most of the peak strain energy density values differ. The location of the highest strain energy density values occurs at the correct spot in the rezoning case where it is shifted to the left for the nonrezoning case. This shift to the left lies in the region of the inverted elements thus giving rise to false values. These

191

differences are indicative of an improvement in the solution caused by the rezoning. Selection of rezoning indicators would also appear appropriate.

8.3 Impacting Cylindrical Rod Problem

The impacting cylindrical rod problem provided an excellent study of the rezoning method for a dynamic problem. The problem is essentially identical to the upsetting billet problem except no rigid die is creating the deformation. The velocity of the object at impact to a rigid surface causes the deformation of the body. This problem allows for the comparison and verification of the self adaptive rezoning method and rezoning indicators derived from eigenvalue tests, that were developed in this investigation, for a dynamic problem. For the nonrezoning case the problem was able to run to completion. Using the rezoning technique of this investigation the problem was run to completion with two rezonings. This indicates that the distortions for this problem were not as extreme as seen in the upsetting billet problem. The assumption of a rigid die with perfect friction, caused the extreme distortions in the upsetting billet problem. In this problem no friction was assumed, thus allowing the deforming elements to slide along the rigid surface. It is interesting to note that this creates larger aspect ratios in the distorted

192

elements. The upsetting billet problem caused mainly skew angle distortions with a few taper ratio distortions. In the impacting cylindrical rod problem the element distortions were aspect ratio, taper ratio, and skew angle. Skew angle distortions seem to appear in all cases. The nature of this problem allowed for the examination of large aspect ratio values not seen in the upsetting billet problem.

This problem exhibited a behavior of distorting the elements in the lower portion of the mesh (Figure 7.4) to an extreme in the first two or three microseconds of elapsed time. This distortion was caused by stopping the momentum of the object near its base by the rigid surface. The elements above this region continued on the downward travel causing the lower elements of the mesh to become distorted. At some time increment, the lowest portion of the body actually began to rebound from the surface to cause additional deformation in these lower regions. The incompressible nature of the elements in plastic deformation allowed the mesh to be pushed out and curled up at the lower right had corner of the mesh (Figure 7.21). This deformation behavior is what made this problem ideal for rezoning.

Rezoning of the lower portion of the mesh was required to obtain accurate results in the region. Displacements, strains, and stresses in this region are

considered important to the analyst. Two rezonings

achieved the improvement in accuracy to the lower mesh

region as well as maintaining valid elements throughout

the other regions of the mesh.

By comparison of the shape and element values of the

finite element mesh, at each rezoning point, it was

judged that the selection of the rezoning indicator

values was appropriate. Higher or lower values of

rezoning indicators would allow for too much distortion

or not enough deformation capability. These effects have

already been explained. The two rezonings required for

this problem shows how a little effort in correction of

distorted elements can increase the accuracy of the

results. For many similar problems which require

rezoning, only a few rezonings would be necessary.

8.3.1 Comparison to Similar Problems in the Literature

Several examples in the literature are similar in

nature to this example problem of an impacting

cylindrical rod [11, 24, 56-60].

References [56, 58, 59] contain early examples of

tests and studies of the plastic behavior of materials

which were examined using impacting cylindrical rods.

The materials used, geometries, and impacting conditions

varied. None of the cases exactly matched the one used

in this investigation. The finite element method did not

exist at the time References [56, 58, 59] were written. No direct comparisons to the model used in this investigation can be made.

Reference [57] is a study of soft-body impact. An example of an impacting cylindrical rod to a rigid surface was examined. The final deformation shape of the mesh is very similar to the shape observed in this investigation. In this reference, however, the material was modeled as a gelatin substance and the impacting velocities were quite a bit smaller. The model also used three dimensional elements. No direct comparisons are legitimate other than the similarities in overall shape of the deformation.

In Reference [11] a cylindrical rod was impacted against a thick flat plate. Velocities were on the same order of magnitude as used in this investigation. Different geometries, materials, and element types were used. Triangular elements were used. A rezoning process was incorporated into the solution process. The results of the problem seem to be excellent for triangular elements. No comparisons can be made other than to note that the overall deformation was similar. Since this model struck a flat plate instead of a rigid surface this created a slightly different problem. It is interesting to note that the curling of the material at the outer edge of the model also occurred in this model.

The model used in Reference [24] is much similar to the model used in this investigation. The geometries and material properties differ, but in both problems the cylindrical rod strikes a rigid surface. The overall deformation patterns of both are similar. The deformation of the elements in the lower portion of the mesh is equivalent in both models. The strain gradients also appear to be equivalent given the differences between the models. The initial velocity prior to impact for Reference [24] is 227 meters per second, about one fourth the value used in this investigation.

Reference [60] studied the dynamic yield point of materials by impacting cylindrical rods to a rigid surface and correlated the results to finite element models. A variety of dimensions and materials were used. The finite element models used in Reference [60] were in agreement with the actual test data of the impacting cylindrical rods. It is interesting to note that overall mesh shapes of the models, including shapes of the elements, is very similar to the results of this investigation. An interesting case study within Reference [60] was an impact case where the outer edges of the rod began to curl upward. This was demonstrated in the model used in this investigation. Contours of plastic strain also seemed to be comparable.

No detailed comparisons of the impacting cylindrical

rod used in this investigation to those cited in the literature can be made due to the differences in the models and test conditions. A general overall comparison has been established. This helps to validate the use of the rezoning method and rezoning indicators derived from eigenvalue tests developed in this investigation. Actual test data or another validated finite element models would be required to make a detailed comparison of the effectiveness of the rezoning method used in this investigation.

8.3.2 Comparison to a Nonrezoning Case

Figure 7.21 illustrates the deformations induced upon the elements in the mesh for the nonrezoning case. Almost the entire lower portion of the mesh is flagged as being distorted or near the distortion limits. Such results would not provide an accurate solution.

Figure 7.26 illustrates the mesh of the same problem at the same point in the solution as shown in Figure 7.21. This case is for the completed solution using rezoning. A few distortions are present. Upon examination of the values, the distortions just exceeded the limits set by the rezoning indicators. A solution for this case can definitely be considered more accurate. Two rezonings is not a high price to pay for the increased accuracy and the completion of the solution.

197

8.3.3 Comparison to Strain Jump Values

Strain jump values for the impacting cylindrical rod problem are listed in Table C.1 through Table C.4 in Appendix C. Extreme jumps or discontinuities between the strain values that occur at a given node shared by several elements is indicative of inaccuracies in the solution. Elements which connect to this node are providing quite different results in strain for the same nodal position. In some cases this can be expected where a steep strain gradient exists. A steep strain gradient is a natural tendency given the nature of the problem. In cases of constant strain this would not be expected.

In this problem strain jumps were relatively high in the regions undergoing large deformations. This is expected since the model undergoes quite a bit of deformation in the lower region. Upon comparison of the strain jump values for the non rezoning case (Table C.1) to those for the rezoning case (Table C.2 through Table C.4) one finds that the values for the nonrezoning case can be an order of magnitude higher. This is drastic for the strain values under consideration. Comparison of the final solution for the nonrezoning and rezoning cases indicate a factor of about five in difference between maximum values Values of large strain jumps correspond nicely with regions of the mesh which are flagged for rezoning. Slightly less values are noticed in regions of

the mesh which are within twenty percent of reaching the rezoning indicator limits.

8.3.4 Comparison to Equivalent Plastic Strain Values

Figures C.1, C.4, C.7, and C.10 in Appendix C are contour plots of equivalent plastic strain for the impacting cylindrical rod problem. These contour plots provide a visual inspection of the mesh for regions of steep gradients of equivalent plastic strain. These regions of steep gradient could be indicative of large deformations confined to a small region. They could also be considered regions of discontinuities in solution values and hence inaccurate results.

Visual examination of the rezoning contour plots seems to indicate smooth transitions of strain throughout the mesh rising to peak values in the critical regions. Elements flagged for rezoning occurred only within the regions of steep gradients. The smoothness of the contours is indicative of an accurate solution.

Comparison of the final mesh of the nonrezoning case to the rezoning case illustrates a few minor differences in strain values. Some of the contour shapes and peak strain values differ. This is indicative of an improvement in the solution caused by the rezoning. The slight difference as compared to the more extreme differences of the upsetting billet problem is indicative

199

of the need for only two rezonings. Selection of
rezoning indicators also appears to be appropriate.

8.3.5 Comparison to Mises Stress Values

Figures C.2, C.5, C.8, and C.11 in Appendix C are
contour plots of Mises stress values for the impacting
cylindrical rod problem. These contour plots provide a
visual inspection of the mesh for regions of steep
gradients of Mises stress. These regions of steep
gradients could be indicative of discontinuities in
solution values and hence inaccurate results.

Visual examination of the rezoning contour plots
seems to indicate smooth transitions of stress throughout
the mesh rising to peak values in the critical regions.
The smoothness of the contours is indicative of an
accurate solution.

Comparison of the final mesh of the nonrezoning to
the rezoning case illustrates slight differences in
stress values obtained. Some of the contour shapes and
peak stress values differ. Once again the fact that only
two rezonings were required accounts for the less
dramatic difference. The rezoning case does cause
improvement in the solution. Selection of rezoning
indicators would also appear appropriate.

8.3.6 Comparison to Strain Energy Density Values

Figures C.3, C.6, C.9, and C.12 in Appendix C are contour plots of strain energy density for the impacting cylindrical rod problem. These contour plots provide a visual inspection of the mesh for regions of steep gradients of strain energy density. These regions of steep gradients could be indicative of large deformations and strains as well as expenditure of energy confined to a small region. They could also be considered regions of discontinuities in solution values and hence inaccurate results.

Visual examination of the rezoning contour plots seems to indicate smooth transitions of strain energy density throughout the mesh rising to peak values in the critical regions. The smoothness of the contours is indicative of an accurate solution.

Comparison of the final mesh of the nonrezoning case to the rezoning case illustrates the difference in strain energy density values obtained. The contour patterns and peak strain energy density values differ. The location of the steepest gradients of strain energy density occurs at the point of extreme element distortion in the nonrezoning case. These steep gradients are indicative of inaccuracies in the solution cause by distorted elements. Selection of rezoning indicators with regards to this problem would appear to be appropriate.

8.4 Mesh Manipulations

Rezoning can be summed up as a manipulative procedure on the finite element mesh to improve upon the accuracy and solution process. The mesh must first be examined. In this investigation a computer program accomplishes this quite efficiently. The mesh must then be remeshed or a new mesh created. This is a key part of the rezoning process. The new mesh in essence, is representative of the amount of improvement in the solution due to rezoning. The validity of the new mesh is closely tied to the remapping of element variables from the old mesh.

8.4.1 Finite Element Mesh Inspection

The finite element mesh inspection computer program is listed in Appendix A. This computer program performed exceptionally well in determining the maximum or minimum values of the geometrical measures of aspect ratio, taper ratio, and skew angle. The rezoning indicator values provided the means to flag each element of the mesh that exceeded the distortion limits set by the rezoning indicators.

The computer program requires node and element input files at each increment or time step in the solution process. It performs a quick check on the finite element mesh and determines the geometrical measures of each

element and compares this value to the rezoning indicator values. This program can be easily incorporated into a finite element code so that the mesh checking procedure is automatically made at each time step or increment. This permits prompt rezoning leading to increased solution accuracy.

This mesh inspection program is limited to linear four node quadrilateral elements. The basic ideas incorporated into the program could be extended to second order eight node quadrilateral elements or to other types of elements as well. Several modifications would have to be incorporated which are dependent upon the differences of the other type of element being examined.

8.4.2 Remeshing Technique

The remeshing technique used in this investigation is based upon user intervention. The user must examine the rezoning indicator information and determine how to create a new valid and well shaped mesh required for the rezoning process. This is not an extremely difficult task if one uses a computer aided design package or a finite element pre and post processor to help create the new mesh. The information generated by the rezoning indicators for increments or time steps prior, after, and at the point of rezoning aid the analyst in deciding where and how to remesh. This process was followed in

this investigation.

The remeshing process seemed to work well given a few iterations on each new mesh created. It proved, however, to be a tedious and labor intensive process. It was also subject to error due to the human intervention required. The automation of this process would require an expert system or some type of artificial intelligence to incorporate the decision making process of the analyst. Meshing techniques would have to be incorporated that can generate the desired meshes based upon the decisions arrived at by the expert system. With the derivation of the rezoning indicators, the only major obstacle in developing a self adaptive rezoning algorithm is the development of this remeshing expert system.

8.4.3 Remapping Technique

The remapping technique used in this investigation is the algorithm which is part of the finite element code ABAQUS. ABAQUS' code contains an interactive rezoner which has an automatic remapping of solution variables to the new mesh. The technique is an adequate remapper for a self adaptive rezoning algorithm. The only fault was that the automatic remapping was not applied to dynamic related quantities such as velocities. An independent interpolation method was used to interpolate velocities to the new mesh for dynamic problems.

8.5 Recommendations

In order to create an automatic self adaptive rezoner one must first develop an automatic remesher. Development of such a remesher requires an expert system based on the rezoning indicators and the self adaptive rezoning procedure. Various mapping and mesh creation techniques would be required for it to be universal in nature.

Further verification and correlation of the rezoning indicators must be accomplished. This would provide a solid foundation for using the rezoning indicators in the self adaptive rezoning algorithm. Further correlation with additional example problems which vary in application, loading and model description will help to build this foundation. Correlation with empirical tend to further establish the validity of the techniques used. Deriving rezoning indicators for other types and orders of elements, as well as using various material models will help to solidify the approach taken. Derivation of the rezoning indicators by the eigenvalue testing method, however, must be used in order to properly correlate the differences in element types and orders as well as material models, for added validation to the approach taken to quantify rezoning indicator values developed in this investigation.

REFERENCES

REFERENCES

1. Babuska, I., and W. C. Rheinboldt. "A Posteriori Error Estimates for the Finite Element Method." <u>Inter-national Journal of Numerical Methods in Engineering</u>, 12 (1978): 1597-1015.

2. Babuska, I., and W. C. Rheinboldt. <u>A Survey of A Posteriori Error Estimators and Adaptive Approaches in in the Finite Element Method</u> (Institute of Physical Science and Technology, 1982), Technical Note BN-981.

3. Babuska, I., and W. C. Rheinboldt. "Computational Error Estimates and Adaptive Processes for some Non-linear Structural Problems." <u>Computational Methods in Applied Mechanics and Engineering</u>, 34 (1982): 895-937.

4. Babuska, I., and W. C. Rheinboldt. "Error Estimates for Adaptive Finite Element Computations." <u>SIAM Journal of Numerical Analysis</u>, 15 (1978): 736-754.

5. Babuska, I., O. C. Zienkiewicz, J. Gago, and E. R. De A. Oliveria. <u>Accuracy Estimates and Adaptive Refinement in Finite Element Computations</u>, Chichester: John Wiley and Sons, 1986.

6. Roberti, P., M. A. Melkanoff. "Self-Adaptive Stress Analysis Based on Stress Convergence." <u>International Journal for Numerical Methods in Engineering</u>, 24 (1987): 1973-1992.

7. Shepard, M. S., M. A. Yerry, and P. L. Baehmann. "Auto-matic Mesh Generation Allowing for Efficient A Priori and A Posteriori Mesh Refinements." <u>Computer Methods in Applied Mechanics and Engineering</u>, 55 (1986) 161-180.

8. Weiser, A. <u>Local-Mesh, Local-Order, Adaptive Finite Element Method with A Posteriori Error Estimators for Elliptic Partial Differential Equations</u> (New Haven: Yale University, 1981), Technical Report No. 213.

9. Timoshenko, S., and J. N. Goodier. <u>Theory of Elasticity</u>. New York: McGraw-Hill, 1951.

10. Belytschko, T., and T. J. R. Hughes. <u>Computational Methods for Transient Analysis, Volume 1 in Computational Methods in Mechanics</u>, North-Holland: Elsevier Science Publishers, 1983.

11. Chou, P. C., D. Liang, and L. Wu. "Mesh Rezoning for a Dynamic Triangular Finite-Elements Hydrocode." <u>Finite Elements in Analysis and Design</u>, 4 (1988): 175-192.

12. Crawford, R. H., D. C. Anderson, and W. N. Waggenspack. "Mesh Rezoning of 2D Isoparametric Element by Inversion." <u>International Journal for Numerical Methods in Engineering</u>, 28 (1989): 523-531.

13. Guerra, F. M. <u>Finite Element Analysis for the Adaptive Method of Rezoning</u> (Austin: The Texas Institute for Computational Mechanics at the University of Texas at Austin, 1987), TICOM Report 78-7.

14. Gelten, C. J. M., and J. E. de Jong. "A Method to Redefine a Finite Element Mesh and its Applications to Metal Forming and Crack Growth Analysis." <u>International Finite Element Congress</u>, (1981): 65-85.

15. Gelten, C. J. M., and A. W. A. Konter. "Application of Mesh-Rezoning in the Updated Lagrangian Method to Forming Analyses." <u>Numerical Methods in Industrial Forming Processes</u>, (1982): 511-521.

16. Guoji, L., P. Xianguang, and H. Yijian. "DIFO-2 User Oriented Finite Element Method Program for Die Forging." <u>NAMRC Proceedings</u>, 13 (1985): 442-447.

17. Hibbit, H. D., Karlsson, and Sorensen. <u>The ABAQUS Theory Manual (Version 4.8)</u>, 1989.

18. Hibbit, H. D., Karlsson, and Sorensen. <u>The ABAQUS Users' Manual (Version 4.8)</u>, 1989.

19. Hoffman, R. E., F. M. Guerra, and D. L. Humphrey. "Practical Applications of Adaptive Mesh Refinement (Rezoning)." <u>Computers and Structures</u>, 12 (1980): 639-655.

20. Horak, H. G., E. M. Jones, J. W. Kodis, and M. T. Sandford II. "An Algorithm for the Discrete Rezoning of Lagrangian Meshes." <u>Journal of Computational Physics</u>, 26 (1978): 277-284.

21. Oh, S. I., J. P. Tang, and A. Badwy. "Finite Element Mesh Rezoning and its Application to Metal Forming Analyses." _Advances in Techniques of Plasticity_, 2 (1984): 1051.

22. Ramshaw, J. D. "Conservative Rezoning Algorithm for Generalized Two-Dimensional Meshes." _Journal of Computational Physics_, 59 (1985): 193-199.

23. Hughes, T. J. R. "Generalization of Selective Integration Procedures to Anisotropic and Nonlinear Media." _International Journal for Numerical Methods in Engineering_, 12 (1982): 1413-1418.

24. Hallquist, J. O. _NIKE2D - A Vectorized Implicit, Finite Deformation, Finite Element Code for Analyzing the Static and Dynamic Response of 2-D Solids with Inter-active Rezoning and Graphics_ (New Mexico: Lawrence Livermore National Laboratory, 1986), UCID-19677, Revision 1.

25. Flanagan, D. P., and T. Belytschko. "A Uniform Strain Hexahedron and Quadrilateral with Orthogonal Hourglass Control." _International Journal for Numerical Methods in Engineering_, 17 (1981): 679-706.

26. Bathe, K. J. _Finite Element Procedures in Engineering Analysis_, New Jersey: Prentice-Hall, Inc., 1982.

27. Cook, R. D., D. S. Malkus, and M. E. Plesha. _Concepts and Applications of Finite Element Analysis_, New York: John Wiley and Sons, 1989.

28. Jones, R. E. _QMESH: A Self-Organizing Mesh Generation Program_ (Albuquerque: Sandia Laboratories, 1974), SLA-73-1088.

29. Arney, D. C. "An Adaptive Mesh Algorithm for Solving Systems of Time Dependent Partial Differential Equations." Doctoral Dissertation, Rensselaer Polytechnic Institute, 1985.

30. _ABAQUS_, Version 4.9. Computer Software. Providence: Hibbitt, Karlsson, and Sorensen, Inc., 1991. Disk.

31. _SDRC's IDEAS Supertab_, Version 4.0. Computer Software. Cincinnati: Structural Dynamics Research Corporations, Inc., 1988. Disk.

32. Rigby, G. L., and G. M. McNeice. "A Strain Energy
    Basis for Studies of Element Stiffness Matricies."
    AIAA Journal, 10 (1972): 1490-1493.

33. Babuska, I. *Finite Element Workshop 1980* (Maryland:
    University of Maryland, 1980), Technical Note BN-940.

34. Botkin, M. E. "An Adaptive Finite Element Technique
    for Plate Structures." *AIAA Journal*, 23 (1984): 812-
    814.

35. Carey, G. F. "A Mesh Refinement Scheme for Finite
    Element Calculations." *Computer Methods in Applied
    Mechanics and Engineering*, 7 (1976): 93-105.

36. Desai, C. S., and J. F. Abel. *Introduction to the
    Finite Element Method A Numerical Method for
    Engineering Analysis*, New York: Van Nostrand Reinhold
    Company, 1972.

37. Kittur, M. G., and R. L. Huston. "Finite Element Mesh
    Refinement Criteria for Stress Analysis." *Computers
    and Structures*, 32 (1990): 251-255.

38. Melosh, R. J., and P. V. Marcal. "An Energy Basis for
    Mesh Refinement of Structural Continua."
    *International Journal for Numerical Methods in
    Engineering*, 11 (1977): 1083-1091.

39. Rheinboldt, W. C. *Adaptive Mesh Refinement Process for
    Finite Element Solutions* (Pittsburgh: Institute for
    Computational Mathematics and Applications, University
    of Pittsburgh, 1980), Technical Report ICMA-80-14.

40. Baehmann, D. L., S. L. Wittchen, M. S. Shepard, K. R.
    Grice, and M. A. Yerry. *Robust Geometrically Based
    Automatic 2-D Mesh Generation* (Troy: Center for
    Interactive Computer Graphics, 1986), TR-86007.

41. Denayer, A. "Automatic Generation of Finite Element
    Meshes." *Computers and Structures*, 9 (1978): 359-364.

42. Frederich, C. O., Y. C. Wong, and F. W. Edge. "Two
    Dimensional Automatic Mesh Generation for Structural
    Analysis." *International Journal for Numerical
    Methods in Engineering*, 2 (1970): 113-144.

43. Haber, R., M. S. Shepard, J. F. Abel, R. H. Gallagher, and D. P. Greenberg. "A General Two-Dimensional, Graphical Finite Element Preprocessor Utilizing Discrete Transfinite Mappings." International Journal for Numerical Methods in Engineering, 17 (1981): 1015-1044.

44. Nikuchi, N. "Adaptive Grid-Design Methods for Finite Element Analysis." Computer Methods in Applied Mechanics and Engineering, 55 (1986): 129-160.

45. Shepard, M. S. Approaches to the Automatic Generation and Control of Finite Element Meshes (Troy: Center for Interactive Computer Graphics, Rensselaer Polytechnic Institute, 1987), TR-87005, CIGG, RPI.

46. Shepard, M. S., K. R. Grice, and M. K. Georges. "Some Recent Advances in Automatic Mesh Generation." Modern Methods for Automating Finite Element Mesh Generation, New York: ASCE, 1986.

47. Thompson, J. F. "A Survey of Dynamically-Adaptive Grids in the Numerical Solution of Partial Differential Equations." Applied Numerical Mathematics, 1 (1985): 3-27.

48. Thompson, J. F. Numerical Grid Generation Foundations and Applications, New York: Elsevier Science Publishing Company, 1985.

49. Wordenweber, B. "Finite Element Mesh Generation." Computer Aided Design, 16 (1984): 285-291.

50. Yerry, M. A., and M. S. Shepard. "Finite Element Mesh Generation Based on a Modified Quadtree Approach." IEEE Computer Graphics and Applications, 3 (1983): 36-46.

51. Rogers, D. F., and J. A. Adams. Mathematical Elements for Computer Graphics, New York: McGraw-Hill Publishing Company, 1990.

52. Dukowicz, J. K., and J. W. Kodis. "Accurate Conservative Remapping (Rezoning) for Arbitrary Lagrangian-Eulerian Computations." SIAM Journal for Scientific and Statistical Computing, 8 (1987): 305-321.

53. Dukowicz, J. K. "Conservative Rezoning (Remapping) for General Quadrilateral Meshes." Journal of Computational Physics, 54 (1987): 441-424.

54. Lippmann, H., Editor, <u>Metal Forming Plasticity</u>, IUTAM Symposium Tutzing/Germany, New York: Springer-Verlag, 1978.

55. Hibbit, H. D., Karlsson, and Sorensen. <u>The ABAQUS Example Problems Manual (Version 4.8)</u>, 1989.

56. Fireman, E. L., J.S. Koehler, and F. Seitz. <u>The Set Added to Compressed Cylinders After Impact</u> (National Defense Research Committee, 1944), Armor and Ordinance Report No. A-258, OSRD No. 3331.

57. Brockman, R. A. <u>Finite Element Analysis of Soft-Body Impact</u> (Dayton: Flight Dynamics Laboratory, Wright Patterson Air Force Base, 1984), AFWAL-TR-84-3055.

58. Seitz, F. <u>The Testing of Metals in Compression at High Rates of Strain</u> (National Defense Research Committee, 1943), Armor and Ordinance Report No. A-174.

59. Simpson, O. C., E. L. Fireman, and J. S. Koehler. <u>High Speed Compression Testing of Copper Crusher Cylinders and Spheres</u> (National Defense Research Committee, 1944), Armor and Ordinance Report No. A-257, OSRD No. 3330.

60. Wilkins, M. L., and M. W. Guinan. "Impact of Cylinders on a Rigid Boundary." <u>Journal of Applied Physics</u>, 44 (1973): 1200-1206.

BIBLIOGRAPHY

BIBLIOGRAPHY

1. Bathe, K. J., E. Ramm, and E. L. Wilson. "Finite Element Formulations for Large Deformation Dynamic Analysis." _International Journal for Numerical Methods in Engineering_, 9 (1975): 353-386.

2. Brockenbrough, R. L., and B. G. Johnston. _USS Steel Design Manual_. Pittsburgh: United States Steel Corporation, 1981.

3. Dieter, G. E. _Mechanical Metallurgy_. New York: McGraw-Hill Book Company, 1987.

4. Fung, Y. C. _Foundations of Solid Mechanics_. New Jersey: Prentice-Hall, 1965.

5. Gopinathan, V. _Plasticity Theory and its Application in Metal Forming_. New York: John Wiley and Sons, 1982.

6. Gaudreau, G. L., and J. O. Hallquist. "Recent Developments in Large Scale Finite Element Lagrangian Hydrocode Technology." _Computer Methods in Applied Mechanics and Engineering_, 33 (1982): 725-757.

7. Hibbitt, H. D., P. V. Marcal, and J. R. Rice. "A Finite Element Formulation for Problems of Large Strain and Large Displacement." _International Journal of Solids and Structures_, 6 (1970): 1069-1086.

8. Key, S. W. "A Finite Element Procedure for the Large Deformation Dynamic Response of Axisymmetric Solids." _Computer Methods in Applied Mechanics and Engineering_, 4 (1974): 195-218.

9. Matthies, H., and G. Strang. "The Solution to Nonlinear Finite Element Equations." _International Journal for Numerical Methods in Engineering_, 14 (1979): 1613-1626.

10. McMeeking, R. M., and J. R. Rice. "Finite-Element Formulations for Problems of Large Elastic-Plastic Deformation." _International Journal of Solids and Structures_, 11 (1975): 601-616.

APPENDICES

APPENDIX A

MESH EXAMINATION COMPUTER PROGRAM

MESH EXAMINATION COMPUTER PROGRAM

The following computer program is used to examine the finite element mesh at each time step or increment in the solution process. It computes the maximum aspect ratio, minimum taper ratio, and the maximum and minimum skew angles for each quadrilateral element.

A file is created which lists the aspect ratios, taper ratios, and skew angles for all the elements. A flag is set for each element which violates any one of the rezoning indicators and the flag appears in the column associated with the type of distortion. The integer number one indicates that an element is flagged for rezoning while a zero means that no geometrical measures have exceeded the rezoning indicator values. The program also determines if an element has coincident nodes and if the element has become inverted.

The program is written in fortran and could easily be integrated into a self adaptive rezoning algorithm. The program is valid for the examination of finite element meshes which only contain four node quadrilateral elements. An element and a node file must be supplied to the program under the names of elements.txt and nodes.txt respectively. Examples of these files are also included.

217

```
C
C       THIS PROGRAM DETERMINES THE GEOMETRICAL SHAPE
C       CONDITIONS OF THE ELEMENTS IN THE MESH.   EACH
ELEMENT C       IS EXAMINED AND THE ELEMENTS WHICH ARE
FOUND TO BE
C       GEOMETRICALLY DISTORTED ARE FLAGED AS CANDIDATES
FOR
C       REZONING.
C
C       READ NODE AND ELEMENT LISTS AND ENTER THE LISTS
INTO
C       TWO ARRAYS NAMED NODE(I,J) AND ELM(I,J).
C
        INTEGER ELM(500,4),ELMFLAG(500,9),IDNODE(500)
        INTEGER IDELM(500)
        REAL NODE(500,2),VALAR(500),VALTR(500),VALSKL(500)
        REAL VALSKU(500)
        INTEGER FLAGAR,FLAGTR,FLAGVT,FLAGCN,FLAGTH,FLAGCL
        INTEGER ELMID,COIN12,COIN13,COIN14,COIN23,COIN24
        INTEGER COIN34
        INTEGER FLAGSU,FLAGSL,FLAGSK
        WRITE(*,*) 'STARTING PROGRAM GEOMETRY'
        PI=3.141592654
C
C    ENTER THE TYPE OF ELEMENT AND DETERMINE LIMIT VALUES
C    FOR DISTORTION CASES AR, TR, SK
C
        WRITE(*,*) 'ENTER THE TYPE OF ELEMENT'
        WRITE(*,*) '(1) 4 NODE AXISYMMETRICAL
QUADRILATERAL'
        WRITE(*,*) '(2) 4 NODE PLANE STRAIN QUADRILATERAL'
        WRITE(*,*) '(3) 4 NODE PLANE STRESS QUADRILATERAL'
        READ(*,*) ITYPE
        IF (ITYPE .EQ. 1) THEN
            ARLIM=18.37837
            TRLIM=0.549424
            SKLLIM=50.0
            SKULIM=130.0
        END IF
        IF (ITYPE .EQ. 2) THEN
            ARLIM=18.59468
            TRLIM=0.579587
            SKLLIM=42.99092
            SKULIM=137.00908
        END IF
        IF (ITYPE .EQ. 3) THEN
            ARLIM=16.79966
            TRLIM=0.630321
            SKLLIM=51.9744
            SKULIM=128.0256
        END IF
```

```
C
C   READ DATA FROM NODE AND ELEMENT FILES
C
      OPEN(501,FILE='NODES.TXT',STATUS='OLD')
      WRITE(*,*) 'BEFORE FIRST DO AND AFTER FISRT OPEN'
      DO 10 I=1,500
         WRITE(*,*) 'I=',I
         READ(501,*,END=11) IDNODE(I),NODE(I,1),NODE(I,2)
         INODE=INODE+1
   10 CONTINUE
   11 CONTINUE
C  11 FORMAT(1X,I2,F4.1,F4.1,F4.1)
      CLOSE(501,STATUS='KEEP')
      WRITE(*,*) 'FIRST FILE CLOSED ABOUT TO OPEN SECOND'
      OPEN(502,FILE='ELEMENTS.TXT',STATUS='OLD')
      WRITE(*,*) 'ENTERING SECOND DO LOOP'
      DO 12 I=1,500
         WRITE(*,*) 'I=',I
         READ(502,*,END=16)IDELM(I),ELM(I,1),
     +   ELM(I,2),ELM(I,3),ELM(I,4)
         IELM=IELM+1
   12 CONTINUE
   16 CONTINUE
      CLOSE(502,STATUS='KEEP')
C
C     WRITE OUT NUMBER OF NODES AND ELEMENTS
C
      WRITE(*,*) 'INODE=',INODE
      WRITE(*,*) 'IELM=',IELM
C
C     PRINT OUT NODE AND ELEMENT LISTS TO VERIFY METHOD
C
      WRITE(*,*) 'BEFORE PRINT OUT OF LISTS'
      DO 13 I=1,INODE
         WRITE(*,*) 'IDNODE=',IDNODE(I)
         WRITE(*,*) 'NODE2=',NODE(I,1)
         WRITE(*,*) 'NODE3=',NODE(I,2)
         WRITE(*,*) 'IDELEM=',IDELM(I)
         WRITE(*,*) 'ELEM1=',ELM(I,1)
         WRITE(*,*) 'ELEM2=',ELM(I,2)
         WRITE(*,*) 'ELEM3=',ELM(I,3)
         WRITE(*,*) 'ELEM4=',ELM(I,4)
   13 CONTINUE
C
C     LOOP OVER EACH ELEMENT
C
      DO 14 J=1,IELM
C
C     COMPUTE EACH ELEMENTS NODE COORDINATES
C
         ELMID=IDELM(J)
```

```fortran
                   NODE1=ELM(J,1)
                   NODE2=ELM(J,2)
                   NODE3=ELM(J,3)
                   NODE4=ELM(J,4)
                   DO 83 K1=1,INODE
                     IF (IDNODE(K1) .EQ. NODE1) THEN
                        XN1=NODE(K1,1)
                        YN1=NODE(K1,2)
                     END IF
                     IF (IDNODE(K1) .EQ. NODE2) THEN
                        XN2=NODE(K1,1)
                        YN2=NODE(K1,2)
                     END IF
                     IF (IDNODE(K1) .EQ. NODE3) THEN
                        XN3=NODE(K1,1)
                        YN3=NODE(K1,2)
                     END IF
                     IF (IDNODE(K1) .EQ. NODE4) THEN
                        XN4=NODE(K1,1)
                        YN4=NODE(K1,2)
                     END IF
   83          CONTINUE
C
C         WRITE OUT EACH OF THE VALUES AS A CHECK
C
              WRITE(*,*) 'ELMID=',ELMID
              WRITE(*,*) 'NODE1=',NODE1
              WRITE(*,*) 'NODE2=',NODE2
              WRITE(*,*) 'NODE3=',NODE3
              WRITE(*,*) 'NODE4=',NODE4
              WRITE(*,*) 'XN1=',XN1
              WRITE(*,*) 'XN2=',XN2
              WRITE(*,*) 'XN3=',XN3
              WRITE(*,*) 'XN4=',XN4
              WRITE(*,*) 'YN1=',YN1
              WRITE(*,*) 'YN2=',YN2
              WRITE(*,*) 'YN3=',YN3
              WRITE(*,*) 'YN4=',YN4
C
C         DETERMINE IF ANY ELEMENT NODE POINTS ARE COINCIDENT
C
              IF ((XN1 .EQ. XN2) .AND. (YN1 .EQ. YN2)) THEN
                 COIN12=1
                ELSE
                 COIN12=0
              END IF
              IF ((XN1 .EQ. XN3) .AND. (YN1 .EQ. YN3)) THEN
                 COIN13=1
                ELSE
                 COIN13=0
              END IF
```

220

```fortran
      IF ((XN1 .EQ. XN4) .AND. (YN1 .EQ. YN4)) THEN
          COIN14=1
        ELSE
          COIN14=0
      END IF
      IF ((XN2 .EQ. XN3) .AND. (YN2 .EQ. YN3)) THEN
          COIN23=1
        ELSE
          COIN23=0
      END IF
      IF ((XN2 .EQ. XN4) .AND. (YN2 .EQ. YN4)) THEN
          COIN24=1
        ELSE
          COIN24=0
      END IF
      IF ((XN3 .EQ. XN4) .AND. (YN3 .EQ. YN4)) THEN
          COIN34=1
        ELSE
          COIN34=0
      END IF
      FLAGCN=0
      IF (COIN12 .EQ. 1) THEN
          FLAGCN=1
      END IF
      IF (COIN13 .EQ. 1) THEN
          FLAGCN=1
      END IF
      IF (COIN14 .EQ. 1) THEN
          FLAGCN=1
      END IF
      IF (COIN23 .EQ. 1) THEN
          FLAGCN=1
      END IF
      IF (COIN24 .EQ. 1) THEN
          FLAGCN=1
      END IF
      IF (COIN34 .EQ. 1) THEN
          FLAGCN=1
      END IF
C
C     WRITE OUT COINCIDENT ELEMENT NODE POINT FLAGS
C
      WRITE(*,*) 'COIN12=',COIN12
      WRITE(*,*) 'COIN13=',COIN13
      WRITE(*,*) 'COIN14=',COIN14
      WRITE(*,*) 'COIN23=',COIN23
      WRITE(*,*) 'COIN24=',COIN24
      WRITE(*,*) 'COIN34=',COIN34
      WRITE(*,*) 'FLAGCN',FLAGCN
C
C     WRITE OUT IF WE HAVE A COINCIDENT NODAL POINT AND
```

221

```fortran
C        SKIP TO THE NEXT ELEMENT
C
         IF (FLAGCN .EQ. 1) THEN
            WRITE(*,*) 'A COINCIDENT NODE FOR
ELEMENT',ELMID
            GOTO 17
         END IF
C
C        COMPUTE THE EDGE VALUES
C

EDGEA=SQRT((XN2-XN1)*(XN2-XN1)+(YN2-YN1)*(YN2-YN1))

EDGEB=SQRT((XN3-XN2)*(XN3-XN2)+(YN3-YN2)*(YN3-YN2))

EDGEC=SQRT((XN4-XN3)*(XN4-XN3)+(YN4-YN3)*(YN4-YN3))

EDGED=SQRT((XN1-XN4)*(XN1-XN4)+(YN1-YN4)*(YN1-YN4))
C
C        WRITE OUT THE EDGE VALUES
C
         WRITE(*,*)  'EDGEA=',EDGEA
         WRITE(*,*)  'EDGEB=',EDGEB
         WRITE(*,*)  'EDGEC=',EDGEC
         WRITE(*,*)  'EDGED=',EDGED
C
C        COMPUTE ALL POSSIBLE ASPECT RATIOS
C
         RAB=EDGEA/EDGEB
         RAD=EDGEA/EDGED
         RCB=EDGEC/EDGEB
         RCD=EDGEC/EDGED
         RBA=EDGEB/EDGEA
         RBC=EDGEB/EDGEC
         RDA=EDGED/EDGEA
         RDC=EDGED/EDGEC
C
C        WRITE OUT POSSIBLE ASPECT RATIO VALUES
C
         WRITE(*,*)  'RAB=',RAB
         WRITE(*,*)  'RAD=',RAD
         WRITE(*,*)  'RCB=',RCB
         WRITE(*,*)  'RCD=',RCD
         WRITE(*,*)  'RBA=',RBA
         WRITE(*,*)  'RBC=',RBC
         WRITE(*,*)  'RDA=',RDA
         WRITE(*,*)  'RDC=',RDC
C
C        DETERMINE LARGEST ASPECT RATIO AND SET FLAGS
C
         AR=RAB
```

222

```fortran
      IF (RAD .GT. AR) THEN
          AR=RAD
      END IF
      IF (RCB .GT. AR) THEN
          AR=RCB
      END IF
      IF (RCD .GT. AR) THEN
          AR=RCD
      END IF
      IF (RBA .GT. AR) THEN
          AR=RBA
      END IF
      IF (RBC .GT. AR) THEN
          AR=RBC
      END IF
      IF (RDA .GT. AR) THEN
          AR=RDA
      END IF
      IF (RDC .GT. AR) THEN
          AR=RDC
      END IF
      IF (AR .GE. ARLIM) THEN
          FLAGAR=1
        ELSE
          FLAGAR=0
      END IF
C
C     WRITE OUT LARGEST ASPECT RATIO AND ITS FLAG VALUE
C
      WRITE(*,*) 'AR=',AR
      WRITE(*,*) 'FLAGAR=',FLAGAR
C
C     COMPUTE ALL POSSIBLE TAPER RATIOS
C
      RAC=EDGEA/EDGEC
      RCA=EDGEC/EDGEA
      RBD=EDGEB/EDGED
      RDB=EDGED/EDGEB
C
C     WRITE OUT POSSIBLE TAPER RATIO VALUES
C
      WRITE(*,*) 'RAC=',RAC
      WRITE(*,*) 'RCA=',RCA
      WRITE(*,*) 'RBD=',RBD
      WRITE(*,*) 'RDB=',RDB
C
C     DETERMINE SMALLEST TAPER RATIO AND SET FLAGS
C
      TR=RAC
      IF (RCA .LT. TR) THEN
          TR=RCA
```

```
          END IF
          IF (RBD .LT. TR) THEN
              TR=RBD
          END IF
          IF (RDB .LT. TR) THEN
              TR=RDB
          END IF
          IF (TR .LE. TRLIM) THEN
              FLAGTR=1
            ELSE
              FLAGTR=0
          END IF
C
C     WRITE OUT SMALLEST TAPER RATIO AND ITS FLAG VALUE
C
          WRITE(*,*) 'TR=',TR
          WRITE(*,*) 'FLAGTR=',FLAGTR
C
C     CALC CROSS PRODUCT TO DETERMINE INVERTED ELEMENTS
C
          V12X23=(XN2-XN1)*(YN3-YN2)-(YN2-YN1)*(XN3-XN2)
          V23X34=(XN3-XN2)*(YN4-YN3)-(YN3-YN2)*(XN4-XN3)
          V34X41=(XN4-XN3)*(YN1-YN3)-(YN4-YN3)*(XN1-XN4)
          V41X12=(XN1-XN4)*(YN2-YN1)-(YN1-YN4)*(XN2-XN1)
C
C     WRITE OUT VALUES OF CROSS PRODUCTS
C
          WRITE(*,*) 'V12X23=',V12X23
          WRITE(*,*) 'V23X34=',V23X34
          WRITE(*,*) 'V34X41=',V34X41
          WRITE(*,*) 'V41X12=',V41X12
C
C     SET FLAGS FOR CROSS PRODUCTS THAT IS FOR INVERSION
C
          IF (V12X23 .LE. 0.0) THEN
              INVRT2=1
            ELSE
              INVRT2=0
          END IF
          IF (V23X34 .LE. 0.0) THEN
              INVRT3=1
            ELSE
              INVRT3=0
          END IF
          IF (V34X41 .LE. 0.0) THEN
              INVRT4=1
            ELSE
              INVRT4=0
          END IF
          IF (V41X12 .LE. 0.0) THEN
              INVRT1=1
```

224

```fortran
            ELSE
                INVRT1=0
            END IF
            FLAGVT=0
            IF (INVRT1 .EQ. 1) THEN
                FLAGVT=1
            END IF
            IF (INVRT2 .EQ. 1) THEN
                FLAGVT=1
            END IF
            IF (INVRT3 .EQ. 1) THEN
                FLAGVT=1
            END IF
            IF (INVRT4 .EQ. 1) THEN
                FLAGVT=1
            END IF
C
C       WRITE OUT FLAGS FOR ELEMENT INVERSION
C
            WRITE(*,*) 'INVRT1=',INVRT1
            WRITE(*,*) 'INVRT2=',INVRT2
            WRITE(*,*) 'INVRT3=',INVRT3
            WRITE(*,*) 'INVRT4=',INVRT4
            WRITE(*,*) 'FLAGVT=',FLAGVT
C
C       CALCULATE THE DOT PRODUCT TO DETERMINE ANGLES
C
C         IF (ICL412 .EQ. 1) THEN
C             THETA1=PI
C             GOTO 22
C         END IF
            T1=(XN4-XN1)*(XN2-XN1)+(YN4-YN1)*(YN2-YN1)
            THETA1=ACOS(T1/(EDGED*EDGEA))
            IF (INVRT1 .EQ. 1) THEN
                THETA1=2.0*PI-THETA1
            END IF
            T2=(XN1-XN2)*(XN3-XN2)+(YN1-YN2)*(YN3-YN2)
            THETA2=ACOS(T2/(EDGEA*EDGEB))
            IF (INVRT2 .EQ. 1) THEN
                THETA2=2.0*PI-THETA2
            END IF
            T3=(XN2-XN3)*(XN4-XN3)+(YN2-YN3)*(YN4-YN3)
            THETA3=ACOS(T3/(EDGEB*EDGEC))
            IF (INVRT3 .EQ. 1) THEN
                THETA3=2.0*PI-THETA3
            END IF
            T4=(XN3-XN4)*(XN1-XN4)+(YN3-YN4)*(YN1-YN4)
            THETA4=ACOS(T4/(EDGEC*EDGED))
            IF (INVRT4 .EQ. 1) THEN
                THETA4=2.0*PI-THETA4
            END IF
```

225

```
C
C       CONVERT FROM RADIANS TO DEGREES
C
        WT1=THETA1*180.0/PI
        WT2=THETA2*180.0/PI
        WT3=THETA3*180.0/PI
        WT4=THETA4*180.0/PI
C
C     SET SKEW ANGLE FLAGS FOR BOTH UPPER AND LOWER
VALUES
C
C
C   LOWER LIMIT
C
        SKL=WT1
        IF (WT2 .LT. SKL) THEN
            SKL=WT2
        END IF
        IF (WT3 .LT. SKL) THEN
            SKL=WT3
        END IF
        IF (WT4 .LT. SKL) THEN
            SKL=WT4
        END IF
        FLAGSL=0
        IF (SKL .LE. SKLLIM) THEN
            FLAGSL=1
          ELSE
            FLAGSL=0
        END IF
C
C     WRITE OUT SMALLEST SKEW ANGLE AND ITS FLAG VALUE
C
        WRITE(*,*) 'SKL=',SKL
        WRITE(*,*) 'FLAGSL=',FLAGSL
C
C   UPPER LIMIT
C
        SKU=WT1
        IF (WT2 .GT. SKU) THEN
            SKU=WT2
        END IF
        IF (WT3 .GT. SKU) THEN
            SKU=WT3
        END IF
        IF (WT4 .GT. SKU) THEN
            SKU=WT4
        END IF
        FLAGSU=0
        IF (SKU .GE. SKULIM) THEN
            FLAGSU=1
```

```fortran
            ELSE
               FLAGSU=0
            END IF
            FLAGSK=0
            IF ((FLAGSL .EQ. 1) .OR. (FLAGSU .EQ. 1)) THEN
               FLAGSK=1
            END IF
C
C      WRITE OUT LARGEST SKEW ANGLE AND SK FLAG VALUE
C
            WRITE(*,*) 'SKU=',SKU
            WRITE(*,*) 'FLAGSKU=',FLAGSKU
            WRITE(*,*) 'FLAGSK=',FLAGSK
C
C      WRITE OUT ELEMENT ANGLES
C
            WRITE(*,*) 'THETA1=',WT1
            WRITE(*,*) 'THETA2=',WT2
            WRITE(*,*) 'THETA3=',WT3
            WRITE(*,*) 'THETA4=',WT4
            WRITE(*,*) 'FLAGSK=',FLAGSK
C
C      WRITE OUT ALL FLAGS AND VALUES TO ARRAYS
C
   17       CONTINUE
            ELMFLAG(J,1)=ELMID
            ELMFLAG(J,2)=FLAGAR
            ELMFLAG(J,3)=FLAGTR
            ELMFLAG(J,4)=FLAGSK
            ELMFLAG(J,5)=FLAGCN
C            ELMFLAG(J,6)=FLAGCL
            ELMFLAG(J,6)=FLAGVT
            VALAR(J)=AR
            VALTR(J)=TR
            VALSKL(J)=SKL
            VALSKU(J)=SKU
   14    CONTINUE
C     WRITE OUT FLAG AND VALUE ARRAYS TO A FILE
         OPEN(555,FILE='FLAGS.TXT',STATUS='NEW')
         WRITE(555,*) '  ELMID  AR        TR        SKL
SKU
     +FAI  FTR FSK FCN FVT'
         DO 15 J=1,IELM
           WRITE(555,99) ELMFLAG(J,1),VALAR(J),
     +VALTR(J),VALSKL(J),
     +VALSKU(J),ELMFLAG(J,2),ELMFLAG(J,3),ELMFLAG(J,4),
     +ELMFLAG(J,5),ELMFLAG(J,6)
   15    CONTINUE
   99    FORMAT(1X,I7,F9.4,F8.4,F10.4,F10.4,I4,I4,I4,I4,I4)
         CLOSE(555,STATUS='KEEP')
         END
```

Element and node input files follow.

Element input file.

Element number and associated node numbers

1	1	2	102	101
2	2	3	103	102
3	3	4	104	103
4	4	5	105	104
5	5	6	106	105
6	6	7	107	106
7	7	8	108	107
8	8	9	109	108
9	9	10	110	109
10	10	11	111	110
11	11	12	112	111
12	12	13	113	112
101	101	102	202	201
102	102	103	203	202
103	103	104	204	203
104	104	105	205	204
105	105	106	206	205
106	106	107	207	206
107	107	108	208	207
108	108	109	209	208
109	109	110	210	209
110	110	111	211	210
111	111	112	212	211
112	112	113	213	212
201	201	202	302	301
202	202	203	303	302
203	203	204	304	303
204	204	205	305	304
205	205	206	306	305
206	206	207	307	306
207	207	208	308	307
208	208	209	309	308
209	209	210	310	309
210	210	211	311	310
211	211	212	312	311
212	212	213	313	312
301	301	302	402	401
302	302	303	403	402
303	303	304	404	403
304	304	305	405	404
305	305	306	406	405
306	306	307	407	406
307	307	308	408	407
308	308	309	409	408

309	309	310	410	409
310	310	311	411	410
311	311	312	412	411
312	312	313	413	412
401	401	402	502	501
402	402	403	503	502
403	403	404	504	503
404	404	405	505	504
405	405	406	506	505
406	406	407	507	506
407	407	408	508	507
408	408	409	509	508
409	409	410	510	509
410	410	411	511	510
411	411	412	512	511
412	412	413	513	512
501	501	502	602	601
502	502	503	603	602
503	503	504	604	603
504	504	505	605	604
505	505	506	606	605
506	506	507	607	606
507	507	508	608	607
508	508	509	609	608
509	509	510	610	609
510	510	511	611	610
511	511	512	612	611
512	512	513	613	612
601	601	602	702	701
602	602	603	703	702
603	603	604	704	703
604	604	605	705	704
605	605	606	706	705
606	606	607	707	706
607	607	608	708	707
608	608	609	709	708
609	609	610	710	709
610	610	611	711	710
611	611	612	712	711
612	612	613	713	712
701	701	702	802	801
702	702	703	803	802
703	703	704	804	803
704	704	705	805	804
705	705	706	806	805
706	706	707	807	806
707	707	708	808	807
708	708	709	809	808
709	709	710	810	809
710	710	711	811	810
711	711	712	812	811

712	712	713	813	812
801	801	802	902	901
802	802	803	903	902
803	803	804	904	903
804	804	805	905	904
805	805	806	906	905
806	806	807	907	906
807	807	808	908	907
808	808	809	909	908
809	809	810	910	909
810	810	811	911	910
811	811	812	912	911
812	812	813	913	912
901	901	902	1002	1001
902	902	903	1003	1002
903	903	904	1004	1003
904	904	905	1005	1004
905	905	906	1006	1005
906	906	907	1007	1006
907	907	908	1008	1007
908	908	909	1009	1008
909	909	910	1010	1009
910	910	911	1011	1010
911	911	912	1012	1011
912	912	913	1013	1012
1001	1001	1002	1102	1101
1002	1002	1003	1103	1102
1003	1003	1004	1104	1103
1004	1004	1005	1105	1104
1005	1005	1006	1106	1105
1006	1006	1007	1107	1106
1007	1007	1008	1108	1107
1008	1008	1009	1109	1108
1009	1009	1010	1110	1109
1010	1010	1011	1111	1110
1011	1011	1012	1112	1111
1012	1012	1013	1113	1112
1101	1101	1102	1202	1201
1102	1102	1103	1203	1202
1103	1103	1104	1204	1203
1104	1104	1105	1205	1204
1105	1105	1106	1206	1205
1106	1106	1107	1207	1206
1107	1107	1108	1208	1207
1108	1108	1109	1209	1208
1109	1109	1110	1210	1209
1110	1110	1111	1211	1210
1111	1111	1112	1212	1211
1112	1112	1113	1213	1212

Node input file.

Node number	X coord.	Y coord.
1	0.	0.
2	8.33333E-04	0.
3	1.66667E-03	0.
4	2.50000E-03	0.
5	3.33333E-03	0.
6	4.16667E-03	0.
7	5.00000E-03	0.
8	5.83333E-03	0.
9	6.66667E-03	0.
10	7.50000E-03	0.
11	8.33333E-03	0.
12	9.16667E-03	0.
13	1.00000E-02	0.
101	0.	1.25000E-03
102	8.33333E-04	1.25000E-03
103	1.66667E-03	1.25000E-03
104	2.50000E-03	1.25000E-03
105	3.33333E-03	1.25000E-03
106	4.16667E-03	1.25000E-03
107	5.00000E-03	1.25000E-03
108	5.83333E-03	1.25000E-03
109	6.66667E-03	1.25000E-03
110	7.50000E-03	1.25000E-03
111	8.33333E-03	1.25000E-03
112	9.16667E-03	1.25000E-03
113	1.00000E-02	1.25000E-03
201	0.	2.50000E-03
202	8.33333E-04	2.50000E-03
203	1.66667E-03	2.50000E-03
204	2.50000E-03	2.50000E-03
205	3.33333E-03	2.50000E-03
206	4.16667E-03	2.50000E-03
207	5.00000E-03	2.50000E-03
208	5.83333E-03	2.50000E-03
209	6.66667E-03	2.50000E-03
210	7.50000E-03	2.50000E-03
211	8.33333E-03	2.50000E-03
212	9.16667E-03	2.50000E-03
213	1.00000E-02	2.50000E-03
301	0.	3.75000E-03
302	8.33333E-04	3.75000E-03
303	1.66667E-03	3.75000E-03
304	2.50000E-03	3.75000E-03
305	3.33333E-03	3.75000E-03
306	4.16667E-03	3.75000E-03
307	5.00000E-03	3.75000E-03
308	5.83333E-03	3.75000E-03
309	6.66667E-03	3.75000E-03

```
310     7.50000E-03  3.75000E-03
311     8.33333E-03  3.75000E-03
312     9.16667E-03  3.75000E-03
313     1.00000E-02  3.75000E-03
401        0.        5.00000E-03
402     8.33333E-04  5.00000E-03
403     1.66667E-03  5.00000E-03
404     2.50000E-03  5.00000E-03
405     3.33333E-03  5.00000E-03
406     4.16667E-03  5.00000E-03
407     5.00000E-03  5.00000E-03
408     5.83333E-03  5.00000E-03
409     6.66667E-03  5.00000E-03
410     7.50000E-03  5.00000E-03
411     8.33333E-05  5.00000E-03
412     9.16667E-03  5.00000E-03
413     1.00000E-02  5.00000E-03
501        0.        6.25000E-03
502     8.33333E-04  6.25000E-03
503     1.66667E-03  6.25000E-03
504     2.50000E-03  6.25000E-03
505     3.33333E-03  6.25000E-03
506     4.16667E-03  6.25000E-03
507     5.00000E-03  6.25000E-03
508     5.83333E-03  6.25000E-03
509     6.66667E-03  6.25000E-03
510     7.50000E-03  6.25000E-03
511     8.33333E-03  6.25000E-03
512     9.16667E-03  6.25000E-03
513     1.00000E-02  6.25000E-03
601        0.        7.50000E-03
602     8.33333E-04  7.50000E-03
603     1.66667E-03  7.50000E-03
604     2.50000E-03  7.50000E-03
605     3.33333E-03  7.50000E-03
606     4.16667E-03  7.50000E-03
607     5.00000E-03  7.50000E-03
608     5.83333E-03  7.50000E-03
609     6.66667E-03  7.50000E-03
610     7.50000E-03  7.50000E-03
611     8.33333E-03  7.50000E-03
612     9.16667E-03  7.50000E-03
613     1.00000E-02  7.50000E-03
701        0.        8.75000E-03
702     8.33333E-04  8.75000E-03
703     1.66667E-03  8.75000E-03
704     2.50000E-03  8.75000E-03
705     3.33333E-03  8.75000E-03
706     4.16667E-03  8.75000E-03
707     5.00000E-03  8.75000E-03
708     5.83333E-03  8.75000E-03
```

```
709      6.66667E-03 8.75000E-03
710      7.50000E-03 8.75000E-03
711      8.33333E-03 8.75000E-03
712      9.16667E-03 8.75000E-03
713      1.00000E-02 8.75000E-03
801         0.       1.00000E-02
802      8.33333E-04 1.00000E-02
803      1.66667E-03 1.00000E-02
804      2.50000E-03 1.00000E-02
805      3.33333E-03 1.00000E-02
806      4.16667E-03 1.00000E-02
807      5.00000E-03 1.00000E-02
808      5.83333E-03 1.00000E-02
809      6.66667E-03 1.00000E-02
810      7.50000E-03 1.00000E-02
811      8.33333E-03 1.00000E-02
812      9.16667E-03 1.00000E-02
813      1.00000E-02 1.00000E-02
901         0.       1.12500E-02
902      8.33333E-04 1.12500E-02
903      1.66667E-03 1.12500E-02
904      2.50000E-03 1.12500E-02
905      3.33333E-03 1.12500E-02
906      4.16667E-03 1.12500E-02
907      5.00000E-03 1.12500E-02
908      5.83333E-03 1.12500E-02
909      6.66667E-03 1.12500E-02
910      7.50000E-03 1.12500E-02
911      8.33333E-03 1.12500E-02
912      9.16667E-03 1.12500E-02
913      1.00000E-02 1.12500E-02
1001        0.       1.25000E-02
1002     8.33333E-04 1.25000E-02
1003     1.66667E-03 1.25000E-02
1004     2.50000E-03 1.25000E-02
1005     3.33333E-03 1.25000E-02
1006     4.16667E-03 1.25000E-02
1007     5.00000E-03 1.25000E-02
1008     5.83333E-03 1.25000E-02
1009     6.66667E-03 1.25000E-02
1010     7.50000E-03 1.25000E-02
1011     8.33333E-03 1.25000E-02
1012     9.16667E-03 1.25000E-02
1013     1.00000E-02 1.25000E-02
1101        0.       1.37500E-02
1102     8.33333E-04 1.37500E-02
1103     1.66667E-03 1.37500E-02
1104     2.50000E-03 1.37500E-02
1105     3.33333E-03 1.37500E-02
1106     4.16667E-03 1.37500E-02
1107     5.00000E-03 1.37500E-02
```

```
1108    5.83333E-03 1.37500E-02
1109    6.66667E-03 1.37500E-02
1110    7.50000E-03 1.37500E-02
1111    8.33333E-03 1.37500E-02
1112    9.16667E-03 1.37500E-02
1113    1.00000E-02 1.37500E-02
1201         0.     1.50000E-02
1202    8.33333E-04 1.50000E-02
1203    1.66667E-03 1.50000E-02
1204    2.50000E-03 1.50000E-02
1205    3.33333E-03 1.50000E-02
1206    4.16667E-03 1.50000E-02
1207    5.00000E-03 1.50000E-02
1208    5.83333E-03 1.50000E-02
1209    6.66667E-03 1.50000E-02
1210    7.50000E-03 1.50000E-02
1211    8.33333E-03 1.50000E-02
1212    9.16667E-03 1.50000E-02
1213    1.00000E-02 1.50000E-02
```

APPENDIX B

RESULTS FROM THE UPSETTING BILLET PROBLEM

RESULTS FROM THE UPSETTING BILLET PROBLEM

The following figures and tables are results from the upsetting billet problem which simulates a metal forming process. Contour plots of equivalent plastic strain, Mises stress, and strain energy density are shown in Figure B.1 through Figure B.27. Each figure corresponds to either equivalent plastic strain, Mises stress, or strain energy density for a particular rezoning point or at the completion of the solution. Cases of the completed solution for nonrezoning also appear. Table listings of strain jump values at the nodes of the elements flagged for rezoning and those within twenty percent of being flagged are shown in Table B.1 through Table B.9.

PEEQ

	VALUE				
1	+2.00E-07	5	+8.00E-01	9	+1.60E+00
2	+2.00E-01	6	+1.00E+00	10	+1.80E+00
3	+4.00E-01	7	+1.20E+00	11	+2.00E+00
4	+6.00E-01	8	+1.40E+00		
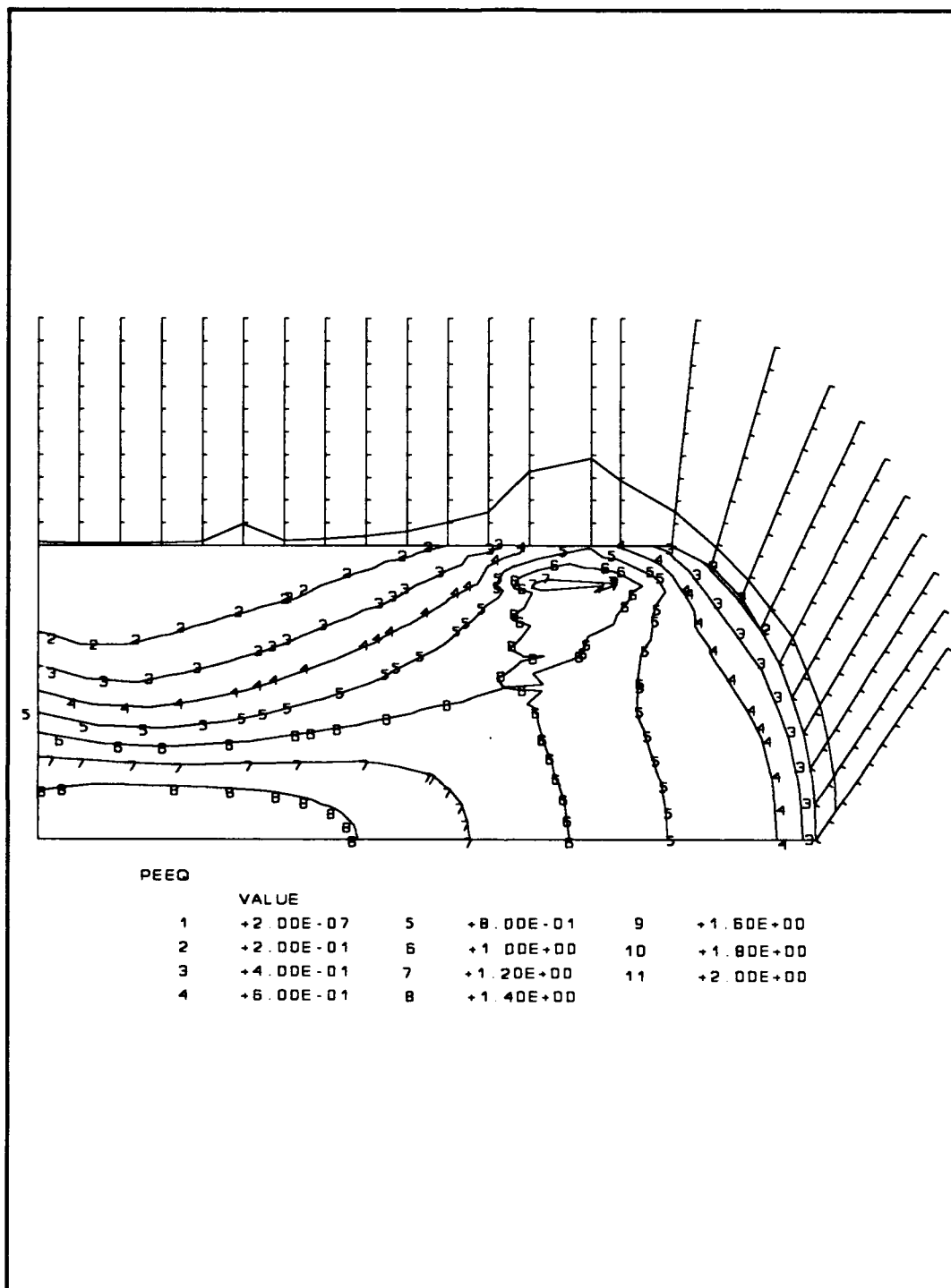
Figure B.1.   Contour plot of equivalent plastic strain for the point of termination for the nonrezoning case of the upsetting billet

237

MISES

	VALUE						
1	+3.00E+02	4	+9.00E+08	7	+1.80E+09	10	+2.70E+09
2	+3.00E+08	5	+1.20E+09	8	+2.10E+09	11	+3.00E+09
3	+6.00E+08	6	+1.50E+09	9	+2.40E+09		
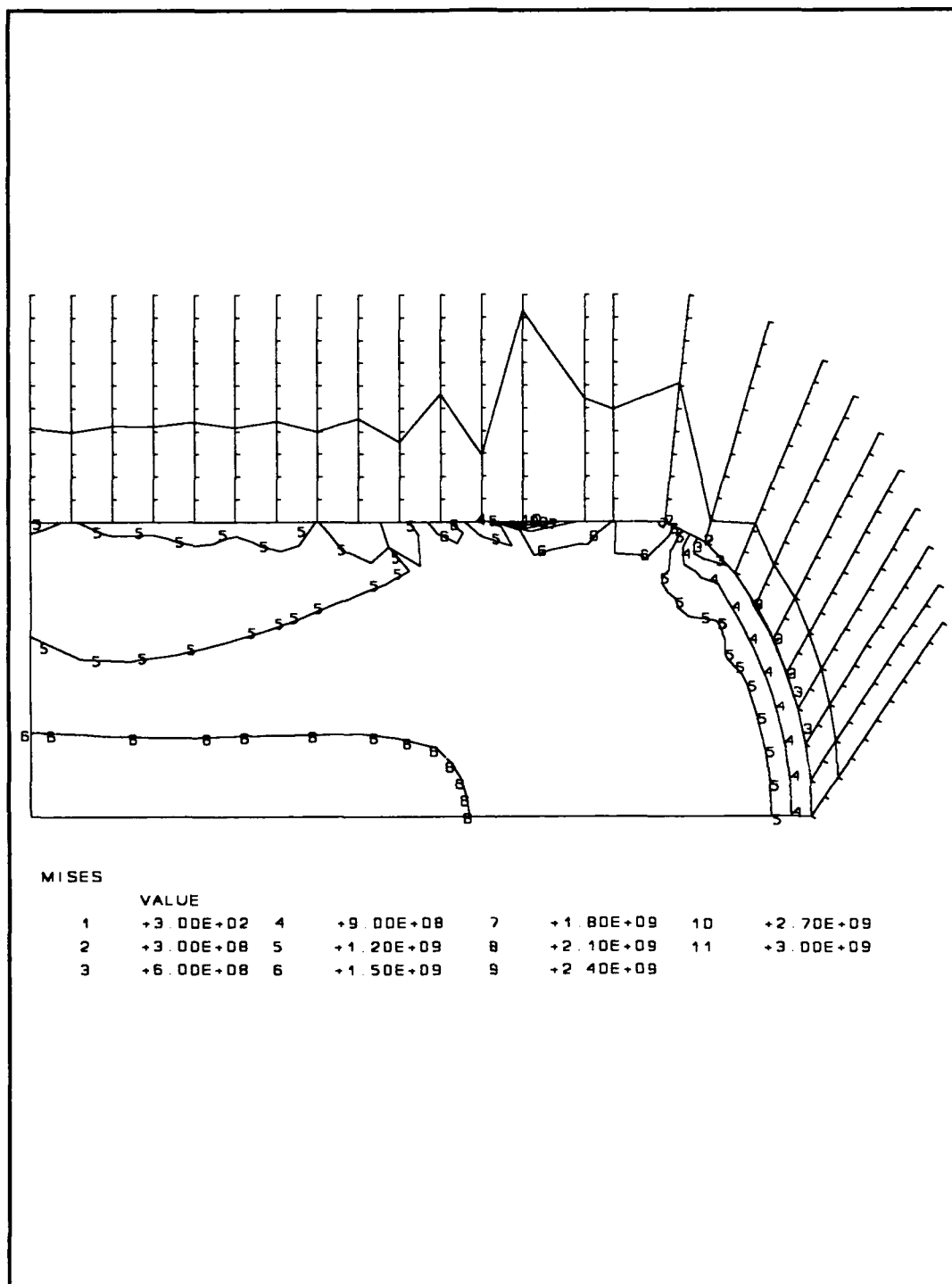
Figure B.2. Contour plot of Mises stress for the point of termination for the nonrezoning case of the upsetting billet

SENER

	VALUE						
1	+2.00E+00	4	+6.00E+06	7	+1.20E+07	10	+1.80E+07
2	+2.00E+06	5	+8.00E+06	8	+1.40E+07	11	+2.00E+07
3	+4.00E+06	6	+1.00E+07	9	+1.60E+07		
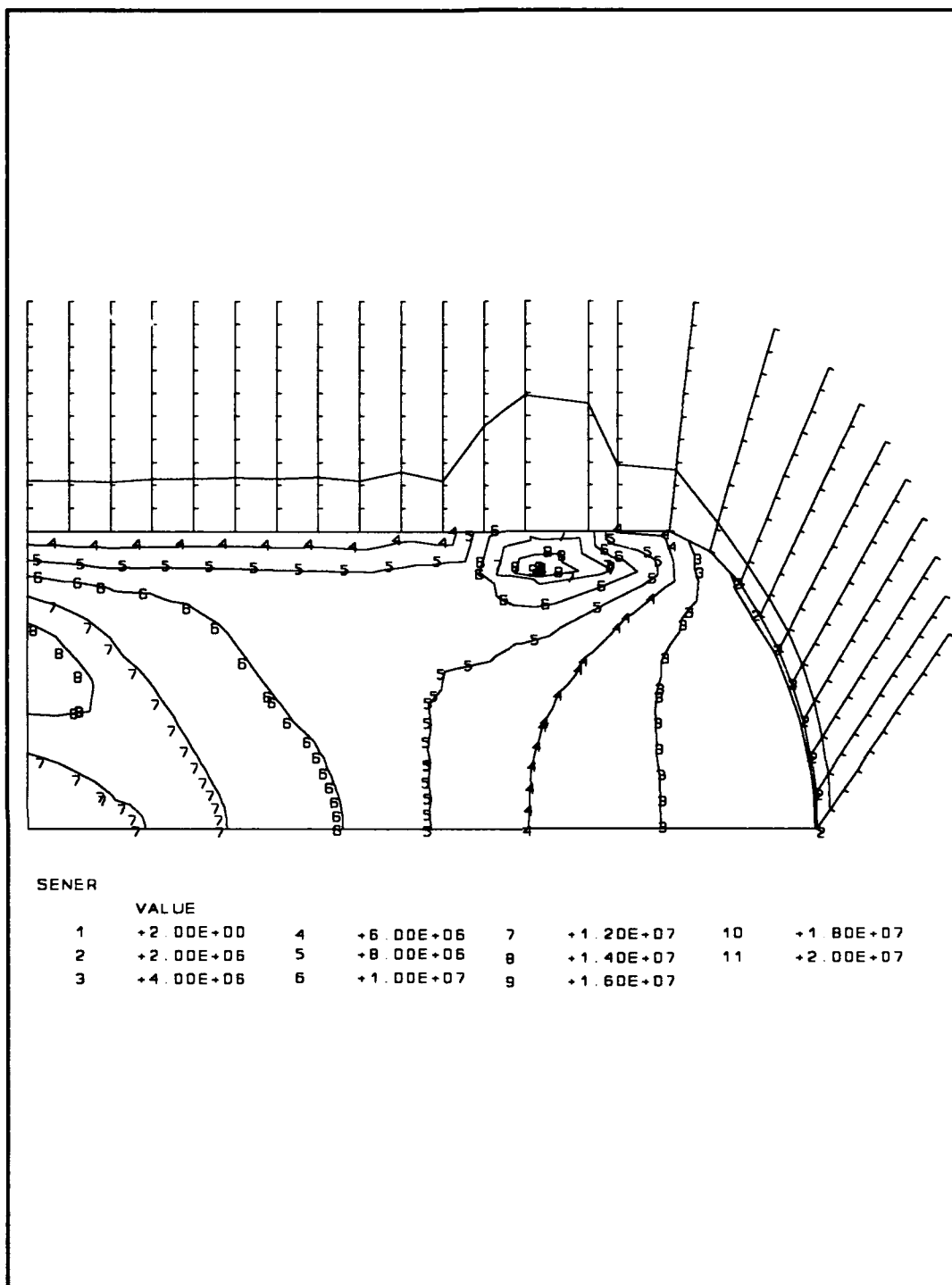
Figure B.3. Contour plot of strain energy density for the point of termination for the nonrezoning case of the upsetting billet

239

Table B.1.   Strain jump values for elements flagged for rezoning and those within twenty percent for the nonrezoning case of the upsetting billet problem

NODE	SJP11	SJP22	SJP33	SJP12
403	0.1087	0.1531	4.4257E-02	0.3299
404	5.8574E-02	8.8652E-02	6.1517E-02	7.0910E-02
405	6.3749E-02	0.1296	6.5147E-02	0.1592
406	6.1816E-02	7.4349E-02	6.3445E-02	2.3932E-02
407	4.1947E-02	9.3432E-02	5.9968E-02	0.1033
502	9.8379E-02	0.1628	6.4428E-02	0.7069
503	7.5396E-02	9.8475E-02	6.6235E-02	0.1989
504	0.1091	0.1887	7.9210E-02	0.2785
505	6.5466E-02	6.7889E-02	7.8712E-02	3.0310E-02
506	5.8595E-02	0.1330	7.4008E-02	0.1971
507	7.9917E-02	6.2654E-02	6.7713E-02	1.4708E-02
508	6.7636E-02	9.6878E-02	6.2028E-02	0.1224
602	1.4998E-02	7.6449E-02	8.4243E-02	0.5125
603	0.1769	0.2717	9.4519E-02	0.4704
604	4.6682E-02	6.7258E-02	0.1010	6.9186E-02
605	0.1142	0.2098	9.5356E-02	0.3247
606	6.9404E-02	3.0024E-02	8.7081E-02	5.8353E-02
607	6.9527E-02	0.1474	7.7930E-02	0.2598
608	0.1141	8.0524E-02	6.9220E-02	1.8699E-02
609	9.8652E-02	0.1061	6.2676E-02	0.1221
610	0.1543	0.1471	5.8681E-02	2.2803E-02
702	0.1164	0.2322	0.1168	0.8052
703	2.2474E-02	0.1492	0.1262	0.1489
704	0.1455	0.2698	0.1239	0.3676
705	7.0958E-02	8.1928E-02	0.1134	0.1275
706	0.1386	0.2404	0.1017	0.3929
707	0.1024	1.8540E-02	9.0527E-02	8.5676E-02
708	0.1224	0.2015	7.9614E-02	0.3754
709	0.1513	0.1016	6.9825E-02	2.6138E-02
710	0.1449	0.1410	6.2866E-02	0.1373
711	0.2361	0.2254	6.1734E-02	8.8554E-02
802	4.7234E-02	0.1959	0.1487	0.4192
803	0.1417	0.2933	0.1512	0.3138
804	4.8668E-02	0.1781	0.1399	6.3207E-02
805	0.1347	0.2617	0.1319	0.3168
806	5.0013E-02	0.1436	0.1234	0.1216
807	0.1729	0.2761	0.1142	0.4575
808	0.1211	6.0002E-02	0.1032	0.1089
809	0.2065	0.2872	9.2600E-02	0.5475
810	0.1944	0.1269	7.9920E-02	4.2201E-02
811	0.2523	0.2738	6.6467E-02	0.1085
903	7.2730E-02	0.1998	0.1501	5.4851E-02
904	0.1133	0.2501	0.1366	0.1346

Table B.1 (continued)

905	9.5306E-02	0.2319	0.1375	1.8975E-02
906	0.1478	0.2643	0.1374	0.2266
907	7.9256E-02	0.2146	0.1361	7.7464E-02
908	0.2180	0.3207	0.1312	0.5060
909	0.1051	0.1236	0.1246	0.1503
910	0.3057	0.3881	0.1162	0.8202
911	0.3511	0.2732	9.3264E-02	0.2217
912	0.3918	0.4573	9.6702E-02	0.6479
1005	0.1100	0.2166	0.1074	0.1704
1006	0.1225	0.2357	0.1138	0.1278
1007	0.1665	0.2760	0.1208	0.1534
1008	0.1624	0.2897	0.1279	5.8521E-02
1009	0.2738	0.3716	0.1323	0.4567
1010	0.1253	0.2647	0.1396	0.1887
1011	0.5474	0.5729	0.1372	1.177
1012	0.5947	0.5150	0.1085	1.244
1013	0.2137	0.2996	8.1838E-02	4.3719E-02
1107	9.6497E-02	0.1640	6.7855E-02	0.2243
1108	0.1457	0.2227	7.8364E-02	0.2760
1109	0.2033	0.2934	9.0338E-02	0.3093
1110	0.3120	0.3996	0.1060	0.2537
1111	0.3774	0.5057	0.1280	0.1019
1112	0.8666	0.8729	0.1141	1.814
1113	0.3454	0.2553	0.1020	4.1789E-02
1210	4.5024E-03	8.0536E-03	8.1715E-03	1.7290E-03
1211	3.3283E-03	1.3659E-03	1.3983E-02	5.2741E-03
1212	2.6655E-02	5.8601E-04	1.0573E-02	6.0745E-02

MAXIMUM	0.8666	0.8729	0.1588	1.814
NODE	1112	1112	902	1112
MINIMUM	0.	0.	0.	0.
NODE	1	1	1	1

241

PEEQ

VALUE

1	+5.00E-08	5	+2.00E-01	9	+4.00E-01
2	+5.00E-02	6	+2.50E-01	10	+4.50E-01
3	+1.00E-01	7	+3.00E-01	11	+5.00E-01
4	+1.50E-01	8	+3.50E-01		

Figure B.4. Contour plot of equivalent plastic strain at the point flagged for the first rezoning of the upsetting billet

MISES

	VALUE						
1	+2.00E+02	5	+8.00E+08	9	+1.60E+09
2	+2.00E+08	6	+1.00E+09	10	+1.80E+09
3	+4.00E+08	7	+1.20E+09	11	+2.00E+09
4	+6.00E+08	8	+1.40E+09		

Figure B.5.   Contour plot of Mises stress at the point
flagged for the first rezoning of the upsetting billet

243

SENER

VALUE

1	+6.00E-01	5	+2.40E+06	9	+4.80E+06
2	+6.00E+05	6	+3.00E+06	10	+5.40E+06
3	+1.20E+06	7	+3.60E+06	11	+6.00E+06
4	+1.80E+06	8	+4.20E+06		

Figure B.6. Contour plot of strain energy density at the point flagged for the first rezoning of the upsetting billet

244

Table B.2. Strain jump values for elements flagged for
rezoning and those within twenty percent for the first
rezoning case of the upsetting billet problem

NODE	SJP11	SJP22	SJP33	SJP12
1111	0.1138	0.1550	4.2156E-02	0.1818
1112	0.1627	0.2118	5.2170E-02	0.4883
1113	0.1522	0.1203	3.8374E-02	0.2370
1211	1.9771E-03	1.9998E-03	6.3229E-03	4.2294E-04
1212	7.1671E-03	9.9516E-03	1.3796E-02	9.1070E-03
MAXIMUM	0.2349	0.2118	5.2170E-02	0.4883
NODE	1012	1112	1112	1112
MINIMUM	0.	0.	0.	0.
NODE	1	1	1	1

Figure B.7. Contour plot of equivalent plastic strain at the point flagged for the second rezoning of the upsetting billet

MISES

	VALUE					
1	+5.00E+08	5	+8.60E+08	9	+1.22E+09
2	+5.90E+08	6	+9.50E+08	10	+1.31E+09
3	+6.80E+08	7	+1.04E+09	11	+1.40E+09
4	+7.70E+08	8	+1.13E+09		

Figure B.8. Contour plot of Mises stress at the point flagged for the second rezoning of the upsetting billet

SENER

	VALUE				
1	+7.00E-01	5	+2.80E+06	9	+5.60E+06
2	+7.00E+05	6	+3.50E+06	10	+6.30E+06
3	+1.40E+06	7	+4.20E+06	11	+7.00E+06
4	+2.10E+06	8	+4.90E+06		

Figure B.9. Contour plot of strain energy density at the point flagged for the second rezoning of the upsetting billet

248

Table B.3. Strain jump values for elements flagged for rezoning and those within twenty percent for the second rezoning case of the upsetting billet problem

NODE	SJP11	SJP22	SJP33	SJP12
1112	5.2858E-02	4.5554E-02	1.5595E-02	3.8581E-02
1113	3.4549E-02	2.9818E-02	9.1713E-03	0.1222
1114	0.1610	0.1529	1.1177E-02	0.2947
1213	0.1212	0.1274	7.8805E-03	0.4896
1312	5.2953E-02	6.1623E-02	9.4868E-03	6.5697E-02
1313	7.5287E-02	7.9892E-02	7.6651E-03	0.1871
MAXIMUM	0.1610	0.1529	1.5595E-02	0.4896
NODE	1114	1114	1112	1213
MINIMUM	0.	0.	0.	0.
NODE	1	1	1	1

PEEQ

	VALUE				
1	+9.00E-08	5	+3.60E-01	9	+7.20E-01
2	+9.00E-02	6	+4.50E-01	10	+8.10E-01
3	+1.80E-01	7	+5.40E-01	11	+9.00E-01
4	+2.70E-01	8	+6.30E-01		

Figure B.10.   Contour plot of equivalent plastic strain at the point flagged for the third rezoning of the upsetting billet

MISES

	VALUE				
1	+5.00E+08	5	+9.40E+08	9	+1.38E+09
2	+6.10E+08	6	+1.05E+09	10	+1.49E+09
3	+7.20E+08	7	+1.16E+09	11	+1.60E+09
4	+8.30E+08	8	+1.27E+09		

Figure B.11. Contour plot of Mises stress at the point flagged for the third rezoning of the upsetting billet

SENER

VALUE

1	+9.00E-01	5	+3.60E+06	9	+7.20E+06
2	+9.00E+05	6	+4.50E+06	10	+8.10E+06
3	+1.80E+06	7	+5.40E+06	11	+9.00E+06
4	+2.70E+06	8	+6.30E+06		
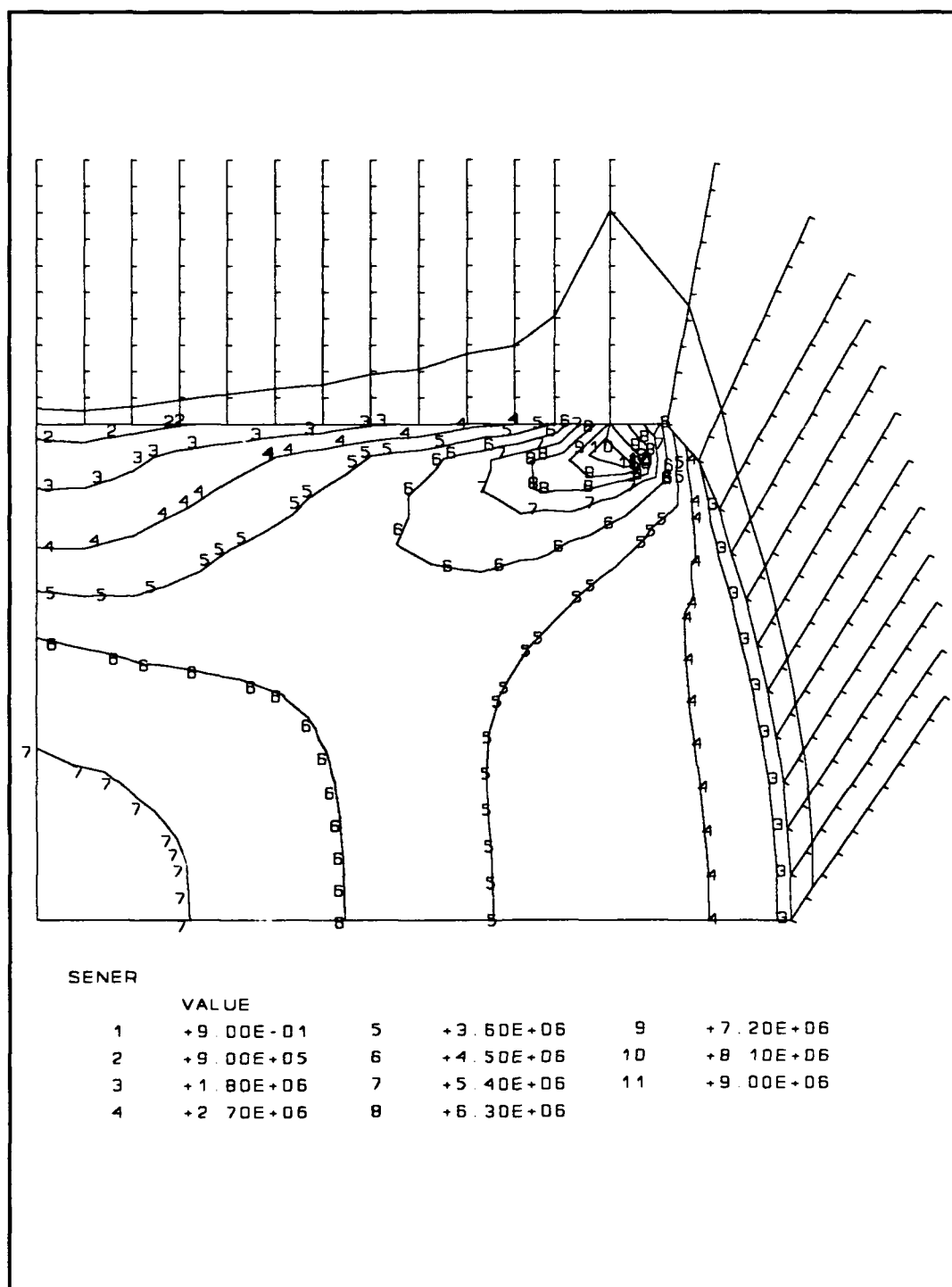
Figure B.12. Contour plot of strain energy density at the point flagged for the third rezoning of the upsetting billet

252

Table B.4. Strain jump values for elements flagged for rezoning and those within twenty percent for the third rezoning case of the upsetting billet problem

NODE	SJP11	SJP22	SJP33	SJP12
909	3.0896E-02	4.8518E-02	2.7023E-02	C.1060
910	2.9980E-02	3.1537E-02	2.3364E-02	7.6816E-02
1009	3.6669E-02	6.3821E-02	2.6996E-02	2.6848E-02
1010	6.0558E-02	8.1115E-02	2.8738E-02	0.1477
1011	2.3587E-02	3.9062E-02	2.6058E-02	9.3531E-02
1012	1.4845E-02	2.5708E-02	2.2944E-02	0.1677
1013	0.1385	0.1254	1.7940E-02	0.1671
1014	0.1738	0.1726	1.7213E-02	0.1713
1110	5.1718E-02	7.1925E-02	1.9937E-02	7.4427E-02
1111	0.1163	0.1268	2.2439E-02	0.1905
1112	9.9883E-02	0.1245	2.4860E-02	3.3268E-02
1113	1.6315E-02	6.1318E-03	2.2087E-02	5.2850E-02
1114	0.3960	0.3977	2.4670E-02	0.3526
1213	7.7226E-03	1.8988E-02	8.4325E-03	0.8184
1310	2.4767E-02	3.2410E-02	7.4690E-03	5.4347E-02
1311	4.5119E-02	5.9032E-02	1.1859E-02	0.1266
1312	0.1012	0.1184	1.6394E-02	7.4013E-02
1313	0.1419	0.1562	1.4384E-02	0.5832

MAXIMUM	0.3960	0.3977	3.3369E-02	0.8184
NODE	1114	1114	802	1213
MINIMUM	0.	0.	0.	0.
NODE	1	1	1	1

253

PEEQ

	VALUE						
1	+1 10E-07	4	+3 30E-01	7	+6 60E-01	10	+9 90E-01
2	+1 10E-01	5	+4 40E-01	8	+7 70E-01	11	+1 10E+00
3	+2 20E-01	6	+5 50E-01	9	+8 80E-01		

Figure B.13.   Contour plot of equivalent plastic strain at the point flagged for the fourth rezoning of the upsetting billet

254

MISES

VALUE

1	+2 00E+02	4	+6 00E+08	7	+1 20E+09	10	+1 60E+09
2	+2 00E+08	5	+8 00E+08	8	+1 40E+09	11	+2 00E+09
3	+4 00E+08	6	+1 00E+09	9	+1 60E+09		

Figure B.14. Contour plot of Mises stress at the point flagged for the fourth rezoning of the upsetting billet

VALUE

SENER	+1.00E+06	4	+3.70E+06	7	+6.40E+06	10	+9.10E+0
2	+1.90E+06	5	+4.60E+06	8	+7.30E+06	11	+1.00E+0
3	+2.80E+06	6	+5.50E+06	9	+8.20E+06		

Figure B.15. Contour plot of strain energy density at the point flagged for the fourth rezoning of the upsetting billet

Table B.5. Strain jump values for elements flagged for rezoning and those within twenty percent for the fourth rezoning case of the upsetting billet problem

NODE	SJP11	SJP22	SJP33	SJP12
913	9.2079E-02	8.4853E-02	1.2486E-02	0.1557
914	8.9564E-03	1.5606E-02	4.7971E-03	2.2316E-02
1012	5.1973E-02	4.1305E-02	1.9670E-02	0.1088
1013	0.2905	0.3060	1.7700E-02	0.5175
1014	7.6891E-02	7.0090E-02	1.2408E-02	8.3253E-02
1112	7.6269E-02	7.6880E-02	1.4097E-02	0.2230
1113	7.9556E-02	6.9390E-02	1.2812E-02	8.7032E-02
MAXIMUM	0.2905	0.3060	2.2617E-02	0.5175
NODE	1013	1013	702	1013
MINIMUM	0.	0.	0.	0.
NODE	1	1	1	1

PEEQ

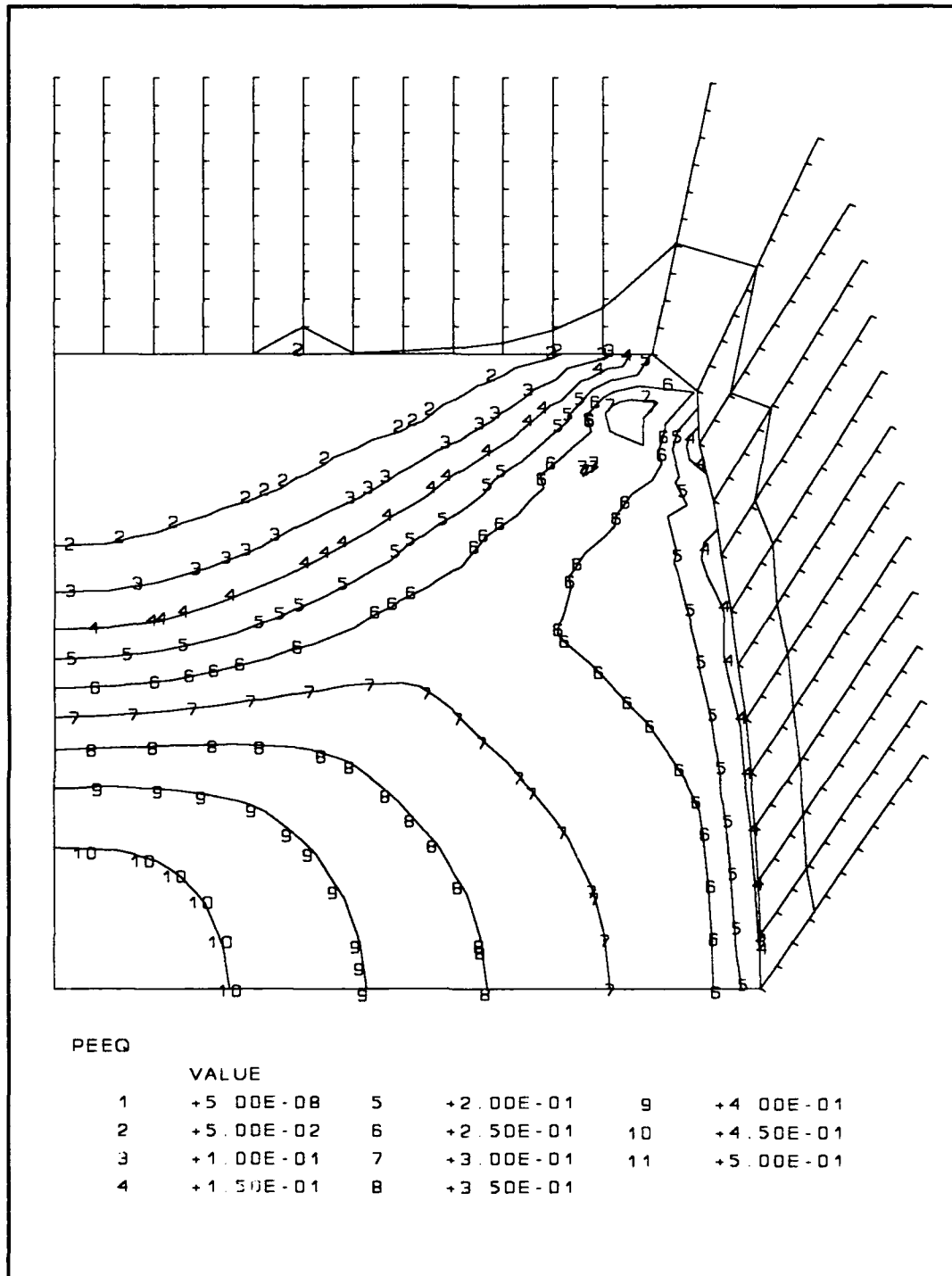|	VALUE						
1	+2.00E-07	4	+6.00E-01	7	+1.20E+00	10	+1.80E+00
2	+2.00E-01	5	+8.00E-01	8	+1.40E+00	11	+2.00E+00
3	+4.00E-01	6	+1.00E+00	9	+1.60E+00		
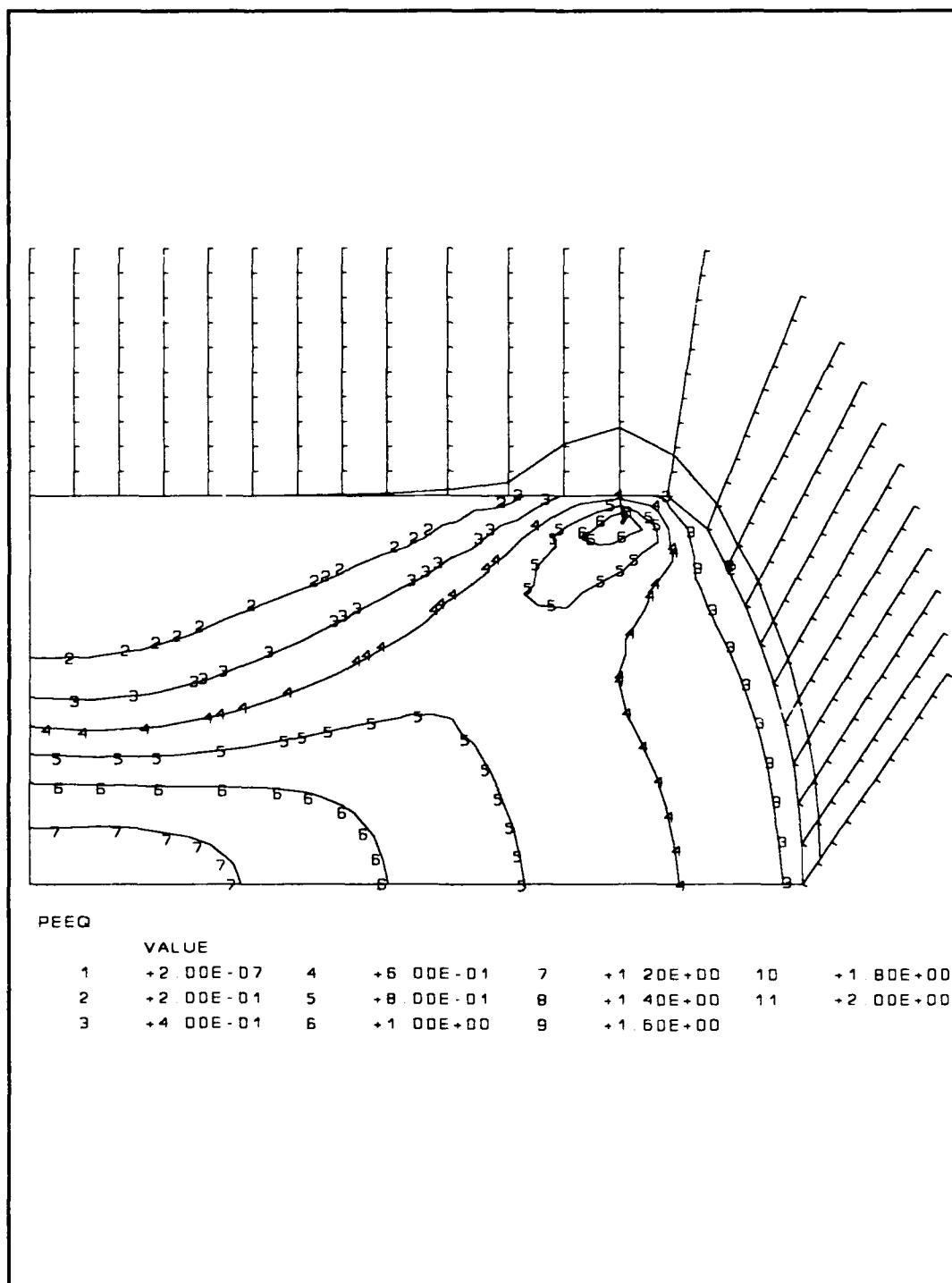
Figure B.16. Contour plot of equivalent plastic strain at the point flagged for the fifth rezoning of the upsetting billet
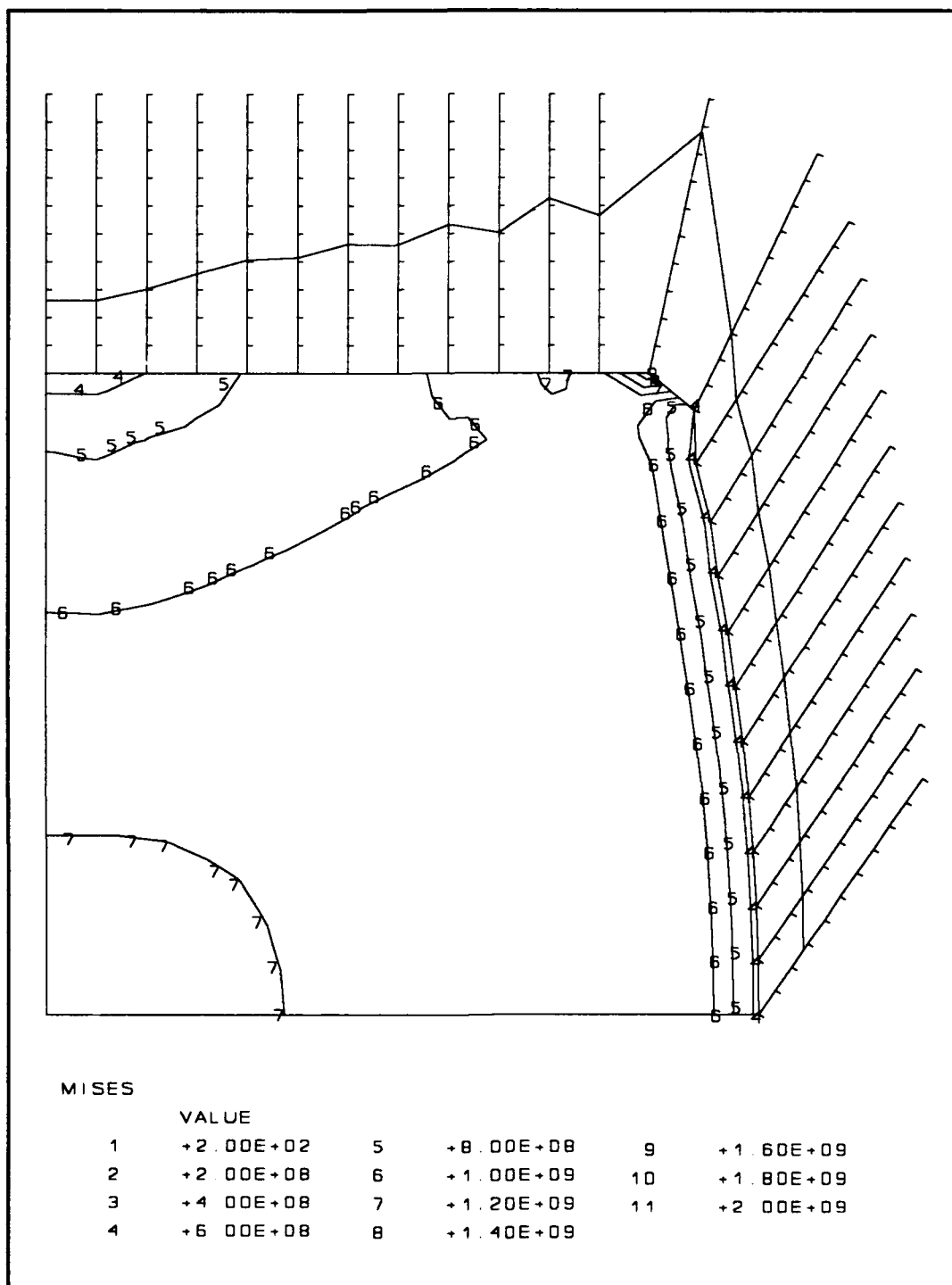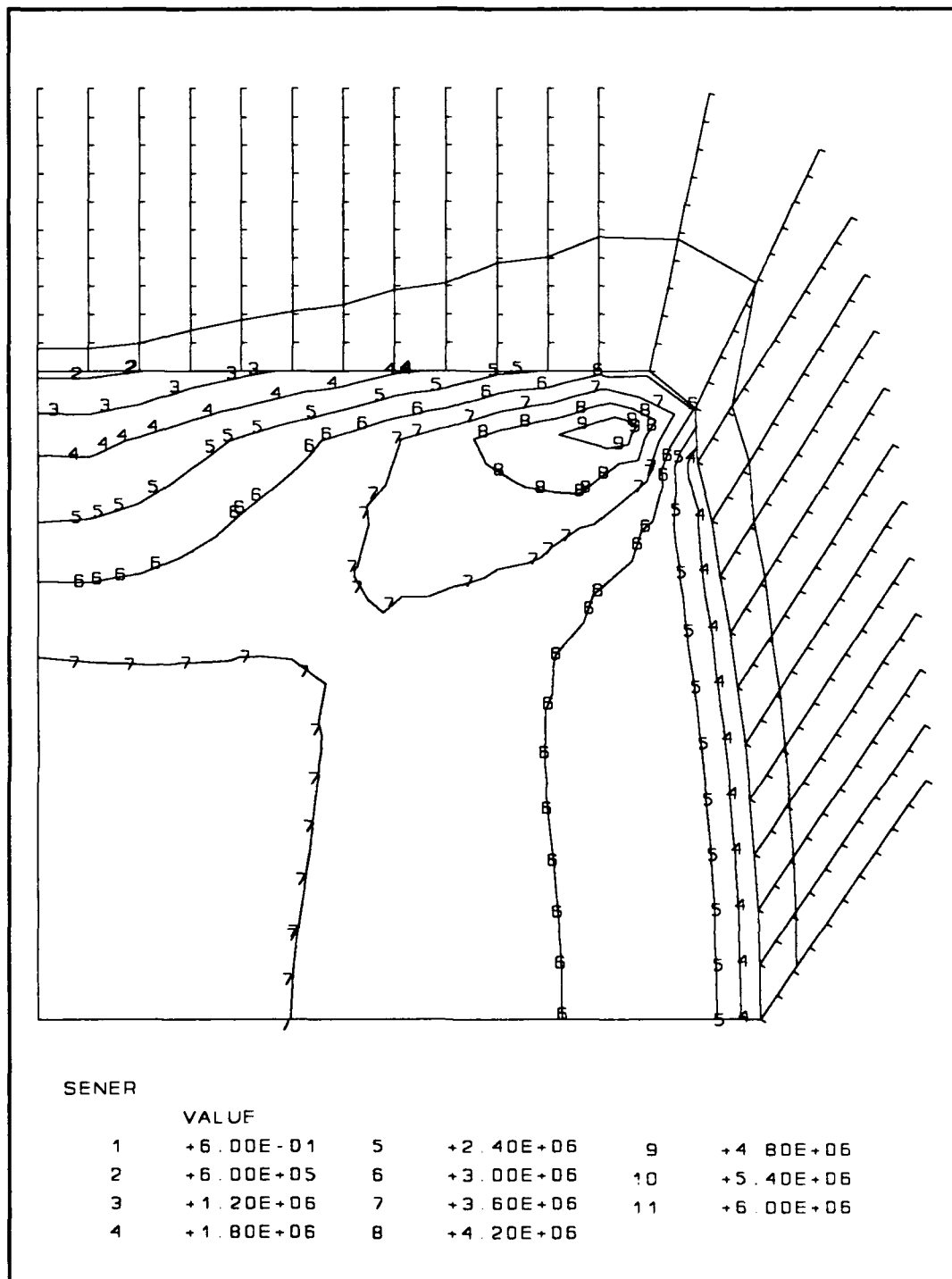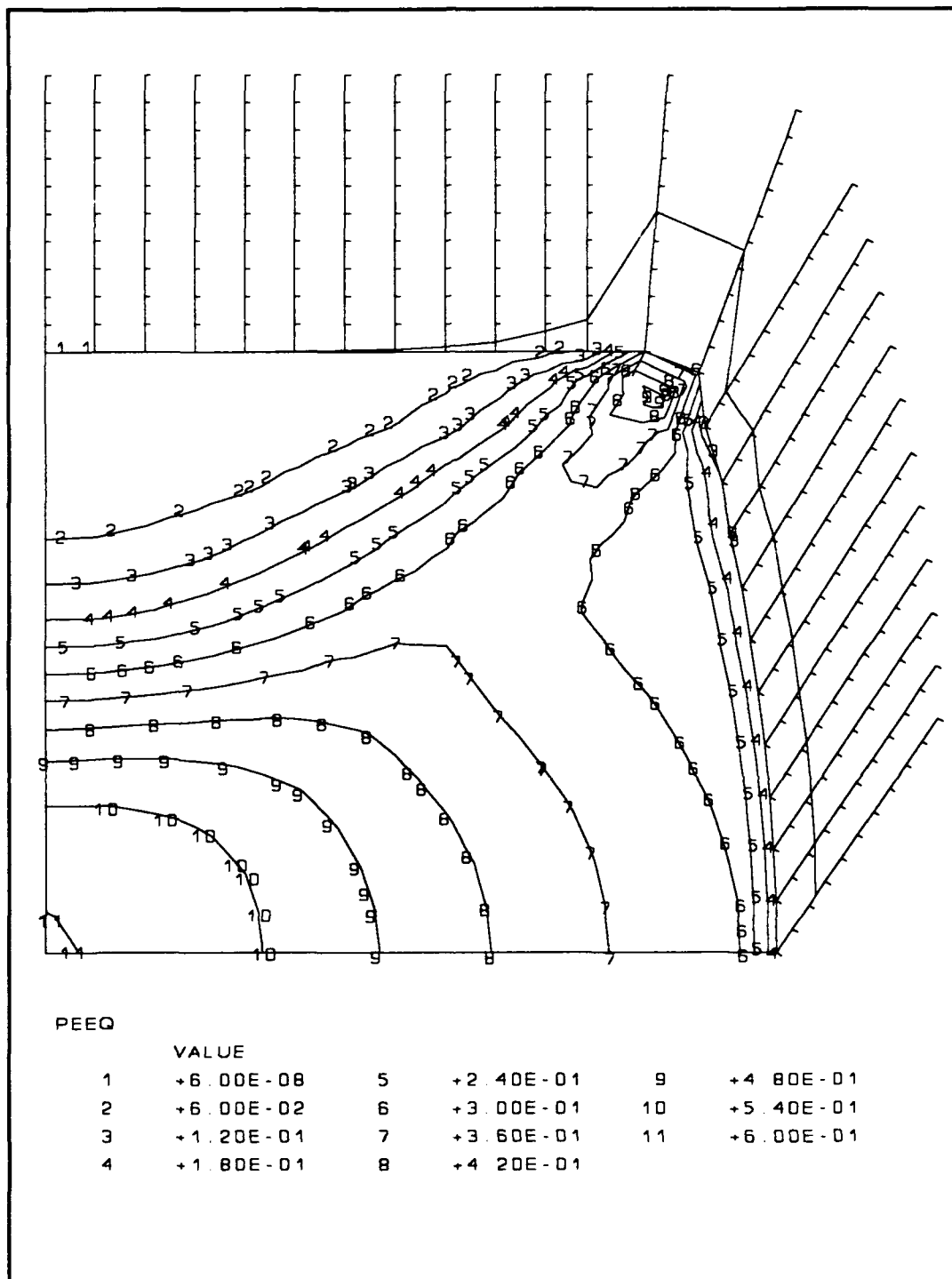
MISES

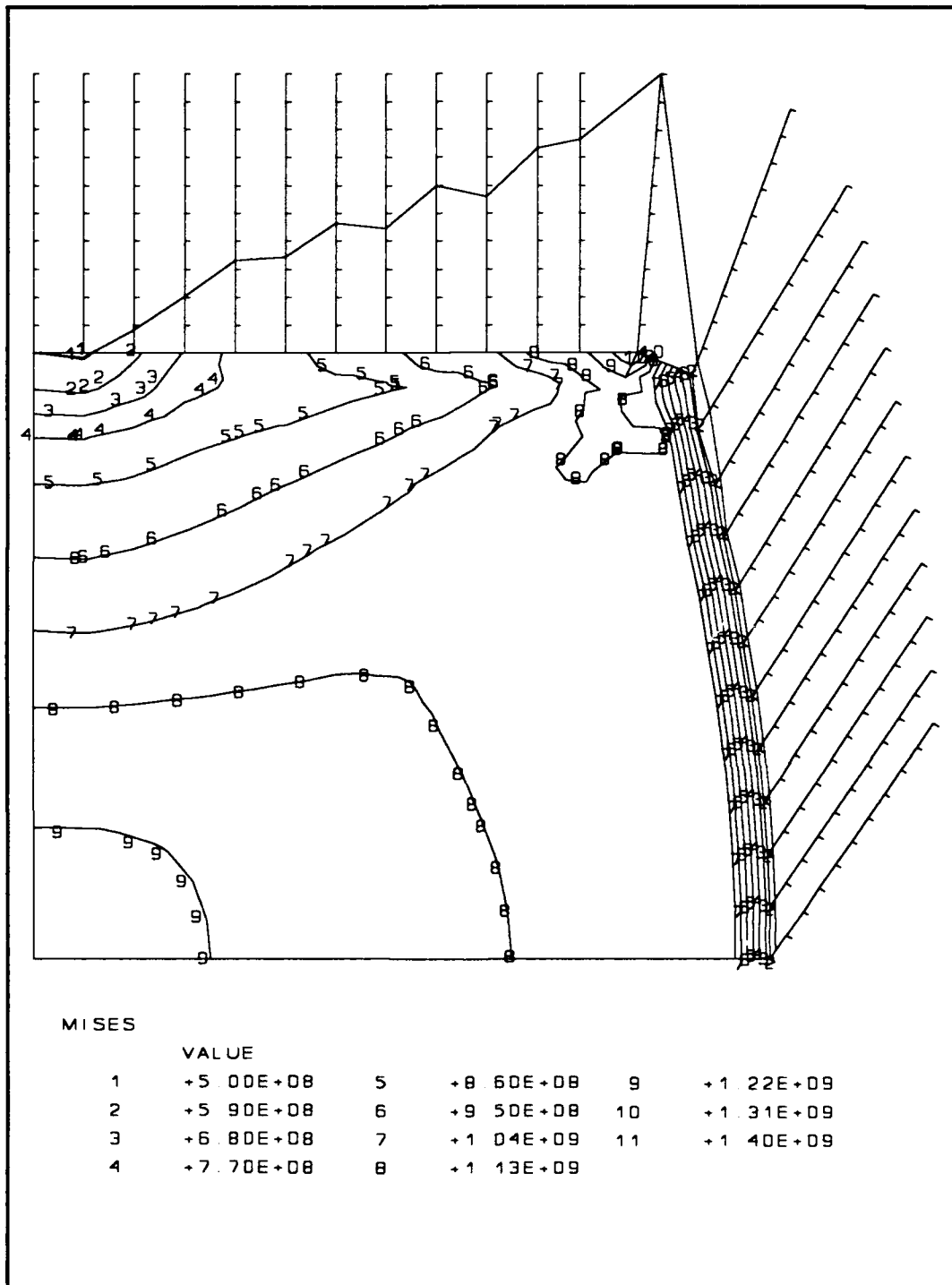|	VALUE						
1	+2 00E+02	4	+6 00E+08	7	+1.20E+09	10	+1 80E+09
2	+2 00E+08	5	+8 00E+08	8	+1 40E+09	11	+2 00E+09
3	+4 00E+08	6	+1 00E+09	9	+1 60E+09		
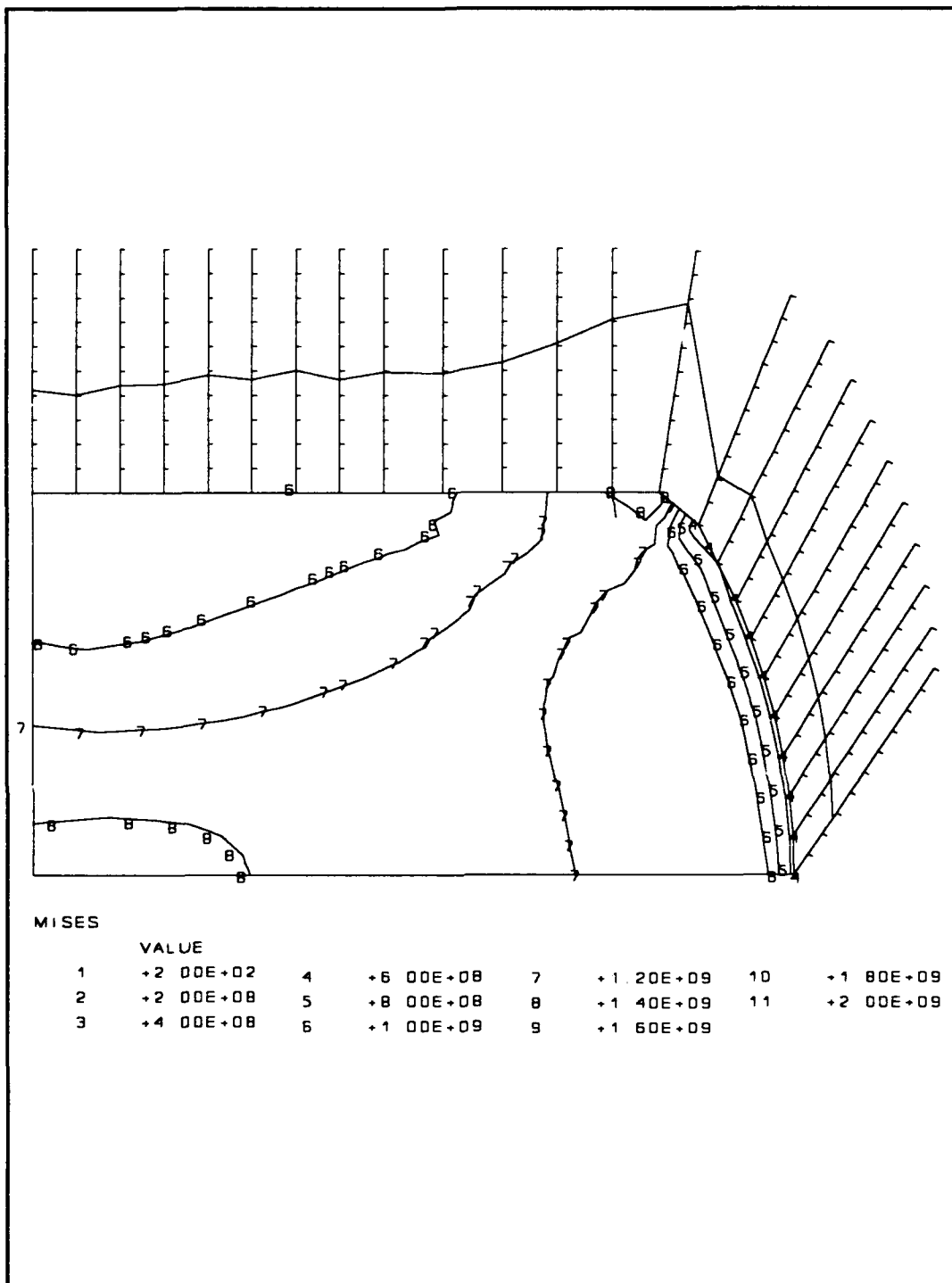
Figure B.17.   Contour plot of Mises stress at the point flagged for the fifth rezoning of the upsetting billet

SENER

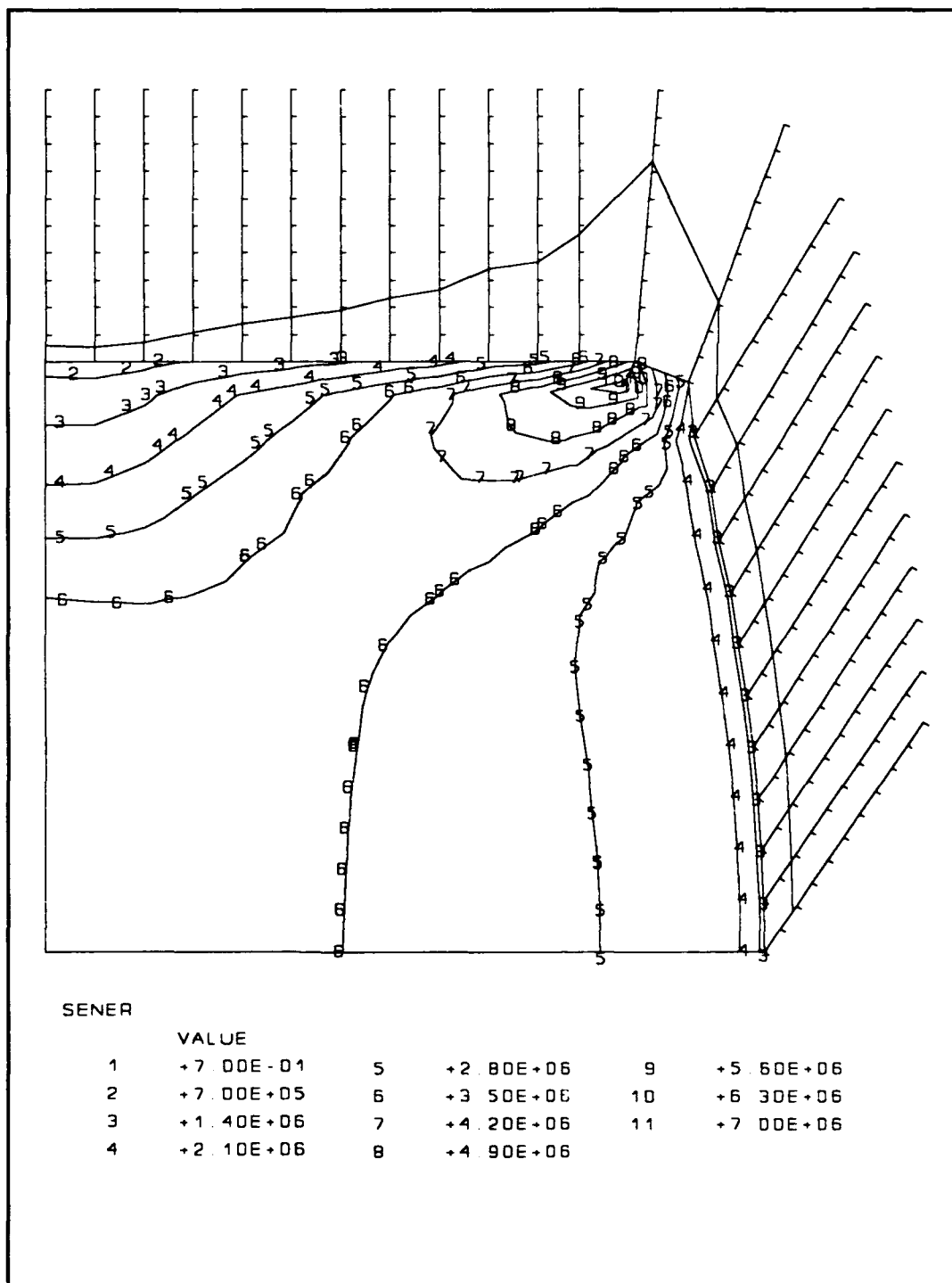|	VALUE						
1	+1.00E+06	4	+4.30E+06	7	+7.60E+06	10	+1.09E+07
2	+2.10E+06	5	+5.40E+06	8	+8.70E+06	11	+1.20E+07
3	+3.20E+06	6	+6.50E+06	9	+9.80E+06		

Figure B.18. Contour plot of strain energy density at the point flagged for the fifth rezoning of the upsetting billet

Table B.6. Strain jump values for elements flagged for rezoning and those within twenty percent for the fifth rezoning case of the upsetting billet problem

NODE	SJP11	SJP22	SJP33	SJP12
913	0.1489	0.1523	9.6085E-03	0.1583
914	6.7766E-02	6.2280E-02	1.1147E-02	1.7455E-02
1011	3.9004E-02	4.4607E-02	2.2758E-02	0.2119
1012	2.6156E-02	3.5150E-02	1.1415E-02	7.7961E-02
1013	0.2906	0.2924	1.3586E-02	0.1430
1014	7.7222E-04	1.2192E-02	1.2571E-02	2.1909E-02
1111	6.0918E-02	5.5426E-02	1.7504E-02	0.1486
1112	4.8595E-02	7.1792E-02	2.9831E-02	0.1408
1113	0.1955	0.1923	1.2794E-02	0.1171
1212	0.2285	0.2196	8.9293E-03	5.6408E-02
1213	0.1089	9.9708E-02	4.7829E-03	0.1312

MAXIMUM	0.2906	0.2924	2.9831E-02	0.2119
NODE	1013	1013	1112	1011

MINIMUM	0.	0.	0.	0.
NODE	1	1	1	1

261

PEEQ

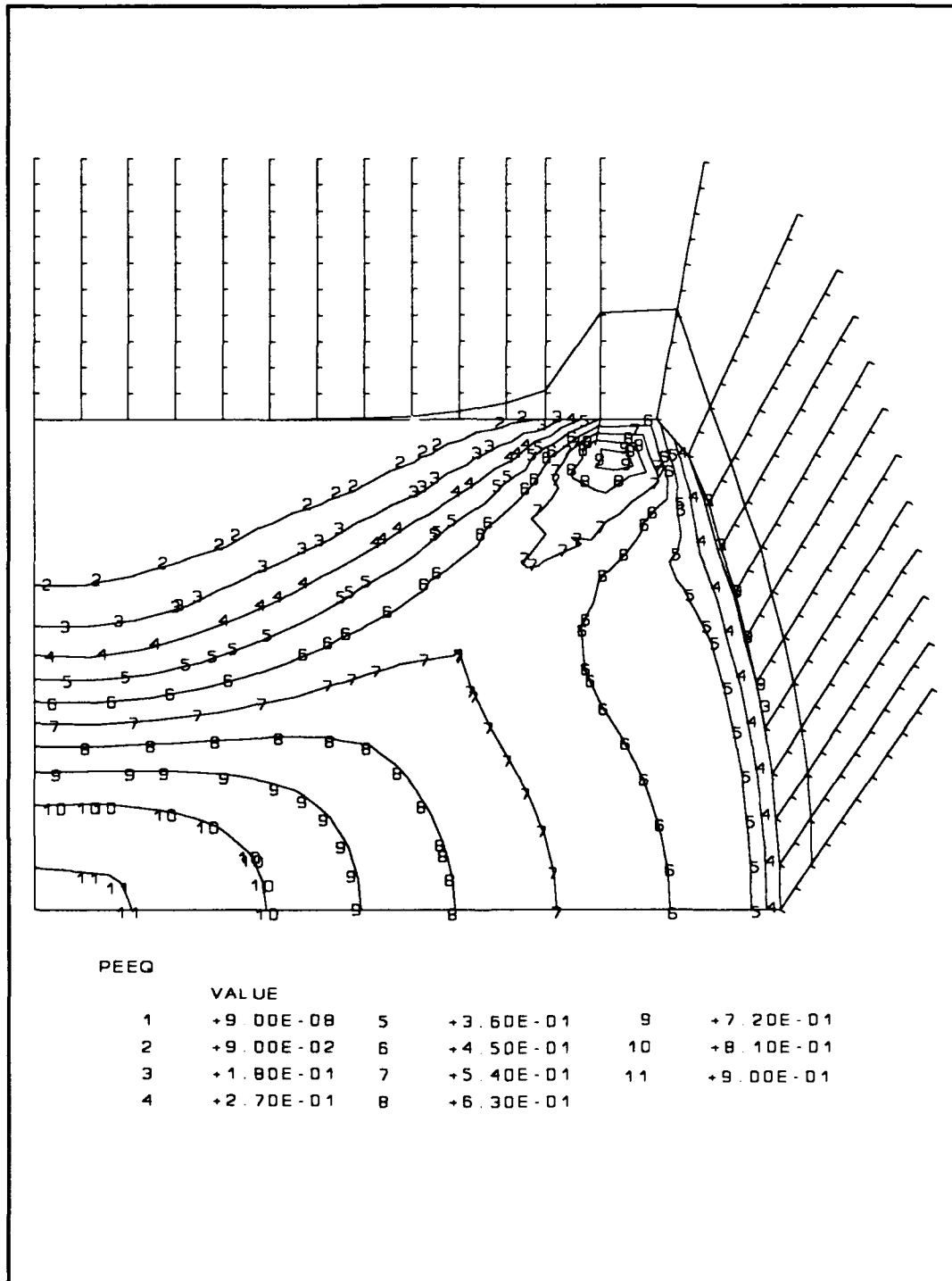|	VALUE				
1	+2.00E-07	4	+6.00E-01	7	+1.20E+00	10	+1.80E+00
2	+2.00E-01	5	+8.00E-01	8	+1.40E+00	11	+2.00E+00
3	+4.00E-01	6	+1.00E+00	9	+1.60E+00	
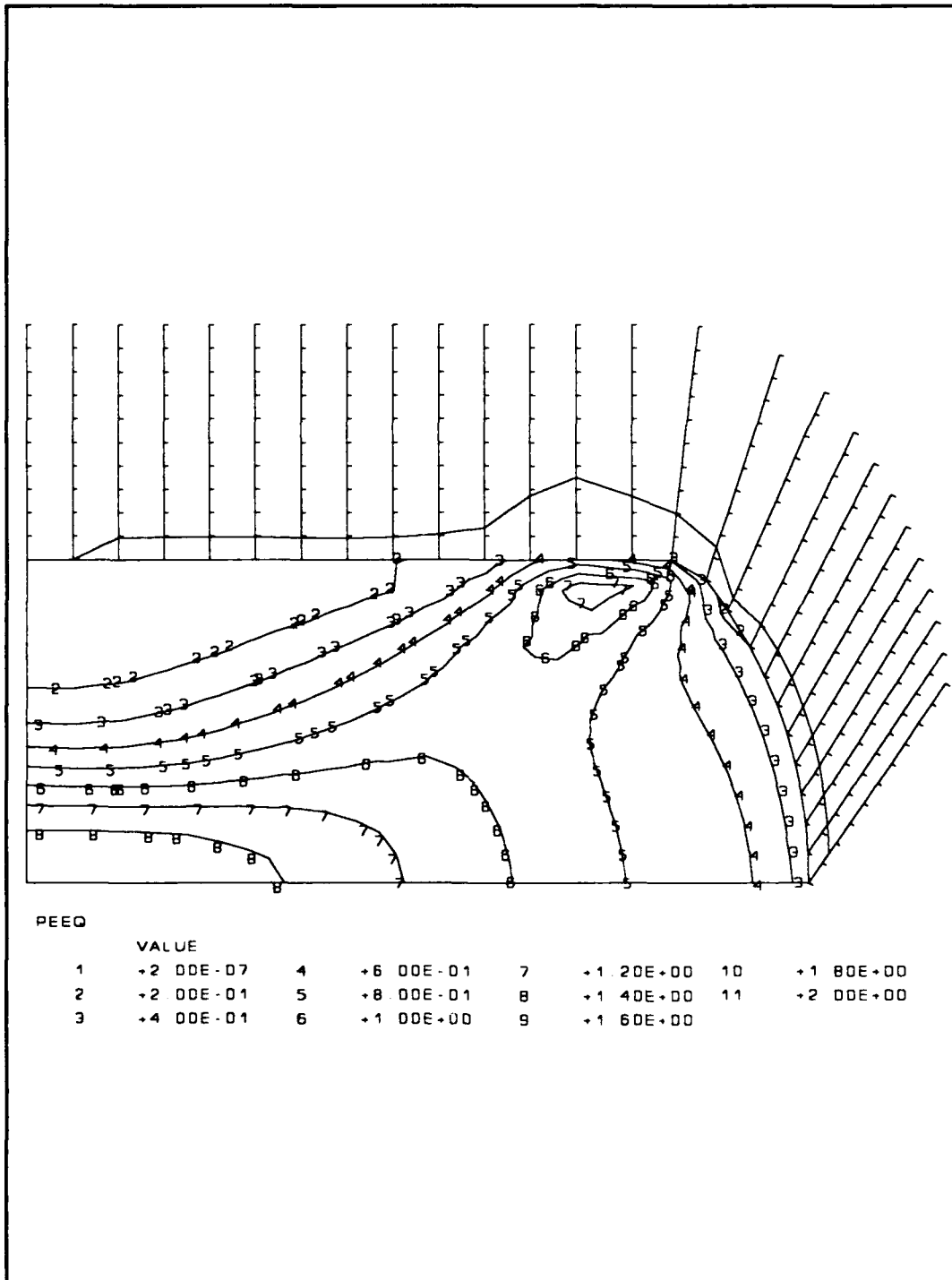
Figure B.19. Contour plot of equivalent plastic strain at the point flagged for the sixth rezoning of the upsetting billet

MISES

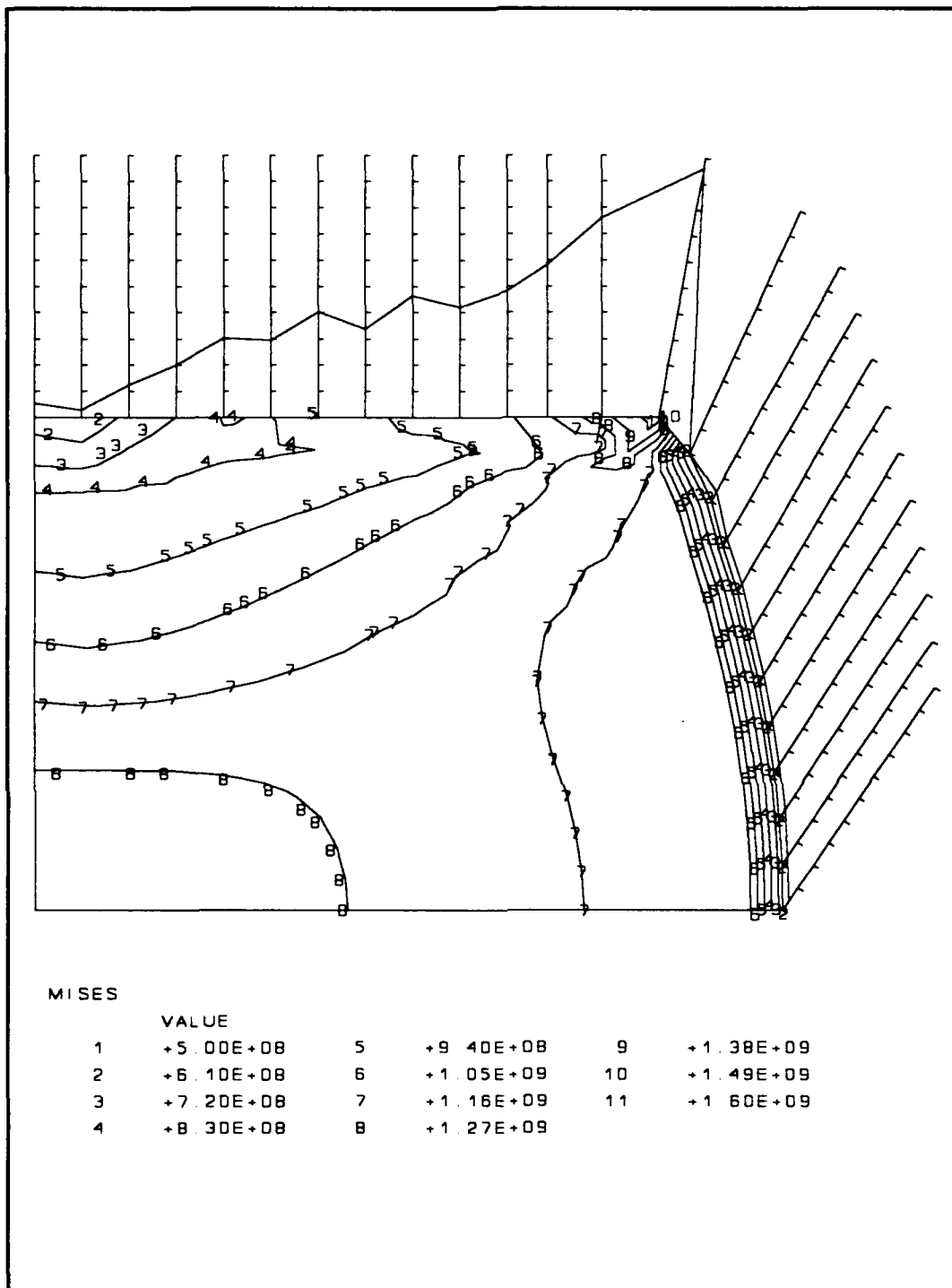|	VALUE							
1	+2.00E+02	4	+6.00E+08	7	+1.20E+09	10	+1.80E+09
2	+2.00E+08	5	+8.00E+08	8	+1.40E+09	11	+2.00E+09
3	+4.00E+08	6	+1.00E+09	9	+1.60E+09		
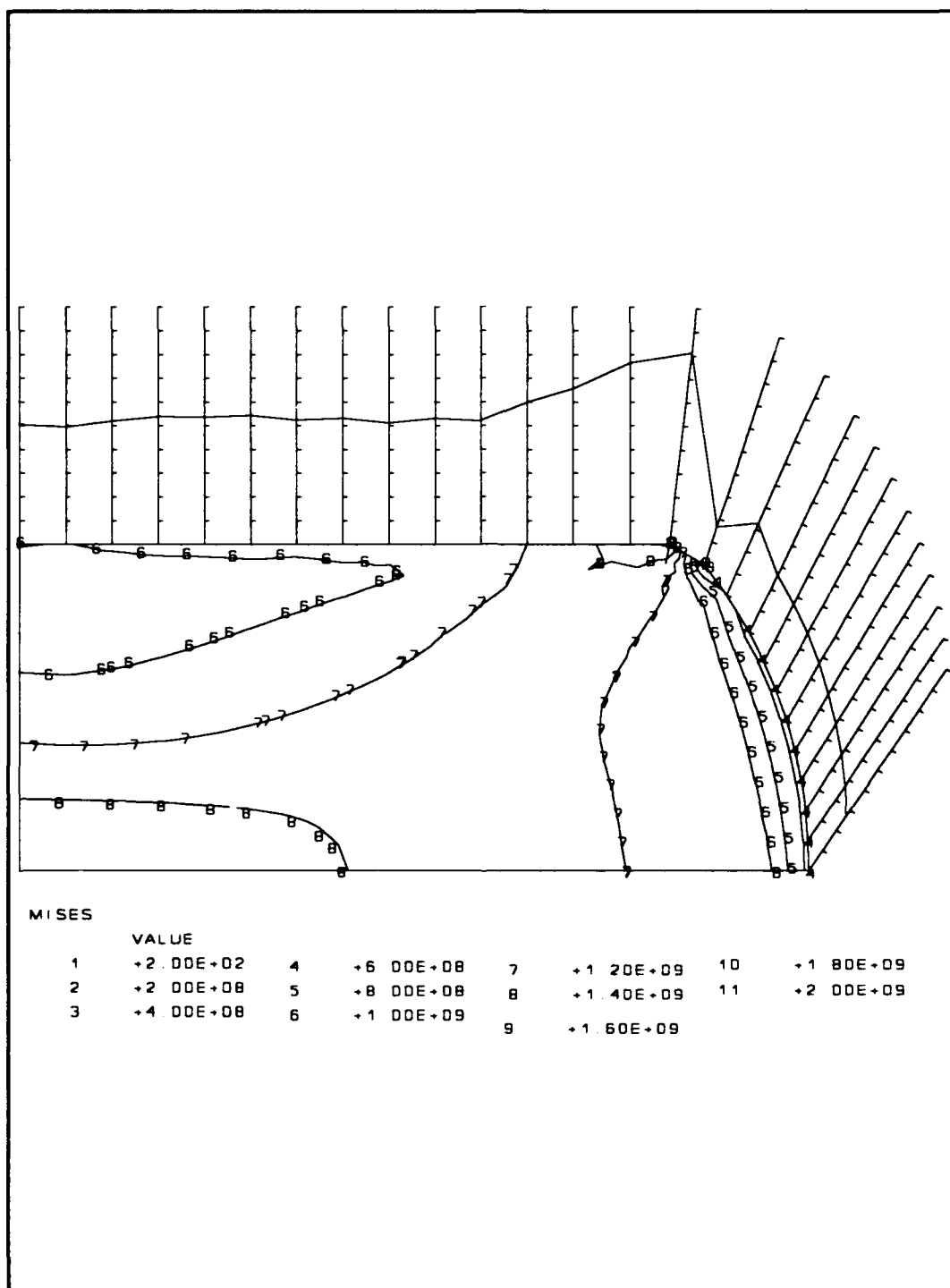
Figure B.20.   Contour plot of Mises stress at the point flagged for the sixth rezoning of the upsetting billet

SENER

	VALUE							
1	+1 00E+06	4	+3 70E+06	7	+6 40E+06	10	+9 10E+06
2	+1 90E+06	5	+4 60E+06	8	+7 30E+06	11	+1 00E+07
3	+2 80E+06	6	+5 50E+06	9	+8 20E+06		
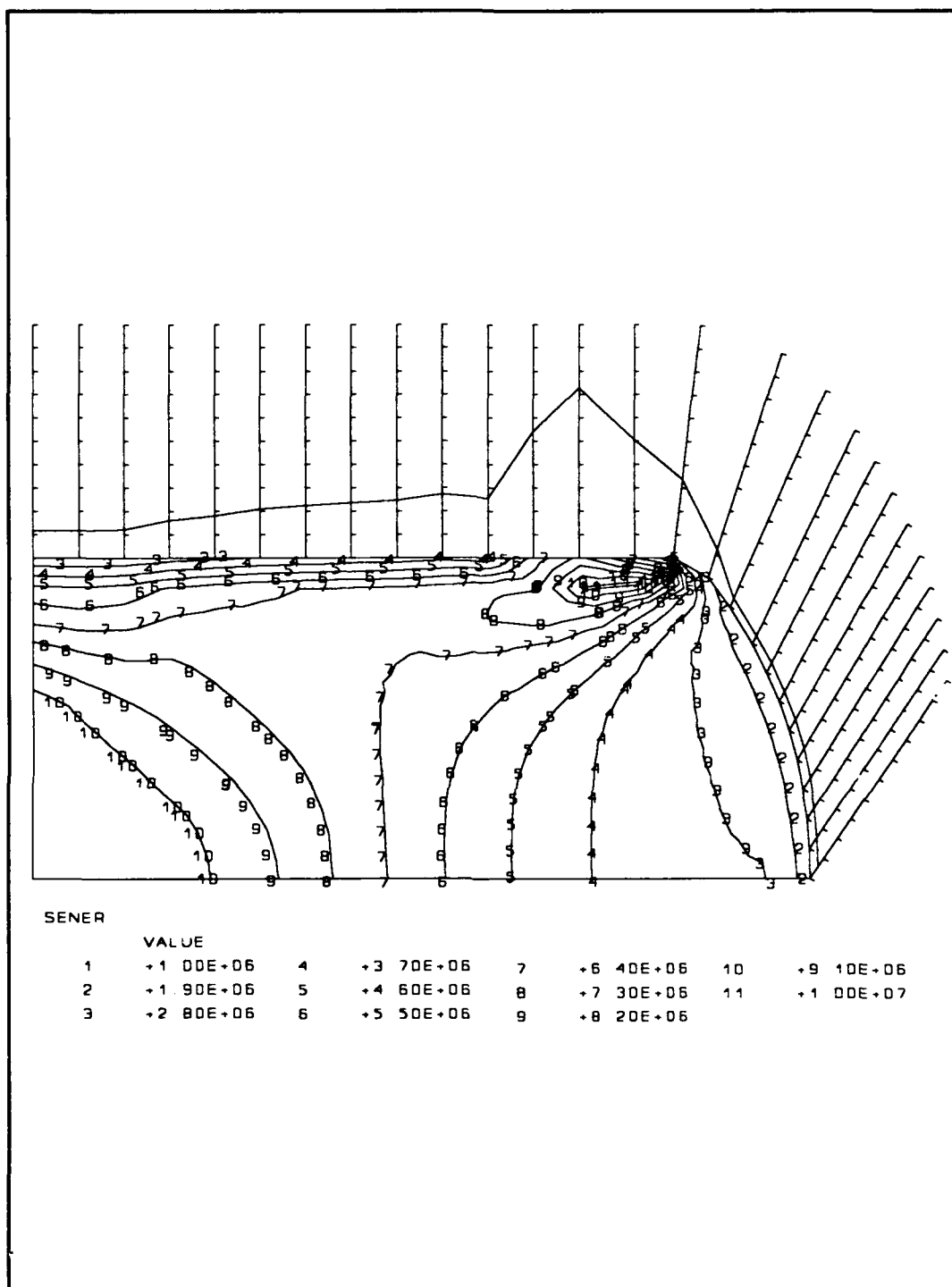
Figure B.21. Contour plot of strain energy density at the point flagged for the sixth rezoning of the upsetting billet

Table B.7. Strain jump values for elements flagged for rezoning and those within twenty percent for the sixth rezoning case of the upsetting billet problem

NODE	SJP11	SJP22	SJP33	SJP12
1014	0.1189	0.1077	2.0098E-02	0.2486
1015	0.1581	0.1576	1.6684E-02	6.8212E-02
1016	9.1012E-02	8.5329E-02	1.3142E-02	0.1261
1114	8.5451E-02	9.0229E-02	2.3210E-02	0.3478
1115	0.3748	0.3773	2.0754E-02	0.7187
1116	6.0648E-03	9.7374E-03	1.6202E-02	4.5026E-02
MAXIMUM	0.3748	0.3773	3.8825E-02	0.7187
NODE	1115	1115	1113	1115
MINIMUM	0.	0.	0.	0.
NODE	1	1	1	1

PEEQ

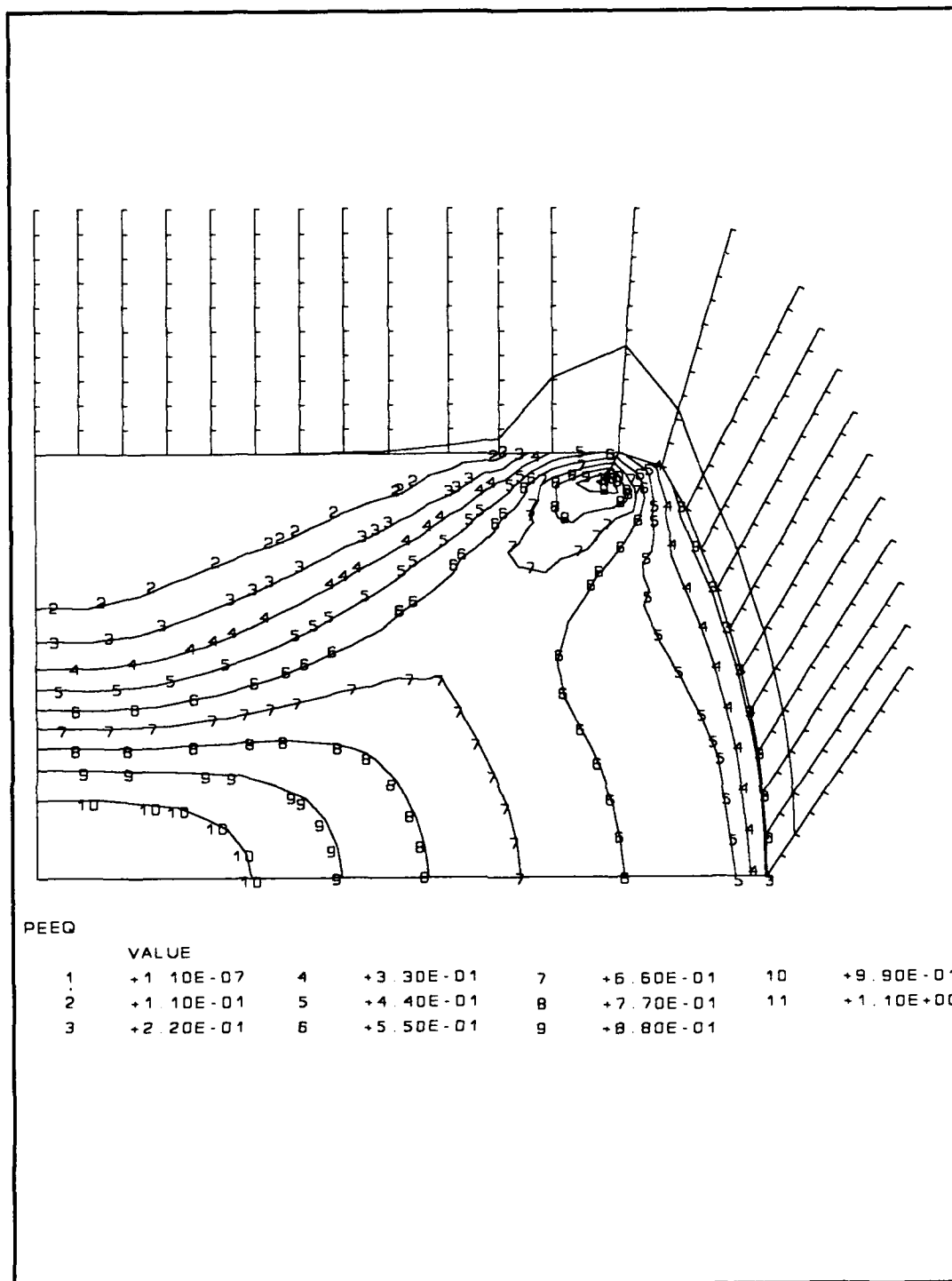|	VALUE						
1	+2.00E-07	4	+6.00E-01	7	+1.20E+00	10	+1.80E+00
2	+2.00E-01	5	+8.00E-01	8	+1.40E+00	11	+2.00E+00
3	+4.00E-01	6	+1.00E+00	9	+1.60E+00		
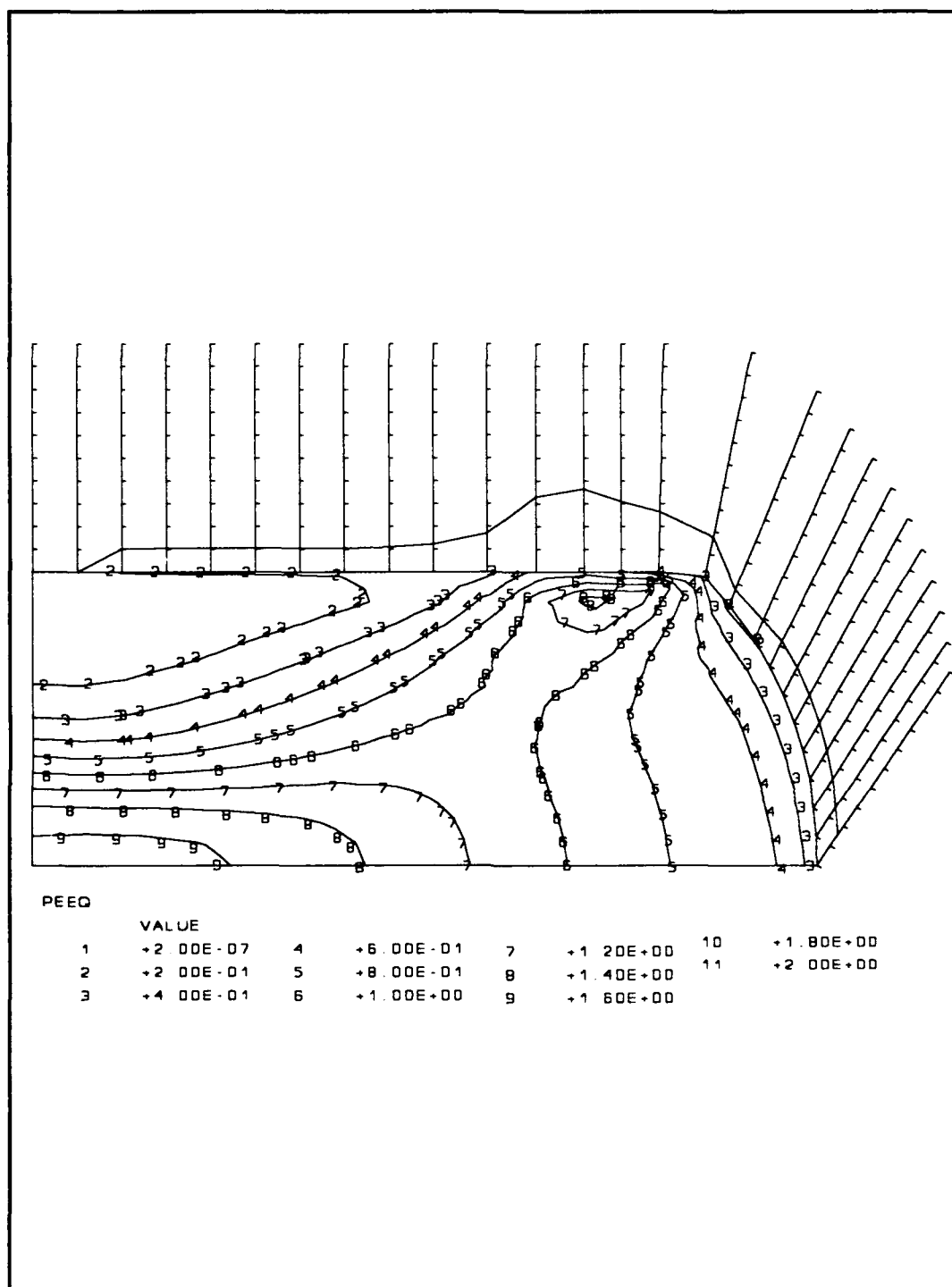
Figure B.22.   Contour plot of equivalent plastic strain at the point flagged for the seventh rezoning of the upsetting billet

266
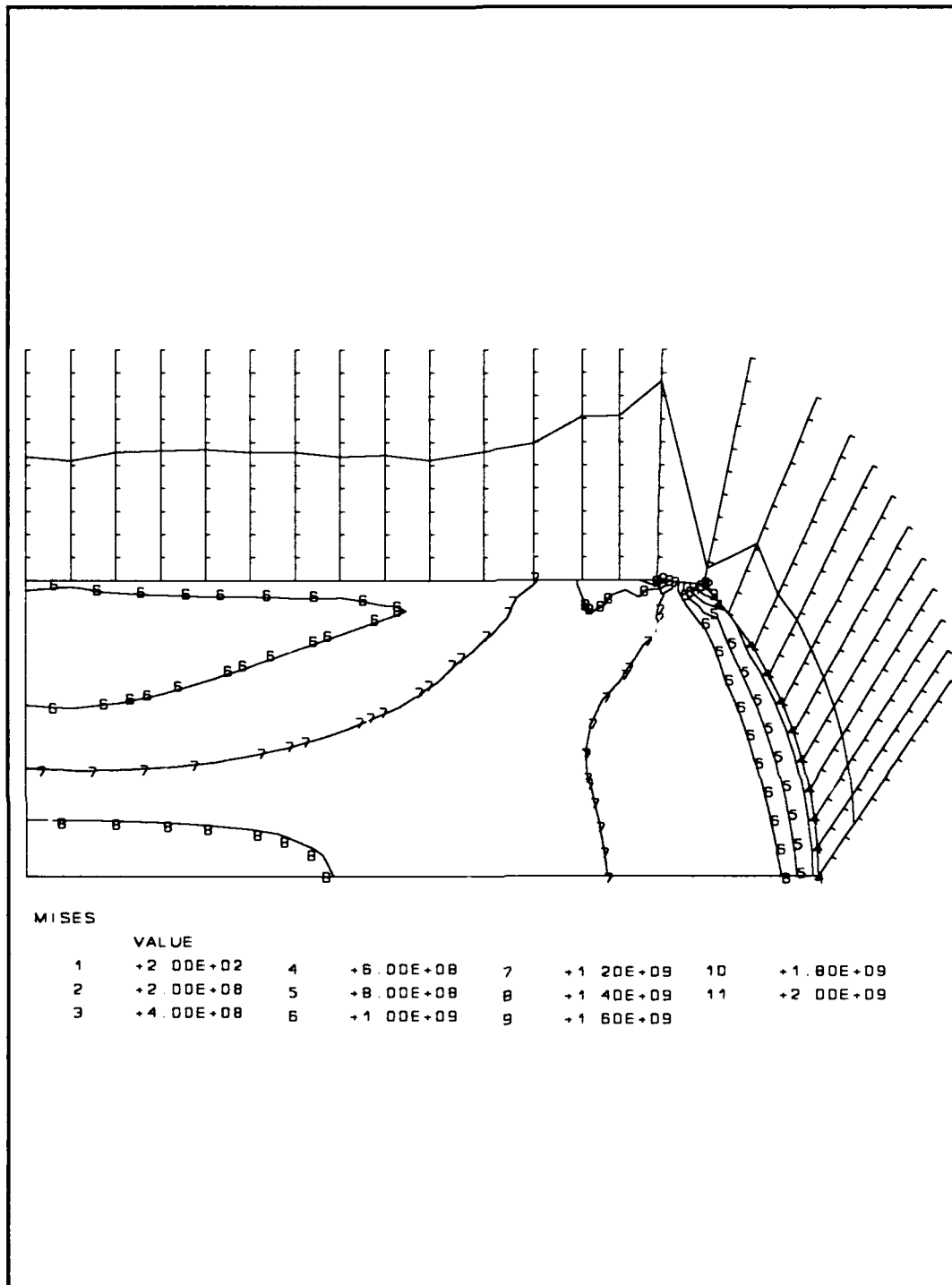
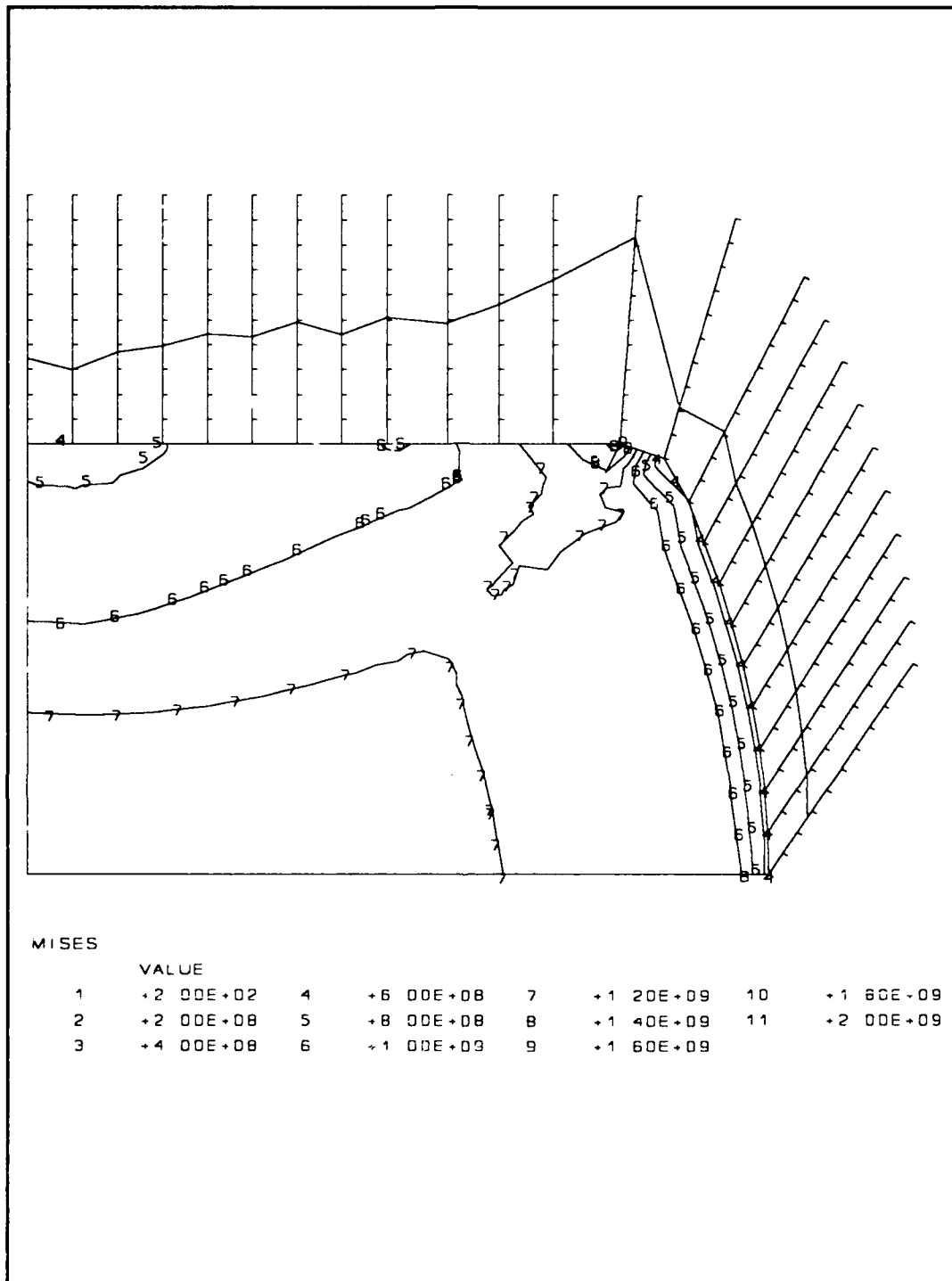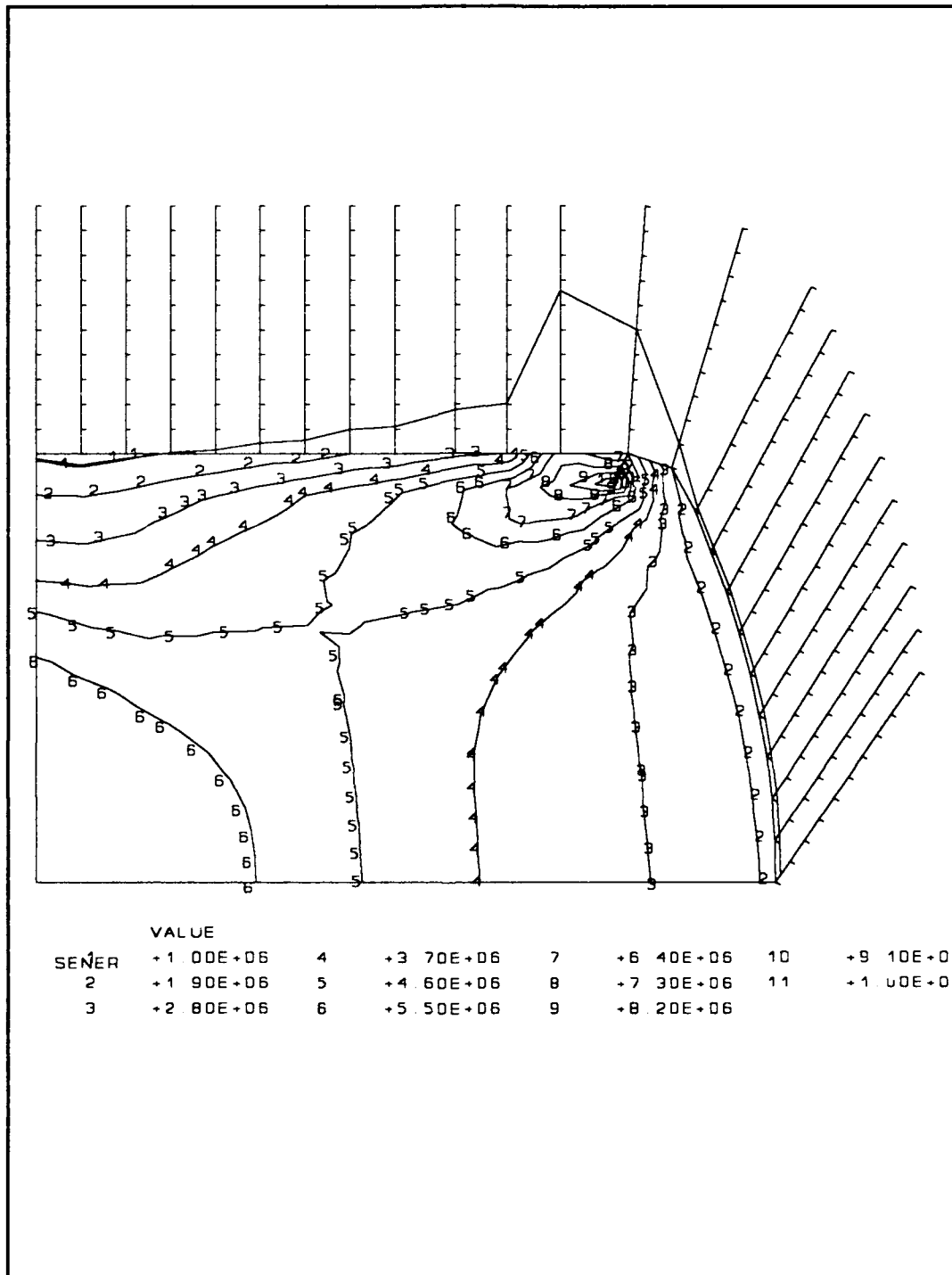**Figure B.23.** Contour plot of Mises stress at the point flagged for the seventh rezoning of the upsetting billet

SENER

VALUE

1	+1.00E+06	4	+4.00E+06	7	+7.00E+06	10	+1.00E+07
2	+2.00E+06	5	+5.00E+06	8	+8.00E+06	11	+1.10E+07
3	+3.00E+06	6	+6.00E+06	9	+9.00E+06		

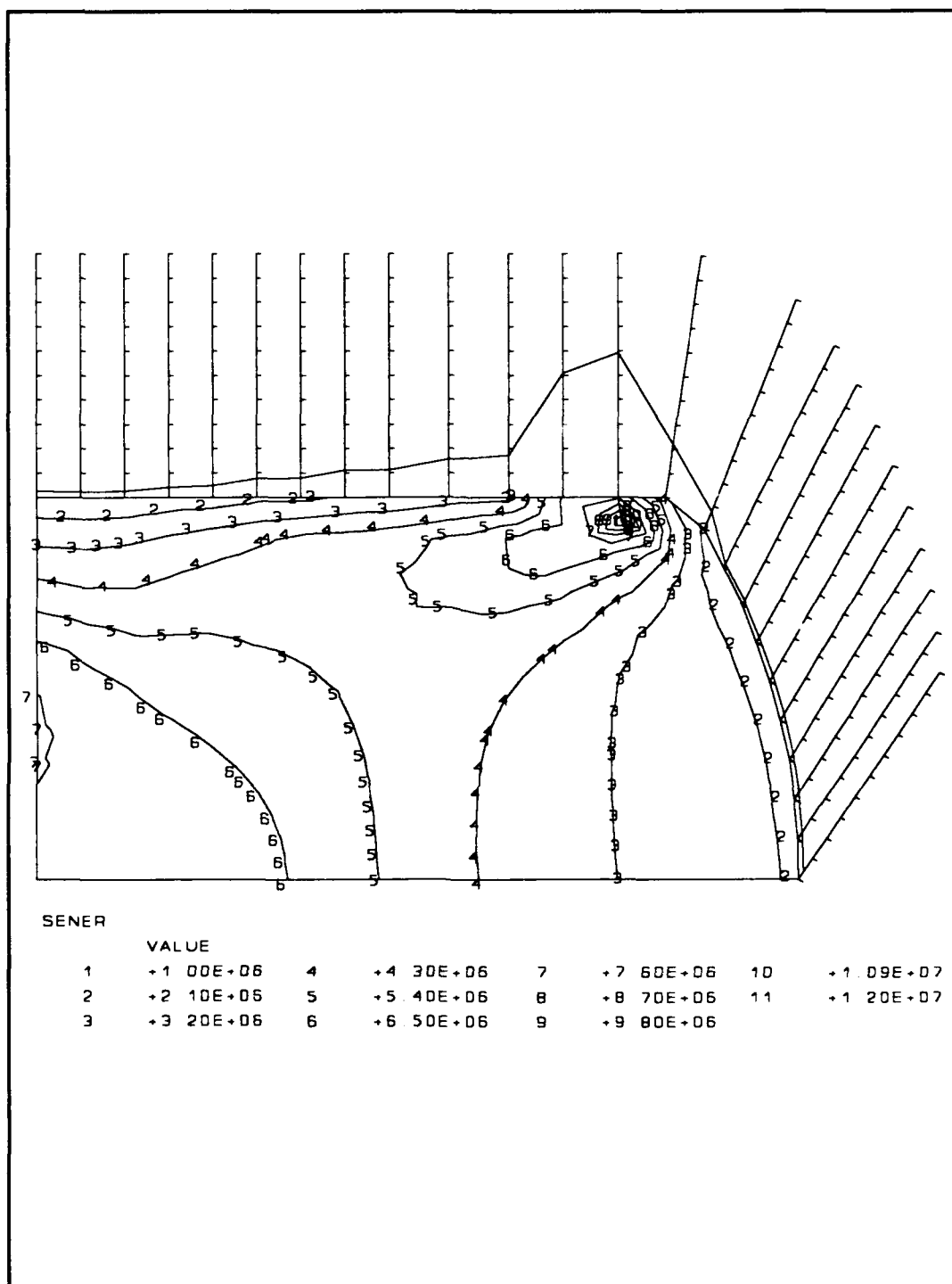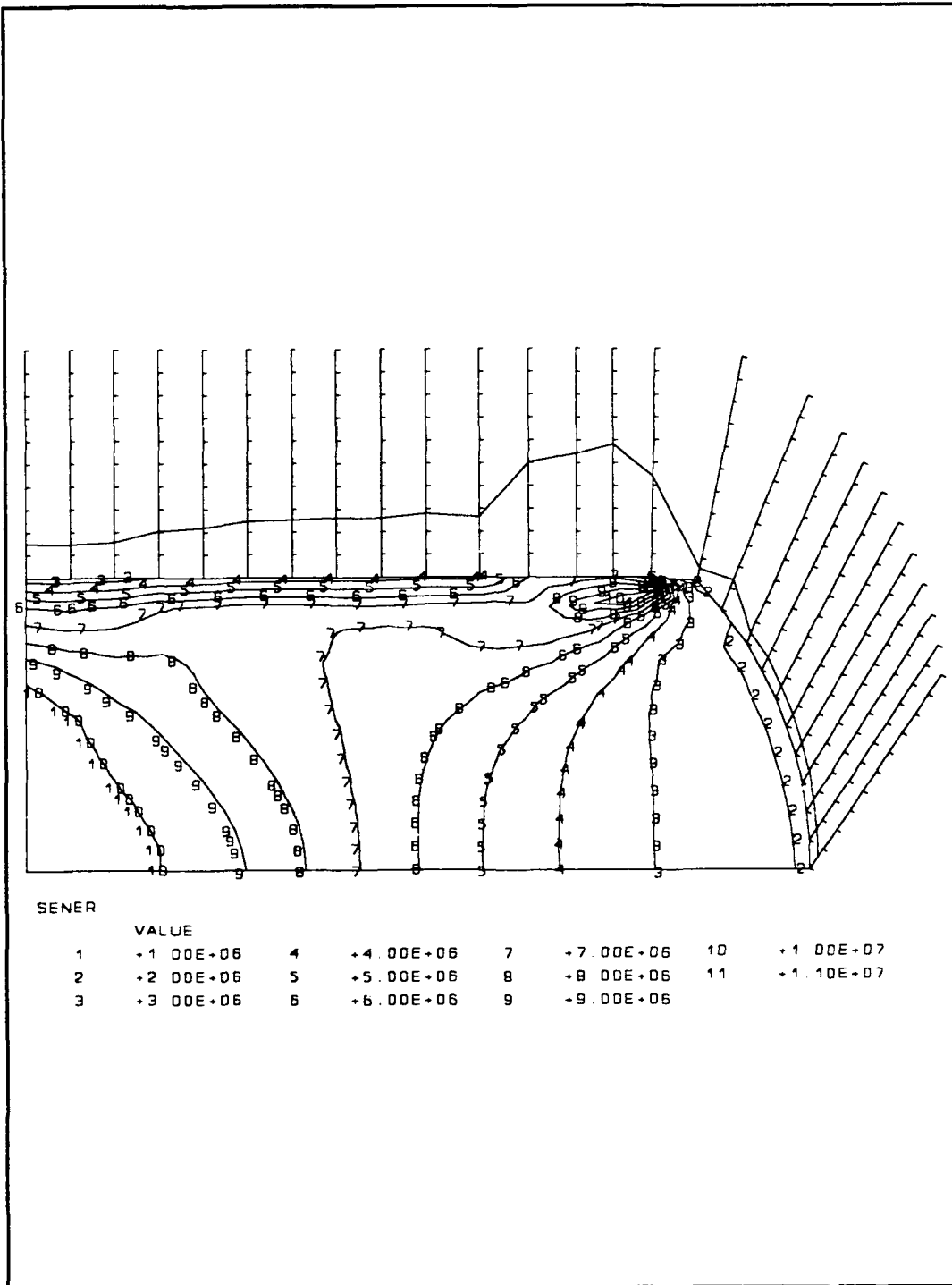Figure B.24.   Contour plot of strain energy density at the point flagged for the seventh rezoning of the upsetting billet

268

Table B.8. Strain jump values for elements flagged for rezoning and those within twenty percent for the seventh rezoning case of the upsetting billet problem

NODE	SJP11	SJP22	SJP33	SJP12
1014	7.9855E-02	8.5844E-02	1.0278E-02	0.1695
1015	0.1980	0.2064	1.1294E-02	0.1466
1016	9.1876E-02	8.8563E-02	8.2710E-03	6.1957E-02
1114	8.7967E-02	0.1014	1.3224E-02	0.1576
1115	0 2143	0.2102	9.9396E-03	0.5591
1116	5.2054E-02	5.6566E-02	8.0256E-03	0.2608
1214	1.3534E-02	7.6348E-03	1.6442E-03	1.9202E-02

MAXIMUM	0.2903	0.2870	1.7889E-02	0.5591
NODE	1212	1212	1113	1115

MINIMUM	0.	0.	0.	0.
NODE	1	1	1	1

PEEQ

VALUE
1	+2.00E-07	4	+6.00E-01	7	+1.20E+00	10	+1.80E+00
2	+2.00E-01	5	+8.00E-01	8	+1.40E+00	11	+2.00E+00
3	+4.00E-01	6	+1.00E+00	9	+1.60E+00		
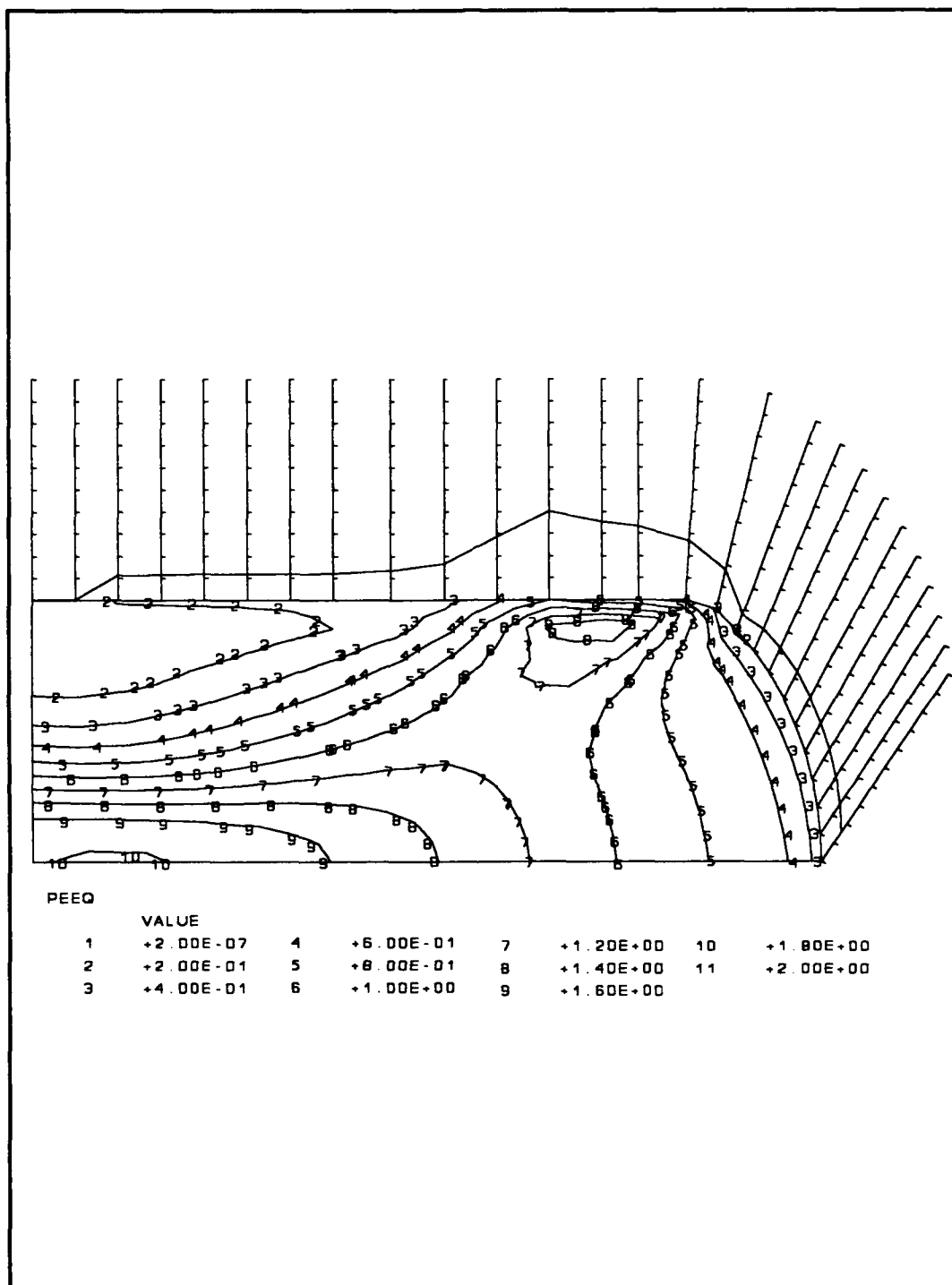
Figure B.25. Contour plot of equivalent plastic strain at the completion of the solution after seven rezonings of the upsetting billet

MISES

	VALUE						
1	+2.00E+02	4	+6.00E+08	7	+1.20E+09	10	+1.80E+09
2	+2.00E+08	5	+8.00E+08	8	+1.40E+09	11	+2.00E+09
3	+4.00E+08	6	+1.00E+09	9	+1.60E+09		
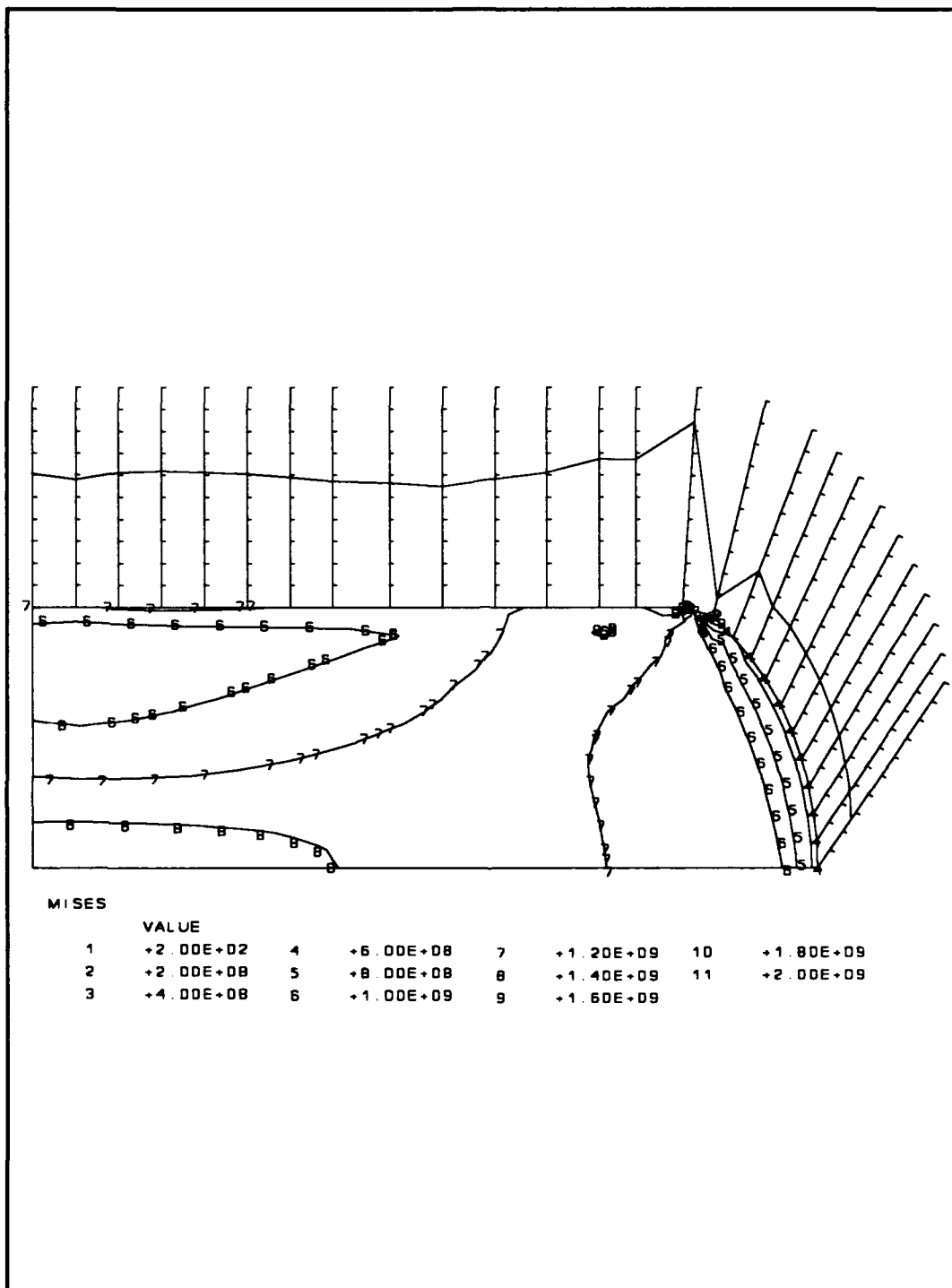
Figure B.26. Contour plot of Mises stress at the completion of the solution after seven rezonings of the upsetting billet

271

SENER   VALUE

1	+2.00E+00	4	+6.00E+06	7	+1.20E+07	10	+1.80E+07
2	+2.00E+06	5	+8.00E+06	8	+1.40E+07	11	+2.00E+07
3	+4.00E+06	6	+1.00E+07	9	+1.60E+07		
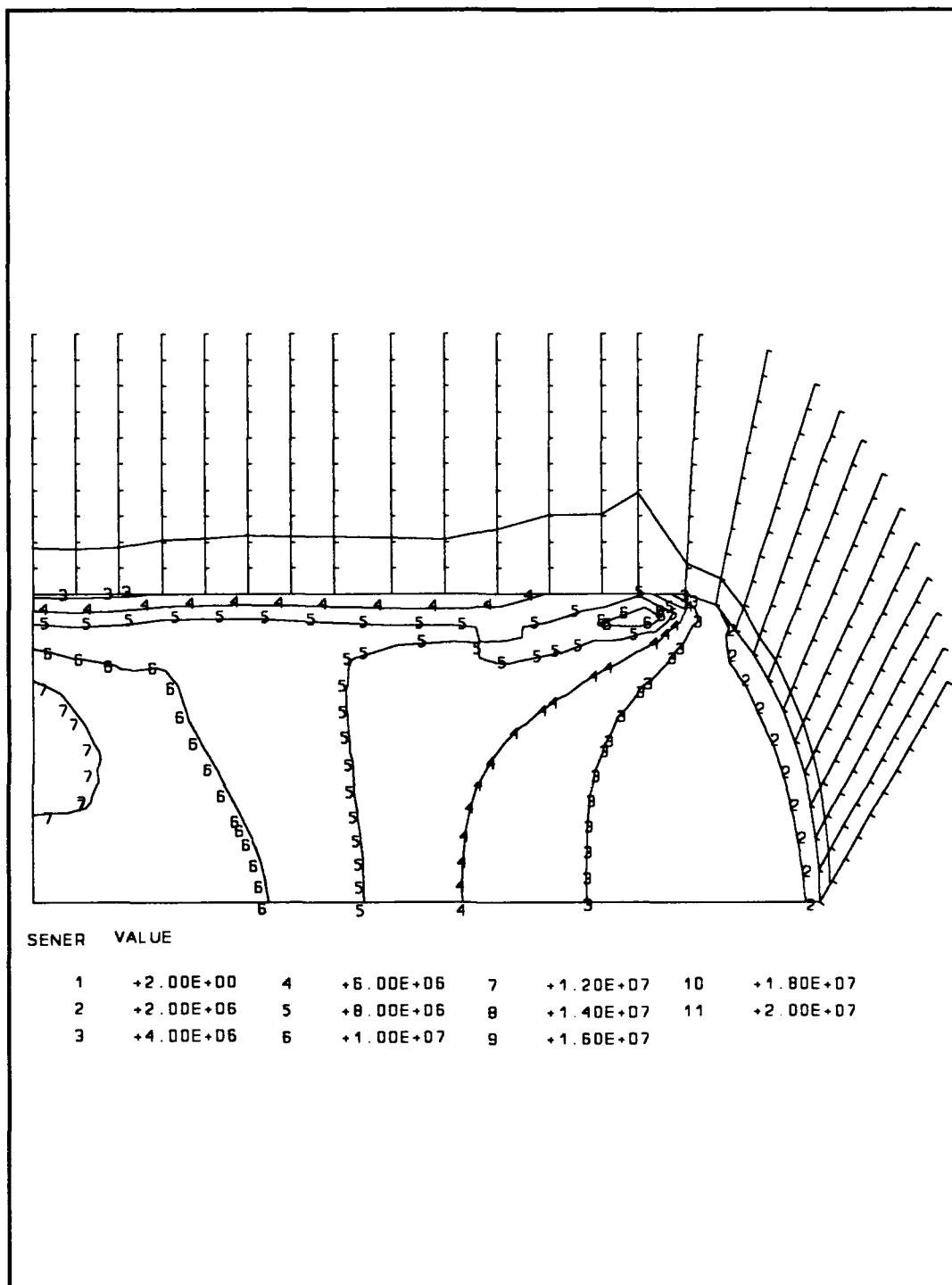
Figure B.27.   Contour plot of strain energy density at the completion of the solution after seven rezonings of the upsetting billet

Table B.9. Strain jump values for elements flagged for rezoning and those within twenty percent for the completed solution of the upsetting billet problem

NODE	SJP11	SJP22	SJP33	SJP12
915	4.8898E-02	5.1015E-02	6.9223E-03	4.7717E-02
916	6.3049E-03	2.4619E-03	2.3446E-03	3.0589E-02
1014	0.1274	0.1312	7.9071E-03	4.1842E-02
1015	0.1165	0.1237	1.3931E-02	0.2146
1016	0.1386	0.1358	1.0510E-02	5.8625E-02
1114	4.9033E-02	7.0610E-02	2.4980E-02	0.3903
1115	0.1691	0.1724	1.1551E-02	0.6818
1116	2.5537E-02	3.5521E-02	9.2248E-03	0.1033
1214	2.4500E-02	3.4480E-02	3.4945E-03	0.1433

MAXIMUM	0.2281	0.2300	2.4980E-02	0.6818
NODE	1212	1212	1114	1115

MINIMUM	0.	0.	0.	0.
NODE	1	1	1	1

APPENDIX C

RESULTS FROM THE IMPACTING CYLINDRICAL ROD PROBLEM

RESULTS FROM THE IMPACTING CYLINDRICAL ROD PROBLEM

The following figures and tables are results from the impacting cylindrical rod problem which simulates a dynamic impact process. Contour plots of equivalent plastic strain, Mises stress, and strain energy density are shown in Figure C.1 through Figure C.12. Each figure corresponds to either equivalent plastic strain, Mises stress, or strain energy density for a particular rezoning point or at the completion of the solution. Cases of the completed solution for nonrezoning also appear. Table listings of strain jump values at the nodes of the elements flagged for rezoning and those within twenty percent of being flagged are shown in Table C.1 through Table C.4.

PEEQ

	VALUE
1	+2.00E-07
2	+2.00E-01
3	+4.00E-01
4	+6.00E-01
5	+8.00E-01
6	+1.00E+00
7	+1.20E+00
8	+1.40E+00
9	+1.60E+00
10	+1.80E+00
11	+2.00E+00

Figure C.1. Contour plot of equivalent plastic strain for the point of completion for the nonrezoning case of the impacting cylindrical rod

276

MISES

	VALUE
1	+2.00E+02
2	+2.00E+08
3	+4.00E+08
4	+6.00E+08
5	+8.00E+08
6	+1.00E+09
7	+1.20E+09
8	+1.40E+09
9	+1.60E+09
10	+1.80E+09
11	+2.00E+09
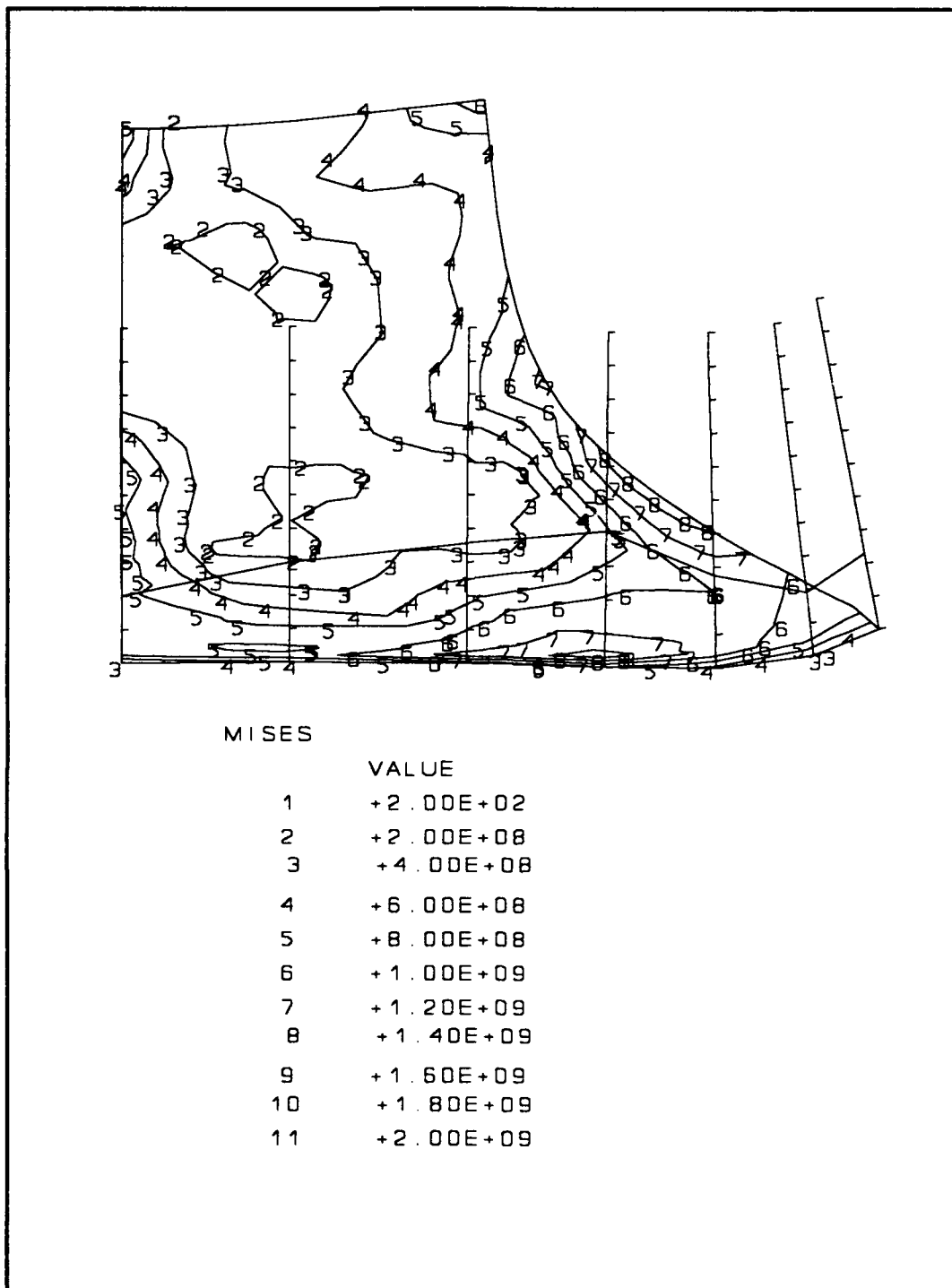
Figure C.2. Contour plot of Mises stress for the point of completion for the nonrezoning case of the impacting cylindrical rod

277

SENER

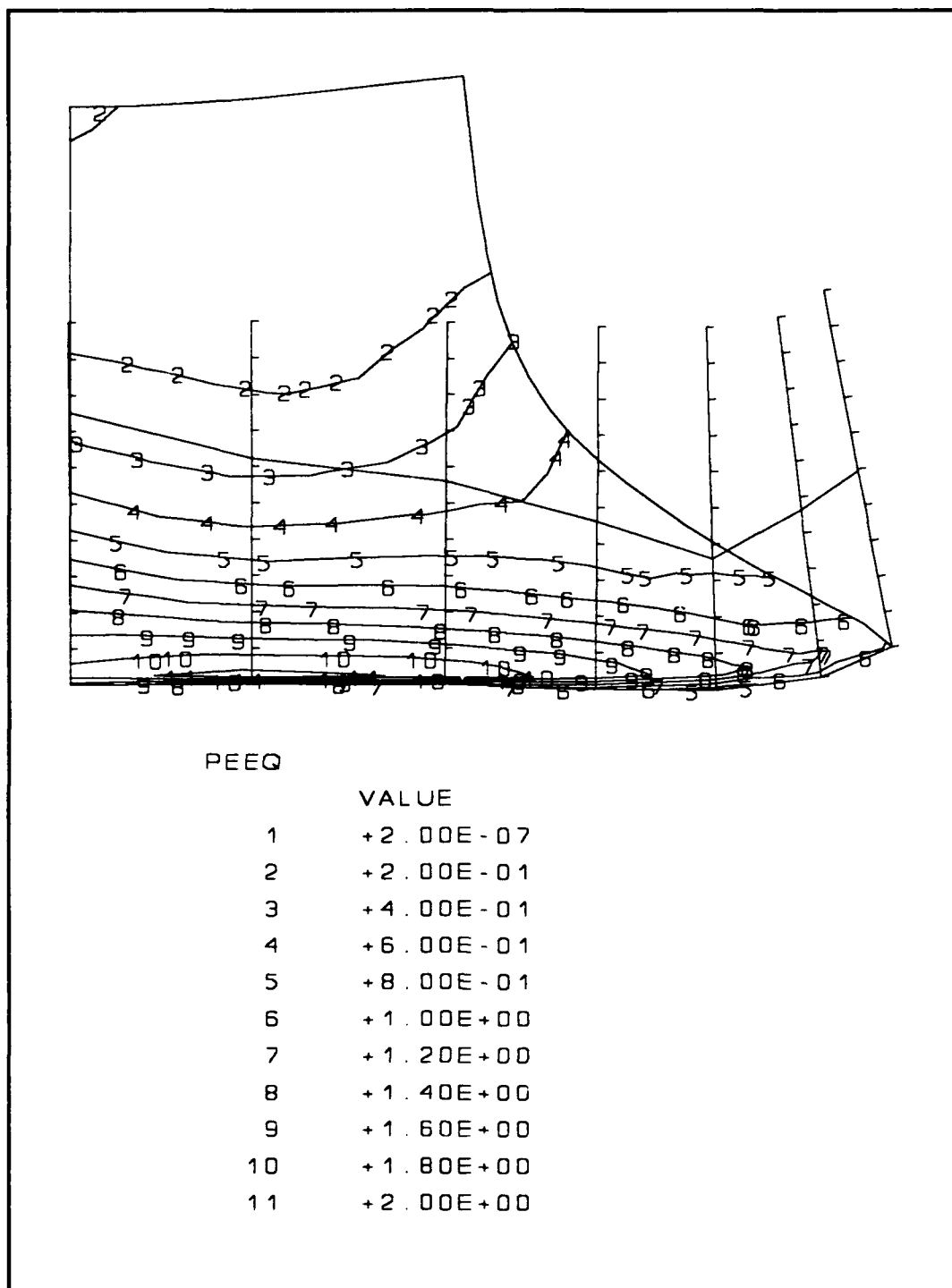|	VALUE
1	+7.00E-01
2	+7.00E+05
3	+1.40E+06
4	+2.10E+06
5	+2.80E+06
6	+3.50E+06
7	+4.20E+06
8	+4.90E+06
9	+5.60E+06
10	+6.30E+06
11	+7.00E+06

Figure C.3. Contour plot of strain energy density for the point of completion for the nonrezoning case of the impacting cylindrical rod
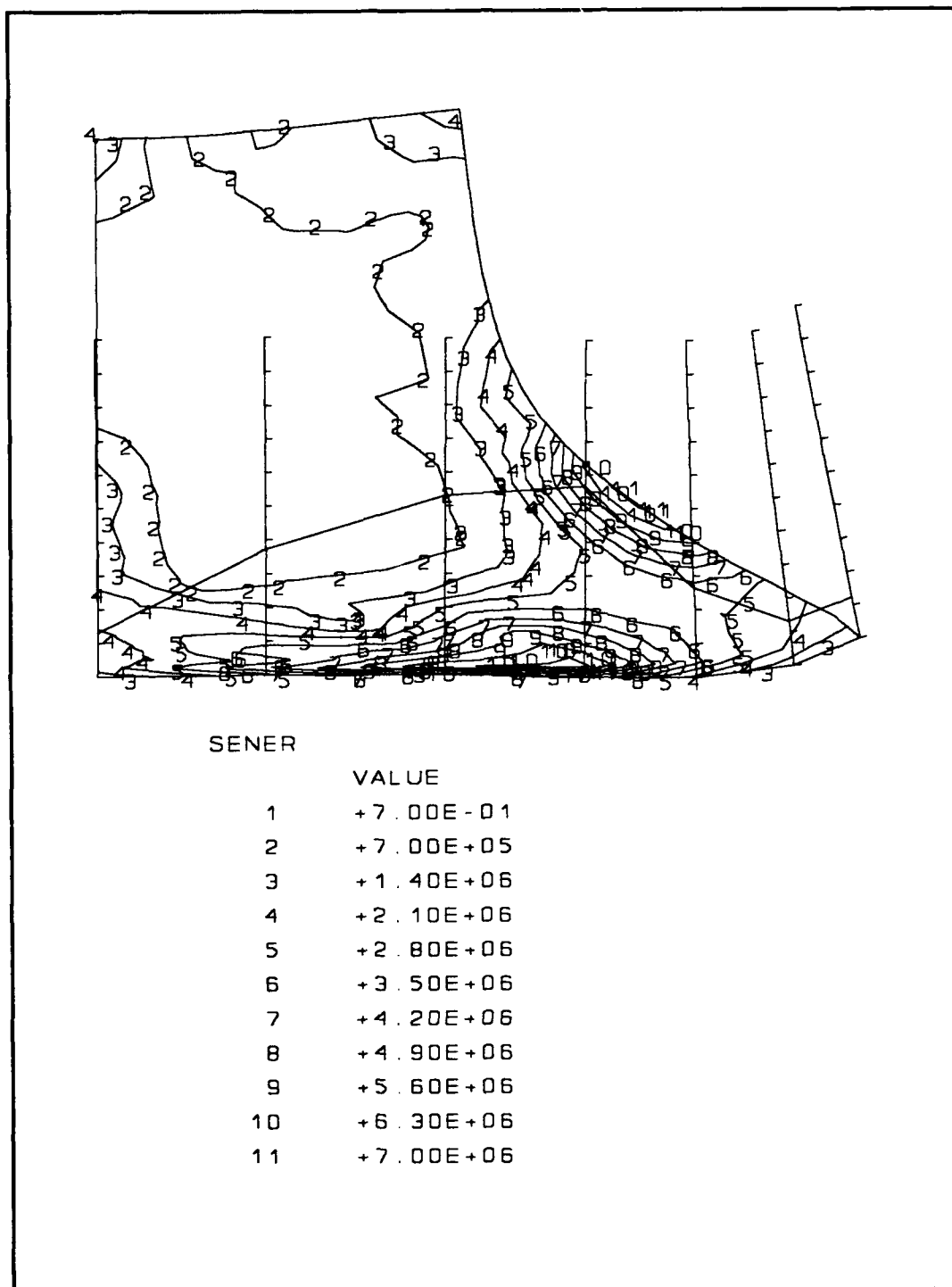
278

Table C.1. Strain jump values for elements flagged for rezoning and those within twenty percent for the completed nonrezoning case of the impacting cylindrical rod

NODE	SJP11	SJP22	SJP33	SJP12
2	2.5507E-02	4.7303E-02	1.8708E-02	0.1392
6	0.3213	0.4112	8.8726E-02	0.4264
101	2.9879E-02	6.6594E-02	3.6296E-02	1.3415E-02
102	3.3352E-02	9.1864E-02	5.5004E-02	0.2864
103	9.6566E-02	0.1507	5.2830E-02	0.4500
104	0.1175	0.1652	8.8138E-02	0.4497
105	0.1457	0.2312	9.8841E-02	0.5306
106	0.4718	0.5725	0.1223	0.6818
107	9.8230E-02	6.4057E-02	3.3566E-02	2.4228E-02
201	2.6730E-02	8.3859E-02	5.6855E-02	2.1395E-02
202	6.2081E-02	0.1436	7.8446E-02	0.4335
203	7.8281E-02	0.1337	6.3455E-02	0.5741
204	0.1405	0.1897	9.9029E-02	0.6251
205	0.2533	0.3400	0.1199	0.5947
206	0.4863	0.5653	0.1460	0.3937
301	1.2002E-02	6.0539E-02	4.9432E-02	2.0820E-02
302	6.6697E-02	0.1428	7.3994E-02	0.5243
303	8.4992E-02	0.1476	6.2091E-02	0.4824
304	0.1615	0.2539	0.1058	0.6566
305	0.3105	0.4027	0.1363	0.5869
306	0.4177	0.5077	0.1595	0.2255
401	1.9428E-02	7.1236E-02	5.1939E-02	2.9777E-02
402	5.6577E-02	0.1313	7.2855E-02	0.5889
403	0.1028	0.1765	7.2447E-02	0.3807
404	0.1760	0.2952	0.1164	0.5686
405	0.3050	0.4122	0.1458	0.5115
406	0.3602	0.4851	0.1630	0.1776
501	1.7242E-02	8.4677E-02	6.7430E-02	4.0156E-02
502	6.3940E-02	0.1464	8.1222E-02	0.6638
503	0.1075	0.1996	9.1310E-02	0.3260
504	0.1746	0.3035	0.1269	0.4787
505	0.2927	0.4064	0.1488	0.4296
506	0.3494	0.4669	0.1602	0.1501
601	1.7888E-02	9.7985E-02	7.9704E-02	4.8226E-02
602	6.3400E-02	0.1507	8.8223E-02	0.6894
603	0.1234	0.2309	0.1072	0.3050
604	0.1516	0.2858	0.1323	0.3710
605	0.2544	0.4015	0.1464	0.3814
606	0.3384	0.4642	0.1529	0.1523
701	1.9216E-02	0.1098	8.9717E-02	4.7622E-02
702	6.6129E-02	0.1661	0.1004	0.6707
703	0.1162	0.2348	0.1181	0.2757
704	0.1329	0.2664	0.1313	0.2863

Table C.1 (continued)

705	0.2217	0.3629	0.1386	0.3308
706	0.3155	0.4500	0.1408	0.1920
801	2.1724E-02	0.1205	9.7810E-02	4.7959E-02
802	7.2442E-02	0.1882	0.1145	0.5944
803	9.8116E-02	0.2216	0.1226	0.2310
804	0.1276	0.2547	0.1251	0.2522
805	0.1822	0.3111	0.1264	0.2928
806	0.2911	0.4203	0.1251	0.2558
902	7.1173E-02	0.1894	0.1185	0.4516
903	7.5991E-02	0.1934	0.1187	0.1890
904	0.1123	0.2265	0.1139	0.2323
905	0.1512	0.2649	0.1115	0.2835
906	0.2610	0.3727	0.1079	0.3188
1003	6.0160E-02	0.1672	0.1068	0.1726
1004	9.0081E-02	0.1893	9.8733E-02	0.1989
1005	0.1251	0.2219	9.4916E-02	0.2552

MAXIMUM	0.4863	0.5725	0.1630	0.6894
NODE	206	106	406	602

MINIMUM	0.	0.	0.	0.
NODE	1	1	1	1
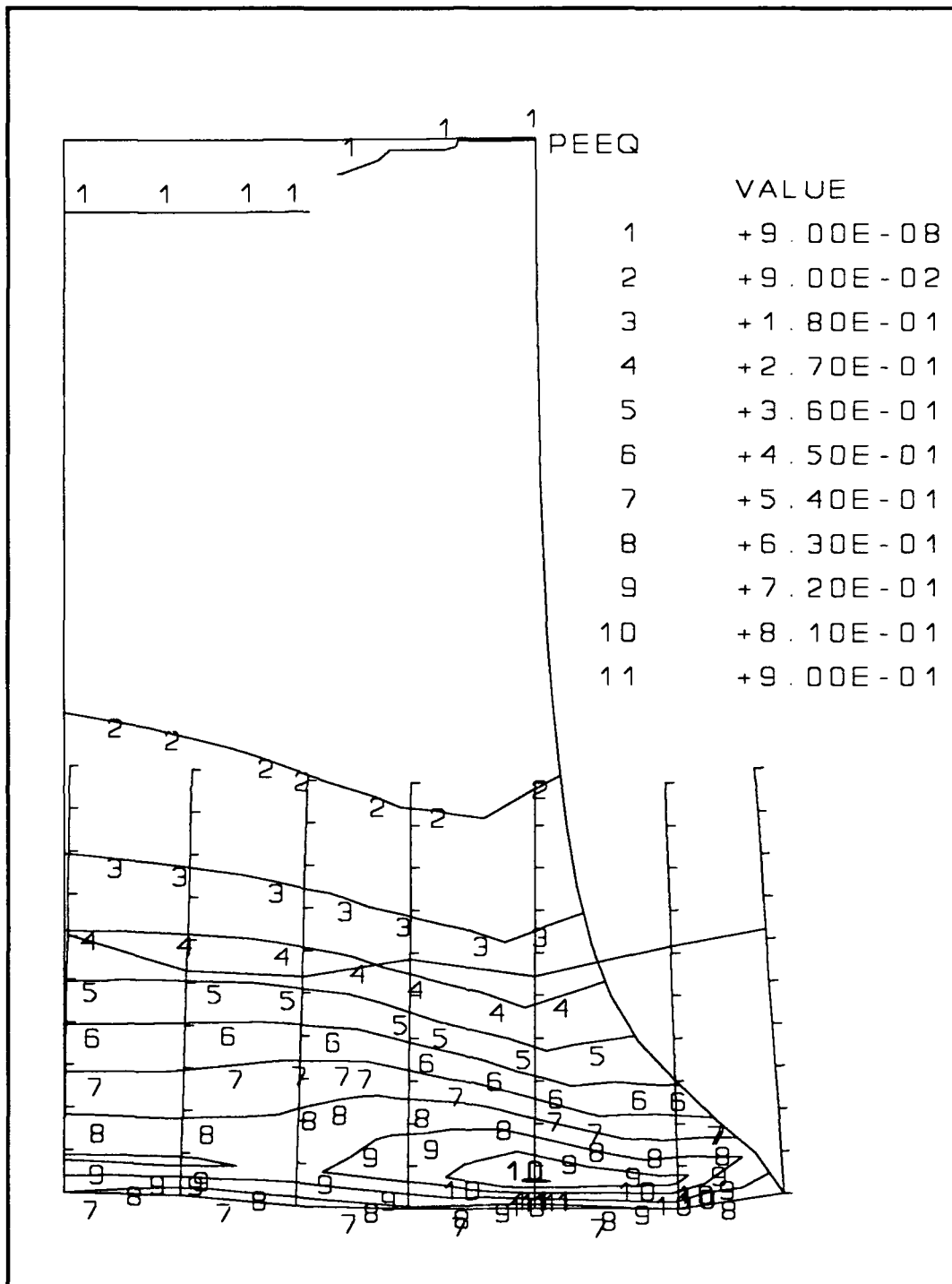
Figure C.4. Contour plot of equivalent plastic strain at the point flagged for the first rezoning of the impacting cylindrical rod
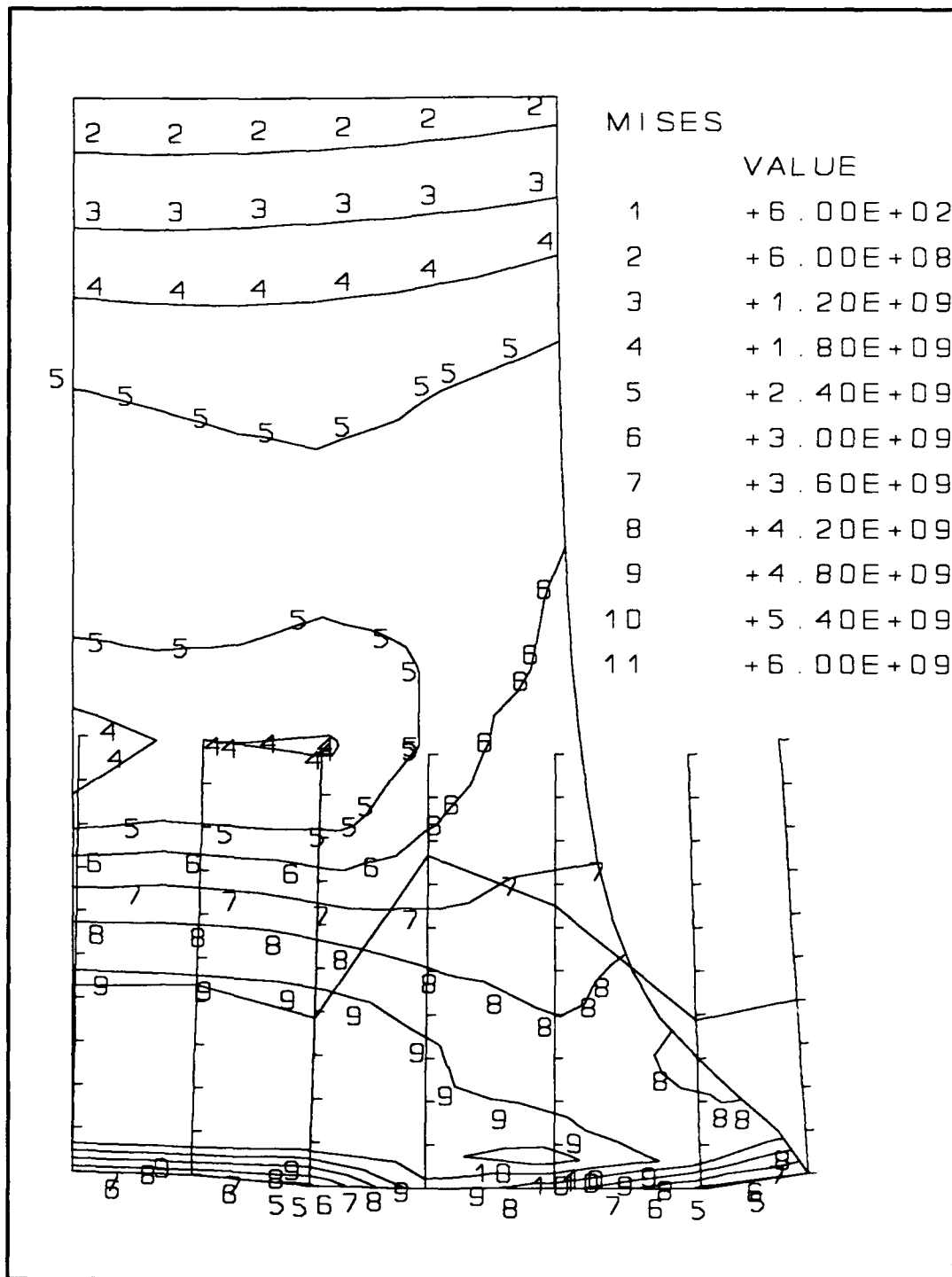
Figure C.5. Contour plot of Mises stress at the point flagged for the first rezoning of the impacting cylindrical rod

282

SENER

	VALUE
1	+6.00E+01
2	+6.00E+07
3	+1.20E+08
4	+1.80E+08
5	+2.40E+08
6	+3.00E+08
7	+3.60E+08
8	+4.20E+08
9	+4.80E+08
10	+5.40E+08
11	+6.00E+08
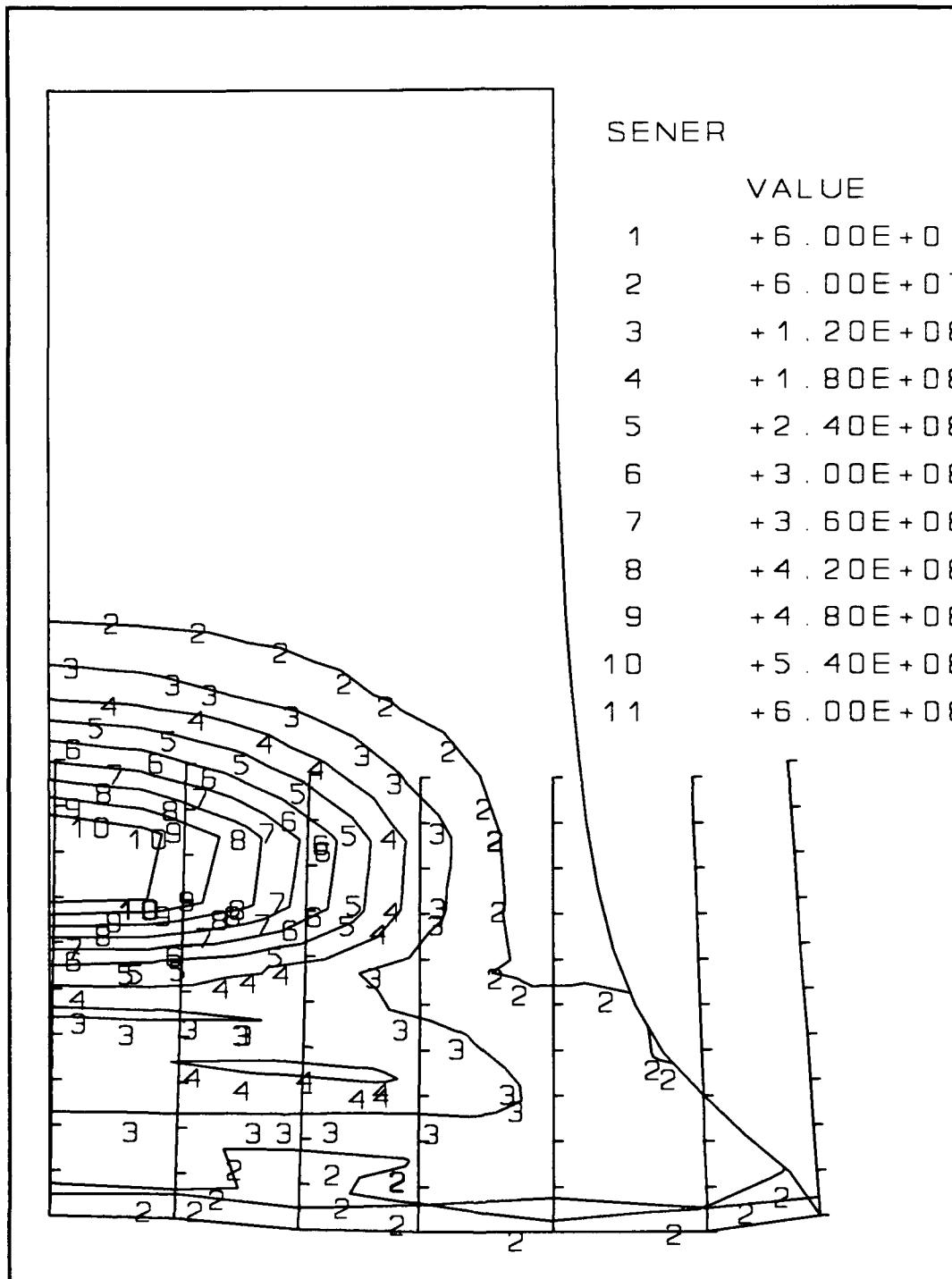
Figure C.6. Contour plot of strain energy density at the point flagged for the first rezoning of the impacting cylindrical rod

Table C.2.   Strain jump values for elements flagged for
rezoning and those within twenty percent for the first
rezoning case of the impacting cylindrical rod

NODE	SJP11	SJP22	SJP33	SJP12
6	0.2212	0.2024	1.7697E-03	0.3480
105	6.4232E-02	9.4914E-02	5.1896E-02	0.1445
106	0.3901	0.4027	4.5110E-02	0.8806
107	9.0363E-02	5.9027E-02	4.3340E-02	7.6385E-02
204	4.8306E-02	0.1027	5.7107E-02	7.8633E-02
205	6.5519E-02	0.1356	6.4642E-02	0.2934
206	0.3790	0.4656	7.9181E-02	0.7632
304	5.0754E-02	6.0166E-02	5.8122E-02	7.0856E-02
305	0.1051	0.1425	6.8045E-02	0.2834
306	0.2780	0.3474	9.4280E-02	0.5509

MAXIMUM	0.3901	0.4656	9.4280E-02	0.8806
NODE	106	206	306	106

MINIMUM	0.	0.	0.	0.
NODE	1	1	1	1

PEEQ

|	VALUE
1	+2.00E-07
2	+2.00E-01
3	+4.00E-01
4	+6.00E-01
5	+8.00E-01
6	+1.00E+00
7	+1.20E+00
8	+1.40E+00
9	+1.60E+00
10	+1.80E+00
11	+2.00E+00
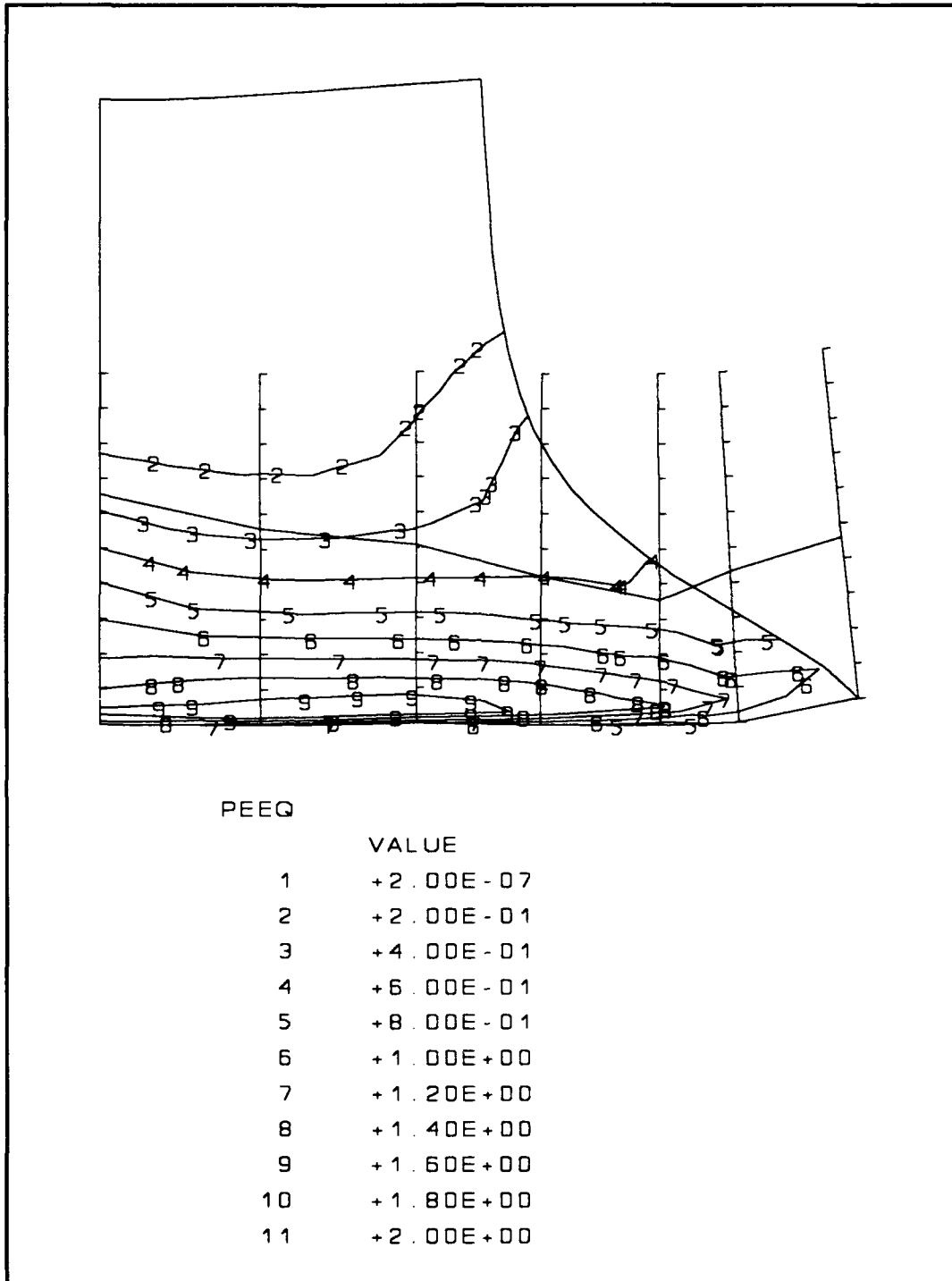
Figure C.7. Contour plot of equivalent plastic strain at the point flagged for the second rezoning of the impacting cylindrical rod

MISES

VALUE

1	+1.00E+09
2	+1.70E+09
3	+2.40E+09
4	+3.10E+09
5	+3.80E+09
6	+4.50E+09
7	+5.20E+09
8	+5.90E+09
9	+6.60E+09
10	+7.30E+09
11	+8.00E+09
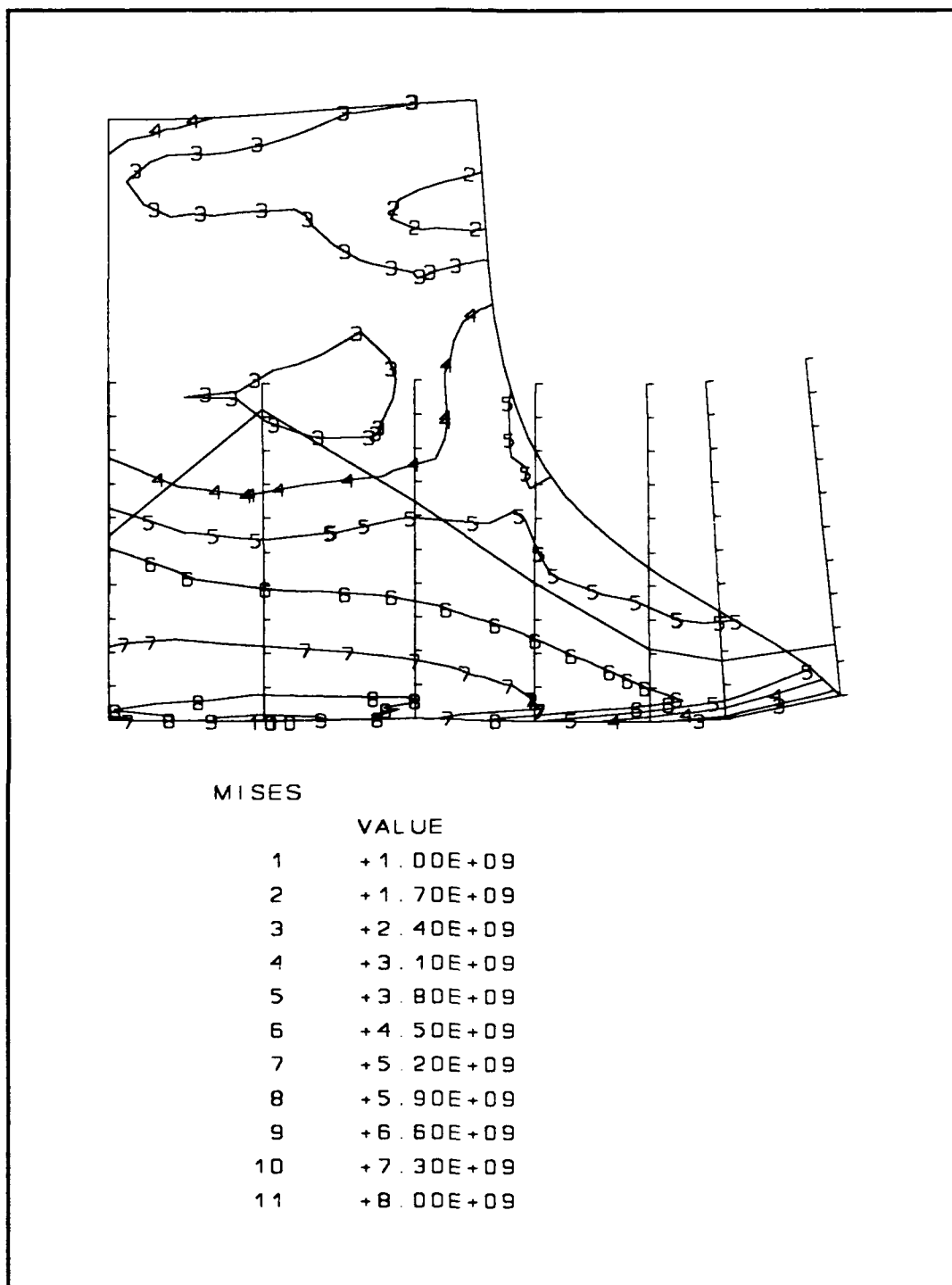
Figure C.8. Contour plot of Mises stress at the point flagged for the second rezoning of the impacting cylindrical rod

286
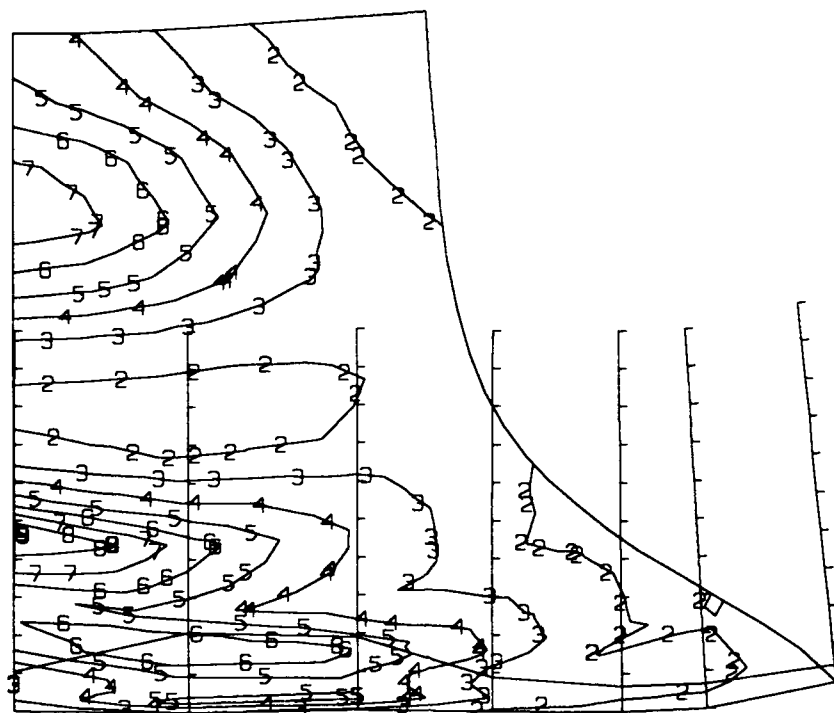
SENER

	VALUE
1	+4.00E+01
2	+4.00E+07
3	+8.00E+07
4	+1.20E+08
5	+1.60E+08
6	+2.00E+08
7	+2.40E+08
8	+2.80E+08
9	+3.20E+08
10	+3.60E+08
11	+4.00E+08

Figure C.9. Contour plot of strain energy density at the point flagged for the second rezoning of the upsetting billet

287

Table C.3. Strain jump values for elements flagged for
rezoning and those within twenty percent for the second
rezoning case of the impacting cylindrical rod

NODE	SJP11	SJP22	SJP33	SJP12
2	5.5823E-02	1.5997E-02	3.3453E-03	0.3633
3	7.9210E-04	5.4914E-02	1.1299E-02	0.3154
6	1.1592E-02	7.0094E-02	7.8879E-02	0.2924
101	1.9331E-02	5.7910E-02	2.9670E-02	3.7229E-03
102	2.3204E-02	7.1929E-02	3.3019E-02	0.3038
103	3.7520E-02	7.2216E-02	1.5454E-02	0.1728
106	3.7426E-02	0.1401	9.2341E-02	5.6507E-02
107	9.2342E-03	1.1391E-02	3.1099E-03	5.7520E-02
202	3.1547E-02	0.1149	3.8023E-02	0.3153
203	7.5559E-02	7.4757E-02	1.0333E-02	7.7200E-02
204	9.3118E-02	0.1605	5.4176E-02	0.2517
205	0.1446	0.2040	7.9322E-02	0.3232
206	4.6789E-02	0.1225	8.2520E-02	3.3073E-02
207	3.8681E-02	4.8100E-02	3.0123E-04	3.3664E-02
302	3.8710E-02	7.6095E-02	4.0009E-02	0.2683
303	0.1129	0.1556	1.5396E-02	0.2925
304	0.1346	0.1787	5.9624E-02	0.3417
305	0.2191	0.2680	8.3023E-02	0.3760
306	9.6619E-02	0.1213	5.4215E-02	7.6008E-02
307	4.6520E-02	3.2786E-02	2.7202E-03	5.2185E-02
402	2.5853E-02	7.6841E-02	3.7215E-02	0.3943
403	8.7416E-02	0.1272	2.7526E-02	0.2585
404	0.1441	0.1850	6.8534E-02	0.3708
501	1.4580E-02	1.2586E-02	2.4874E-02	7.7909E-03
502	3.0520E-02	4.7979E-02	4.2150E-02	0.4853
503	9.2278E-02	0.1137	4.8560E-02	0.2307
504	0.1182	0.1607	7.4764E-02	0.2939
505	0.2747	0.3356	7.8749E-02	0.3286
506	0.2054	0.2594	6.4636E-02	8.0140E-02
601	1.0855E-02	3.0279E-02	4.0706E-02	1.3000E-02
602	7.9114E-02	6.7801E-02	5.1736E-02	0.6113
603	7.4020E-02	0.1041	6.5140E-02	0.1943
604	9.5916E-02	0.1488	7.4891E-02	0.2396
605	0.2446	0.3002	7.6199E-02	0.2622
606	0.1756	0.2239	6.8882E-02	7.7787E-02
701	1.1621E-02	7.4265E-04	4.7666E-02	3.0936E-03
702	7.1919E-02	0.1139	6.1070E-02	0.5768
703	6.0157E-02	0.1254	6.9376E-02	0.1884
704	8.5890E-02	0.1652	7.1706E-02	0.2161
705	0.1802	0.2610	7.4544E-02	0.2046
706	0.1825	0.2258	7.1818E-02	0.1022
801	1.5626E-03	5.3748E-02	5.6808E-02	1.5988E-02
802	4.7764E-02	0.1284	7.3029E-02	0.4493

288

Table C.3 (continued)

803	6.0995E-02	0.1486	7.4382E-02	0.1963
804	8.3098E-02	0.1729	7.1692E-02	0.1891
805	0.1478	0.2397	7.2568E-02	0.2014
806	0.1835	0.2676	7.0025E-02	0.1882
902	3.7431E-02	0.1716	8.1625E-02	0.2628
903	4.5344E-02	0.1673	8.0038E-02	0.1446
904	6.3356E-02	0.1757	7.4401E-02	0.1490
905	8.3084E-02	0.1888	7.1815E-02	0.1793
906	0.1747	0.2639	6.5276E-02	0.2874
MAXIMUM	0.2747	0.3356	9.2341E-02	0.6113
NODE	505	505	106	602
MINIMUM	0.	0.	0.	0.
NODE	1	1	1	1

PEEQ

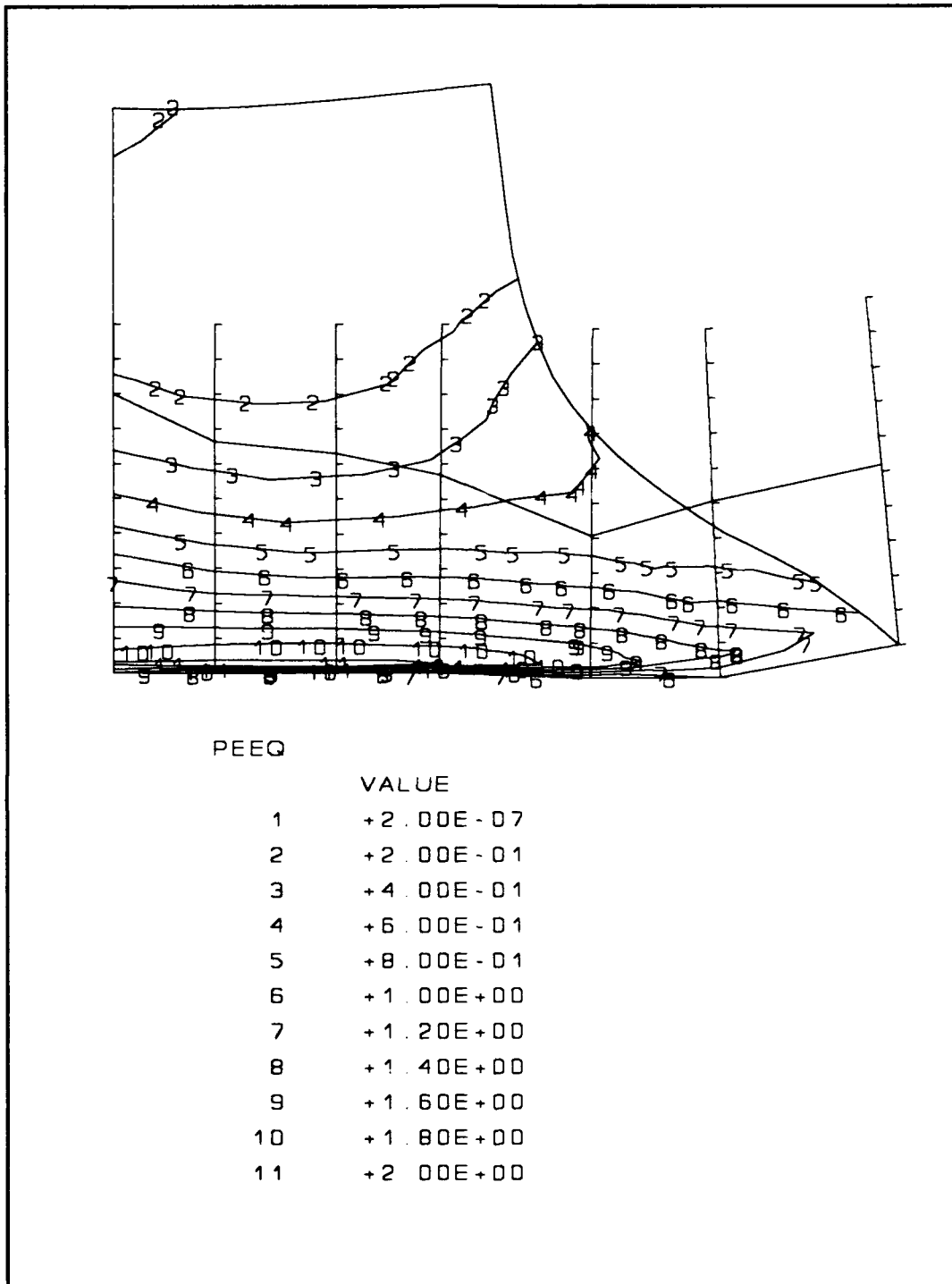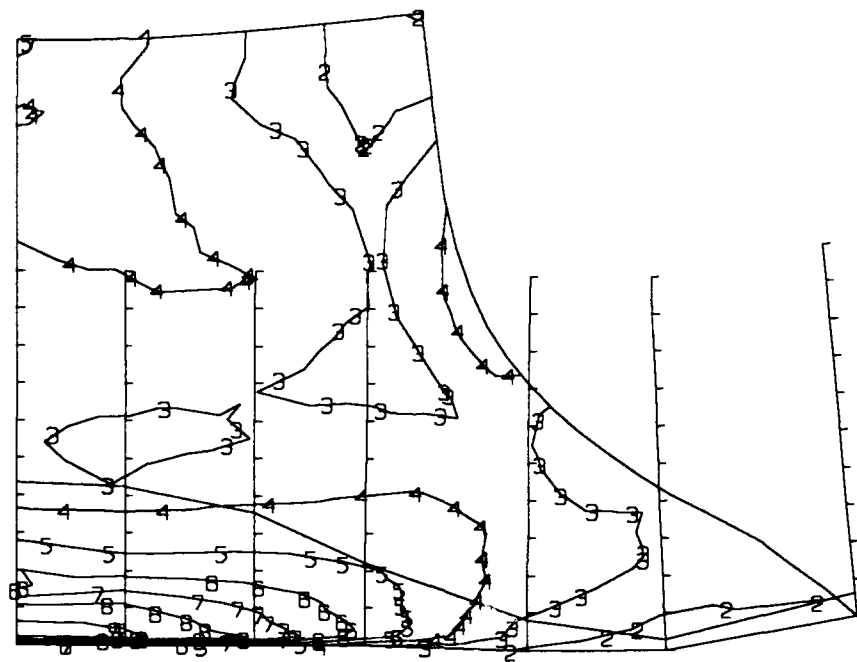|	VALUE
1	+2.00E-07
2	+2.00E-01
3	+4.00E-01
4	+6.00E-01
5	+8.00E-01
6	+1.00E+00
7	+1.20E+00
8	+1.40E+00
9	+1.60E+00
10	+1.80E+00
11	+2.00E+00

Figure C.10.   Contour plot of equivalent plastic strain at the completion of the solution after two rezonings of the impacting cylindrical rod

MISES

	VALUE
1	+4.00E+02
2	+4.00E+08
3	+8.00E+08
4	+1.20E+09
5	+1.60E+09
6	+2.00E+09
7	+2.40E+09
8	+2.80E+09
9	+3.20E+09
10	+3.60E+09
11	+4.00E+09

Figure C.11. Contour plot of Mises stress at the completion of the solution after two rezonings of the impacting cylindrical rod

291

```
SENER

          VALUE
    1     +5.00E+00
    2     +5.00E+06
    3     +1.00E+07
    4     +1.50E+07
    5     +2.00E+07
    6     +2.50E+07
    7     +3.00E+07
    8     +3.50E+07
    9     +4.00E+07
   10     +4.50E+07
   11     +5.00E+07
```
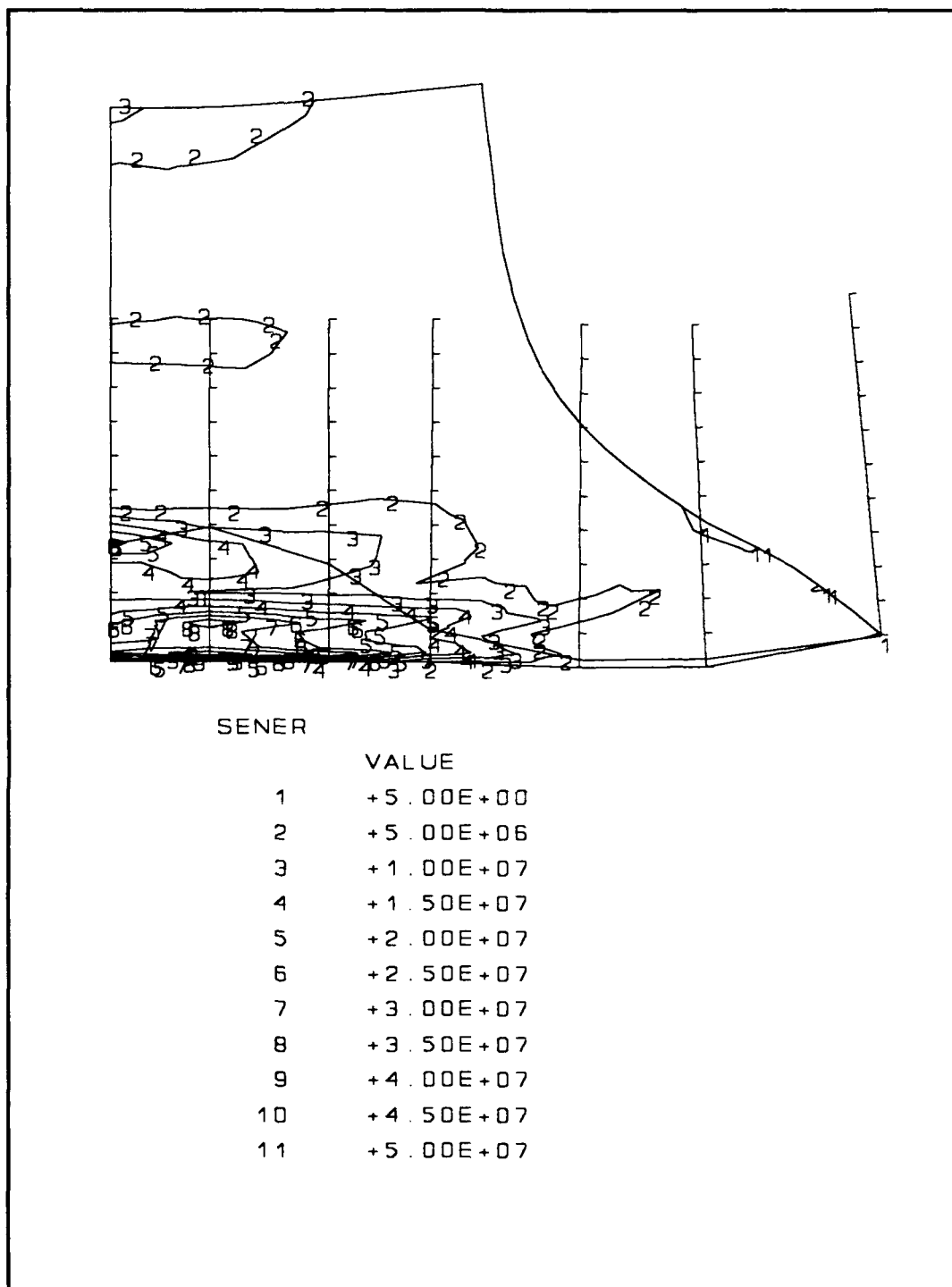
Figure C.12.   Contour plot of strain energy density at the completion of the solution after two rezonings of the impacting cylindrical rod

292

Table C.4. Strain jump values for elements flagged for rezoning and those within twenty percent for the completed solution of the impacting cylindrical rod

NODE	SJP11	SJP22	SJP33	SJP12
5	3.0970E-02	4.8883E-02	2.7757E-02	0.1427
6	2.2486E-02	6.7719E-02	4.8936E-02	0.2652
102	1.0133E-02	1.6223E-02	6.8135E-03	2.8663E-02
103	2.4442E-02	3.7355E-02	8.2218E-03	2.7147E-02
104	8.0744E-03	2.0737E-02	1.7001E-02	0.1268
105	3.9850E-02	5.3764E-02	2.8607E-02	0.1718
106	7.8939E-02	0.1382	6.1876E-02	0.1595
107	5.2838E-03	7.9323E-03	1.5723E-03	1.1892E-03
202	1.2683E-02	2.5585E-02	8.0428E-03	8.7744E-03
203	1.6682E-02	2.9340E-02	4.3758E-03	4.9669E-02
204	1.5986E-02	1.1313E-02	1.6881E-02	7.8854E-02
205	3.7385E-02	5.4799E-02	2.7739E-02	0.1980
206	5.2641E-02	8.8195E-02	4.3490E-02	7.1222E-02
207	1.7887E-03	3.5420E-03	9.8887E-04	2.0093E-02
302	1.3265E-02	2.8002E-02	7.2024E-03	5.4183E-02
303	2.3220E-02	2.9243E-02	4.3418E-03	4.2694E-02
304	1.6430E-02	3.8273E-02	2.1420E-02	4.3119E-02
305	2.9775E-02	5.0882E-02	2.8508E-02	0.1757
306	2.3179E-02	3.6604E-02	2.4433E-02	4.6458E-02
307	1.4008E-03	3.0415E-03	3.5799E-03	4.8215E-03
404	2.9442E-02	4.6636E-02	2.1253E-02	2.8440E-02
405	5.1527E-02	7.5627E-02	3.0958E-02	0.1656
406	1.5623E-02	1.1829E-02	1.2834E-02	3.3119E-02
407	9.7292E-04	2.0247E-03	4.2460E-03	7.3644E-03
504	3.6298E-02	5.2872E-02	1.9547E-02	3.4029E-02
505	8.4293E-02	0.1055	2.6760E-02	0.1821
506	2.2319E-02	2.0844E-02	1.3564E-02	2.1826E-02
507	8.6197E-03	1.0291E-02	3.8614E-03	6.2326E-03
704	2.2287E-02	3.2704E-02	2.0206E-02	4.6715E-02
705	5.5985E-02	8.0207E-02	2.8351E-02	9.3384E-02
804	1.7322E-02	1.9174E-02	2.0325E-02	3.0457E-02
805	5.2425E-02	6.6138E-02	2.8855E-02	7.5535E-02
MAXIMUM	8.4293E-02	0.1382	6.1876E-02	0.2652
NODE	505	106	106	6
MINIMUM	0.	0.	0.	0.
NODE	1	1	1	1

REPORT DOCUMENTATION PAGE

Form Approved
OMB No. 0704-0188

AGENCY USE ONLY (Leave blank)	2. REPORT DATE March 1992	3. REPORT TYPE AND DATES COVERED Final

TITLE AND SUBTITLE A METHOD OF SELF ADAPTIVE REZONING FOR THE CASE OF LARGE DEFORMATION FINITE ELEMENT PROBLEMS UTILIZING REZONING INDICATORS DERIVED FROM EIGENVALUE TESTING	5 FUNDING NUMBERS
AUTHOR(S) B. L. Croft	

PERFORMING ORGANIZATION NAME(S) AND ADDRESS(ES) Naval Command, Control and Ocean Surveillance Center (NCCOSC) RDT&E Division (NRaD) San Diego, CA 92152–5000	8. PERFORMING ORGANIZATION REPORT NUMBER NRaD TD 2275

SPONSORING/MONITORING AGENCY NAME(S) AND ADDRESS(ES) Naval Command, Control and Ocean Surveillance Center (NCCOSC) RDT&E Division (NRaD) San Diego, CA 92152–5000	10. SPONSORING/MONITORING AGENCY REPORT NUMBER

1. SUPPLEMENTARY NOTES

2a. DISTRIBUTION/AVAILABILITY STATEMENT	12b. DISTRIBUTION CODE

3. ABSTRACT *(Maximum 200 words)*

A method for self adaptive rezoning is delineated based upon finite element modeling assumptions of structural problems involving large deformations and strains. Linear isoparametric quadrilateral elements using selective reduced integration are examined.

Geometrical measures of an element are defined in terms of aspect ratio, taper ratio, and skew angel. The amount of distortion of an element is related to these terms when compared to the same terms for an ideal element. An algorithm is developed to examine the finite element mesh, element by element, to quantify the geometrical relationships which are needed to quantify the amount of distortion.

Results of eigenvalue testing quadrilateral elements is used to derive rezoning indicators. The process is theoretically and mathematically sound, but must be derived empirically due to the nonlinear nature of the stiffness matrix. A ratio of the strain energy density of an ideal to a distorted element is used in determining the rezoning indicators.

A remeshing technique is developed which requires user intervention and is based upon information determined by the rezoning indicators. An automatic remapping scheme is used to remap the element variables from the old mesh to the new rezoned mesh. Two example problems are examined.

4. SUBJECT TERMS self adaptive rezoning eigenvalue testing finite element mesh remapping linear isoparametric quadrilateral elements remeshing			15 NUMBER OF PAGES 316
			16 PRICE CODE

7 SECURITY CLASSIFICATION OF REPORT UNCLASSIFIED	18. SECURITY CLASSIFICATION OF THIS PAGE UNCLASSIFIED	19 SECURITY CLASSIFICATION OF ABSTRACT UNCLASSIFIED	20 LIMITATION OF ABSTRACT SAME AS REPORT

21a. NAME OF RESPONSIBLE INDIVIDUAL	21b. TELEPHONE *(include Area Code)*	21c. OFFICE SYMBOL
B. L. Croft	(619) 553–3458	Code 981

INITIAL DISTRIBUTION